Applied Molecular Quantum Electrodynamics: Geometric aspects of the efficiency of photonic interactions

Jack Stephen Ford

For the qualification of PhD

University of East Anglia

School of Chemistry

Submitted September 2015

Abstract

This thesis presents applications of molecular quantum electrodynamics (MQED) to the analysis of resonance energy transfer (RET), molecular absorption and emission, and light scattering by molecules. An MQED framework describes such processes as a series of microscopic photonic interaction events. Multi-interaction processes entail intermediate states of the system's evolution remaining unspecified, requiring careful interpretation. RET, as modified by coupling with the nearest molecule of the surrounding refractive medium, is investigated. Special attention is given to a system geometry where unmodified RET is impossible, so coupling with the third chromophore is essential. Two distinct treatments are given to emission by a multi-chromophore system, distinguished by different ways of framing the quantum system: Either all photons are virtual and chromophores share excitation, or real photons interact with a single unspecified chromophore. Anomalously high fluorescence-anisotropy is explainable with the latter analysis. Off-resonant light is known to modify the absorption behaviour of molecules: This weak-interaction is analysed with an MQED formulation modified by field dressing, modelling advanced media effects in the condensed phase. Within the electric-dipole approximation, hyper-Rayleigh scattering (HRS) is considered forbidden for centrosymmetric molecules: By including higher-multipole interactions, mechanisms enabling conventionally-forbidden HRS are discovered. For each process analysed, the main results are predictions for the efficiency or observable rate. The relative positions and orientations of the molecules and fields are the key variables, so the rate equations are typically complicated functions thereof. Where rate equations depend on molecular orientation, it is often appropriate to calculate the average value over all orientations, giving results applicable to the fluid phase. System geometry may exert very fine control – a process forbidden in one case may become allowed by a minor change of one chromophore's alignment. This thesis contributes to understanding the precise requirements of molecular geometry that must inform the design of energy-transfer systems.

Contents

Total length: 179 pages, approx. 36000 words.

Acknowledgements

My postgraduate studentship has been supported by a Doctoral Training Account from the Engineering and Physical Sciences Research Council.

I am very grateful to my supervisor, Professor David Andrews, for his invaluable guidance and advice through the last five years. I could not have asked for more attentive and constructive supervision, which has enabled a term of productive and very varied research.

The QED group at UEA has been a pleasure to be part of – David has fostered a collective of researchers with diverse talents who support each other's work and share a real spirit of camaraderie. I especially commend David Bradshaw and Matthew Williams, my co-authors on several peer-reviewed publications, for being model collaborators.

I would like to thank my UEA mentors, Sue Roe and Ryan Tebbit, for helping me to organise myself and my work, and for providing general advice as I begin aspiring toward a research career.

Lastly and most importantly, infinite thanks are due to my parents for supporting and assisting me during my university years. Without Mum's frequent help in breaking my writer's block, this thesis would consist almost entirely of equations and figures linked by "$\Rightarrow$" and "$\therefore$" operators. And without the Dad Taxi Co., my work week would have involved far too many rainy winter evenings loitering for hours in Norwich Bus Station.

Chapter 1: **Introduction**

1. Thesis overview

This thesis concerns various processes of molecular absorption or emission of light, electronic energy transfer, and light scattering. All these forms of light-matter interaction may in principle be reduced to a series of microscopic photonic interaction events. The formalism of molecular quantum electrodynamics (MQED) understands each individual interaction event to consist of a single chromophore changing its electronic state while creating or annihilating a photon.

I intend to describe several different forms of interaction and molecular transition in an MQED framework. This thesis extends the direct application of MQED methods to certain common physical processes that are conventionally analysed with other theoretical approaches, and introduces novel developments to existing QED analyses.

The two parts of Chapter 2 are an introduction to molecular QED theory and the calculation methods applied in the research of chapters 3-6. Certain features of the theory require careful interpretation, as the analysis may involve counter-intuitive results of quantum mechanics, or contain implicit assumptions that limit its applications.

Chapter 2a explains the necessity of quantum electrodynamic methods for the analysis of photonic interactions, and provide the theoretical framework that is employed in the analysis and calculations of the subsequent chapters. It then explores the complications that arise in the treatment of multi-interaction processes – in principle, interaction events may occur in any time-order and the intermediate states of a system's evolution are unspecified. Appendix 8a assists in explaining the mathematical patterns governing event-ordering.

Chapter 2b outlines the standard method of calculating a rotational average of molecular response tensors, which is necessary for evaluating the rate of a process where the molecule(s) are randomly oriented or stochastically rotate. Appendix 8b contains the full data required for an explicit calculation. This method is used to calculate rotationally-averaged rate equations in chapters 3a, 4b, 5 and 6.

For each photonic process explored in the chapters 3-6, the main results of the MQED analysis are to derive the predicted transition efficiency or observable interaction rate. The relative positions and orientations of the system's molecules and fields are usually the key variables to determine efficiency, so the final rate equations are typically functions of the lengths and angles in the system geometry.

Chapter 3 is in two parts, concerning processes of resonance energy transfer (RET). Chapter 3a discusses the nature of RET in its two-body and third-body-modified forms, and provides detailed analysis of the case in which the nearest molecule of surrounding matter constitutes the third body. This directly links the bulk material properties of a medium to the microscopic photonic interactions of RET. Appendix 8c is part of the electrodynamic coupling derivation that is central to the analysis of RET applied in chapters 3a, 3b and 4a. Chapter 3b gives special attention to a system geometry in which two-body RET is naturally forbidden – coupling with the third chromophore is absolutely necessary for RET, and so the precise position and orientation of this chromophore is critical.

Chapter 4 is in two parts, concerning the emission of one or two photons by a system of multiple chromophores – emission behaviour is complicated by delocalisation of the initial excitation between the chromophores. Chapter 4a explores the consequences of pairwise electrodynamic coupling, both within a two-nanoemitter system and between individual nanoemitters and the detector unit. Appendix 8d gives a mathematical treatment of the quantum mechanics of a two-chromophore exciton, where the coupling leads to unspecified excitation-sharing between emitter units. Chapter 4b disregards explicit coupling and models the fluorescence of a multi-chromophore complex in solution, where the sharing of excitation is itself a quantum measurement phenomenon.

Chapter 5 concerns the absorption of one or two photons by a molecule, with the involvement of an additional non-resonant beam of light modifying this process. The forward-scattering of auxiliary light is additional to the absorption, forming a single process of up to four distinct interaction events. Analysis of the case of a molecule in solution requires rotational averaging and a discussion of how media properties influence the character of interacting light.

Chapter 6 concerns high-order processes of hyper-Rayleigh scattering (HRS) by a molecule. Within a theoretical analysis that uses the standard electric-dipole

approximation for all interactions, HRS is known to be forbidden for high-symmetry molecules. But by including interaction behaviours beyond the electric-dipole approximation in the analysis, this chapter describes mechanisms that enable such conventionally-forbidden HRS.

Chapter 7 concludes with commentary on the preceding chapters, noting how the many different photonic processes are connected by similar MQED models and methodology. The limitations of the theoretical framework are discussed briefly, along with considerations of quantum-measurement interpretation. The various novel findings of this thesis are noted, together with their potential applications and areas for further research.

2. List of publications

Chapters 3-6 of this thesis report six distinct research projects undertaken during my postgraduate studentship. As part of this work, several journal articles and conference papers have been published. Each thesis chapter has been written to expand upon the findings and discussion contained in the corresponding publications, and to bring the projects together into a coherent thesis on geometric aspects of interaction efficiency. While all publications have been cited where appropriate, here is a complete self-bibliography in chronological order.

[1] D.L. Andrews and J.S. Ford, "Electronic Energy Transport in Nanomaterials: Influence of Host Structure": *Proc. SPIE*, **8459** (2012), p. 0C.
[2] J.S. Ford, D.S. Bradshaw, and D.L. Andrews, "Signatures of Exciton Coupling in Paired Nanoemitters": *J. Phys. Chem. C* **117**, 12393 (2013).
[3] D.L. Andrews and J.S. Ford, "Resonance Energy Transfer: Influence of Neighboring Matter Absorbing in the Wavelength Region of the Acceptor": *J. Chem. Phys.* **139**, (2013).
[4] D.S. Bradshaw, J.S. Ford, and D.L. Andrews, "On the Detection of Characteristic Optical Emission from Electronically Coupled Nanoemitters": *Proc. SPIE*, **8807** (2013), p. 03.

[5] J.S. Ford and D.L. Andrews, "Geometrical Effects on Resonance Energy Transfer between Orthogonally-Oriented Chromophores, Mediated by a Nearby Polarisable Molecule": *Chem. Phys. Lett.* **591**, 88 (2014).

[6] J.M. Leeder, M.M. Coles, J.S. Ford, and D.L. Andrews, "Designing Media for the Local Control of Nanoscale Absorption, Transmission, and Energy Transfer": *Proc. SPIE*, **9126** (2014), p. 15.

[7] J.S. Ford, D.S. Bradshaw, and D.L. Andrews, "Engaging New Dimensions in Nonlinear Optical Spectroscopy Using Auxiliary Beams of Light": *Proc. SPIE*, **9136** (2014), p. 1C.

[8] J.S. Ford and D.L. Andrews, "One- and Two-Photon Absorption in Solution: The Effects of a Passive Auxiliary Beam": *J. Chem. Phys.* **141**, (2014).

[9] M.D. Williams, J.S. Ford, and D.L. Andrews, "Mechanisms Universally Permitting Hyper-Rayleigh Scattering": *Proc. SPIE*, **9347** (2015), p. 11.

[10] M. D. Williams, J. S. Ford, and D. L. Andrews, "Hyper-Rayleigh Scattering in Centrosymmetric Systems": *J. Chem. Phys.* **143**, 124301 (2015).

–

Chapter 2: **Calculation framework**

2a: **MQED theory**

1. MQED: Photonic interactions of molecules

Quantum electrodynamics is the essential framework for any microscopic analysis of molecule-light interactions. A semiclassical model, with quantum-mechanical molecules influenced by Maxwellian fields, fails to correctly describe processes such as spontaneous emission. A classical vacuum with no radiation offers no perturbation to a molecule's stationary states, so any excited state should be perfectly stable. Quantum electrodynamics, by treating radiation as quantum particles (photons) subject to uncertainty relations, permits quantum fluctuations in photon-number as a source of perturbation.[1–3]

As an example interaction, consider Rayleigh scattering – a process well-known as the cause of the atmosphere's light blue colour. The naive or semi-classical model is light (which may or may not be quantised as photons) bouncing off a molecule in a single event, like a microscopic form of reflection – this is implied by the word "scattering". But the photonic description is two distinct microscopic interaction events: the absorption of an input photon and the creation of a new photon of the same wavelength.

While most of this thesis concerns interactions of photons with whole molecules, the theory can equally be applied to photonic interactions of individual optically-active sites (chromophores) affixed to some larger matrix. The words "molecule" and "chromophore" can be understood as interchangeable in most contexts.

When applying any of these theoretical results to a specific real system, care must be taken to ensure that the chromophores are adequately separated in space – all interactions are understood to entail a minimum number of photons being exchanged between chromophores that remain distinct, with their individual states. If there is close physical contact between the molecules, then their electronic wavefunctions will significantly overlap, so each molecule no longer has a discrete state that only changes in response to creation or annihilation of identified photons. If wavefunctions overlap sufficiently that a chemical bond is formed, then it becomes incorrect to describe the chromophores as distinct objects

whose interactions are mediated purely by the passage of photons through the vacuum between their two positions.

All electromagnetic interactions of molecules are described as discrete interactions with the (quantised, retarded) electromagnetic field. These interactions are perturbations of the molecules' states, so perturbation-theory methods may be used to evaluate the quantum amplitudes of molecular transition processes in terms of molecule-radiation interaction Hamiltonian operators.

In principle, all theory serves the goal of making predictions for the observable outputs of interactions (physical observables such as emission of radiation, or net change in a molecule's electronic excitation), which may be tested. For a process where the system of interest undergoes a change in overall state, the theoretical analysis methods outlined in this chapter can deliver a prediction of the rate of the transition. This may be verified by quantitatively measuring observable signals that are diagnostic of the final state produced by the process.

2. Feynman diagrams

In fundamental quantum field theory, the interactions of elementary particles are shown with Feynman diagrams, with conservation of four-momentum ensured by rules governing line gradients. A Feynman diagram illustrates a particular movement of particles through spacetime, each constituent subsystem occupying several states during the evolution.

Feynman diagrams are well-suited to the systems considered in this thesis, because it is possible to show the specifics of each individual photon-interaction and the time-order of the events. Unlike the classic diagrams of Richard Feynman et al which describe general interactions of particles,[4] this thesis deals with molecules limited to non-relativistic motion, and so the form of all Feynman diagrams is limited to vertical molecule-lines with photons shown as diagonal waves.

Whole molecules generally remain at non-relativistic speeds, within a Born-Oppenheimer approximation. The Feynman diagrams used in molecular quantum electrodynamics can thus be made to obey the simple rule that molecule lines remain vertical. The speed of light being constant, all photons are wavy lines with

the same gradient. This approximation removes all other relativistic considerations from the Feynman diagram structure.

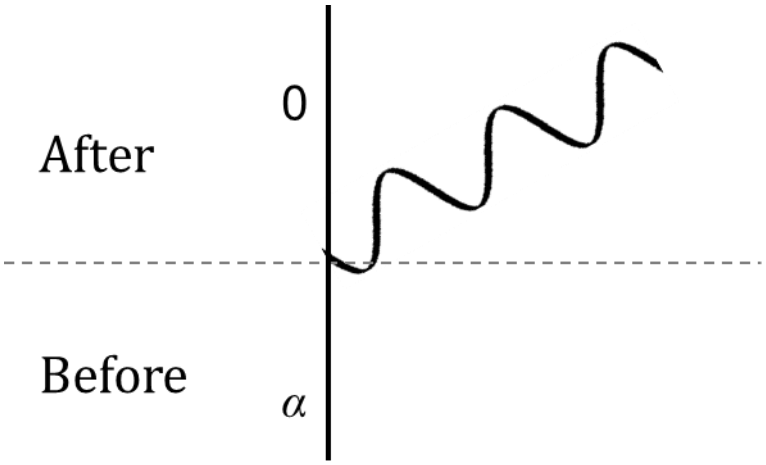

Figure 2a.1: An elementary molecular Feynman diagram. This shows a molecule's spontaneous emission of one photon, while relaxing from an excited state α to the ground state 0. The vertical axis is time and the horizontal axis is a spatial coordinate, so the slope of the photon's line indicates propagation to the right at speed *c*.

The information that Feynman diagrams are used to convey in non-relativistic molecular quantum electrodynamics does not include intricacies such as four-momentum. All that is shown is motionless molecules interacting with the field and photons that are either virtual (bounded at both ends by interactions within the system) or real (connecting the system to the outside, so directly observable). Since the relative positions are drawn so abstractly as to be useless, and the virtual photons are always implied to consist of a great many possible radiation modes, the only physical information that these Feynman diagrams successfully convey is the core connectivity and time-order of the photonic interactions within a process.

See appendix 8a for an overview of a complementary method for diagrammatically representing multi-interaction photonic processes: State-sequence diagrams have certain mathematical advantages,[5,6] and have been usefully applied to many of the problems in this thesis.[3,7,8]

3. Radiation states and the interaction Hamiltonian

Photons, as physically observable particles, are described solely in terms of their tangible properties which may perturb the matter they interact with. A radiation mode describes the microscopic structure of the electric and magnetic fields. The decomposition of a system's radiation into a set of discrete modes, each occupied by an integer number of photons, is the quantum version of a classical field mode decomposition.[9,10] The states of a system's radiation are quantified by the Fock number q, which is the number of photons of a specific mode in the system.

This thesis uses a decomposition of electromagnetic fields into the set of plane-wave modes. Each such mode is defined by the wavevector **k**, describing the propagation direction and the wavelength $\lambda = 2\pi k^{-1}$, and the polarisation state η. The Fock states of radiation are thus labelled $|q,\mathbf{k},\eta\rangle$. A plane wave has the unique property that the field structure is paraxial at all points along the axis of propagation **k**, such that the wavefronts of constant phase are parallel planes normal to the **k** axis. All positions along this axis are equivalent, so the position of an interaction does not need to be uniquely defined – in any other choice of mode decomposition, it is necessary to specify that the interacting chromophore is positioned at the origin of the mode expansion, and carefully construct the Fock states to accommodate this requirement.

When moving from a semi-classical formulation to a fully-quantum molecular electrodynamics, the relevant Hamiltonian energy operator for the quantum-mechanical system must be reformed. Quantum radiation, composed of Fock states $|q,\mathbf{k},\eta\rangle$, is now part of the system, so it has its own distinct Hamiltonian term. The system Hamiltonian operator is thus conventionally decomposed into three components, summing over the various molecules ξ:

$$H = H_{\text{radiation}} + \sum_{\xi}\left(H_{\text{molecule}} + H_{\text{interaction}}\right) \tag{2a.1}$$

The interaction Hamiltonian term for each molecule ξ is expressible as a multipolar expansion. With the radiation imposing transverse electric displacement field $\mathbf{d}^{\perp}$ and magnetic field **b** on the location of ξ:[1,11]

$$H_{\text{interaction}}(\xi) = -\varepsilon_0^{-1}\boldsymbol{\mu}\cdot\mathbf{d}^{\perp} - \varepsilon_0^{-1}Q_{ij}\nabla_j d_i^{\perp} - \mathbf{m}\cdot\mathbf{b} + \ldots \tag{2a.2}$$

Subscripts *i*,*j*,*k*,*l* are Cartesian indices, each representing an unspecified member of the standard-basis set $\{x,y,z\}$. This thesis makes extensive use of the Einstein convention of implied summation over repeat indices: If R_x represents the *x*-component of a vector **R**, then $R_i S_i = R_x S_x + R_y S_y + R_z S_z = \mathbf{R}\cdot\mathbf{S}$.

In equation (2a.2), **μ**, **Q** and **m** are the electric dipole (E1), electric quadrupole (E2) and magnetic dipole (M1) response operators of molecule ξ. In principle, the series continues with an infinite number of E*N* and M*N* terms. This description of the interaction as a combination of multipole moments with increasing order is a series expansion, following from a multipolar decomposition of the interaction potential's distribution about the molecule's position. The pseudo-numerical "-pole" names reflect the fact that permanent multipoles are idealised potential distributions with 2^N poles, centred on the molecule's position. The N=0 multipoles are not included – electric monopoles are merely permanent charges, and magnetic monopoles are physically impossible.

It is usually sufficient to include only the first term of the H_{int} expansion – this is the electric dipole (E1) approximation. This is satisfactory when the radiation wavelength is sufficiently long that there is no variation in the fields over the extent of the molecule. The transition electric dipole moments for each transition (labelled $\boldsymbol{\mu}^{FI}$ below) are then the only relevant molecular properties. This form of the multipolar expansion, which neglects longitudinal fields and delivers the E1 approximation as a leading term, is consistent with the Power-Zineau-Wooley canonical formulation of MQED interactions.[12,13] Any multipolar-tensor-coupling formulation (such as the E1 approximation) necessarily presupposes a QED framework.[14,15]

Each interaction event may be described with a Dirac bracket – this gives the quantum amplitude for the interaction process, as discussed in the following section 4. Using the E1 approximation, $H_{\text{int}} = (-\varepsilon_0^{-1})\boldsymbol{\mu}\cdot\mathbf{d}^{\perp}$, the molecule-plus-radiation system is transformed from its initial state I to a final state F with amplitude:

$$\begin{aligned}\left\langle F\left|H_{\text{int}}\right|I\right\rangle &= \left\langle \text{Mol}_F + \text{Rad}_F \left| H_{\text{int}} \right| \text{Mol}_I + \text{Rad}_I \right\rangle \\ &= -\varepsilon_0^{-1} \left\langle \text{Mol}_F \left| \boldsymbol{\mu} \right| \text{Mol}_I \right\rangle \cdot \left\langle \text{Rad}_F \left| \mathbf{d}^{\perp} \right| \text{Rad}_I \right\rangle\end{aligned} \qquad (2a.3)$$

The molecular Dirac bracket vector is the electric dipole moment of the molecule's transition, conventionally labelled $\boldsymbol{\mu}^{FI}$. Given that the fields belong to the radiation, which consists of photons in various Fock states, the quantum description of transverse electric displacement field $\mathbf{d}^{\perp}$ is expressed as a mode expansion in terms of the plane-wave mode parameters $\mathbf{k}$ and η:

$$\mathbf{d}^{\perp} = i\sum_{\mathbf{k},\eta}\left(\frac{\hbar\varepsilon_0 ck}{2V}\right)^{1/2}\left[\mathbf{e}_{(\eta,\mathbf{k})}a_{(\mathbf{k},\eta)}\exp(i\,\mathbf{k}\cdot\mathbf{r}_{\xi}) - \overline{\mathbf{e}}_{(\eta,\mathbf{k})}a^{\dagger}_{(\mathbf{k},\eta)}\exp(-i\,\mathbf{k}\cdot\mathbf{r}_{\xi})\right] \tag{2a.4}$$

A single photon and a molecule ξ (transitioning $\xi_F \leftarrow \xi_I$) will therefore interact as described by the Dirac bracket:

$$\begin{aligned}\left\langle F\left|H_{\text{int}}\right|I\right\rangle = -i\mu_i^{\xi_F\xi_I}\sum_{\mathbf{k},\eta}\left(\frac{\hbar ck}{2\varepsilon_0 V}\right)^{1/2}\Big(\quad & e_{(\mathbf{k},\eta)i}\exp(i\,\mathbf{k}\cdot\mathbf{r}_{\xi})\left\langle Rad_F\left|a_{(\mathbf{k},\eta)}\right|Rad_I\right\rangle \\ & - \overline{e}_{(\mathbf{k},\eta)i}\exp(-i\,\mathbf{k}\cdot\mathbf{r}_{\xi})\left\langle Rad_F\left|a^{\dagger}_{(\mathbf{k},\eta)}\right|Rad_I\right\rangle\Big)\end{aligned} \tag{2a.5}$$

The photon annihilation operator $a_{(\eta,\mathbf{k})}$ and the photon creation operator $a^{\dagger}_{(\eta,\mathbf{k})}$ operate on Fock states of radiation $\left|q,\mathbf{k},\eta\right\rangle$ according to standard quantum algebra rules:

$$a_{(\eta,\mathbf{k})}\left|q,\mathbf{k},\eta\right\rangle = q^{1/2}\left|(q-1),\mathbf{k},\eta\right\rangle \tag{2a.6}$$

$$a^{\dagger}_{(\eta,\mathbf{k})}\left|q,\mathbf{k},\eta\right\rangle = (q+1)^{1/2}\left|(q+1),\mathbf{k},\eta\right\rangle \tag{2a.7}$$

The letter q here represents the mode occupation number of a plane-wave Fock state – loosely, this is the number of photons within the system volume V that have polarization state η and wavevector $\mathbf{k}$. If a different set of electromagnetic modes is used to describe the system's radiation, the Fock states would be defined differently – there would be an alternative annihilation operator a and creation operator $a^{\dagger}$ for this set of modes, and they would change the Fock numbers for the relevant states according to equations (2a.6) and (2a.7).

A logical consequence of these algebra rules is that the two Dirac bracket terms of equation (2a.5) are both always zero, unless one of the two following possibilities hold true:

- Photon creation – the number of photons in the (**k**, η) mode **increases** by one in the course of the interaction:

$$\begin{aligned} &\left|Rad_F\right\rangle = \left|Rad_I + 1_{(\mathbf{k},\eta)}\right\rangle \\ &\therefore \left\langle F\left|H_{\text{int}}\right|I\right\rangle = +i\mu_i^{\xi_F\xi_I}\sum_{\mathbf{k},\eta}\left(\frac{\hbar ck}{2\varepsilon_0 V}\right)^{1/2}\bar{e}_{(\mathbf{k},\eta)i}\exp(-i\,\mathbf{k}\cdot\mathbf{r}_\xi) \end{aligned} \tag{2a.8}$$

- Photon annihilation – the number of photons in the (**k**, η) mode **decreases** by one in the course of the interaction:

$$\begin{aligned} &\left|Rad_F\right\rangle = \left|Rad_I - 1_{(\mathbf{k},\eta)}\right\rangle \\ &\therefore \left\langle F\left|H_{\text{int}}\right|I\right\rangle = -i\mu_i^{\xi_F\xi_I}\sum_{\mathbf{k},\eta}\left(\frac{\hbar ck}{2\varepsilon_0 V}\right)^{1/2}e_{(\mathbf{k},\eta)i}\exp(i\,\mathbf{k}\cdot\mathbf{r}_\xi) \end{aligned} \tag{2a.9}$$

This is, indirectly, a proof of the postulate that fields and molecules only interact via the creation or annihilation of a single photon at the molecule.

4. Quantum amplitude and process rate

In quantum mechanics, a system's state transition is a wavefunction-collapse from one state to another, due to some perturbation. We cannot mechanistically predict such microscopic events, merely the probabilities of them occurring. So instead of deriving precise predictions of transition times we must settle for calculations of the average rate of transition occurrence.

For the F←I transition, the crucial variable is the quantum amplitude M_{FI}. Most generally, this is the Hamiltonian matrix element of the perturbation transforming I into F, expressible as a Dirac bracket:

$$M_{FI} = \left\langle F\left|H'\right|I\right\rangle \tag{2a.10}$$

The operator H' is a perturbation Hamiltonian, describing the total energy exchanged in the transition. For transitions involving a single microscopic interaction, the role of this H' can be taken by the molecular interaction Hamiltonian H_{int} described in the previous section. So for a single-event process, equation (2a.8) or (2a.9) gives the process quantum amplitude M_{FI}.

"Fermi's golden rule" (actually Dirac's rule, called "golden" by Fermi) is the basis of any calculation of the rate of a system's discrete state transition. This

probabilistic rate, Γ_{FI}, is the probability of the F←I transition's occurrence per unit time. It may be interpreted as the mean lifetime of the state I, or as the expected average abundance of the state F as a function of time. If the system's destination F is a continuum of possibilities with density-of-states ρ_F , the Fermi rule is stated as:

$$\Gamma_{FI} = 2\pi\hbar^{-1}\rho_F \left|M_{FI}\right|^2 \qquad (2a.11)$$

This square-modulus function is a form of the Born rule, relating observation-probability to the Dirac brackets of state-overlap. The applicability of the Fermi rule to a particular transition rests on how accurately a single constant value for ρ_F describes the nature of the system's state *F*.

A quantum amplitude M_{FI} is a complex quantity, with units of energy because H' is an energy operator. Like a wavefunction, it is an abstract mathematical object that only indirectly describes the observable properties of the transition. The square-modulus has a real physical interpretation via the Born rule, but the complex argument does not. However, the complex argument does have important effects on quantum interference, described below.

5. Multi-component quantum amplitudes

Quantum amplitudes *M* obey a version of the superposition principle – the "true" M_{FI} is the total of a (linear, unweighted) sum of all possible amplitudes that connect the same states *F* and *I*. All physical mechanisms, involving all combinations of any number of feasible perturbations, contribute to the sum as terms in M_{FI}. This principle has been poetically described as "everything that can happen does happen",[16] and forms the basis for path-integral calculations in pure QED.[4] The magnitude of each individual component M_{FI} is a measure of that particular mechanism's efficiency as a method for executing the F←I transition.

The Fermi rule's square-modulus dependence on the *total* amplitude creates quantum interference in the transition rate of processes with multiple M_{FI} components. When there are *n* distinct amplitude components, the Fermi rate consists of *n* squared-amplitudes plus *n*(*n*-1)/2 cross-terms of interference between pairs. For example, with *n*=3:

$$\begin{aligned}\Gamma_{FI} &= 2\pi\hbar^{-1}\rho_F \left|M_{FI}^A + M_{FI}^B + M_{FI}^C\right|^2 \\ &= 2\pi\hbar^{-1}\rho_F \Big\{ \left|M_{FI}^A\right|^2 \\ &\qquad + 2\,\mathrm{Re}\left(M_{FI}^A \bar{M}_{FI}^B\right) + \left|M_{FI}^B\right|^2 \\ &\qquad + 2\,\mathrm{Re}\left(M_{FI}^A \bar{M}_{FI}^C\right) + 2\,\mathrm{Re}\left(M_{FI}^B \bar{M}_{FI}^C\right) + \left|M_{FI}^C\right|^2 \Big\}\end{aligned} \tag{2a.12}$$

An overbar denotes complex conjugation. The sign and magnitude of the cross-terms depend on the complex arguments of the two quantum amplitudes that interfere. This means that including additional transition mechanisms does not necessarily simply add to the rate – quantum interference may be constructive or destructive.

In equation (2a.10), identifying H' with H_{int} follows from first-order perturbation theory: The physical interaction of photon and molecule, described by H_{int}, is the perturbation that transforms $|I\rangle$ into $|F\rangle$. For example, in figure 2a.1, the pre-interaction system labelled "Before" is $|I\rangle$, the resulting state labelled "After" is $|F\rangle$, and the interaction event (molecular relaxation plus photon creation) defines the transition. But when the transition F←I requires more than one distinct interaction event, the state I is followed by intermediate eras (R, S, T, etc.) before the system evolves to F. Each microscopic transition from one state to another is then a separate perturbation H_{int}, so a *K*-interaction process must be described by K^{th}-order perturbation theory. This means that in general, the quantum amplitude M_{FI} is given by the K^{th} term of a perturbative expansion:[10,17]

$$M_{FI} = \langle F|H_{\text{int}}|I\rangle + \sum_R \frac{\langle F|H_{\text{int}}|R\rangle\langle R|H_{\text{int}}|I\rangle}{E_I - E_R} + \sum_{R,S} \frac{\langle F|H_{\text{int}}|S\rangle\langle S|H_{\text{int}}|R\rangle\langle R|H_{\text{int}}|I\rangle}{(E_I - E_R)(E_I - E_S)} + \ldots \tag{2a.13}$$

This expansion is another sum over various *M*s for different mechanisms, since in principle a process F←I may proceed via a varying number of interactions. But practically, if a process requires a minimum of *K* interactions, then the first K–1 terms of the expansion shall vanish and the K^{th} term shall be the most significant by far.

For processes entailing more than one interaction event, the initial state I is abolished by the first event to occur, and the final state F is ushered in by the last one to occur. During the time between these two events, the system is in intermediate states (labelled R, S, T, etc.). The summation over all possible

mechanisms, as in equation (2a.12), necessarily includes a sum over all possible intermediate states that the system may occupy in the course of each transition pathway. This is indicated by the big sigma operator summing over R, S, T in the terms of the perturbative expansion (2a.13). Importantly, the derivation of this expansion specifically excludes the states I and F from the set of R, and from the set of S, etc.[18]

Without any observation of the system during these intermediate eras, all possibilities for the molecular state must be included – all of the molecule's realisable stationary states, and in principle also countless "virtual" states with a total energy value that is not in the set of proper eigenfunctions. The full sum-over-states may be infinite, but the quantum amplitudes involving the stationary states will usually be the leading significant terms.

The sum must even include intermediate states that violate the requirement of total energy conservation at each event. The strict law of energy conservation applies to the states I and F, so any energy imbalance will last only as long as the intermediate states. If the intermediate eras are of short duration (compared to Planck's constant $\hbar$ divided by the magnitude of the energy imbalance) then fleeting non-conservation is permitted. This is in accordance with the time-energy uncertainty principle – the total energy content of the system in state R has uncertainty inversely proportional to the lifetime of R, whereas I and F are of unbounded duration and thus certain energy. The denominators of equation (2a.13) indicate that the magnitude of each energy imbalance is inversely proportional to that mechanism's quantum amplitude contribution.

This argument for temporary non-conservation of energy also applies to other conservative quantities: the states I and F have well-defined values for the linear momentum and angular momentum of each molecule, yet unobserved intermediate states are not required to maintain these properties. These unseen imbalances do not cause any overall change to the position or orientation of molecules undergoing multi-interaction processes, as any such change would constitute an observation of the reality of certain intermediate states R.

6. Damping and resonance

In the minimal description of each photonic process, the system states I and F are taken to be of infinite duration – giving them a finite lifetime would be to include additional state transitions before or after the process. This infinite duration requires that all mechanisms for the decay of these states are neglected. This is reasonable when I or F involve the molecules' ground states, which should be perfectly stable. But the intermediate states R, S, T are short-lived, so it is necessary to include some description of their decay tendencies.

When each photonic process is described as a minimum number of photons being exchanged between chromophores, this deliberately ignores many other possible interactions. A complete description of a system's behaviour must also include each molecule exchanging rotational and/or kinetic energy with its neighbours. In the condensed phase, these neighbours are disordered solvent molecules, so the system is coupled to a thermal bath with a huge number of degrees of freedom. Any energy transferred into the thermal bath is unlikely to ever return coherently to the system. This coupling manifests as a tendency of the molecular states to decay via irreversible thermal dissipation.[19]

In a density matrix formalism, the evolution of such an open quantum system (weak coupling to a stochastic bath) is described by a master equation in Lindblad form:[20]

$$\frac{d}{dt}\rho = \frac{-i}{\hbar}[H,\rho] + \sum \gamma \left(L\rho L^{\dagger} - L^{\dagger}L\rho/2 - \rho L^{\dagger}L/2 \right) \qquad \text{(2a.14)}$$

The first term is the standard Liouville-von Neumann equation for the evolution of a closed quantum system with density matrix ρ, equivalent to the Schrödinger equation. The effects of dissipative coupling with the environment are described by the Lindbladian terms with a set of decay constants γ. The Lindblad operators L represent the open system's contribution to the system-bath interactions.[21,22]

The variable γ_r is the decay constant of molecular state *r* due to thermal dissipation – in the language of harmonic oscillators, this is the *damping* experienced by that state. A stable ground state immune from decay has no damping, so $\gamma_0 = 0$.

According to equation (2a.13), the quantum amplitude for any multi-interaction process is a function of the differences in total system energy between state I and each intermediate state R, S, T. For each energy difference factor, separating out the molecule and radiation energies yields

$$\left(E_I - E_R\right) = E_0 + E_I^{\text{Rad}} - E_r - E_R^{\text{Rad}} = E_{0r} \pm \hbar ck \tag{2a.15}$$

where E_{0r} is the difference in molecular energy (between state 0 in era I and state r in era R) and k is the wavenumber of the interacting photon in the R←I transition. Energy $\hbar ck$ is added or subtracted from the system depending on whether the photon is being created or annihilated.

Within the QED formalism of this chapter, the decay tendency of each intermediate molecular state *r, s, t* enters the description of multi-interaction processes via a damping modification to these energy difference factors:

$$\left(E_I - E_R\right) = E_{0r} \pm \hbar ck + i\hbar c\gamma_r \tag{2a.16}$$

The imaginary damping term is not derived directly from the perturbative expansion (2a.13). The form of this modification is a phenomenological expediency, intended to encapsulate dynamics of the system beyond the minimal photon-molecule interactions, without explicitly including the many additional system-bath interactions.[23–25]

Technically, the appearance of an imaginary part in the energy difference $\left(E_I - E_R\right)$ may be interpreted as non-Hermiticity of the R←I interaction Hamiltonian operator, H_{int}. This breaks time-symmetry for the R←I transition, and this time-asymmetry represents the irreversibility of the decay process (tending toward thermal equilibrium). Under Noether's theorem, any time-asymmetry is equivalent to the system failing to satisfy overall conservation of energy. Therefore, energy exchanges with the thermal bath have been incorporated into the QED system model in the form of energy discrepancies at each state transition. (This is distinct from the explicit non-conservation described in the previous section.)

Apart from the need to include thermal dissipation effects into the QED analysis for completeness, damping becomes a very important contribution to system behaviour under certain conditions. For choice molecular states *r*, it is possible

that the energy contribution of the interacting photon is equal to the molecular transition, a condition of *resonance*:

$$\pm\hbar ck = E_{0r} \tag{2a.17}$$

With no damping, this means the molecule-radiation interaction is perfectly energy-conservative at the R←I transition, and hence $E_I = E_R$. At resonance, the unmodified perturbative equation (2a.13) predicts an *unbounded* rate of transition. But in fact, the rates of real second-order transitions are observed to vary with radiation frequency such that there is a well-behaved maximum at resonance. The addition of imaginary damping to the energy-differences results in the predicted rate having a Lorentzian spectrum in *k* near resonance:[26,27]

$$\Gamma \propto \frac{1}{\left(E_{0r} \pm \hbar ck\right)^2 + \left(\hbar c\gamma_r\right)^2} \tag{2a.18}$$

At exact resonance, $E_{0r} \pm \hbar ck = 0$, the damping term entirely dominates the energy denominator, and so the *peak* transition rate has an inverse-square proportionality to the damping, $\Gamma \propto \gamma_r^{-2}$. This makes the damping magnitude an indirectly measurable quantity.

7. Time-ordering

A process consisting of *K* distinct interaction events may proceed with those events occurring in any order. Each of the *K!* time-orderings involves the system transitioning through a unique sequence of (*K*-1) intermediate states R, S, T, etc. When the perturbative expansion sums over all possible intermediate states, this includes a summation over all of the *K!* time-orderings.

For example, consider a process of resonance energy transfer from a donor molecule to an acceptor molecule, the focus of chapter 3. There are two Feynman diagrams for this, showing a transfer of electronic excitation from one molecule to another via a photon:

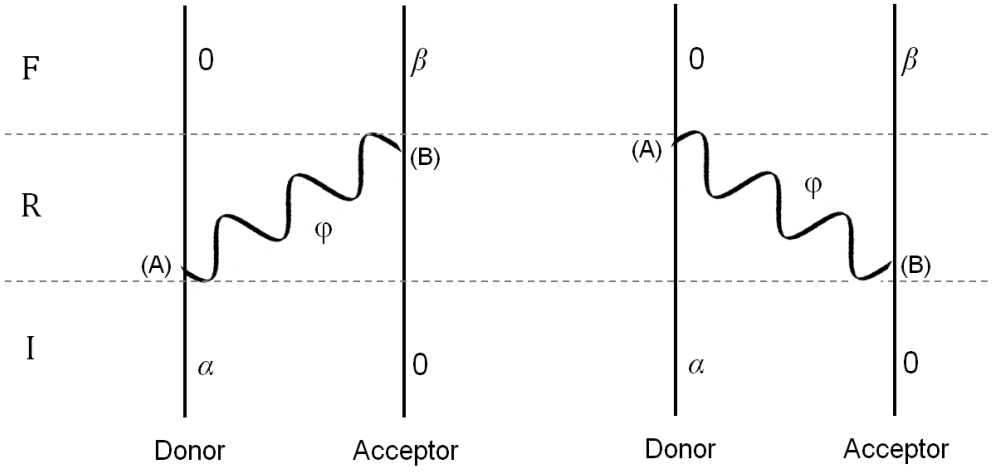

Figure 2a.2: Resonance energy transfer. Left: The Donor molecule interacts with radiation in the event labelled (A), relaxing from excited state α to ground state 0 and creating the photon φ; then the photon annihilates at the Acceptor in the event labelled (B), this interaction exciting it to state β. Right: The Acceptor molecule is excited and creates photon φ in the event labelled (B); then the photon annihilates at the Donor which relaxes in the event labelled (A).

The two events mark transitions in which the molecules and the field change state. These states are only disturbed by the interaction events, and so in describing the entire system, the events (A) and (B) execute the system's transition between overall states I, R, F. It is the non-relativistic approximation which enables us to unambiguously divide the entire system's time history into three discrete eras without worrying about the relativity of simultaneity. The two events punctuate three eras in the system's history, each characterised by an overall system state. See appendix 8a for an alternative representation of this process.

The system's "true" state R is unspecified, due to the era lasting too short a time for any real measurement. The two time-orderings of (A) and (B) each provide equally many possibilities for R. The sum over intermediate states R includes an indefinite integration over the infinite possibilities for wavevector and polarisation of the photon φ, even those that create an energy imbalance. In fact the (B)(A) time-ordering (the right Feynman diagram of figure 2a.2) *always* involves some energy non-conservation, but the (A)(B) time-ordering is only perfectly conservative if the photon energy $\hbar c\varphi$ has exactly the correct value.

Time-ordering falls within the category of unspecified mechanistic information – the total quantum amplitude of a multi-event process is the sum of the amplitudes for each time-ordering. For a *K*-interaction process: the total quantum amplitude must first be decomposed into a sum of *K!* terms, each being the amplitude for the process limited to one time-ordering; then each of those terms must be decomposed into an (infinite) sum, each term of which is the amplitude for the process limited to a specific sequence of intermediate states.

[1] D. P. Craig and T. Thirunamachandran, *Molecular Quantum Electrodynamics*, 2nd ed. (Dover Publications, Mineola, New York, 1998).

[2] A. Salam, "Molecular Quantum Electrodynamics in the Heisenberg Picture: A Field Theoretic Viewpoint": *Int. Rev. Phys. Chem.* **27**, 405 (2008).

[3] Akbar Salam, *Molecular Quantum Electrodynamics: Long-Range Intermolecular Interactions* (Wiley, Hoboken, NJ, 2010).

[4] R.P. Feynman and A.R. Hibbs, *Quantum Mechanics and Path Integrals: Emended Edition* (Dover Publications, Incorporated, 2012).

[5] R.D. Jenkins, D.L. Andrews, and L.C.D. Romero, "A New Diagrammatic Methodology for Non-Relativistic Quantum Electrodynamics": *J. Phys. B At. Mol. Opt. Phys.* **35**, 445 (2002).

[6] Weisstein, Eric W, "Hasse Diagram": *MathWorld - Wolfram Web Resour.* (n.d.).

[7] D.L. Andrews and J.S. Ford, "Resonance Energy Transfer: Influence of Neighboring Matter Absorbing in the Wavelength Region of the Acceptor": *J. Chem. Phys.* **139**, (2013).

[8] Daniels, Gareth J. and Andrews, David L., "The Electronic Influence of a Third Body on Resonance Energy Transfer (Corrected Article)": *J. Chem. Phys.* **117**, 6882 (2002).

[9] G. Grynberg, A. Aspect, and C. Fabre, *Introduction to Quantum Optics: From the Semi-Classical Approach to Quantized Light* (Cambridge University Press, Cambridge, 2010).

[10] William H. Louisell, *Quantum Statistical Properties of Radiation*, Wiley Classics Library Edition 1990 (John Wiley & Sons, New York, 1973).

[11] E.A. Power and T. Thirunamachandran, "On the Nature of the Hamiltonian for the Interaction of Radiation with Atoms and Molecules: (e/mc)p.A, −μ.E, and All That": *Am. J. Phys.* **46**, 370 (1978).

[12] P.W. Atkins and R.G. Woolley, "The Interaction of Molecular Multipoles with the Electromagnetic Field in the Canonical Formulation of Non-Covariant Quantum Electrodynamics": *Proc. R. Soc. Lond. Math. Phys. Eng. Sci.* **319**, 549 (1970).

[13] M. Babiker, E.A. Power, and T. Thirunamachandran, "On a Generalization of the Power-Zienau-Woolley Transformation in Quantum Electrodynamics and Atomic Field Equations": *Proc. R. Soc. Lond. Math. Phys. Eng. Sci.* **338**, 235 (1974).

[14] R.G. Woolley, "Molecular Quantum Electrodynamics": *Proc. R. Soc. Lond. Math. Phys. Eng. Sci.* **321**, 557 (1971).

[15] R.G. Woolley, "Gauge Invariance and Multipole Moments": *Adv. Quantum Chem.* **Volume 32**, 167 (1998).

[16] B. Cox and J. Forshaw, *The Quantum Universe* (Allen Lane, London, 2011).

[17] A. Salam, "Quantum Electrodynamics Effects in Atoms and Molecules": *Wiley Interdiscip. Rev. Comput. Mol. Sci.* **5**, 178 (2015).

[18] E.A. Power, *Introductory Quantum Electrodynamics* (American Elsevier Publishing Company, 1965).

[19] C. Cohen-Tannoudji, J. Dupont-Roc, and G. Grynberg, *Atom-Photon Interactions, Basic Processes and Applications* (Wiley, New York, 1992).

[20] Stephen L. Adler, "Derivation of the Lindblad Generator Structure by Use of the Itô Stochastic Calculus": *Phys Lett A* **265**, 58 (2000).

[21] Crispin W. Gardiner and Peter Zoller, *Quantum Noise*, 3rd ed. (Springer, Berlin, 2004).

[22] D. F. Walls and G. J. Milburn, *Quantum Optics*, 2nd ed. (Springer, Berlin, 2008).

[23] D. L. Andrews, S. Naguleswaran, and G. E. Stedman, "Phenomenological Damping of Nonlinear-Optical Response Tensors": *Phys Rev A* **57**, 4925 (1998).

[24] D. L. Andrews, L. C. Dávila-Romero, and G. E. Stedman, "Polarizability and the Resonance Scattering of Light: Damping Sign Issues": *Phys Rev A* **67**, 55801 (2003).

[25] R. Chang, P.T. Leung, and D.P. Tsai, "Effects of Gain Medium on the Plasmonic Enhancement of Forster Resonance Energy Transfer in the Vicinity of a Metallic Particle or Cavity": *Opt. Express* **22**, 27451 (2014).

[26] P. R. Berman, R. W. Boyd, and P. W. Milonni, "Polarizability and the Optical Theorem for a Two-Level Atom with Radiative Broadening": *Phys Rev A* **74,** (2006).

[27] P. W. Milonni, R. Loudon, P. R. Berman, and S. M. Barnett, "Linear Polarizabilities of Two- and Three-Level Atoms": *Phys Rev A* **77,** 43835 (2008).

–

Chapter 2: **MQED calculation framework**

2b: **Rotational average of molecular response tensors**

1. Introduction

In each of the following chapters, MQED methods are employed to calculate the rate of a certain photonic process as a function of the orientation of the chromophores. If the orientation is static and known, the MQED results may be used to directly predict the observable process rate.

This chapter describes a method for integrating the MQED rate result (for a static chromophore) over the three Euler angles of chromophore orientation, delivering a rotational average of the process rate. Chevron brackets $\langle\ \rangle$ denote that this operation has been applied to a quantity: If rate Γ is a function of orientation, then $\langle\Gamma\rangle$ is the average value of Γ for the whole orientation-space formed by the three Euler angles.

This average is the correct observable rate for photonic processes in which a stochastically-oriented molecule interacts with fields that are fixed in the laboratory frame: Interactions of an arbitrarily-oriented molecule with virtual photons that couple with fixed chromophores (chapter 3a); laboratory-fixed light beams interacting with a freely-rotating chromophore such as a molecule in liquid solution (chapters 5 and 6); etc.

Even if the unfixed chromophore is not rapidly rotating but is static in a randomly-determined orientation relative to the fixed fields, the result of Euler angle integration is an ensemble average over many systems, which undergo the photonic process with different values for that orientation.

2. Reference frames

As implied by the scalar products in equation (2a.2), every interaction rate term is proportional to a scalar product of field vectors and a molecular response tensor. Using the Einstein convention of implied summation over repeated indices *i*:

$$\Gamma \propto \left[\text{fields}\right]_{i123\ldots iN} T_{i123\ldots iN} \tag{2b.1}$$

To calculate this scalar product, the field vectors and the molecular response tensor must both be expressed in terms of Cartesian components with respect to a common reference frame.

The radiation is fixed in the laboratory frame, meaning that its polarization vectors $\boldsymbol{e}$ (or the coupling tensor **V** that describes virtual radiation) have invariant Cartesian components in the laboratory-fixed basis set $\{x,y,z\}$. Laboratory-fixed tensor components are indicated with Roman indices: $i,j,k,l\ldots$ or $i1,i2,i3\ldots$

A molecule's response tensor is determined by the intrinsic electronic geometry of the internal structure, and rotates with the molecule, so the laboratory-frame Cartesian components vary with the Euler angles of orientation. The tensor components in a molecule-fixed reference frame, with unit vectors $\{x',y',z'\}$, are invariant, so this is the natural frame for expressing these quantities. The orthogonal set $\{x',y',z'\}$ would typically be defined by molecular symmetry elements such as a principal rotation axis. Molecule-fixed tensor components are indicated with Greek indices: $\lambda,\gamma,\epsilon,\zeta\ldots$ or $\lambda 1, \lambda 2, \lambda 3\ldots$

The laboratory-fixed tensor components $T_{i123\ldots iN}$ will vary as the molecule rotates, but the molecule-fixed components $T_{\lambda 123\ldots\lambda N}$ are invariant quantities intrinsic to the molecule's physical composition. It is therefore necessary to evaluate each laboratory-fixed component as a function of the natural components and a product of cosines relating the unit vectors of the two reference frames.

$$T_{i123\ldots iN} = T_{\lambda 123\ldots\lambda N}\ \ l_{i1\lambda 1}\ l_{i2\lambda 2}\ l_{i3\lambda 3}\cdots l_{iN\lambda N} \tag{2b.2}$$

The dimensionless scalar $l_{i1\lambda 1}$ is the cosine of the angle between the (laboratory-fixed) unit vector with hanging index $i1$ and the (molecule-fixed) unit vector with hanging index $\lambda 1$. The factor consisting of N cosines is a double-tensor (a tensor with components in both frames) which describes the relationship between the two frames, as determined by the Euler angles. The rotationally-averaged double-tensor is conventionally labelled $I^{(N)}$.

$$I^{(N)} \equiv \left\langle l_{i1\lambda 1} l_{i2\lambda 2} l_{i3\lambda 3}\cdots l_{iN\lambda N}\right\rangle \tag{2b.3}$$

The double-tensor is the only factor in rate equation (2b.1) influenced by the molecule's orientation. Crucially, this means that a rotational average of this factor accomplishes the averaging of the process rate.

$$\langle \Gamma \rangle \propto \left[\text{fields}\right]_{i123\ldots iN} T_{\lambda 123\ldots \lambda N} I^{(N)} \tag{2b.4}$$

Apart from a brief discussion of N=1 and N=3 averages in chapter 3a, and a borrowed N=7 result in chapter 6, this thesis only contains explicit evaluations of rotational averages with even N values, up to 8.

3. The Thirunamachandran method

The rotational-average of the double-tensor is calculated according to a standard method:[1–3]

$$I^{(N)} = f_r^{(N)} m_{rs}^{(N)} g_s^{(N)} \tag{2b.5}$$

With even N values, each $f_r^{(N)}$ is a tensor consisting of a product of $N/2$ Kronecker deltas, cast in the laboratory-fixed coordinates i such that each $f_r^{(N)}$ index-contracts with the field vectors. Each possible value of the index r produces a $f_r^{(N)}$ with a distinct permutation of the N indices. The set of possible r values has cardinality that depends on N:

$$r \in \left\{1, 2, 3, \cdots |r|\right\} \tag{2b.6}$$

$$|r| = \frac{(N-1)!}{\prod_{x=1}^{N/2-1}(2x)} = 1\times 3\times 5\times \cdots (N-1) \tag{2b.7}$$

The elementary case is N=2, which yields the single tensor $f_1^{(2)} = \delta_{i12}$, specifying a dot product of the field vector that has hanging index $i1$ and the field vector that has hanging index $i2$. An average with N=4 yields three pair-of-delta tensors $f_r^{(4)}$:

$$\begin{aligned} f_1^{(4)} &= \delta_{i12}\delta_{i34} \\ f_2^{(4)} &= \delta_{i13}\delta_{i24} \\ f_3^{(4)} &= \delta_{i14}\delta_{i23} \end{aligned} \tag{2b.8}$$

An average with *N*=6 yields fifteen triple-delta tensors $f_r^{(6)}$, following the pattern of specifying all unique *i*-index pairings. An average with *N*=8 yields 105 quad-delta tensors $f_r^{(8)}$.[4] These results are provided in Appendix 8b.

The tensors $g_s^{(N)}$ are identical in form to $f_r^{(N)}$, but the Kronecker deltas are cast in terms of the molecule-fixed coordinates λ such that each $g_s^{(N)}$ index-contracts with the molecular response tensor.

The elements $m_{rs}^{(N)}$ are defined by the following matrix-inversion relation, inferred from equations (A2.13) and (A2.10) of ref.[1]:

$$m^{(N)} = \mathbf{S}^{-1} \tag{2b.9}$$

$$S_{rs} = f_r^{(N)} \cdot f_s^{(N)} \tag{2b.10}$$

The matrix **S** consists of Kronecker delta inner-products, so equation (2b.10) always produces a single-valued dimensionless scalar, a real number. For example, in the *N*=6 case, the top-right corner element of **S** is:

$$S_{1;15} = f_1^{(6)} \cdot f_{15}^{(6)} = \delta_{ij}\delta_{kl}\delta_{mn}\delta_{in}\delta_{jm}\delta_{kl} = 9 \tag{2b.11}$$

The matrix-inverse of **S** is then calculated, yielding the $m^{(N)}$ matrix. Therefore, the elements $m_{rs}^{(N)}$ are likewise real numbers.[5,6] Appendix 8b reports the results of all $m_{rs}^{(N)}$ for even values of *N* up to 8. Notably, the $m^{(N)}$ matrices obey the formula $\sum_{r,s} m_{rs}^{(N)} = (N+1)^{-1}$.[4]

Each rotationally-averaged rate term is thus expressible as a multiple index-contraction, with implied summation over all *N* laboratory-fixed indices *i* in the set{*x*,*y*,*z*}, over all *N* molecule-fixed indices λ in the set {*x'*,*y'*,*z'*}, over *r* in the set defined by equation (2b.6), and over *s* in the same set.

$$\begin{aligned} \langle \Gamma \rangle &\propto \left[\text{fields}\right]_{i123\ldots iN} T_{\lambda 123\ldots \lambda N}\, I^{(N)} \\ &\propto \left[\text{fields}\right]_{i123\ldots iN} f^{(N)}_{r;\, i123\ldots iN}\, m^{(N)}_{rs}\, g^{(N)}_{s;\, \lambda 123\ldots \lambda N}\, T_{\lambda 123\ldots \lambda N} \end{aligned} \tag{2b.12}$$

4. Degeneracy and natural invariants

It may be that the laboratory-fixed field "tensor", labelled [fields], contains vectors that are indistinguishable. Situations like this are especially likely in rate terms that are derived from the square modulus of a single quantum amplitude for an E1 interaction – each field vector **e** must appear alongside its complex conjugate, which is equal if there is no imaginary part. An arbitrary fourth-rank example would be:

$$\left[\text{fields}\right]_{i1234} = e_{i1}\, e_{i2}\, b_{i3}\, k_{i4} \tag{2b.13}$$

Here, the two vectors **e** are identical, so the tensor labelled [fields] has $i1 \leftrightarrow i2$ index-symmetry.

The effect of this symmetry on the rotational average evaluation is that several r values may yield identical results for the contraction with $f_r^{(N)}$. Also, in cases where the fields are produced by plane radiation, the vectors **e** have no imaginary part so $(\mathbf{e}\cdot\bar{\mathbf{e}}) = 1$, and this may produce further degeneracy. In this example there is degeneracy between r=2 and r=3:

$$\begin{aligned}
\left[e_{i1}e_{i2}b_{i3}k_{i4}\right] f_1^{(4)} &= (\mathbf{b}\cdot\mathbf{k}) \\
\left[e_{i1}e_{i2}b_{i3}k_{i4}\right] f_2^{(4)} &= (\mathbf{e}\cdot\mathbf{b})(\mathbf{e}\cdot\mathbf{k}) \\
\left[e_{i1}e_{i2}b_{i3}k_{i4}\right] f_3^{(4)} &= (\mathbf{e}\cdot\mathbf{b})(\mathbf{e}\cdot\mathbf{k})
\end{aligned} \tag{2b.14}$$

In evaluating the implied sum over r in equation (2b.10), the set of *unique* values of the contraction $\left[\text{fields}\right]_{i123\ldots iN} f_r^{(N)}$ must be identified, and their coefficients $m_{rs}^{(N)}$ are the sum of elements of $m^{(N)}$ with the corresponding degenerate r values:

$$\sum\nolimits_r \left[e_{i1}e_{i2}b_{i3}k_{i4}\right] f_{r;\,i1234}^{(4)}\, m_{rs}^{(4)} = (\mathbf{b}\cdot\mathbf{k})\, m_{1s}^{(4)} + (\mathbf{e}\cdot\mathbf{b})(\mathbf{e}\cdot\mathbf{k})\left(m_{2s}^{(4)} + m_{3s}^{(4)}\right) \tag{2b.15}$$

In equation (2b.3), the double-tensor consisting of N cosines couples each i-index with the λ-index of the same number. The Latin-Greek symmetry of the double-tensor is reflected in the diagonal symmetry of the $m^{(N)}$ matrices. Any i-index-symmetry in the contraction $\left[\text{fields}\right]_{i123\ldots iN} f_r^{(N)}$ must be reflected by λ-index-symmetry in the contraction $g_s^{(N)} T_{\lambda 123\ldots\lambda N}$, over the same numbers. Even without this induced symmetry, it may be that the molecular response tensor $T_{\lambda 123\ldots\lambda N}$ has intrinsic λ-index-symmetry due to the nature of the molecule's state transition.

The effect of this symmetry on the rotational average evaluation is that several *s* values may yield identical results for the contraction with $g_s^{(N)}$. An arbitrary fourth-rank example would be a *T* tensor with $\lambda 3 \leftrightarrow \lambda 4$ index-symmetry, resulting in degeneracy between *s*=2 and *s*=3:

$$\begin{aligned} T_{\lambda 1234}\, g_1^{(4)} &= T_{\lambda 1122} \\ T_{\lambda 1234}\, g_2^{(4)} &= T_{\lambda 1212} \\ T_{\lambda 1234}\, g_3^{(4)} &= T_{\lambda 1221} = T_{\lambda 1212} \end{aligned} \qquad (2b.16)$$

As in the laboratory-fixed half of the calculation, the implied sum over *s* requires that the set of *unique* values of the contraction $g_s^{(N)} T_{\lambda 123\ldots\lambda N}$ must be identified, and their coefficients $m_{rs}^{(N)}$ are the sum of elements of $m^{(N)}$ with the corresponding degenerate *s* values:

$$\sum\nolimits_s T_{\lambda 1234}\, g_{s;\,\lambda 1234}^{(4)}\, m_{rs}^{(4)} = T_{\lambda 1122}\, m_{r1}^{(4)} + T_{\lambda 1212}\left(m_{r2}^{(4)} + m_{r3}^{(4)}\right) \qquad (2b.17)$$

Each unique $g_s^{(N)} T_{\lambda 123\ldots\lambda N}$ result (in this example, $T_{\lambda 1122}$ and $T_{\lambda 1212}$) is a scalar produced by a limited sum over the $T_{\lambda 123\ldots\lambda N}$ Cartesian components, λ-index contracting along a particular molecule symmetry defined by the structure of $g_s^{(N)}$. These scalars are the "natural invariants" of the molecular response tensor for this electronic state-transition – as a set, they represent different aspects of the molecule's capacity to perform the various forms of charge-redistribution required.

The natural invariants contain information about how the molecule's structure influences its QED interactions. Evaluating a subset of them as equal to zero constitutes a selection rule forbidding a certain kind of transition. It is well known that the selection rules for any interaction may be inferred from analysis of the components of molecular response tensors.[7,8]

See chapter 6 for a worked example of a *N*=8 calculation.

[1] D. P. Craig and T. Thirunamachandran, "Rotational Averaging of Tensors": *Mol. Quantum Electrodyn.*, Dover Paperback (Dover Publications, Mineola, New York, 1998), pp. 310–315.

[2] H. Jeffreys, "On Isotropic Tensors": *Math. Proc. Camb. Philos. Soc.* **73**, 173 (1973).

[3] T. Bancewicz, "Excess Hyperpolarizabilities: The Irreducible Tensor Approach": *J. Math. Chem.* **50**, 1570 (2012).

[4] D.L. Andrews and W.A. Ghoul, "Eighth Rank Isotropic Tensors and Rotational Averages": *J. Phys. Math. Gen.* **14**, 1281 (1981).

[5] D. L. Andrews and T. Thirunamachandran, "On Three-Dimensional Rotational Averages": *J. Chem. Phys.* **67**, 5026 (1977).

[6] W.M. McClain, "Polarization Dependence of Three-Photon Phenomena for Randomly Oriented Molecules": *J. Chem. Phys.* **57**, 2264 (1972).

[7] D.L. Andrews and T. Thirunamachandran, "Hyper−Raman Scattering by Chiral Molecules": *J. Chem. Phys.* **70**, 1027 (1979).

[8] R. Piron, S. Brasselet, D. Josse, J. Zyss, G. Viscardi, and C. Barolo, "Matching Molecular and Optical Multipoles in Photoisomerizable Nonlinear Systems": *J Opt Soc Am B* **22**, 1276 (2005).

–

Chapter 3: **Resonance energy transfer modified by a third chromophore**

3a: **Influence of near-resonant surrounding matter**

1. Introduction

Resonance energy transfer (RET) is well known to occur in natural photosynthesis and its synthetic analogues,[1,2] and energy-harvesting dendrimers and block copolymers likewise depend on efficient transfer of excitation between resonant chromophores.[3–5] A detailed analysis of the advanced quantum features of this familiar process, and the effects unique to multi-chromophore systems, can give insights useful to the design of various novel energy-harvesting materials.[6–9]

This chapter provides an MQED description of RET as a photonic process,[10–13] with focus on the process being modified by interactions with a third chromophore that does not directly compete as an acceptor, such as molecules of the medium. In many true photosynthetic systems involving an RET donor-acceptor pair, there are nearby chromophores who absorb at a wavelength that is just a little shorter than the wavelength-equivalent of the transfer energy.[14] This analysis discovers which specific properties of such nearby near-resonant chromophores will enhance or inhibit the efficiency of RET.[15]

A simple three-chromophore model of modified-RET is constructed as an extension of elementary two-body RET.[16] Familiar MQED methods are then applied to derive equations for the rate of this process in terms of system geometry and the electronic properties of the chromophores. The completely general rate expression is an intricate function of relative positions and orientations,[17] so for ease of calculation the focus is then on providing actionable results for particular limiting cases of simple geometry.

2. Three-body RET

The MQED description of (unmodified) RET entails two molecules/chromophores: the donor, D, and the acceptor, A. The donor loses

energy in the process, and in the simplest case this means that it relaxes from some initial excited state, α, to its ground state, 0. The acceptor is excited by an equal amount, to some excited state of its own, β. These two molecular transitions are coupled by a mediating photon, ϕ, which is created at one of the interaction events and annihilated at the other.

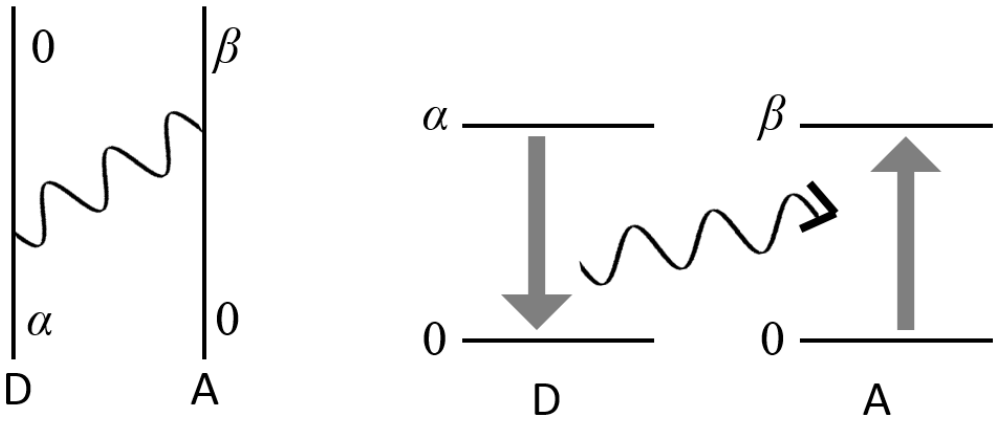

Figure 3a.1: Non-relativistic Feynman diagram (left) and Jablonski-like energy level diagram (right), illustrating two-body RET. See also figure 2a.2.

A process of third-body-modified RET is constructed by the addition of a third chromophore, M, coupled to the RET system by additional virtual photons. The minimal coupling (which will dominate a sum-over-states) is via a single photon, *p*, interacting with M and one of the RET pair. Figure 3a.2 illustrates one possible configuration for this coupling scheme – in this example it is chromophore D that interacts with *p*, connecting the RET system to M.

The four interaction events are distinct, with the individual labels (W), (X), (Y) and (Z). At each event, one of the chromophores (M, D, A) undergoes a transition between states (0, α, *r*, β) and one photon (φ, *p*) is either created or annihilated. The four events may occur in any time-ordering, such that there are 4*!* = 24 possible permutations. There are 23 Feynman diagrams in addition to figure 3a.2 that also describe the same overall process.

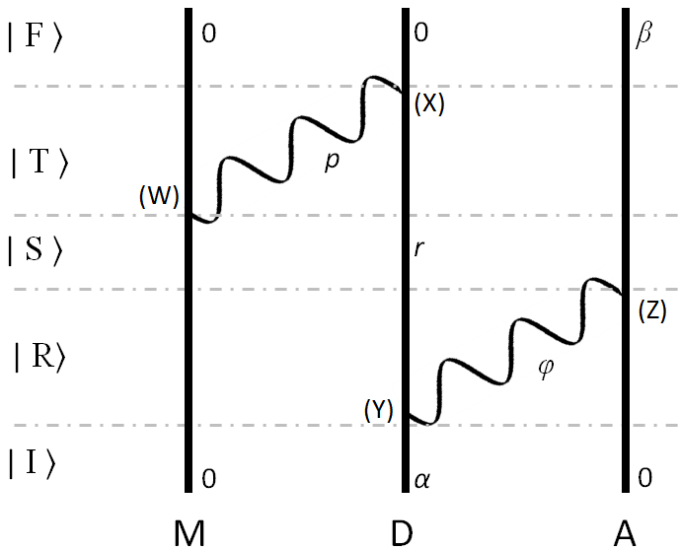

Figure 3a.2: Feynman diagram of third-body-modified RET – specifically, the YZWX time-ordering for the MDA coupling configuration. Event (W) is the interaction of M with photon *p*, considered a *static* interaction as M undergoes no transition and the *permanent* dipole of its state 0 is engaged; (X) is the interaction of D with photon *p*; (Y) is the interaction of D with photon *φ*; and (Z) is the excitation of A. The four events transform the overall system state from the initial $|\,\mathrm{I}\,\rangle$ to the final $|\,\mathrm{F}\,\rangle$ via three intermediate states.

Regardless of the order of the four events, they punctuate five eras in the system's evolution, labelled chronologically I, R, S, T, F. The sum-over-states encompasses all possibilities for the system's states R, S, T. The many components of this sum are decomposed first by coupling configuration, then by time-ordering, then by the possible states of the photons and molecules within each era.

The above photon-connectivity of the system (M coupled to D; D coupled to A) is labelled the "MDA coupling configuration". The shorthand "MDA" serves as a direct illustration of the coupling: M-D, D-A. Without introducing a third photon, it is possible for the exact same modified-RET process to occur via a mechanism with M coupled to A, and D coupled to just one of the others. These are the DAM and DMA configurations.

Intuitively, the coupling configuration should specify the direction of photon propagation, and thus dictate the chromophores' relative positions. But in general the photon wavevectors are *not* strictly limited to the line from their creation position to their annihilation position. The sum-over-states includes a sum over all

orientations for the wavevectors, calculated as an integration over the polar and azimuthal angles (see Appendix 8c) – the possible wavevector orientations that are misaligned from the proper creation-annihilation line give smaller contributions to the total quantum amplitude. Similarly, if the relative positions of the chromophores are such that one of the three coupling configurations is unfavourable, this will simply result in that configuration's quantum amplitude component being smaller.

Ref.[18] previously addressed this problem in terms of the same three coupling configurations. The bottom-up approach pursued here aims at a more detailed treatment of the influences of bulk matter surroundings on the RET process.

3. Derivation for the MDA coupling configuration

Consider interaction event (W), as shown in figure 3a.2. Applying the electric dipole approximation, the interaction of a photon *p* with a molecule M transitioning T←S has the Dirac bracket:

$$\left\langle T\left|H_{\text{int}}^{(W)}\right|S\right\rangle = -i\mu_i^{M_0M_0}\sum_{\mathbf{p},\mathbf{e}_{(\text{p})}}\left(\frac{\hbar cp}{2\varepsilon_0 V}\right)^{1/2}\Big(\quad e_{(\text{p})i}\exp(i\,\mathbf{p}\cdot\mathbf{r}_M)\left\langle Rad_T\left|a_{\text{p}}\right|Rad_S\right\rangle \\ -\bar{e}_{(\text{p})i}\exp(-i\,\mathbf{p}\cdot\mathbf{r}_M)\left\langle Rad_T\left|a_{\text{p}}^{\dagger}\right|Rad_S\right\rangle\Big) \tag{3a.1}$$

This is an applied form of equation (2a.5). The symbols **p** represents the photon's wavevector, and the non-bold version, *p* is the magnitude. The subscript *i* here is a Cartesian index, using the Einstein convention of implied summation over repeated tensor indices: there is a scalar product of the molecule's transition dipole moment vector $\boldsymbol{\mu}^{\text{M}}$ and the radiation mode's polarisation vectors $\mathbf{e}_{(p)}$. Overbars denote complex conjugation. The vector $\mathbf{r}_M$ is the (relative) position of the molecule M where this interaction occurs. The operators a_{p} and $a_{\text{p}}^{\dagger}$ are the photon annihilation and creation operators for the radiation mode **p**. The volume of quantization, *V*, usually represents the average amount of space occupied by one photon, but for a single-photon interaction this is arbitrary.

As explained by equations (2a.5-7), at least one of these two Dirac bracket terms must be zero for any particular pair of occupation numbers for radiation mode **p** in

Rad_S and Rad_T. Therefore there are two possible solutions to equation (3a.1). Either event (W) is a photon **p** creation event (as in figure 3a.2):

$$\left\langle T \left| H_{\text{int}}^{(W)} \right| S \right\rangle = +i\mu_i^{M_0 M_0} \sum_{\mathbf{p},\mathbf{e}_{(\text{p})}} \left(\frac{\hbar c p}{2\varepsilon_0 V} \right)^{1/2} \bar{e}_{(\text{p})i} \exp(-i\mathbf{p}\cdot\mathbf{r}_M) \left\langle Rad_T \left| a_{\text{p}}^{\dagger} \right| Rad_S \right\rangle \quad (3a.2)$$

or event (W) is a photon **p** annihilation event:

$$\left\langle T \left| H_{\text{int}}^{(W)} \right| S \right\rangle = -i\mu_i^{M_0 M_0} \sum_{\mathbf{p},\mathbf{e}_{(\text{p})}} \left(\frac{\hbar c p}{2\varepsilon_0 V} \right)^{1/2} e_{(\text{p})i} \exp(i\mathbf{p}\cdot\mathbf{r}_M) \left\langle Rad_T \left| a_p \right| Rad_S \right\rangle \quad (3a.3)$$

The **p**-creation solution (3a.2) is non-zero only if the occupation number of mode **p** in Rad_T is one greater than that in Rad_S; the **p**-annihilation solution (3a.3) is non-zero only if the occupation number of mode **p** in Rad_T is one less than that in Rad_S. Which of these two solutions applies to any particular Dirac bracket in the quantum amplitude calculation depends on the time-ordering of the four events.

Every time-ordering of the four events necessarily involves one creation and one annihilation event for photon *p*, and one of each for photon *φ*. However, which named event corresponds to each of these phenomena varies between the 24 time-orderings. Events (W) and (X) create and annihilate the photon *p*, but it is whichever occurs first that creates *p* and whichever follows that annihilates *p*. Events (Y) and (Z) have the same relationship with photon *φ*.

For any particular time-ordering, the quantum amplitude of the four-interaction process is the fourth-order term of the perturbative expansion, equation (2a.13):

$$M_{FI} = \sum_{R,S,T} \frac{\left\langle F \left| H_{\text{int}} \right| T \right\rangle \left\langle T \left| H_{\text{int}} \right| S \right\rangle \left\langle S \left| H_{\text{int}} \right| R \right\rangle \left\langle R \left| H_{\text{int}} \right| I \right\rangle}{\left[E_{IT}^{\text{D}} + E_{IT}^{\text{A}} - E_T^{rad} \right] \left[E_{IS}^{\text{D}} + E_{IS}^{\text{A}} - E_S^{rad} \right] \left[E_{IR}^{\text{D}} + E_{IR}^{\text{A}} - E_R^{rad} \right]} \quad (3a.4)$$

$$= \left(\frac{\hbar c}{2\varepsilon_0 V} \right)^2 \sum_{p,e_{(p)},\phi,e_{(\phi)}} \frac{p\phi \;\; \bar{e}_{(p)a} e_{(p)b} \bar{e}_{(\phi)c} e_{(\phi)d} \;\; \mu_i^{M_o M_o} \mu_j^{D_o D_r} \mu_k^{D_r D_\alpha} \mu_l^{A_\beta A_o}}{\left[E_{\alpha T}^{\text{D}} + E_{0T}^{\text{A}} - E_T^{rad} \right] \left[E_{\alpha S}^{\text{D}} + E_{0S}^{\text{A}} - E_S^{rad} \right] \left[E_{\alpha R}^{\text{D}} + E_{0R}^{\text{A}} - E_R^{rad} \right]}$$
$$\times \exp\left(i\mathbf{p}.(\mathbf{r}_{pAnn.} - \mathbf{r}_{pCre.}) + i\boldsymbol{\varphi}.(\mathbf{r}_{\phi Ann.} - \mathbf{r}_{\phi Cre.}) \right)$$

Energy differences for molecule X are written as $E_{AB}^X \equiv E_A^X - E_B^X$, where E_A^X is the total molecular energy of X in state A.

The Cartesian index labels *a, b, c, d* on the polarisation vectors are wildcards representing an unspecified permutation of the indices *i, j, k, l*. Index *a* shall be the same as that on the **μ** creating photon *p*, index *b* shall be the same as that on

the **μ** annihilating photon *p*, index *c* shall be the same as that on the **μ** creating photon *φ*, and index *d* shall be the same as that on the **μ** annihilating photon *φ*. Note that μ_i always describes the event (W) interaction and μ_l always describes the event (Z) interaction, but the correspondence of moments μ_j and μ_k to events (X) and (Y) depends on which comes first in the given time-ordering. And μ_k necessarily comes before μ_j.

The intricate correspondences outlined in the above paragraph – between the objective events (W), (X), (Y), (Z); the creation/annihilation events of photons; photon polarisations bearing the indices *a, b, c, d*; the chromophore transition events with moments μ_i, μ_j, μ_k, μ_l – can be best understood by considering how the Feynman diagram of figure 3a.2 is modified by changing the time-ordering. Also, figure 8a.6 illustrates the molecule and radiation states in all 24 time-orderings.

Equation (3a.4) is constructed to describe *any one* of the 24 event-orderings, since the big sigma entails an implicit summation over all of them. State-specific variables such as $E^{\mathrm{D}}_{\alpha R}$ and E^{rad}_{S} can be straightforwardly evaluated by choosing one time-ordering of the four events and reading the states from the relevant Feynman diagram – e.g. all the E^{Rad} terms will deliver 0, $\hbar cp$, $\hbar c\varphi$, or $\hbar c(p+\varphi)$. The **r** vectors are the relative positions of whichever interaction events create and annihilate the photons *p* and *φ* – e.g. $\mathbf{r}_{pAnn.}$ is the position of the interaction at which photon *p* is annihilated (at M or at D, depending on time-ordering). Similarly, the Cartesian indices on the polarisation vectors **e** depend on the time-ordering. Each is in a scalar product with one of the transition dipole moments **μ** determined by which molecular transition creates or annihilates each photon, so the indices *a, b, c, d* must be understood to represent one of the 24 permutations of *i, j, k, l*.

The general amplitude, including all 24 event-orderings seamlessly, can be found by adding together 24 terms of the form of equation (3a.4). The big sigma's summation over radiation modes **p** and **ϕ** is achieved by taking the limit of infinite *V*, and recasting the sum over modes as triple integrations over **p**-space and over **ϕ**-space. The details of this derivation are included in Appendix 8c.

$$M_{FI} = (2\pi)^{-2}\left(2\varepsilon_0\right)^{-2}\mu_i^{\mathrm{M_o M_o}}\mu_l^{\mathrm{A_\beta A_o}}\sum_{\mathrm{D}_r}\left\{\frac{\mu_j^{\mathrm{D_o D}_r}\mu_k^{\mathrm{D}_r\mathrm{D}_\alpha}}{E^{\mathrm{D}}_{\alpha r}}+\frac{\mu_k^{\mathrm{D_o D}_r}\mu_j^{\mathrm{D}_r\mathrm{D}_\alpha}}{E^{\mathrm{D}}_{\alpha r}-\hbar ck}\right\}$$
$$\times\left(\nabla^2\delta_{ij}-\nabla_i\nabla_j\right)R^{-1}_{\mathrm{MD}}\left(\nabla'^2\delta_{kl}-\nabla'_k\nabla'_l\right)R^{-1}_{\mathrm{DA}}\exp\left(ikR_{\mathrm{DA}}\right) \qquad (3a.5)$$

Nomenclature: $\mathbf{R}_{\mathrm{AB}}\equiv\mathbf{r}_{\mathrm{A}}-\mathbf{r}_{\mathrm{B}}$; $\nabla_j\equiv\dfrac{\partial}{\partial R_{\mathrm{MD}\,j}}$; $\nabla'_l\equiv\dfrac{\partial}{\partial R_{\mathrm{DA}\,l}}$; $k\equiv\dfrac{E^{\mathrm{D}}_{\alpha 0}}{\hbar c}=\dfrac{E^{\mathrm{A}}_{\beta 0}}{\hbar c}$.

This is the whole quantum amplitude for the MDA configuration. The complete result makes no mention of the photon properties **p**, **ϕ**, $\mathbf{e}_{(\mathrm{p})}$, or $\mathbf{e}_{(\phi)}$, because all possible values have now been included in the sum-over-states. This is in keeping with the photons being considered virtual.

In this MDA coupling configuration, the D chromophore undergoes a two-interaction transition via some intermediate state *r*, and the above result includes a sum over every possible D_r as the last remaining component of the general sum-over-states. The general damped polarisability tensor, as given below for molecule X transitioning f←0, is capable of describing any such two-interaction transition. See equation 5.2.7 of ref.[19]. The arguments *-k'* and *k* are the wavenumbers of the two interacting photons – a positive sign signifies a photon created at molecule X; negative sign indicates annihilation at X. The wavenumber γ_r^X represents damping imposed on molecular state X_r (see section 6 of chapter 2a).

$$\alpha_{ij}^{\mathrm{X}_f\mathrm{X}_0}\left(-k';k\right)=-\sum_{X_r}\left[\frac{\mu_i^{\mathrm{X}_f\mathrm{X}_r}\mu_j^{\mathrm{X}_r\mathrm{X}_0}}{E^X_{r0}-\hbar c\,k-i\hbar c\,\gamma_r^X}+\frac{\mu_j^{\mathrm{X}_f\mathrm{X}_r}\mu_i^{\mathrm{X}_r\mathrm{X}_0}}{E^X_{r0}+\hbar c\,k'\pm i\hbar c\,\gamma_r^X}\right] \qquad (3a.6)$$

In this nomenclature, the big sigma in Equation (3a.5) is now expressible as the relevant transition polarisability, $\alpha_{jk}^{\mathrm{D}_0\mathrm{D}_\alpha}(-k;0)$.

Likewise, the second line of Equation (3a.5) is precisely expressible in terms of the rank-two electrodynamical coupling tensor which is ubiquitous in two-body RET work.[12] Cartesian cosines are denoted $\hat{R}_j\equiv R_j/R$.

$$V_{ij}\left(k;\mathbf{R}\right)\equiv\left(4\pi\varepsilon_0\right)^{-1}R^{-3}\exp\left(ikR\right)$$
$$\times\left[\left(\delta_{ij}-3\hat{R}_i\hat{R}_j\right)-ikR\left(\delta_{ij}-3\hat{R}_i\hat{R}_j\right)-k^2R^2\left(\delta_{ij}-\hat{R}_i\hat{R}_j\right)\right] \qquad (3a.7)$$
$$=\left(4\pi\varepsilon_0\right)^{-1}R^{-1}\exp\left(ikR\right)\left[\nabla^2\delta_{ij}-\nabla_i\nabla_j\right]$$

Equation (3a.5) is thus concisely expressed as a product involving just five tensors:

$$M_{\mathrm{MDA}} = \mu_i^{\mathrm{M}_o\mathrm{M}_o}\; V_{ij}\left(0;\mathbf{R}_{\mathrm{MD}}\right)\; \alpha_{jk}^{\mathrm{D}_o\mathrm{D}_\alpha}(-k;0)\; V_{kl}\left(k;\mathbf{R}_{\mathrm{DA}}\right)\; \mu_l^{\mathrm{A}_\beta\mathrm{A}_o} \tag{3a.8}$$

The arguments of the coupling tensor $V_{kl}\left(k;\mathbf{R}_{\mathrm{DA}}\right)$ indicate that it describes the transfer of energy $\hbar ck$ over the distance $\mathbf{R}_{\mathrm{DA}}$ via a virtual photon – this is the RET coupling. The coupling tensor $V_{ij}\left(0;\mathbf{R}_{\mathrm{MD}}\right)$ connects the third body M to chromophore D, but zero energy is exchanged – this is *static* coupling between the permanent dipole of M and the transition polarisability of D, as illustrated by the creation and annihilation of photon *p* in figure 3a.2. A semiclassical interpretation would describe the latter coupling as the permanent dipole of M inducing a perturbation in the transition dipole moment of D's relaxation.

4. Other coupling configurations

The five factors of Equation (3a.8) each correspond a coupling phenomenon as illustrated by the Feynman diagram for the MDA energy transfer process (Figure 3a.2). Figure 3a.3 makes this correspondence explicit:

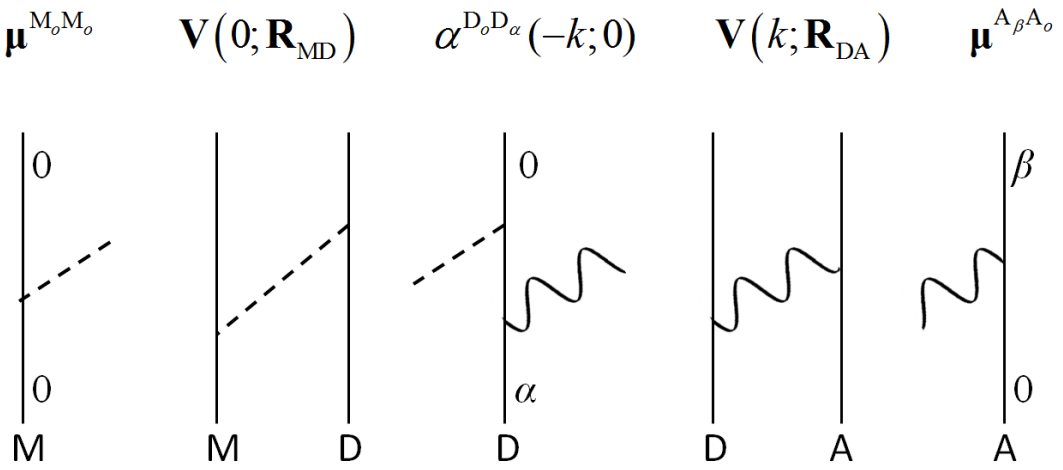

Figure 3a.3: The five factors of M_{MDA} each correspond to a coupling component of figure 3a.2, as they each describe one aspect of the electrodynamics of the process.

With this correspondence in mind, the Feynman diagrams for the DAM and DMA configurations enable a straightforward derivation of quantum amplitude formulae by substitution of variables. The DAM amplitude is constructed by direct analogy from Equation (3a.8):

$$M_{\mathrm{DAM}} = \mu_i^{\mathrm{D_o D_\alpha}}\ V_{ij}\left(k;\mathbf{R}_{\mathrm{DA}}\right)\ \alpha_{jk}^{\mathrm{A_\beta A_o}}(0;k)\ V_{kl}\left(0;\mathbf{R}_{\mathrm{AM}}\right)\ \mu_l^{\mathrm{M_o M_o}} \tag{3a.9}$$

The DMA configuration, in which the M chromophore directly mediates the transfer of energy, is structurally similar to two-step RET with no distinct time-delay.[20] The amplitude is constructed similarly:

$$M_{\mathrm{DMA}} = \mu_i^{\mathrm{D_o D_\alpha}}\ V_{ij}\left(k;\mathbf{R}_{\mathrm{DM}}\right)\ \alpha_{jk}^{\mathrm{M_o M_o}}(-k;k)\ V_{kl}\left(k;\mathbf{R}_{\mathrm{MA}}\right)\ \mu_l^{\mathrm{A_\beta A_o}} \tag{3a.10}$$

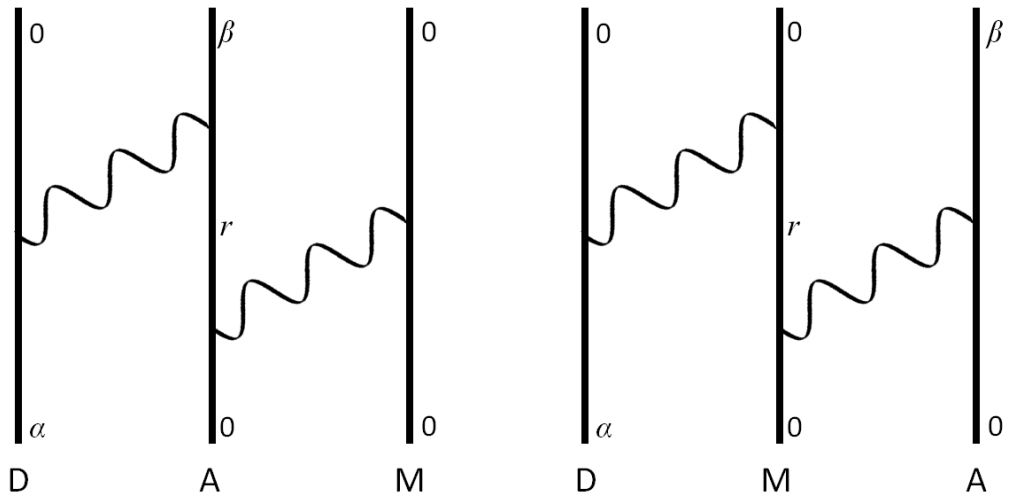

Figure 3a.4: Feynman diagrams for the other two three-body configurations: DAM (left), and DMA (right). These have exactly the same structure as figure 3a.2, differing only in the chromophore and state labels appropriate to each configuration.

Within this formalism, two-body RET (not involving any M) is described as the DA configuration. It has a three-factor quantum amplitude:

$$M_{\mathrm{DA}} = \mu_i^{\mathrm{D_o D_\alpha}}\ V_{il}\left(k;\mathbf{R}_{\mathrm{DA}}\right)\ \mu_l^{\mathrm{A_\beta A_o}} \tag{3a.11}$$

The full derivation involves the second term of the perturbative expansion, as it is a two-interaction process. For this reason, M_{DA} will usually be much greater in magnitude than the amplitudes of the three M-modified RET configurations.

The Fermi rule gives the measurable rate for a process as proportional to the square modulus of the total quantum amplitude. The four configuration amplitudes derived above all connect the same initial state I to the same final state F, such that they all describe the same RET process, so its total amplitude is their sum. This delivers ten rate terms according to the pattern of equation (2a.12).

$$\begin{aligned}\Gamma_{FI} &= 2\pi\hbar^{-1}\rho_F \left|M_{\mathrm{DA}} + M_{\mathrm{MDA}} + M_{\mathrm{DAM}} + M_{\mathrm{DMA}}\right|^2 \\ &= 2\pi\hbar^{-1}\rho_F \left\{ \left|M_{\mathrm{DA}}\right|^2 \right. \\ &\qquad + 2\,\mathrm{Re}\left(\bar{M}_{\mathrm{DA}} M_{\mathrm{DMA}}\right) + \left|M_{\mathrm{MDA}}\right|^2 \\ &\qquad + 2\,\mathrm{Re}\left(\bar{M}_{\mathrm{DA}} M_{\mathrm{DAM}}\right) + 2\,\mathrm{Re}\left(\bar{M}_{\mathrm{MDA}} M_{\mathrm{DAM}}\right) + \left|M_{\mathrm{DAM}}\right|^2 \\ &\qquad + 2\,\mathrm{Re}\left(\bar{M}_{\mathrm{DA}} M_{\mathrm{MDA}}\right) + 2\,\mathrm{Re}\left(\bar{M}_{\mathrm{MDA}} M_{\mathrm{DMA}}\right) \\ &\qquad \left. + 2\,\mathrm{Re}\left(\bar{M}_{\mathrm{DAM}} M_{\mathrm{DMA}}\right) + \left|M_{\mathrm{DMA}}\right|^2 \right\}\end{aligned} \tag{3a.12}$$

5. Specific geometries

Each of the 10 terms in rate equation (3a.12) is challenging to directly relate to measurements and molecular properties. To most readily elicit the physical significance of this result, it is necessary to introduce some simplifying assumptions about the physical system.

The focus is now on the case of the three molecules being separated by a distance that is significantly less than k^{-1}, but not in direct contact. That is to say, the molecules are close together as measured by the wavelength corresponding to the exchanged energy, but still at sufficient separation for there to be no significant electron wavefunction overlap. The chromophores must remain distinct units, whose only interactions with each other are via the two specific virtual photons p and ϕ included in the Feynman diagrams of figure 3a.2 and figure 3a.4. In the **V** tensor definition (3a.7), this is the case of $kR \ll 1$. Each coupling tensor in equations (3a.8-11) therefore reduces to:

$$\lim_{kR\to 0} V_{ij}\left(k;\mathbf{R}\right) = \left(4\pi\varepsilon_0\right)^{-1} R^{-3}\left(\delta_{ij} - 3\hat{R}_i\hat{R}_j\right) \tag{3a.13}$$

This reduced coupling tensor has no imaginary part and no dependence on k. The dependence on R, the magnitude of the molecules' separation, is given solely by the factor R^{-3}, such that the coupling strength will decline monotonically with increasing distance. This justifies a focus on the near-zone, as any M molecules

that are further away will give a comparatively insignificant contribution to the RET process.

To further simplify the system for the sake of enabling calculation of testable results, it is necessary to restrict the transition dipole moment vectors $\boldsymbol{\mu}^{\mathrm{D_o D_\alpha}}$ and $\boldsymbol{\mu}^{\mathrm{A_\beta A_o}}$ to be parallel. In all the geometric expressions in this section, the orientation of these vectors shall be labelled the system's Cartesian *z*-axis.

The main aim of this calculation is to identify the dependence of RET on the relative position and the electronic properties of the chromophore M, which represents the nearest molecule/chromophore of the matter surrounding D and A. When D and A are in solution, M will be the nearest solvent molecule; when D and A are protein chromophores, M will be the nearest other chromophore. In either scenario, the spatial orientation of M cannot reasonably be specified as a known variable – a complete treatment in terms of the specific orientation of M is thus unnecessary. Thus, in each instance of $\boldsymbol{\mu}^{\mathrm{M_0 M_0}}$ and $\alpha^{\mathrm{M_o M_o}}(-k;k)$ the (unknown) orientation of M must be replaced with an average of all its possible orientations.

Figure 3a.5 summarises the results of a rotational average over the orientation of $\boldsymbol{\mu}^{\mathrm{M_0 M_0}}$ for each of the ten rate terms of equation (3a.12). These are attained by application of the Euler-angle-integration method of tensor averaging explained in chapter 2b, section 2.

	DA	MDA	DAM	DMA
DA	$\lvert M_{\mathrm{DA}}\rvert^2$			
MDA	$\langle \mu_i^{\mathrm{M_o M_o}} \rangle$ $\propto I^{(1)}$	$\langle \mu_i^{\mathrm{M_o M_o}} \mu_j^{\mathrm{M_o M_o}} \rangle$ $\propto I^{(2)}$		
DAM	$\langle \mu_i^{\mathrm{M_o M_o}} \rangle$ $\propto I^{(1)}$	$\langle \mu_i^{\mathrm{M_o M_o}} \mu_j^{\mathrm{M_o M_o}} \rangle$ $\propto I^{(2)}$	$\langle \mu_i^{\mathrm{M_o M_o}} \mu_j^{\mathrm{M_o M_o}} \rangle$ $\propto I^{(2)}$	
DMA	$\langle \alpha_{ij}^{\mathrm{M_o M_o}} \rangle$ $\propto I^{(2)}$	$\langle \mu_i^{\mathrm{M_o M_o}} \alpha_{jk}^{\mathrm{M_o M_o}} \rangle$ $\propto I^{(3)}$	$\langle \mu_i^{\mathrm{M_o M_o}} \alpha_{jk}^{\mathrm{M_o M_o}} \rangle$ $\propto I^{(3)}$	$\langle \alpha_{ij}^{\mathrm{M_o M_o}} \alpha_{kl}^{\mathrm{M_o M_o}} \rangle$ $\propto I^{(4)}$

Figure 3a.5: The rank of an average over M's orientation, applied to each of the terms of equation (3a.12). The terms with odd-order double-tensor are vanishing.

The rotational-average theory of ref.[21] yields the trivial result $I^{(1)} = 0$. The double-tensor $I^{(3)}$ is index-antisymmetric,[21] yet the two terms involving $I^{(3)}$ entail an index-contraction with the polarisability tensor $\alpha_{jk}^{\mathrm{M_o M_o}}(-k;k)$, which is index-symmetric because equation (3a.6) has intrinsic *i*/*j* symmetry given the arguments –*k* and *k*.[22] Hence the four terms that yield $I^{(1)}$ or $I^{(3)}$ vanish with the application of the rotational average.

The surviving six contributions to Equation (3a.12) consist of: the two-body RET rate not involving M, which will usually be the dominant term; two rate terms which involve M participating via the polarisability $\alpha^{\mathrm{M_o M_o}}(-k;k)$, i.e. those derived from the DMA configuration; and three terms which involve M participating via the static dipole $\boldsymbol{\mu}^{\mathrm{M_0 M_0}}$, i.e. those derived from the MDA and DAM configurations. What this means for the dependence of RET efficiency on the properties of nearby chromophores, is that the two-body RET process will be modified by two distinct influences – certain contributions to the rate represent the modification imposed by the polarisabilty of the surroundings, and others represent the modification by a permanent polarity of M.

Due to M_{DA} being a two-interaction amplitude and thus of low-order perturbation, it is expected that the two-body RET rate, $\left|M_{\mathrm{DA}}\right|^2$, will dominate the sum in equation (3a.12). The same argument also implies that $\mathrm{Re}\left(\bar{M}_{\mathrm{DA}}\, M_{\mathrm{DMA}}\right)$ should be the most significant of the five surviving rate terms that involve M. The remaining four corrections will only become significant under circumstances where the two-body RET mechanism is disproportionately unfavourable, such that M_{DA} is severely reduced – that is the focus of chapter 3b.

Before application of the rotational average over M orientations, the term $\mathrm{Re}\left(\bar{M}_{\mathrm{DA}}\, M_{\mathrm{DMA}}\right)$entails the real part of an intricate inner product of four complex tensors:

$$\begin{aligned}\mathrm{Re}\left(\bar{M}_{DA} M_{DMA}\right) = \mu_i^{D_o D_\alpha}\, \mu_m^{D_o D_\alpha}\; \mu_l^{A_\beta A_o}\, \mu_n^{A_\beta A_o} \\ \times \mathrm{Re}\left[V_{ij}\left(k;\mathbf{R}_{DM}\right)\, V_{kl}\left(k;\mathbf{R}_{MA}\right)\, \bar{V}_{mn}\left(k;\mathbf{R}_{DA}\right)\; \alpha_{jk}^{M_o M_o}(-k;k)\right]\end{aligned} \tag{3a.14}$$

The rotational average imposes a factor of $I^{(2)} = \delta_{jk}\,\delta_{\lambda\nu}/3$on the polarisability tensor, transforming it into $\alpha_{\lambda\lambda}^{M_o M_o}/3 = \mathrm{Tr}\left(\alpha^{M_o M_o}\right)$. This trace-polarisability will

have positive sign if the primary absorption band of M is of *slightly greater* energy than the transferred energy $\hbar ck$.

Equation (3a.13) is the relevant **V** definition for this system. The assumption of $\boldsymbol{\mu}^{\mathrm{D_o D_\alpha}}$ and $\boldsymbol{\mu}^{\mathrm{A_\beta A_o}}$ lying on the z-axis implies that the indices *i*, *l*, *m* and *n* are now limited to *z*. Now, the averaged form of equation (3a.12) therefore evaluates in full detail as:

$$\begin{aligned}\left\langle \Gamma_{FI} \right\rangle &= \frac{2\pi\rho_F}{\hbar}\left\{ \left|M_{\mathrm{DA}}\right|^2 + 2\left\langle \mathrm{Re}\left(\bar{M}_{DA} M_{\mathrm{DMA}}\right)\right\rangle + \ldots \right\} \\ &= \frac{\rho_F}{48\pi^2\hbar\varepsilon_0^3}\left|\mu^{\mathrm{D_o D_\alpha}}\right|^2 \left|\mu^{\mathrm{A_\beta A_o}}\right|^2 R_{DA}^{-3}\left(1-3\hat{R}_{DAz}^2\right) \\ &\quad \times \Big\{ \quad 6\pi\varepsilon_0 R_{DA}^{-3}\left(1-3\hat{R}_{DAz}^2\right) \\ &\qquad + \mathrm{Re}\left(\mathrm{Tr}\,\alpha^{M_o M_o}(-k;k)\right) \\ &\qquad\quad \times R_{DM}^{-3} R_{MA}^{-3}\left[1-3\hat{R}_{DMz}^2 - 3\hat{R}_{MAz}^2 + 9\hat{R}_{DMz}\hat{R}_{MAz}\left(\hat{R}_{DM}\cdot\hat{R}_{MA}\right)\right] \\ &\qquad + \ldots \Big\}\end{aligned} \tag{3a.15}$$

The first line of the expansion, $6\pi\varepsilon_0 R_{DA}^{-3}(1-3\hat{R}_{DAz}^2)$, is the two-body RET rate; the next term contains all variables attributable to the influence of M (the nearest chromophore of a passively-interacting medium) modifying the process via DMA coupling. Notably, this influence is determined only by the relative position and the trace-polarisability of M, and its *sign* specifies whether M's influence amplifies or diminishes RET. In general, larger (more polarisable) molecules M that come nearer to the donor-acceptor pair should induce the greatest (positive or negative) rate modification.

If the trace-polarisability factor is expressed in volume form,

$$\alpha' \equiv \frac{3}{4\pi\varepsilon_0}\mathrm{Re}\left(\mathrm{Tr}\,\alpha^{M_o M_o}(-k;k)\right) \tag{3a.16}$$

and all common factors are removed from (3a.15), then the two leading RET rate terms are expressible as:

$$\left\langle \Gamma_{FI} \right\rangle \propto \left[1-3\hat{R}_{DAz}^2\right] + \frac{2}{9}\left(\frac{\alpha' R_{DA}^3}{R_{DM}^3 R_{MA}^3}\right)\left[1-3\hat{R}_{DMz}^2 - 3\hat{R}_{MAz}^2 + 9\hat{R}_{DMz}\hat{R}_{MAz}\left(\hat{R}_{DM}\cdot\hat{R}_{MA}\right)\right] \tag{3a.17}$$

If the three inter-chromophore separation distances are approximately equal, then the modification term is proportional to the ratio of M's polarisability volume to the cube of this distance.

The dependence on M's position is a very complicated function of the relative separation and orientation of D and A as well as their dipole orientation, *z*. It is thus not feasible to predict a rigorous relationship between the location of M and the RET rate modification. However, the result does allow the sign and degree of modification to be calculated for any specific system geometry.

A very simple example solution is the case of the three chromophores forming a half-square triangle with apex M (i.e. $R_{DA} = \sqrt{2}R_{DM} = \sqrt{2}R_{MA}$) with the *z*-axis oriented orthogonal to the plane of this triangle. The solution to equation (3a.17) for this geometry is:

$$\left\langle \Gamma_{FI} \right\rangle \propto 1 + \frac{2^{5/2}}{9}\left(\frac{\alpha'}{R_{DM}^3}\right) \tag{3a.18}$$

The two-body RET rate is set to 1, so the second term represents the relative rate modification. If α' is the volume of a spherical M, then a reasonable value for the separation R_{DM} would be triple the radius of M. This volume ratio produces a weak but detectable rate enhancement of 9.8%.

6. Polarisability and refractive index

The polarisability tensor $\alpha_{ij}^{\mathrm{M_0M_0}}\left(-k;k\right)$, which is the time-symmetric inert scattering tensor of the molecule M as defined by equation (3a.6), has been shown to be the principal factor (other than relative position) determining the role of M in modifying RET.

The double-interaction of M in the DMA coupling configuration (see figure 3a.3) is identifiable as simple scattering because: there is conservation of energy in the two interaction events within the subsystem consisting of M and radiation; M undergoes no overall molecular transition; and the transition dipole moments $\boldsymbol{\mu}^{\mathrm{M_0M}_r}$ and $\boldsymbol{\mu}^{\mathrm{M}_r\mathrm{M_0}}$ are chosen to have no imaginary part. These facts together imply that $\mu_i^{\mathrm{M_0M}_r}\mu_j^{\mathrm{M}_r\mathrm{M_0}} = \mu_j^{\mathrm{M_0M}_r}\mu_i^{\mathrm{M}_r\mathrm{M_0}}$.

The polarisability includes a sum over the complete set of intermediate states M_r, which are all the possible stationary states for the molecule M. Of particular interest is the excited state whose energy (relative to M_0) is closest to the transfer energy, $\hbar ck$. The denominators of equation (3a.6) show that polarisability is at a maximum and at its most wavelength-dependent near to resonance, so now the near-resonant case is explored in more detail. The nearest-to-resonant intermediate state is labelled M_ε. In the sum over M_r, this may be separated out:

$$\begin{aligned}\alpha_{ij}^{M_0M_0}(-k;k) = -\hbar^{-1}c^{-1} \\ \times\Bigg\{ \mu_i^{M_0M_\varepsilon}\mu_j^{M_\varepsilon M_0}\left[\frac{\Delta_\varepsilon + i\gamma_\varepsilon}{{\Delta_\varepsilon}^2+\gamma_\varepsilon^2}+\frac{\Delta_\varepsilon + 2k \mp i\gamma_\varepsilon}{\left(\Delta_\varepsilon+2k\right)^2+\gamma_\varepsilon^2}\right] \\ +\sum_{r\neq\varepsilon}\mu_i^{M_0M_r}\mu_j^{M_rM_0}\left[\frac{k_{r0}-k+i\gamma_r}{\left(E_{r0}^M/\hbar c-k\right)^2+\gamma_r^2}+\frac{k_{r0}+k\mp i\gamma_r}{\left(E_{r0}^M/\hbar c+k\right)^2+\gamma_r^2}\right]\Bigg\}\end{aligned} \tag{3a.19}$$

The variables $E_{\varepsilon 0}^M$ and γ_ε are electronic properties intrinsic to the species M. The energy-separation of M_ε from resonance is represented by the difference $\Delta_\varepsilon = E_{\varepsilon 0}^M/\hbar c - k$. The situation of exact resonance, $E_{\varepsilon 0}^M = \hbar ck$, corresponds to $\Delta_\varepsilon = 0$. Importantly, this chapter assumes that M does *not* have any stationary state at exact resonance, as this would make it a second acceptor chromophore A.

In the case of $\hbar ck$ being very close in energy to a stationary state of M, so the difference Δ_ε is small, so all $r \neq \varepsilon$ terms (the second line of equation (3a.19)) and the anti-resonant ε term (the second fraction in the first line) become comparatively negligible. The real trace polarisability featuring in equation (3a.15) can then be approximated as:

$$\mathrm{Re}\left(\mathrm{Tr}\,\alpha_{ij}^{M_0M_0}(-k;k)\right) = -(\hbar c)^{-1}\mu^{M_0M_\varepsilon}\mu^{M_\varepsilon M_0}\frac{\Delta_\varepsilon}{{\Delta_\varepsilon}^2+\gamma_\varepsilon^2} \tag{3a.20}$$

This function of Δ_ε and γ_ε can be further simplified by truncating the Taylor series expansions that arise in the two extreme cases. Either relatively weak damping:

$$\begin{aligned}&\gamma_\varepsilon << |\Delta_\varepsilon| \\ &\therefore \mathrm{Re}\left(\mathrm{Tr}\,\alpha_{ij}^{M_0M_0}(-k;k)\right) \approx -(\hbar c)^{-1}\mu^{M_0M_\varepsilon}\mu^{M_\varepsilon M_0}\left[\Delta_\varepsilon^{-1}-\gamma_\varepsilon^2\Delta_\varepsilon^{-3}\right]\end{aligned} \tag{3a.21}$$

or relatively heavy damping:

$$\begin{aligned} &\gamma_\varepsilon >> |\Delta_\varepsilon| \\ &\therefore \mathrm{Re}\left(\mathrm{Tr}\,\alpha_{ij}^{M_0M_0}(-k;k)\right) \approx -(\hbar c)^{-1}\,\mu^{M_0M_\varepsilon}\mu^{M_\varepsilon M_0}\left[\Delta_\varepsilon\gamma_\varepsilon^{-2} - \Delta_\varepsilon{}^3\gamma_\varepsilon^{-4}\right] \end{aligned} \tag{3a.22}$$

When interpreted as functions of *k*, these equations describe the influence of the transfer energy $\hbar ck$ on the magnitude of equation (3a.15)'s M-modification term. This is because the polarisability of M is the only variable in equation (3a.15) that varies with *k*.

If RET is understood as the short-range limit of *radiative* energy transfer, the wavenumber may be interpreted as $k = 2\pi/\lambda$, where λ is the wavelength of the ideal non-virtual photon carrying the energy $\hbar ck$ from D to A. This perspective is conceptually at variance with this chapter's two-virtual-photon description of modified RET, but it illustrates the physical insights. Molecules of the surrounding matter modify the rate of energy transfer via their polarisability, and the modification varies according to the wavelength. Wavelength-specific modification of photon behavior by the polarisability of the medium is commonly addressed in terms of macroscopic optical properties.

A close analogy can be drawn with the wavelength-dependence of the refractive index *n* of a medium comprised of molecules of species M. The density form of the Clausius-Mossotti relation expresses the polarisability of a substance present in number-density *N*, as a function of the refractive index *n* of the pure substance:

$$\alpha = 3N^{-1}\frac{n^2-1}{n^2+2} \tag{3a.23}$$

It has already been postulated that there is an isotropic distribution of orientations for molecule M. This is consistent with the polarisability itself being isotropic, with diagonal scalar elements that are equal and may each be identified with the Clausius-Mossotti result. Then the scalar polarisability in equation (3a.15) is exactly triple the real part of this result:

$$\mathrm{Re}\left(\mathrm{Tr}\,\alpha_{ij}^{M_0M_0}(-k;k)\right) = 3\,\mathrm{Re}\,\alpha = 9N^{-1}\,\frac{\mathrm{Re}\left(n^2\right)^2 + \mathrm{Re}\left(n^2\right) + \mathrm{Im}\left(n^2\right)^2 - 2}{\mathrm{Re}\left(n^2\right)^2 + 4\,\mathrm{Re}\left(n^2\right) + \mathrm{Im}\left(n^2\right)^2 + 4} \tag{3a.24}$$

This treats *n* as the refractive index of a bulk medium consisting of unaligned M molecules. RET occurs between individual molecules D and A, which are surrounded by this medium. The scenario best described by this formulation is

low-concentration solutes D and A present in a liquid M solution, but it may still in principle be usefully applied to chromophores embedded in photosynthetic proteins or dendrimers.

Equation (3a.24) can be rearranged to give a prediction for the medium's refractive index given a certain polarisability for the constituents M. Provided that n^2 has no imaginary part, this comes to:

$$\mathrm{Re}(n) = \left| \frac{2N\,\mathrm{Re}(\mathrm{Tr}\,\alpha) + 9}{9 - N\,\mathrm{Re}(\mathrm{Tr}\,\alpha)} \right|^{1/2} \qquad (3a.25)$$

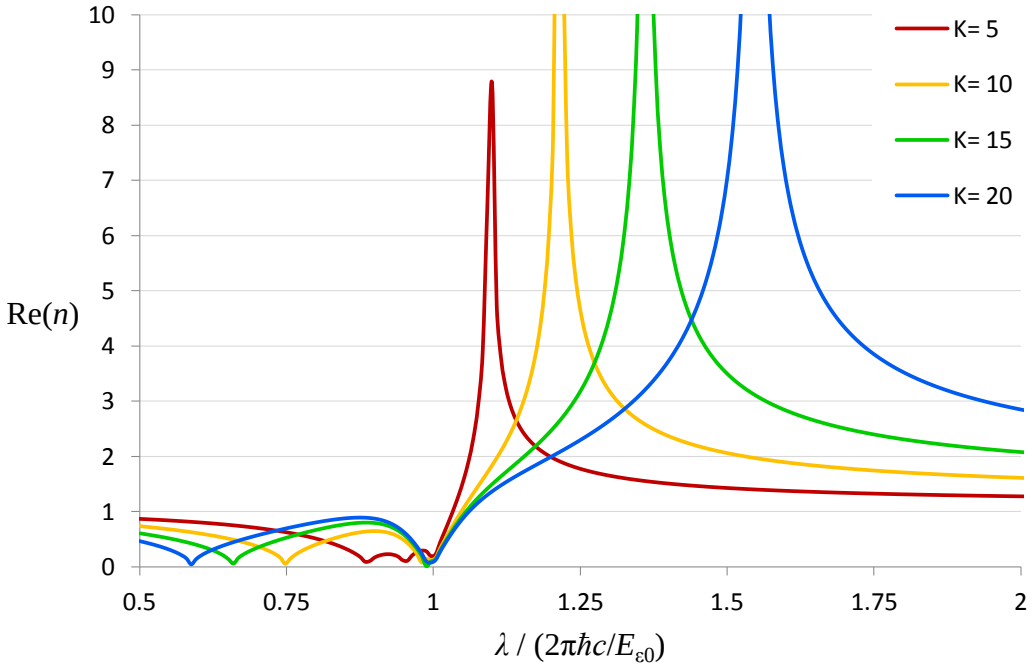

Figure 3a.6: Refractive index of the medium M as a function of the transfer-energy wavelength, λ, with abscissa normalised to the resonance condition. Equation (3a.25) is plotted in the form:

$$\mathrm{Re}(n) = \left| \frac{2K\left(\hbar^{-1}c^{-1}E_{\varepsilon 0} - 2\pi\lambda^{-1}\right)\left[\left(\hbar^{-1}c^{-1}E_{\varepsilon 0} - 2\pi\lambda^{-1}\right)^2 + \gamma^2\right]^{-1} + 9}{9 - K\left(\hbar^{-1}c^{-1}E_{\varepsilon 0} - 2\pi\lambda^{-1}\right)\left[\left(\hbar^{-1}c^{-1}E_{\varepsilon 0} - 2\pi\lambda^{-1}\right)^2 + \gamma^2\right]^{-1}} \right|^{1/2}$$

This graph uses a value for damping, $\gamma = (4\pi)^{-1}\hbar^{-1}c^{-1}E_{\varepsilon 0}$, which is within the weak limit described by equation (3a.21). The parameter K is defined as $K \equiv \hbar^{-1}c^{-1}N\mu^{M_0M_\varepsilon}\mu^{M_\varepsilon M_0}$, in units of $E_{\varepsilon 0} = 1$. The near-zero at $\lambda = 2\pi\hbar c / E_{\varepsilon 0}$ represents weakly-damped resonance.

Equation (3a.20) and the relation $\Delta_\varepsilon = E_{\varepsilon 0}^M / \hbar c - 2\pi/\lambda$ combine to give the real trace polarisability $\mathrm{Re}(\mathrm{Tr}\,\alpha)$ as a function of the ideal wavelength λ. Thus, equation (3a.25) provides $\mathrm{Re}(n)$ as a function of λ and of N, as illustrated by figure 3a.6. Note that the results of section 5 assume the wavelength λ to be slightly longer than the resonance condition. The number-density of M molecules, N, is an indirect measure of the inter-chromophore distance – the average distance should have an inverse cube-root proportionality to N.

7. Discussion

The results of section 4 stand alone as a complete description of the factors determining the rate of modified-RET – but only if we have complete knowledge of each chromophore's relative position, orientation, the energy of each stationary state, and all the transition dipole moments involving each stationary state. This condition may be approached in the case of strictly-aligned chromophores within a rigid protein structure, such as natural photosynthetic complexes.

It has been identified that with an isotropic medium, molecular polarisability is the principal property of the surrounding matter responsible for modifying RET. Polarisability is at a maximum near to resonance, so matter that is near-resonant will have the greatest effect on RET efficiency – but exact resonance would lead to the medium molecules competing for the role of final energy acceptor, which lies outside of this analysis.

Equation (3a.24) is unique for directly linking the bulk refractive index of a material to the effect that its individual molecules have upon the microscopic process of RET. In the case of a homogenous medium that is a mixture of several near-resonant molecular species, the relevant refractive index is that of a pure sample of whichever species M is closest to the RET pair. When attempting to detect a third-body modification compared to the two-body RET rate, it is not possible to remove the third molecule M without completely taking the donor and acceptor out of solution, but the RET efficiency of a donor-acceptor complex may be measured in solutions with differing refractive index.

The more conventional refraction-correction to RET involves a redefinition of the coupling tensor $\mathbf{V}$,[23,24] and this has been successfully used to analyse

photosynthetic systems by treating the protein scaffold as a refractive environment.[25,26] If this chapter employed such an approach, the polarisability of molecule M would be unrelated to *n*, and the **V** tensors of equations (3a.8-11) would receive the modifying factor $(n^2+2)^2/9n^2$. But that would result in a RET rate dependence on *n* inconsistent with equation (3a.15), which is justified by the QED derivations of this chapter. The discrepancy comes from the two formulations describing different coupling scenarios – this chapter deals with a specific M chromophore identified as the nearest medium molecule, so the space between D and M cannot be filled with matter that modifies coupling with its non-unity refractive index.

[1] J. L. Herek, N. J. Fraser, T. Pullerits, P. Martinsson, T. Polivka, H. Schee, R. J. Cogdell, and V. Sundstrom, "B800 to B850 Energy Transfer Mechanism in Bacterial LH2 Complexes Investigated by B800 Pigment Exchange": *Biophys. J.* **78**, 2590 (2000).

[2] D. L. Andrews, S. P. Li, J. Rodriguez, and J. Slota, "Development of the Energy Flow in Light-Harvesting Dendrimers": *J. Chem. Phys.* **127**, 134902 (2007).

[3] J. Barber, "Biological Solar Energy": *Philos. Trans. R. Soc. Math. Phys. Eng. Sci.* **365**, 1007 (2007).

[4] S.-C. Lo and P. L. Burn, "Development of Dendrimers: Macromolecules for Use in Organic Light-Emitting Diodes and Solar Cells": *Chem Rev* **107**, 1097 (2007).

[5] G. R. Fleming, G. S. Schlau-Cohen, K. Amarnath, and J. Zaks, "Design Principles of Photosynthetic Light-Harvesting": *Faraday Discuss.* **155**, 27 (2012).

[6] B. Valeur, *Molecular Fluorescence* (Wiley-VCH, Weinheim, 2002).

[7] F. Barigelletti and L. Flamigni, "Photoactive Molecular Wires Based on Metal Complexes": *Chem. Soc. Rev.* **29**, 1 (2000).

[8] Z. Tan, R. Kote, W. N. Samaniego, S. J. Weininger, and W. G. McGimpsey, "Intramolecular Singlet-Singlet and Triplet-Triplet Energy Transfer in Adamantyl-Linked Trichromophores": *J Phys Chem A* **103**, 7612 (1999).

[9] V. Balzani, P. Ceroni, A. Juris, M. Venturi, S. Campagna, F. Puntoriero, and S. Serroni, "Dendrimers Based on Photoactive Metal Complexes. Recent Advances": *Coord. Chem. Rev.* **219**, 545 (2001).

[10] D. L. Andrews and B. S. Sherborne, "Resonant Excitation Transfer: A Quantum Electrodynamical Study": *J. Chem. Phys.* **86**, 4011 (1987).

[11] D. L. Andrews, "A Unified Theory Of Radiative And Radiationless Molecular Energy Transfer": *J. Chem. Phys.* **135**, 195 (1989).

[12] D. L. Andrews and D. S. Bradshaw, "Virtual Photons, Dipole Fields and Energy Transfer: A Quantum Electrodynamical Approach": *Eur. J. Phys.* **25**, 845 (2004).

[13] D. Beljonne, C. Curutchet, G. D. Scholes, and R. J. Silbey, "Beyond Forster Resonance Energy Transfer in Biological and Nanoscale Systems": *J Phys Chem B* **113**, 6583 (2009).

[14] R.E. Blankenship, *Molecular Mechanisms of Photosynthesis* (Blackwell, Oxford, 2002).

[15] D.L. Andrews and J.S. Ford, "Resonance Energy Transfer: Influence of Neighboring Matter Absorbing in the Wavelength Region of the Acceptor": *J. Chem. Phys.* **139**, (2013).

[16] D.L. Andrews and J.S. Ford, "Electronic Energy Transport in Nanomaterials: Influence of Host Structure": *Proc. SPIE*, **8459** (2012), p. 0C.

[17] G.D. Scholes, G.R. Fleming, A. Olaya-Castro, and R. van Grondelle, "Lessons from Nature about Solar Light Harvesting": *Nat Chem* **3**, 763 (2011).

[18] Daniels, Gareth J. and Andrews, David L., "The Electronic Influence of a Third Body on Resonance Energy Transfer (Corrected Article)": *J. Chem. Phys.* **117**, 6882 (2002).

[19] D. P. Craig and T. Thirunamachandran, *Molecular Quantum Electrodynamics*, 2nd ed. (Dover Publications, Mineola, New York, 1998).

[20] Akbar Salam, "Mediation of Resonance Energy Transfer by a Third Molecule": *J. Chem. Phys.* **136**, 014509 (2012).

[21] D. P. Craig and T. Thirunamachandran, "Rotational Averaging of Tensors": *Mol. Quantum Electrodyn.*, Dover Paperback (Dover Publications, Mineola, New York, 1998), pp. 310–315.

[22] D. L. Andrews and T. Thirunamachandran, "On Three-Dimensional Rotational Averages": *J. Chem. Phys.* **67**, 5026 (1977).

[23] G. Juzeliūnas, "Molecule-Radiation and Molecule-Molecule Processes in Condensed Media: A Microscopic QED Theory": *Chem. Phys.* **198**, 145 (1995).

[24] S. Caprasecca, C. Curutchet, and B. Mennucci, "Toward a Unified Modeling of Environment and Bridge-Mediated Contributions to Electronic Energy Transfer: A Fully Polarisable QM/MM/PCM Approach": *J. Chem. Theory Comput.* **8**, 4462 (2012).

[25] G. D. Scholes and G. R. Fleming, "On the Mechanism of Light Harvesting in Photosynthetic Purple Bacteria: B800 to B850 Energy Transfer": *J Phys Chem B* **104**, 1854 (n.d.).

[26] C. Curutchet, J. Kongsted, A. Muñoz-Losa, H. Hossein-Nejad, G. D. Scholes, and B. Mennucci, "Photosynthetic Light-Harvesting Is Tuned by the Heterogeneous Polarisable Environment of the Protein": *J. Am. Chem. Soc.* **133**, 3078 (2011).

–

Chapter 3: **Resonance energy transfer modified by a third chromophore**

3b: **Orthogonally-oriented transition dipole moments**

1. Introduction

The precise geometrical arrangement of chromophores – especially the relative orientations of transition dipole moments – significantly influences the efficiency of RET. In the wider literature that covers RET and related processes, the deterministic relationship between relative orientations and RET rate is conventionally described in terms of an orientation factor, κ.[1,2] Much recent theoretical work has explored the issue of optimising the geometry of multi-component RET systems,[3–6] often expressing orientation dependence with a κ function. See equation 2.28 of ref.[7].

$$\kappa_\chi = \left(\hat{\boldsymbol{\mu}}^{\mathrm{D_o D_\alpha}} \cdot \hat{\boldsymbol{\mu}}^{\mathrm{A_\beta A_o}}\right) - \chi\left(\hat{\mathbf{R}}_{\mathrm{DA}} \cdot \hat{\boldsymbol{\mu}}^{\mathrm{D_o D_\alpha}}\right)\left(\hat{\mathbf{R}}_{\mathrm{DA}} \cdot \hat{\boldsymbol{\mu}}^{\mathrm{A_\beta A_o}}\right) \qquad \chi \in \{1, 3\} \tag{3b.1}$$

A well-known result from such work is that the efficiency of short-range Förster RET is proportional to κ_3^2. More generally, RET is forbidden at all ranges if both terms of κ are zero.[8] This condition is met when donor and acceptor dipole moments are oriented orthogonally with respect to each other, *and* one is also perpendicular to the straight line between the molecular positions. Note that in systems where this is true at the midpoint (equilibrium) of the chromophores' vibrations, vibrational displacement may be sufficient to allow RET.[9]

The previous chapter 3a assumes that the donor and acceptor are positioned such that two-body RET (the "DA" configuration) is favourable. Thus the RET rate results are dominated by the unmediated RET process, which is merely modified by quantum interference from third-body interactions. But if the chromophores are situated such that both terms of κ are zero, so the DA configuration cannot contribute, then the RET rate will instead be dominated by indirect-RET mechanisms. This chapter contains the calculations of RET rate in an elementary example of such a DA-forbidden geometry.[10]

2. Quantum amplitudes of RET mechanisms

The donor chromophore D undergoes a decay transition $D_0 \leftarrow D_\alpha$; the acceptor A is excited $A_\beta \leftarrow A_0$; the passive neighbouring molecule M remains in its ground state M_0. A quantity of energy $\hbar ck$ is transferred. This process may proceed via any of four mechanisms, defined by the *coupling configuration*,[11,12] and each of these mechanisms has a distinct quantum amplitude. These are fully derived in chapter 3a and appendix 8c.

- DA coupling: Two-body RET without the involvement of any M.

$$M_{\mathrm{DA}} = \mu_i^{\mathrm{D_o D_\alpha}}\ V_{ij}\left(k;\mathbf{R}_{\mathrm{DA}}\right)\mu_j^{\mathrm{A_\beta A_o}} \tag{3b.2}$$

- MDA coupling: RET with D statically coupled to M.

$$M_{\mathrm{MDA}} = \mu_i^{\mathrm{M_o M_o}}\ V_{ij}\left(0;\mathbf{R}_{\mathrm{MD}}\right)\ \alpha_{jk}^{\mathrm{D_o D_\alpha}}(-k;0)\ V_{kl}\left(k;\mathbf{R}_{\mathrm{DA}}\right)\ \mu_l^{\mathrm{A_\beta A_o}} \tag{3b.3}$$

- DAM coupling: RET with A statically coupled to M.

$$M_{\mathrm{DAM}} = \mu_i^{\mathrm{D_o D_\alpha}}\ V_{ij}\left(k;\mathbf{R}_{\mathrm{DA}}\right)\ \alpha_{jk}^{\mathrm{A_\beta A_o}}(0;k)\ V_{kl}\left(0;\mathbf{R}_{\mathrm{AM}}\right)\ \mu_l^{\mathrm{M_o M_o}} \tag{3b.4}$$

- DMA coupling: Mediated energy transfer, whereby D and A are each coupled only to M.

$$M_{\mathrm{DMA}} = \mu_i^{\mathrm{D_o D_\alpha}}\ V_{ij}\left(k;\mathbf{R}_{\mathrm{DM}}\right)\ \alpha_{jk}^{\mathrm{M_o M_o}}(-k;k)\ V_{kl}\left(k;\mathbf{R}_{\mathrm{MA}}\right)\ \mu_l^{\mathrm{A_\beta A_o}} \tag{3b.5}$$

Separation vector $\mathbf{R}_{\mathrm{AB}}$ is the displacement of the "B" position from the "A" position. The $E1^2$ molecular polarisability tensors $\boldsymbol{\alpha}$ are defined by equation (3a.6). The E1-E1 coupling tensors $\mathbf{V}$ are defined by equation (3a.7).[13] The rate of RET is calculated using the Fermi golden rule, expressed in terms of the four quantum amplitudes by Equation (3a.12).

The Fermi rate term describing the pure unmodified DA process is given by the square modulus of (3b.2). By carefully implementing equations (3a.7) and (3b.1) above, it follows that this rate has the following orientation dependence:[7,8]

$$\begin{aligned}\left|M_{\mathrm{DA}}\right|^2 &\propto R_{\mathrm{DA}}^{-6}\left|\kappa_3 - ikR_{\mathrm{DA}}\kappa_3 - k^2R_{\mathrm{DA}}^2\kappa_1\right|^2 \\ &\propto R_{\mathrm{DA}}^{-6}\ \kappa_3^2\ + k^2R_{\mathrm{DA}}^{-4}\left(\kappa_3^2 - 2\kappa_1\kappa_3\right)\ + k^4R_{\mathrm{DA}}^{-2}\ \kappa_1^2\end{aligned} \tag{3b.6}$$

In the limit where the separation distance R_{DA} is far less than the ideal reduced wavelength k^{-1}, the first term of (3b.6) (with R^{-6} distance-dependence as in Förster RET) dominates, and therefore RET rate is proportional to κ_3^2. In the

opposite limit of $R_{DA} \gg k^{-1}$, the third term (with R^{-2} distance-dependence as in radiative energy transfer) dominates, and so the RET rate is proportional to κ_1^2. At all intermediate scales of separation R_{DA}, there is also contribution to the RET rate from the second term, with orientation factor $\left(\kappa_3^2 - 2\kappa_1\kappa_3\right)$. This analysis rigorously demonstrates that the pure DA form of RET is forbidden when both κ_1 and κ_3 are equal to zero, and this prohibition is effective at all scales of donor-acceptor separation – even in the far-field limit when the mediating photon must be considered wavelike, such that inter-chromophore couplings are subject to appreciable retardation and the Förster theory of RET is inapplicable.[14–16]

This chapter contains the calculations of RET rate in a three-molecule system defined by donor and acceptor dipole moments being oriented orthogonally with respect to each other, and *both* of their dipoles being perpendicular to the vector $\mathbf{R}_{DA}$, as shown by figure 3b.1. This is the most elementary DA-forbidding scenario.

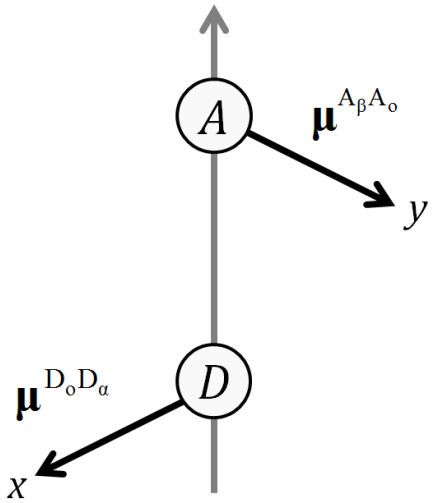

Figure 3b.1: The dipole moments of the donor and the acceptor, and the vector separating their molecular positions, form an orthogonal triad. A Cartesian standard-basis coordinate system may be constructed around these vectors.

3. System specification

The dipole moments of D and A and the separation vector $\mathbf{R}_{DA}$ are aligned as an orthogonal triad. It is therefore most convenient to specify the Cartesian standard-

basis coordinate system according to these directions, and to fix the origin at the position midway between D and A (see figures 3b.1 and 3b.3).

$$\boldsymbol{\mu}^{\mathrm{D_o D_\alpha}} = \hat{\mathbf{x}}\,\mu^{\mathrm{D_o D_\alpha}} \quad ; \quad \boldsymbol{\mu}^{\mathrm{A_\beta A_o}} = \hat{\mathbf{y}}\,\mu^{\mathrm{A_\beta A_o}} \quad ; \quad \mathbf{R}_{\mathrm{DA}} = \hat{\mathbf{z}}\,R_{\mathrm{DA}} \tag{3b.7}$$

In the language of Cartesian hanging indices, the dipole moment factors in the quantum amplitude equations (3b.2-5) reduce to:

$$\mu_i^{\mathrm{D_o D_\alpha}} = \delta_{ix}\,\mu^{\mathrm{D_o D_\alpha}} \quad ; \quad \mu_i^{\mathrm{A_\beta A_o}} = \delta_{iy}\,\mu^{\mathrm{A_\beta A_o}}. \tag{3b.8}$$

In particular, the DA configuration quantum amplitude reduces to:

$$M_{\mathrm{DA}} = \mu^{\mathrm{D_o D_\alpha}}\,V_{xy}\left(k;\mathbf{R}_{\mathrm{DA}}\right)\mu^{\mathrm{A_\beta A_o}} = 0 \tag{3b.9}$$

As intended, this is confirmed to be vanishing, according to the **V** definition.

$$\left(\delta_{xy} - 3\hat{R}_{DAx}\hat{R}_{DAy}\right) - ikR_{DA}\left(\delta_{xy} - 3\hat{R}_{DAx}\hat{R}_{DAy}\right) - k^2R_{DA}^2\left(\delta_{xy} - \hat{R}_{DAx}\hat{R}_{DAy}\right) = 0 \tag{3b.10}$$

When the electronic dipoles of each molecule are taken to be precisely aligned to a single axis, it is implicitly assumed that the molecules have an intrinsic cylindrical symmetry about this one axis. This picture of molecular structure is consistent with a push-pull model of charge displacement.[17–19] The push-pull model also supports the slightly stronger statement of molecular behaviour, that all of the other electronic displacements (static and dynamic dipoles) should likewise align to the molecule's natural axis.

With transition polarisability **α** understood as an $\mathrm{E1}^2$ molecular response tensor, the condition of cylindrical symmetry for D and A results in their **α** tensors having just one nonzero Cartesian component, similar to the dipole moment vectors **μ** above:

$$\alpha_{ij}^{\mathrm{D_o D_\alpha}} = \delta_{ix}\delta_{jx}\,\alpha^{\mathrm{D_o D_\alpha}} \quad ; \quad \alpha_{ij}^{\mathrm{A_\beta A_o}} = \delta_{iy}\delta_{jy}\,\alpha^{\mathrm{A_\beta A_o}} \tag{3b.11}$$

The quantum amplitudes for the other three coupling configurations are thus reduced:

$$M_{\mathrm{MDA}} = \mu_i^{\mathrm{M_o M_o}}\;V_{ix}\left(0;\mathbf{R}_{\mathrm{MD}}\right)\;\alpha^{\mathrm{D_o D_\alpha}}(-k;0)\;V_{xy}\left(k;\mathbf{R}_{\mathrm{DA}}\right)\;\mu^{\mathrm{A_\beta A_o}} = 0 \tag{3b.12}$$

$$M_{\mathrm{DAM}} = \mu^{\mathrm{D_o D_\alpha}}\;V_{xy}\left(k;\mathbf{R}_{\mathrm{DA}}\right)\;\alpha^{\mathrm{A_\beta A_o}}(0;k)\;V_{yi}\left(0;\mathbf{R}_{\mathrm{AM}}\right)\;\mu_i^{\mathrm{M_o M_o}} = 0 \tag{3b.13}$$

$$M_{\mathrm{DMA}} = \mu^{\mathrm{D_o D_\alpha}}\ V_{xi}\left(k;\mathbf{R}_{\mathrm{DM}}\right)\ \alpha_{ij}^{\mathrm{M_o M_o}}(-k;k)\ V_{jy}\left(k;\mathbf{R}_{\mathrm{MA}}\right)\ \mu^{\mathrm{A_\beta A_o}} \tag{3b.14}$$

The MDA and DAM amplitudes come to zero because $V_{xy}\left(k;\mathbf{R}_{\mathrm{DA}}\right) = 0$ as shown by equation (3b.10). The elimination of three of the four coupling configurations leads to a very simple result for the Fermi rate:

$$\left|M_{DA} + M_{\mathrm{MDA}} + M_{\mathrm{DAM}} + M_{\mathrm{DMA}}\right|^2 = \left|M_{\mathrm{DMA}}\right|^2 \tag{3b.15}$$

In this system geometry, with cylindrical symmetry, RET occurs *only* through the DMA mechanism. Some third chromophore M must be coupled to both D and A through its induced dipole moment, acting as a bridge for the excitation. But note that M need not be positioned directly between D and A at all, and if M were actually *bonded* to both D and A (i.e. if there were sufficient electronic wavefunction overlap to enable electron transfer), then this would be a different kind of energy-transfer system altogether.

$$\boldsymbol{\mu}^{\mathrm{D_o D_\alpha}}\ \mathbf{V}\left(k;\mathbf{R}_{\mathrm{DM}}\right)\ \boldsymbol{\alpha}^{\mathrm{M_o M_o}}(-k;k)\ \mathbf{V}\left(k;\mathbf{R}_{\mathrm{MA}}\right)\ \boldsymbol{\mu}^{\mathrm{A_\beta A_o}}$$

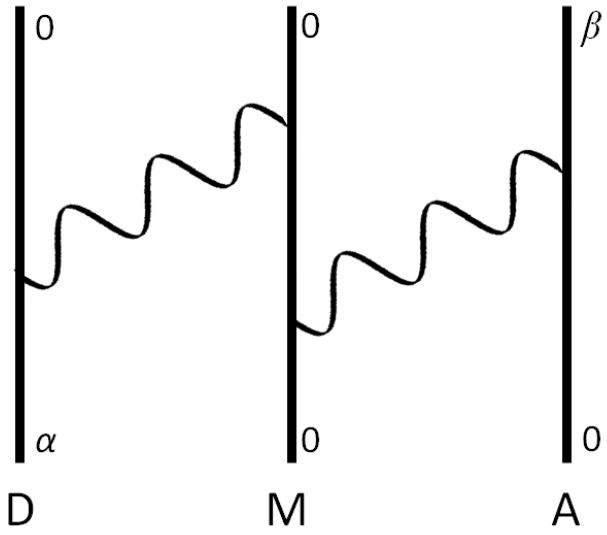

Figure 3b.2: Feynman diagram showing one time-order (of 24) of the DMA mechanism. The five factors of M_{DMA} correspond to coupling elements of the diagram, like in figure 3a.3.

Within the constraints of this system specification, the only remaining geometric variables are the length R_{DA}, the quantity of energy to be transferred $\hbar ck$, and the position and orientation of the crucial molecule M.

4. Position of M

The Cartesian coordinate system has been defined relative to the positions and orientations of the D and A chromophores. For the position of M, it is more natural to replace the *x* and *y* coordinates with an axial distance $\rho \equiv \sqrt{x^2 + y^2}$, and an azimuthal angle ψ defined such that $\psi = 0$ fixes M on the positive *x* axis and $\psi = \pi/2$ fixes M on the positive *y* axis. Figure 3b.3 illustrates these cylindrical coordinates.

The position-dependent factors of M_{DMA} are contained in the two **V** tensors, and each **V** is dominated by the inverse-cube dependence on coupling distance. Within this section, the factor $R_{DM}^{-3} R_{MA}^{-3}$ is labelled η:

$$M_{\mathrm{DMA}} \propto \mathbf{V}\left(k;\mathbf{R}_{\mathrm{DM}}\right) \mathbf{V}\left(k;\mathbf{R}_{\mathrm{MA}}\right) \propto R_{\mathrm{DM}}^{-3} R_{\mathrm{MA}}^{-3} \equiv \eta \tag{3b.16}$$

Usefully, η is symmetric with respect to the ψ coordinate, so the position of M only needs to be defined on the ρz plane.

For any ρ that is greater than $R_{\mathrm{DA}}/2$, the maximum η value is to be found at $z = 0$. For smaller ρ, it is necessary to first define a certain virtual spheroid surface:

$$z^2 + 2\rho^2 = R_{DA}^2/2 \tag{3b.17}$$

This prolate spheroid may be constructed from an ellipse, with minor-axis diameter of R_{DA} and foci located on D and A, rotating about the *z*-axis. For any given $\rho \le R_{\mathrm{DA}}/2$:

- Any nonzero *z* that puts M within the spheroid yields a value of η **greater** than at $z = 0$:

$$\eta\left(0 < |z| < \sqrt{R_{DA}^2/2 - 2\rho^2}\right) > \eta\left(z = 0\right) \tag{3b.18}$$

- Any z which puts M exactly on the spheroid surface yields **the same** η value as $z = 0$:

$$\eta\left(z=\pm\sqrt{R_{DA}^2/2-2\rho^2}\right)=\eta\left(z=0\right) \tag{3b.19}$$

- Any z that puts M outside the spheroid yields a value of η **less** than at $z = 0$:

$$\eta\left(|z|>\sqrt{R_{DA}^2/2-2\rho^2}\right)<\eta\left(z=0\right) \tag{3b.20}$$

With these findings in mind, the following sections specifically concern the $z = 0$ cases, where the coupling distances R_{DM} and R_{MA} are always equal. In full, the quantum amplitude evaluates as a function of the relative molecular positions, contracted with the M polarisability tensor:

$$M_{\mathrm{DMA}}^{z=0}=\left(4\pi\varepsilon_0\right)^{-2}R_{\mathrm{DM}}^{-6}\exp\left(2ikR_{\mathrm{DM}}\right)\,\mu^{\mathrm{D}_o\mathrm{D}_\alpha}\,\mu^{\mathrm{A}_\beta\mathrm{A}_o}\,\alpha_{ij}^{\mathrm{M}_o\mathrm{M}_o}(-k;k)\;\;D_i\,A_j \tag{3b.21}$$

The tensor parts of M_{DMA} are simplified by the vector arguments in the two distinct **V** factors, $\mathbf{R}_{\mathrm{DM}}$ and $\mathbf{R}_{\mathrm{MA}}$, having equal magnitudes. Explicitly:

$$\begin{aligned}
D_i &\equiv \left(1-ikR_{\mathrm{DM}}\right)\left(\delta_{ix}-3\hat{R}_{\mathrm{DM}\,i}\,\hat{R}_{\mathrm{DM}\,x}\right)-k^2R_{\mathrm{DM}}^2\left(\delta_{ix}-\hat{R}_{\mathrm{DM}\,i}\,\hat{R}_{\mathrm{DM}\,x}\right)\\
A_j &\equiv \left(1-ikR_{\mathrm{DM}}\right)\left(\delta_{jy}-3\hat{R}_{\mathrm{MA}\,j}\,\hat{R}_{\mathrm{MA}\,y}\right)-k^2R_{\mathrm{DM}}^2\left(\delta_{jy}-\hat{R}_{\mathrm{MA}\,j}\,\hat{R}_{\mathrm{MA}\,y}\right)\\
\hat{R}_{\mathrm{DM}\,x} &= -\hat{R}_{\mathrm{MA}\,x}=\frac{\rho}{R_{\mathrm{DM}}}\cos\psi\\
\hat{R}_{\mathrm{DM}\,y} &= -\hat{R}_{\mathrm{MA}\,y}=\frac{\rho}{R_{\mathrm{DM}}}\sin\psi\\
\hat{R}_{\mathrm{DM}\,z} &= \hat{R}_{\mathrm{MA}\,z}=\frac{R_{\mathrm{DA}}}{2R_{\mathrm{DM}}}
\end{aligned} \tag{3b.22}$$

In the $z = 0$ regime, $\eta = R_{\mathrm{DM}}^{-6}$. The coordinate ρ specifies some fixed value for the ratio $R_{\mathrm{DA}}/R_{\mathrm{DM}}$, which implies that $\eta \propto R_{\mathrm{DA}}^{-6}$. Consequently, all of the final RET rate results will vary by donor-acceptor separation according to $\left|M_{\mathrm{DMA}}\right|^2 \propto R_{\mathrm{DA}}^{-12}$.

5. Orientation and polarisability of M

Accounting for an arbitrary orientation of the molecule M, it is necessary to define an additional Cartesian reference system, with axes fixed to the molecule's

internal structure. The molecule-fixed coordinates (*x'*,*y'*,*z'*) may be related to the laboratory-fixed coordinates (*x*,*y*,*z*) via Euler angles (*α*,*β*,*γ*). A laboratory-fixed unit vector $\hat{\mathbf{i}}$ is converted to the corresponding molecule-fixed unit vector $\hat{\boldsymbol{\lambda}}$ by a triple rotation:[20]

- First, rotation *α* about the *z*-axis, carrying the *y*-axis into an orientation that the literature calls "the line of nodes";
- then rotation *β* about the line of nodes, carrying the *z*-axis into the *z'*-axis;
- then rotation *γ* about the *z'*-axis, carrying the line of nodes into the *y'*-axis.

And conversion from $\hat{\boldsymbol{\lambda}}$ to $\hat{\mathbf{i}}$ is the inverse of this operation. Therefore, the laboratory-fixed Cartesian components of M's molecular response tensors may be expressed as functions of the natural components, using a triple rotation matrix, **Φ**:

$$\mu_i^M = \Phi_{i\lambda}\,\mu_\lambda^M \tag{3b.23}$$

$$\boldsymbol{\Phi}^{-1} \equiv \begin{pmatrix} \cos\gamma & \sin\gamma & 0 \\ -\sin\gamma & \cos\gamma & 0 \\ 0 & 0 & 1 \end{pmatrix}\begin{pmatrix} \cos\beta & 0 & -\sin\beta \\ 0 & 1 & 0 \\ \sin\beta & 0 & \cos\beta \end{pmatrix}\begin{pmatrix} \cos\alpha & \sin\alpha & 0 \\ -\sin\alpha & \cos\alpha & 0 \\ 0 & 0 & 1 \end{pmatrix} \tag{3b.24}$$

$$\therefore \boldsymbol{\Phi} = \begin{pmatrix} \cos\alpha\cos\beta\cos\gamma - \sin\alpha\sin\gamma & -\cos\alpha\cos\beta\sin\gamma - \sin\alpha\cos\gamma & \cos\alpha\sin\beta \\ \sin\alpha\cos\beta\cos\gamma + \cos\alpha\sin\gamma & -\sin\alpha\cos\beta\sin\gamma + \cos\alpha\cos\gamma & \sin\alpha\sin\beta \\ -\sin\beta\cos\gamma & \sin\beta\sin\gamma & \cos\beta \end{pmatrix}$$

This allows the polarisability tensor in M_{DMA} to be evaluated as a function of the molecule's invariant intrinsic properties and the Euler angles of its orientation:

$$\alpha_{ij}^{\mathrm{M_o M_o}}(-k;k) = \Phi_{i\lambda}\Phi_{j\nu}\,\alpha_{\lambda\nu}^{\mathrm{M_o M_o}}(-k;k) \tag{3b.25}$$

In general, there are nine distinct Cartesian components to M's intrinsic polarisability $\alpha_{\lambda\nu}^{\mathrm{M_o M_o}}(-k;k)$. As a simplified model of molecular response, it is appropriate to neglect off-diagonal ($\delta_{\lambda\nu} = 0$) elements and treat the *y'y'* component as equal to the *x'x'*.

$$\boldsymbol{\alpha}^{\mathrm{M_o M_o}} = \begin{pmatrix} a_{x'x'}^{\mathrm{M_o M_o}} & 0 & 0 \\ 0 & a_{x'x'}^{\mathrm{M_o M_o}} & 0 \\ 0 & 0 & a_{z'z'}^{\mathrm{M_o M_o}} \end{pmatrix} \tag{3b.26}$$

$$\alpha_{ij}^{\mathrm{M_o M_o}}(-k;k) = \left[\Phi_{ix'}\Phi_{jx'} + \Phi_{iy'}\Phi_{jy'}\right]\alpha_{x'x'}^{\mathrm{M_o M_o}}(-k;k) + \Phi_{iz'}\Phi_{jz'}\,\alpha_{z'z'}^{\mathrm{M_o M_o}}(-k;k)$$

This is similar to the assumption of cylindrical symmetry explained in section 3 – molecule M is symmetric with respect to rotation about the *z'* axis. The molecules D and A are described as having perfect cylindrical symmetry and all dipoles lying in the natural axis; but if M were treated in the same manner here, only the *z'z'* component of polarisability would be nonzero. The inclusion of a transverse component $\alpha_{x'x'}^{M_o M_o}(-k;k)$ in the results highlights the RET rate contributions attributable to M's off-axis dipoles.

The Euler angle γ, describing rotation of M about the *z'* axis, is rendered meaningless if the molecular response tensor doesn't discriminate between the *x'* and *y'* axes. For this reason, all functions of γ cancel out of the RET rate calculation.

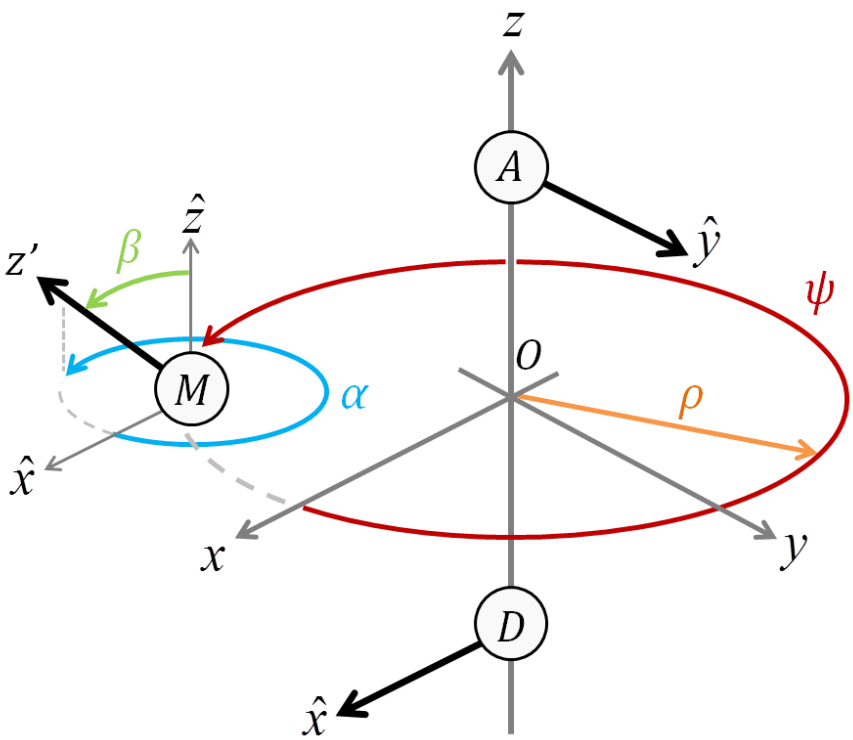

Figure 3b.3: The laboratory-fixed frame is defined with Cartesian coordinates such that molecules D and A lie on the *z*-axis, equidistant from the origin *O*, and have natural dipoles perfectly aligned to the *x* and *y* axes. The molecule M lies on the *xy* plane ($z = 0$) at distance ρ from the *z*-axis and azimuth ψ defined with a right-hand-rule from the *x*-axis. The orientation of M's *z'* axis is described with polar angle β and azimuth α defined similarly to ψ. The angle γ is not shown – it is rotation of M about the *z'* axis.

6. Rate results

6.1 M located on the coordinate origin

The most highly symmetric case is where M is situated midway between D and A, specified by $\rho = 0$. The coordinate ψ has no meaning in this position, and $R_{\mathrm{DM}} = R_{\mathrm{DA}}/2$. Under these conditions, equation (3b.21) yields:

$$\begin{aligned} M_{\mathrm{DMA}}^{\rho=0} &= 2^6 \left(4\pi\varepsilon_0\right)^{-2} \mu^{\mathrm{D_o D_\alpha}} \mu^{\mathrm{A_\beta A_o}} \alpha_{xy}^{\mathrm{M_o M_o}}(-k;k) \\ &\quad \times R_{\mathrm{DA}}^{-6} \exp\left(ikR_{\mathrm{DA}}\right)\left[1-\frac{i}{2}kR_{\mathrm{DA}}-\frac{1}{4}k^2R_{\mathrm{DA}}^2\right]^2 \end{aligned} \tag{3b.27}$$

The polarisability of M has been reduced to one Cartesian component (in the laboratory-fixed frame) by Kronecker deltas in the coupling tensors. This reduces to:

$$\begin{aligned} \alpha_{xy}^{\mathrm{M_o M_o}}(-k;k) &= \left[\Phi_{xx'}\Phi_{yx'}+\Phi_{xy'}\Phi_{yy'}\right]\alpha_{x'x'}^{\mathrm{M_o M_o}}(-k;k)+\Phi_{xz'}\Phi_{yz'}\,\alpha_{z'z'}^{\mathrm{M_o M_o}}(-k;k) \\ &= \left[\alpha_{z'z'}^{\mathrm{M_o M_o}}(-k;k)-\alpha_{x'x'}^{\mathrm{M_o M_o}}(-k;k)\right]\sin\alpha\cos\alpha\sin^2\beta \end{aligned} \tag{3b.28}$$

The orientation function indicates that RET is forbidden where $\beta \in \{0,\ \pi\}$, or where $\alpha \in \{0,\ \pi/2,\ \pi,\ 3\pi/2\}$. These are the cases of $\kappa_3^2 = 0$ for some process of direct RET from D to M, or from M to A. Conversely, the optimum M orientations are found at $\beta = \pi/2$, with $\alpha \in \{\pi/4,\ 3\pi/4,\ 5\pi/4,\ 7\pi/4\}$. These are the cases of the *z'* axis being coplanar to the D and A dipoles and at dihedral angles of 45° to both, such that the two κ_3^2 values are equal. Curiously, the orientation function is independent of kR_{DA}, unlike in the following subsections.

The Fermi rate of RET is proportional to the square modulus of this quantum amplitude:

$$\begin{aligned} \left|M_{\mathrm{DMA}}^{\rho=0}\right|^2 = \ & 16\left(4\pi\varepsilon_0\right)^{-4}\left|\mu^{\mathrm{D_o D_\alpha}}\right|^2\left|\mu^{\mathrm{A_\beta A_o}}\right|^2\left|\alpha_{z'z'}^{\mathrm{M_o M_o}}(-k;k)-\alpha_{x'x'}^{\mathrm{M_o M_o}}(-k;k)\right|^2 \\ & \times R_{\mathrm{DA}}^{-12}\left|4-2ikR_{\mathrm{DA}}-k^2R_{\mathrm{DA}}^2\right|^4 \sin^2\alpha\,\cos^2\alpha\,\sin^4\beta \end{aligned} \tag{3b.29}$$

6.2 The three molecules mutually equidistant

The radial displacement value $\rho = \left(\sqrt{3}/2\right) R_{\mathrm{DA}}$ is a case of particular significance, as this has the three molecules mutually equidistant, $R_{\mathrm{DA}} = R_{\mathrm{DM}} = R_{\mathrm{MA}}$. The three positions form an equilateral triangle, which is a natural result of close-packing for molecules of approximately equal size.

$$M_{\mathrm{DMA}}^{R_{\mathrm{DM}}=R_{\mathrm{DA}}} = \left(4\pi\varepsilon_0\right)^{-2} \exp\left(2ikR_{\mathrm{DA}}\right) R_{DA}^{-6} \;\; \mu^{\mathrm{D_o D_\alpha}} \mu^{\mathrm{A_\beta A_o}} \; D_i \, A_j \, \alpha_{ij}^{\mathrm{M_o M_o}}(-k;k) \tag{3b.30}$$

A full expansion of the polarisability and coupling tensors is required. The tensor part of amplitude (3b.30) expands according to the polarisability equation (3b.26).

$$\begin{aligned} D_i \, A_j \, \alpha_{ij}^{\mathrm{M_o M_o}}(-k;k) = \quad & \alpha_{x'x'}^{\mathrm{M_o M_o}}(-k;k) \left[D_i A_j \Phi_{ix'} \Phi_{jx'} + D_i A_j \Phi_{iy'} \Phi_{jy'} \right] \\ & + \alpha_{z'z'}^{\mathrm{M_o M_o}}(-k;k) \; D_i A_j \Phi_{iz'} \Phi_{jz'} \end{aligned} \tag{3b.31}$$

Each of these three terms has a dimensionless coefficient, whose general form is:

$$D_i A_j \Phi_{i\lambda} \Phi_{j\nu} = \left(D_x \Phi_{x\lambda} + D_y \Phi_{y\lambda} + D_z \Phi_{z\lambda} \right) \left(A_x \Phi_{x\nu} + A_y \Phi_{y\nu} + A_z \Phi_{z\nu} \right) \tag{3b.32}$$

In the present case, the coefficients of (3b.31) are calculated by finding the correct forms of **D** and **A**. The equations (3b.22) must be solved by specifying $\rho = \left(\sqrt{3}/2\right) R_{\mathrm{DA}}$ and $R_{\mathrm{DM}} = R_{\mathrm{DA}}$.

$$\begin{aligned} D_x &= \left(1 - ikR_{\mathrm{DA}}\right)\left(1 - \left(9/4\right)\cos^2\psi\right) - k^2 R_{\mathrm{DA}}^2 \left(1 - \left(3/4\right)\cos^2\psi\right) \\ D_y &= \left(3/4\right)\left[\left(1 - ikR_{\mathrm{DA}}\right)\left(-3\sin\psi\cos\psi\right) - k^2 R_{\mathrm{DA}}^2 \left(-\sin\psi\cos\psi\right)\right] \\ D_z &= \left(\sqrt{3}/4\right)\left[\left(1 - ikR_{\mathrm{DA}}\right)\left(-3\cos\psi\right) - k^2 R_{\mathrm{DA}}^2 \left(-\cos\psi\right)\right] \\ A_x &= \left(3/4\right)\left[\left(1 - ikR_{\mathrm{DA}}\right)\left(3\cos\psi\sin\psi\right) - k^2 R_{\mathrm{DA}}^2 \left(\cos\psi\sin\psi\right)\right] \\ A_y &= \left(1 - ikR_{\mathrm{DA}}\right)\left(1 - \left(9/4\right)\sin^2\psi\right) - k^2 R_{\mathrm{DA}}^2 \left(1 - \left(3/4\right)\sin^2\psi\right) \\ A_z &= \left(\sqrt{3}/4\right)\left[\left(1 - ikR_{\mathrm{DA}}\right)\left(3\sin\psi\right) - k^2 R_{\mathrm{DA}}^2 \left(\sin\psi\right)\right] \end{aligned} \tag{3b.33}$$

Substitution of these components into equation (3b.32) with $\lambda = \nu = x'$ gives the solution for the first coefficient:

$$
\begin{aligned}
&D_i A_j \Phi_{ix'} \Phi_{jx'} = \\
&\{\ \left[\left(1-(9/4)\cos^2\psi\right)-ikR_{\mathrm{DA}}\left(1-(9/4)\cos^2\psi\right)-k^2R_{\mathrm{DA}}^2\left(1-(3/4)\cos^2\psi\right)\right] \\
&\quad\times\left(\cos\alpha\cos\beta\cos\gamma-\sin\alpha\sin\gamma\right) \\
&\quad+(3/4)\left[-3+3ikR_{\mathrm{DA}}+k^2R_{\mathrm{DA}}^2\right]\sin\psi\cos\psi\left(\sin\alpha\cos\beta\cos\gamma+\cos\alpha\sin\gamma\right) \\
&\quad-\left(\sqrt{3}/4\right)\left[-3+3ikR_{\mathrm{DA}}+k^2R_{\mathrm{DA}}^2\right]\cos\psi\left(\sin\beta\cos\gamma\right)\ \} \\
&\times\{\ \left[\left(1-(9/4)\sin^2\psi\right)-ikR_{\mathrm{DA}}\left(1-(9/4)\sin^2\psi\right)-k^2R_{\mathrm{DA}}^2\left(1-(3/4)\sin^2\psi\right)\right] \\
&\quad\times\left(\sin\alpha\cos\beta\cos\gamma+\cos\alpha\sin\gamma\right) \\
&\quad+(3/4)\left[-3+3ikR_{\mathrm{DA}}+k^2R_{\mathrm{DA}}^2\right]\sin\psi\cos\psi\left(\cos\alpha\cos\beta\cos\gamma-\sin\alpha\sin\gamma\right) \\
&\quad+\left(\sqrt{3}/4\right)\left[-3+3ikR_{\mathrm{DA}}+k^2R_{\mathrm{DA}}^2\right]\sin\psi\left(\sin\beta\cos\gamma\right)\ \}
\end{aligned}
\tag{3b.34}
$$

The angle γ has been included at this stage of calculation, even though it is sure to cancel out of the final result. The other two coefficients of (3b.31) are calculated by repeating the substitution with different unit vectors λ and ν.

$$
\begin{aligned}
&D_i A_j \Phi_{iy'} \Phi_{jy'} = \\
&\{\ \left[\left(1-(9/4)\cos^2\psi\right)-ikR_{\mathrm{DA}}\left(1-(9/4)\cos^2\psi\right)-k^2R_{\mathrm{DA}}^2\left(1-(3/4)\cos^2\psi\right)\right] \\
&\quad\times\left(-\cos\alpha\cos\beta\sin\gamma-\sin\alpha\cos\gamma\right) \\
&\quad+(3/4)\left[-3+3ikR_{\mathrm{DA}}+k^2R_{\mathrm{DA}}^2\right]\sin\psi\cos\psi\left(-\sin\alpha\cos\beta\sin\gamma+\cos\alpha\cos\gamma\right) \\
&\quad+\left(\sqrt{3}/4\right)\left[-3+3ikR_{\mathrm{DA}}+k^2R_{\mathrm{DA}}^2\right]\cos\psi\left(\sin\beta\sin\gamma\right)\ \} \\
&\times\{\ \left[\left(1-(9/4)\sin^2\psi\right)-ikR_{\mathrm{DA}}\left(1-(9/4)\sin^2\psi\right)-k^2R_{\mathrm{DA}}^2\left(1-(3/4)\sin^2\psi\right)\right] \\
&\quad\times\left(-\sin\alpha\cos\beta\sin\gamma+\cos\alpha\cos\gamma\right) \\
&\quad+(3/4)\left[-3+3ikR_{\mathrm{DA}}+k^2R_{\mathrm{DA}}^2\right]\sin\psi\cos\psi\left(-\cos\alpha\cos\beta\sin\gamma-\sin\alpha\cos\gamma\right) \\
&\quad-\left(\sqrt{3}/4\right)\left[-3+3ikR_{\mathrm{DA}}+k^2R_{\mathrm{DA}}^2\right]\sin\psi\left(\sin\beta\sin\gamma\right)\ \}
\end{aligned}
\tag{3b.35}
$$

$$
\begin{aligned}
&D_i A_j \Phi_{iz'} \Phi_{jz'} = \\
&\{\ \left[\left(1-(9/4)\cos^2\psi\right)-ikR_{\mathrm{DA}}\left(1-(9/4)\cos^2\psi\right)-k^2R_{\mathrm{DA}}^2\left(1-(3/4)\cos^2\psi\right)\right] \\
&\quad\times\cos\alpha\sin\beta \\
&\quad+(3/4)\left[-3+3ikR_{\mathrm{DA}}+k^2R_{\mathrm{DA}}^2\right]\sin\psi\cos\psi\sin\alpha\sin\beta \\
&\quad+\left(\sqrt{3}/4\right)\left[-3+3ikR_{\mathrm{DA}}+k^2R_{\mathrm{DA}}^2\right]\cos\psi\cos\beta\ \} \\
&\times\{\ \left[\left(1-(9/4)\sin^2\psi\right)-ikR_{\mathrm{DA}}\left(1-(9/4)\sin^2\psi\right)-k^2R_{\mathrm{DA}}^2\left(1-(3/4)\sin^2\psi\right)\right] \\
&\quad\times\sin\alpha\sin\beta \\
&\quad+(3/4)\left[-3+3ikR_{\mathrm{DA}}+k^2R_{\mathrm{DA}}^2\right]\sin\psi\cos\psi\cos\alpha\sin\beta \\
&\quad-\left(\sqrt{3}/4\right)\left[-3+3ikR_{\mathrm{DA}}+k^2R_{\mathrm{DA}}^2\right]\sin\psi\cos\beta\ \}
\end{aligned}
\tag{3b.36}
$$

To calculate the Fermi rate, it is necessary to further simplify this result. Assume that $a_{x'x'}^{\mathrm{M_o M_o}}(-k;k)=0$, such that the transverse component of polarisability is neglected, so the tensor-contraction (3b.31) reduces to one term:

$$D_i\,A_j\,\alpha_{ij}^{\mathrm{M_o M_o}}(-k;k)=D_iA_j\Phi_{iz'}\Phi_{jz'}\;\alpha_{z'z'}^{\mathrm{M_o M_o}}(-k;k) \tag{3b.37}$$

And also assume that $\beta=\pi/2$, such that the *z'* axis is assumed to be coplanar to the D and A dipoles. Then the remaining coefficient becomes:

$$\begin{aligned}
&D_iA_j\Phi_{iz'}\Phi_{jz'}=\\
&2^{-2}\Big[\quad\left\{-9+9ikR_{\mathrm{DA}}+3k^2R_{\mathrm{DA}}^2\right\}\sin\psi\cos\psi\sin\alpha\\
&\qquad+\left\{\left(4-9\cos^2\psi\right)-ikR_{\mathrm{DA}}\left(4-9\cos^2\psi\right)-k^2R_{\mathrm{DA}}^2\left(4-3\cos^2\psi\right)\right\}\cos\alpha\Big]\\
&\times\Big[\quad\left\{-9+9ikR_{\mathrm{DA}}+3k^2R_{\mathrm{DA}}^2\right\}\sin\psi\cos\psi\cos\alpha\\
&\qquad+\left\{\left(4-9\sin^2\psi\right)-ikR_{\mathrm{DA}}\left(4-9\sin^2\psi\right)-k^2R_{\mathrm{DA}}^2\left(4-3\sin^2\psi\right)\right\}\sin\alpha\Big]
\end{aligned} \tag{3b.38}$$

This delivers a result for RET rate as a function of M's azimuthal position ψ and azimuthal orientation α:

$$\begin{aligned}
&\left|M_{\mathrm{DMA}}^{\beta=\pi/2}\right|^2=\\
&2^{-4}\left(4\pi\varepsilon_0\right)^{-4}R_{DA}^{-12}\;\left|\mu^{\mathrm{D_oD_\alpha}}\right|^2\left|\mu^{\mathrm{A_\beta A_o}}\right|^2\left|\alpha_{z'z'}^{\mathrm{M_oM_o}}(-k;k)\right|^2\\
&\times\Big(\quad\left[\left\{3k^2R_{\mathrm{DA}}^2-9\right\}\sin\psi\cos\psi\sin\alpha+\left\{\left(4-9\cos^2\psi\right)-k^2R_{\mathrm{DA}}^2\left(4-3\cos^2\psi\right)\right\}\cos\alpha\right]^2\\
&\quad+\left[9kR_{\mathrm{DA}}\sin\psi\cos\psi\sin\alpha-kR_{\mathrm{DA}}\left(4-9\cos^2\psi\right)\cos\alpha\right]^2\Big)\\
&\times\Big(\quad\left[\left\{3k^2R_{\mathrm{DA}}^2-9\right\}\sin\psi\cos\psi\cos\alpha+\left\{\left(4-9\sin^2\psi\right)-k^2R_{\mathrm{DA}}^2\left(4-3\sin^2\psi\right)\right\}\sin\alpha\right]^2\\
&\quad+\left[9kR_{\mathrm{DA}}\sin\psi\cos\psi\cos\alpha-kR_{\mathrm{DA}}\left(4-9\sin^2\psi\right)\sin\alpha\right]^2\Big)
\end{aligned} \tag{3b.39}$$

6.3 M located at the apex of a right triangle

The radial displacement value $\rho=R_{\mathrm{DA}}/2$ is also a case of interest: The three positions form a right triangle, with M on the right angle. This has the molecule M positioned on the equator of the spheroid discussed in section 4, such that equation (3b.17) is true. Here, the η function is not affected by small changes the

z-coordinate of M's position, so the results of this subsection are applicable even if relative positions are not precisely defined in the *z*-dimension.

$$M_{\mathrm{DMA}}^{\rho=R_{\mathrm{DA}}/2} = 8\left(4\pi\varepsilon_0\right)^{-2} R_{DA}^{-6} \exp\left(2^{1/2} ikR_{\mathrm{DA}}\right) \mu^{\mathrm{D_o D_\alpha}} \mu^{\mathrm{A_\beta A_o}} D_i \; A_j \; \alpha_{ij}^{\mathrm{M_o M_o}}(-k;k) \qquad (3b.40)$$

Again, the tensor-contraction is evaluated according to equation (3b.31). The three coefficients of (3b.31) are calculated by finding the correct forms of **D** and **A**, by solving the equations (3b.22) for the case of $\rho = R_{\mathrm{DA}}/2$ and $R_{\mathrm{DM}} = 2^{-1/2} R_{\mathrm{DA}}$. This method yields:

$$\begin{aligned}
&D_i A_j \Phi_{ix'} \Phi_{jx'} = \\
&\{ \; \left[\left(1-(3/2)\cos^2\psi\right) - 2^{-1/2} ikR_{DA}\left(1-(3/2)\cos^2\psi\right) - 2^{-1}k^2R_{DA}^2\left(1-(1/2)\cos^2\psi\right)\right] \\
&\quad \times\left(\cos\alpha\cos\beta\cos\gamma - \sin\alpha\sin\gamma\right) \\
&\quad + 2^{-1}\left[-3+3\times 2^{-1/2} ikR_{DA} + 2^{-1}k^2R_{DA}^2\right]\sin\psi\cos\psi\left(\sin\alpha\cos\beta\cos\gamma + \cos\alpha\sin\gamma\right) \\
&\quad - 2^{-1}\left[-3+3\times 2^{-1/2} ikR_{DA} + 2^{-1}k^2R_{DA}^2\right]\cos\psi\left(\sin\beta\cos\gamma\right) \; \} \qquad (3b.41) \\
&\times\{ \; \left[\left(1-(3/2)\sin^2\psi\right) - 2^{-1/2} ikR_{DA}\left(1-(3/2)\sin^2\psi\right) - 2^{-1}k^2R_{DA}^2\left(1-(1/2)\sin^2\psi\right)\right] \\
&\quad \times\left(\sin\alpha\cos\beta\cos\gamma + \cos\alpha\sin\gamma\right) \\
&\quad + 2^{-1}\left[-3+3\times 2^{-1/2} ikR_{DA} + 2^{-1}k^2R_{DA}^2\right]\sin\psi\cos\psi\left(\cos\alpha\cos\beta\cos\gamma - \sin\alpha\sin\gamma\right) \\
&\quad + 2^{-1}\left[-3+3\times 2^{-1/2} ikR_{DA} + 2^{-1}k^2R_{DA}^2\right]\sin\psi\left(\sin\beta\cos\gamma\right) \; \}
\end{aligned}$$

$$\begin{aligned}
&D_i A_j \Phi_{iy'} \Phi_{jy'} = \\
&\{ \; \left[\left(1-(3/2)\cos^2\psi\right) - 2^{-1/2} ikR_{DA}\left(1-(3/2)\cos^2\psi\right) - 2^{-1}k^2R_{DA}^2\left(1-(1/2)\cos^2\psi\right)\right] \\
&\quad \times\left(-\cos\alpha\cos\beta\sin\gamma - \sin\alpha\cos\gamma\right) \\
&\quad + 2^{-1}\left[-3+3\times 2^{-1/2} ikR_{DA} + 2^{-1}k^2R_{DA}^2\right]\sin\psi\cos\psi\left(\cos\alpha\cos\gamma - \sin\alpha\cos\beta\sin\gamma\right) \\
&\quad + 2^{-1}\left[-3+3\times 2^{-1/2} ikR_{DA} + 2^{-1}k^2R_{DA}^2\right]\cos\psi\left(\sin\beta\sin\gamma\right) \; \} \qquad (3b.42) \\
&\times\{ \; \left[\left(1-(3/2)\sin^2\psi\right) - 2^{-1/2} ikR_{DA}\left(1-(3/2)\sin^2\psi\right) - 2^{-1}k^2R_{DA}^2\left(1-(1/2)\sin^2\psi\right)\right] \\
&\quad \times\left(-\sin\alpha\cos\beta\sin\gamma + \cos\alpha\cos\gamma\right) \\
&\quad - 2^{-1}\left[-3+3\times 2^{-1/2} ikR_{DA} + 2^{-1}k^2R_{DA}^2\right]\sin\psi\cos\psi\left(\cos\alpha\cos\beta\sin\gamma + \sin\alpha\cos\gamma\right) \\
&\quad - 2^{-1}\left[-3+3\times 2^{-1/2} ikR_{DA} + 2^{-1}k^2R_{DA}^2\right]\sin\psi\left(\sin\beta\sin\gamma\right) \; \}
\end{aligned}$$

$$
\begin{aligned}
&D_i A_j \Phi_{iz'} \Phi_{jz'} = \\
&\{\ \left[\left(1-(3/2)\cos^2\psi\right)-2^{-1/2}ikR_{DA}\left(1-(3/2)\cos^2\psi\right)-2^{-1}k^2R_{DA}^2\left(1-(1/2)\cos^2\psi\right)\right] \\
&\quad\times(\cos\alpha\sin\beta) \\
&\quad+2^{-1}\left[-3+3\times2^{-1/2}ikR_{DA}+2^{-1}k^2R_{DA}^2\right]\sin\psi\cos\psi(\sin\alpha\sin\beta) \\
&\quad+2^{-1}\left[-3+3\times2^{-1/2}ikR_{DA}+2^{-1}k^2R_{DA}^2\right]\cos\psi(\cos\beta)\ \} \\
&\times\{\ \left[\left(1-(3/2)\sin^2\psi\right)-2^{-1/2}ikR_{DA}\left(1-(3/2)\sin^2\psi\right)-2^{-1}k^2R_{DA}^2\left(1-(1/2)\sin^2\psi\right)\right] \\
&\quad\times(\sin\alpha\sin\beta) \\
&\quad+2^{-1}\left[-3+3\times2^{-1/2}ikR_{DA}+2^{-1}k^2R_{DA}^2\right]\sin\psi\cos\psi(\cos\alpha\sin\beta) \\
&\quad-2^{-1}\left[-3+3\times2^{-1/2}ikR_{DA}+2^{-1}k^2R_{DA}^2\right]\sin\psi(\cos\beta)\ \}
\end{aligned}
\tag{3b.43}
$$

As in the previous subsection, it is necessary to simplify this result in order to calculate the Fermi rate. It is now assumed that $a_{x'x'}^{\mathrm{M_o M_o}}(-k;k)=0$, and $\beta=\pi/2$. The tensor-contraction in (3b.40) reduces to one term, specified by (3b.37). The coefficient in the $\rho=R_{\mathrm{DA}}/2$ case is:

$$
\begin{aligned}
&D_i A_j \Phi_{iz'} \Phi_{jz'} \\
&=2\{\ \left[\left(2-3\cos^2\psi\right)-2^{-1/2}ikR_{DA}\left(2-3\cos^2\psi\right)-2^{-1}k^2R_{DA}^2\left(2-\cos^2\psi\right)\right]\cos\alpha \\
&\quad+\left[-3+3\times2^{-1/2}ikR_{DA}+2^{-1}k^2R_{DA}^2\right]\sin\psi\cos\psi\sin\alpha\ \} \\
&\times\{\ \left[\left(2-3\sin^2\psi\right)-2^{-1/2}ikR_{DA}\left(2-3\sin^2\psi\right)-2^{-1}k^2R_{DA}^2\left(2-\sin^2\psi\right)\right]\sin\alpha \\
&\quad+\left[-3+3\times2^{-1/2}ikR_{DA}+2^{-1}k^2R_{DA}^2\right]\sin\psi\cos\psi\cos\alpha\ \}
\end{aligned}
\tag{3b.44}
$$

This delivers a result for RET rate as a function of M's azimuthal position ψ and azimuthal orientation α:

$$
\begin{aligned}
&\left|M_{\mathrm{DMA}}^{\beta=\pi/2}\right|^2 = \\
&16\left(4\pi\varepsilon_0\right)^{-4}R_{DA}^{-12}\left|\mu^{\mathrm{D_o D_\alpha}}\right|^2\left|\mu^{\mathrm{A_\beta A_o}}\right|^2\left|\alpha_{z'z'}^{\mathrm{M_o M_o}}(-k;k)\right|^2 \\
&\times\Big(\ \left[\left\{2-3\cos^2\psi-2^{-1}k^2R_{DA}^2\left(2-\cos^2\psi\right)\right\}\cos\alpha+\left\{2^{-1}k^2R_{DA}^2-3\right\}\sin\psi\cos\psi\sin\alpha\right]^2 \\
&\quad+\left[-2^{-1/2}kR_{DA}\left(2-3\cos^2\psi\right)\cos\alpha+3\times2^{-1/2}kR_{DA}\sin\psi\cos\psi\sin\alpha\right]^2\Big) \\
&\times\Big(\ \left[\left\{2-3\sin^2\psi-2^{-1}k^2R_{DA}^2\left(2-\sin^2\psi\right)\right\}\sin\alpha+\left\{2^{-1}k^2R_{DA}^2-3\right\}\sin\psi\cos\psi\cos\alpha\right]^2 \\
&\quad+\left[-2^{-1/2}kR_{DA}\left(2-3\sin^2\psi\right)\sin\alpha+3\times2^{-1/2}kR_{DA}\sin\psi\cos\psi\cos\alpha\right]^2\Big)
\end{aligned}
\tag{3b.45}
$$

Equation (3b.45) is a continuous function of the M's positional coordinate ψ, M's orientational coordinate α, and the donor-acceptor distance R_{DA}.

The left column of Figure 3b.4 at the end of this chapter shows the output of this function for choice values of the dimensionless scalar kR_{DA}. A full-motion animated plot has also been produced from the same source images, showing the equation outputs for the full continuum of kR_{DA} values – this animation is available at the online version of ref. [10].

7. Discussion

The "DA" mechanism of direct RET is forbidden in donor-acceptor pairs that have a $\kappa_1 = \kappa_3 = 0$ orthogonal geometry. This fact is so well understood that energy transfer within structured polymers can be precisely controlled by manipulating chromophore orientations.[3] This chapter has outlined an additional mechanism which may enable RET in such cases – via the induced dipoles (of transition between the ground state and virtual states) of a nearby polarisable molecule M. In principle, the effects of such additional polarisable chromophores should inform the development of energy transfer systems which rely on precise control of energy flow.

The dependence of RET rate on the precise position and orientation of each chromophore is highly intricate. Just like direct RET is forbidden in the $\kappa_1 = \kappa_3 = 0$ case, the results of this chapter predict very specific geometric conditions where the indirect RET process is either efficient or forbidden. By manipulating chromophore orientation in systems with rigidly-placed chromophores, measurements of energy transfer may test whether equations (3b.29), (3b.39) and (3b.45) correctly describe the higher-order geometric rules. As in the scenarios explored in chapter 3a, the only relevant *intrinsic* property of the chromophore M is the polarisability $\boldsymbol{\alpha}^{M}$. The dependence on k imparted by $\boldsymbol{\alpha}^{M}$ should follow the principles outlined in the polarisability section of chapter 3a.

The "DMA" mechanism must not be confused with two distinct RET steps. The four interaction events all occur as parts of the system's transition F←I, which is considered instantaneous from a macroscopic perspective.The two photons are virtual and the two interactions with chromophore M are of unspecified energy

and time-order – they cannot be meaningfully described as events of $\hbar ck$ absorption followed by $\hbar ck$ emission.

Curiously, the $\rho = 0$ case (section 6.1) shows behaviour similar to the rules governing a beam of light passing through a sequence of polarisers. Consider a beam of unpolarised light propagating upward, which meets a polariser in the horizontal plane aligned to the x axis, then a polariser in the horizontal plane displaced from x by angle α, and finally a polariser in the horizontal plane aligned to the y axis. The efficiency of light transmittance at each interaction is governed by Malus' law – the first polariser shall polarise the beam, the second shall re-align the polarisation and impose a factor of $\cos^2\alpha$ to the beam intensity, and the third shall re-align the polarisation and impose a factor $\cos^2(\alpha - \pi/2)$ of to the beam intensity. The final intensity will be proportional to $(\cos^2\alpha \sin^2\alpha)$; and no transmission can occur if the second polariser is removed. In the RET system of this chapter with $\rho = 0$ and $\beta = \pi/2$, section 6.1 shows that the efficiency of energy transfer is proportional to $(\cos^2\alpha \sin^2\alpha)$; and no transfer can occur if the molecule M is removed.

This kind of correspondence between energy transfer efficiency and the physics of classical waves is to be expected in long-range (radiative) energy transfer processes, as the photons traverse whole wavelengths and may be described as real propagating radiation. But the results of section 6.1 are derived from quantum electrodynamics and are equally valid for short-range RET where the photons are clearly virtual. The Malus dependence on azimuthal orientation of the mediator M is found at all ranges of kR_{DA}, illustrating the essential unity of Förster RET and radiative energy transfer.

[1] B. W. v. d. Meer, "Orientational Aspects in Pair Energy Transfer": *Reson. Energy Transf.*, by D. L. Andrews and Demidov (John Wiley & Sons Ltd, 1999), p. 151.

[2] D.B. VanBeek, M.C. Zwier, J.M. Shorb, and B.P. Krueger, "Fretting about FRET: Correlation between κ and R": *Biophys. J.* **92**, 4168 (n.d.).

[3] S. Ogi, K. Sugiyasu, and M. Takeuchi, "Synthesis and Fluorescence Resonance Energy Transfer Properties of an Alternating Donor–Acceptor Copolymer

Featuring Orthogonally Arrayed Transition Dipoles along the Polymer Backbone": *ACS Macro Lett.* **1**, 1199 (2012).

[4] Akbar Salam, "Mediation of Resonance Energy Transfer by a Third Molecule": *J. Chem. Phys.* **136**, 014509 (2012).

[5] G.D. Scholes, G.R. Fleming, A. Olaya-Castro, and R. van Grondelle, "Lessons from Nature about Solar Light Harvesting": *Nat Chem* **3**, 763 (2011).

[6] G.R. Fleming, G.S. Schlau-Cohen, K. Amarnath, and J. Zaks, "Design Principles of Photosynthetic Light-Harvesting": *Faraday Discuss* **155**, 27 (2012).

[7] D.L. Andrews and G. Juzeliūnas, "Intermolecular Energy Transfer: Retardation Effects": *J. Chem. Phys.* **96**, 6606 (1992).

[8] M.P.E. Lock, D.L. Andrews, and G.A. Jones, "On the Nature of Long Range Electronic Coupling in a Medium: Distance and Orientational Dependence for Chromophores in Molecular Aggregates": *J. Chem. Phys.* **140**, (2014).

[9] H. Langhals, A.J. Esterbauer, A. Walter, E. Riedle, and I. Pugliesi, "Förster Resonant Energy Transfer in Orthogonally Arranged Chromophores": *J. Am. Chem. Soc.* **132**, 16777 (2010).

[10] J.S. Ford and D.L. Andrews, "Geometrical Effects on Resonance Energy Transfer between Orthogonally-Oriented Chromophores, Mediated by a Nearby Polarisable Molecule": *Chem. Phys. Lett.* **591**, 88 (2014).

[11] D.L. Andrews and J.S. Ford, "Resonance Energy Transfer: Influence of Neighboring Matter Absorbing in the Wavelength Region of the Acceptor": *J. Chem. Phys.* **139**, (2013).

[12] Daniels, Gareth J. and Andrews, David L., "The Electronic Influence of a Third Body on Resonance Energy Transfer (Corrected Article)": *J. Chem. Phys.* **117**, 6882 (2002).

[13] D. L. Andrews and D. S. Bradshaw, "Virtual Photons, Dipole Fields and Energy Transfer: A Quantum Electrodynamical Approach": *Eur. J. Phys.* **25**, 845 (2004).

[14] G. Juzeliūnas and D.L. Andrews, "Quantum Electrodynamics of Resonance Energy Transfer": *Adv. Chem. Phys.* **112**, 357 (2007).

[15] D.L. Andrews, "Mechanistic Principles and Applications of Resonance Energy Transfer": *Can. J. Chem.* **86**, 855 (2008).

[16] Akbar Salam, *Molecular Quantum Electrodynamics: Long-Range Intermolecular Interactions* (Wiley, Hoboken, NJ, 2010).

[17] F. Terenziani, C. Katan, E. Badaeva, S. Tretiak, and M. Blanchard-Desce, "Enhanced Two-Photon Absorption of Organic Chromophores: Theoretical and Experimental Assessments": *Adv. Mater.* **20**, 4641 (2008).

[18] J. Del Nero, F.M. de Souza, and R.B. Capaz, "Molecular Electronics Devices: A Short Review": *J. Comput. Theor. Nanosci.* **7**, 503 (2010).

[19] K.S. Suslick, C.T. Chen, G.R. Meredith, and L.T. Cheng, "Push-Pull Porphyrins as Nonlinear Optical Materials": *J. Am. Chem. Soc.* **114**, 6928 (1992).

[20] R. N. Zare, *Angular Momentum* (Wiley, New York, 1988).

–

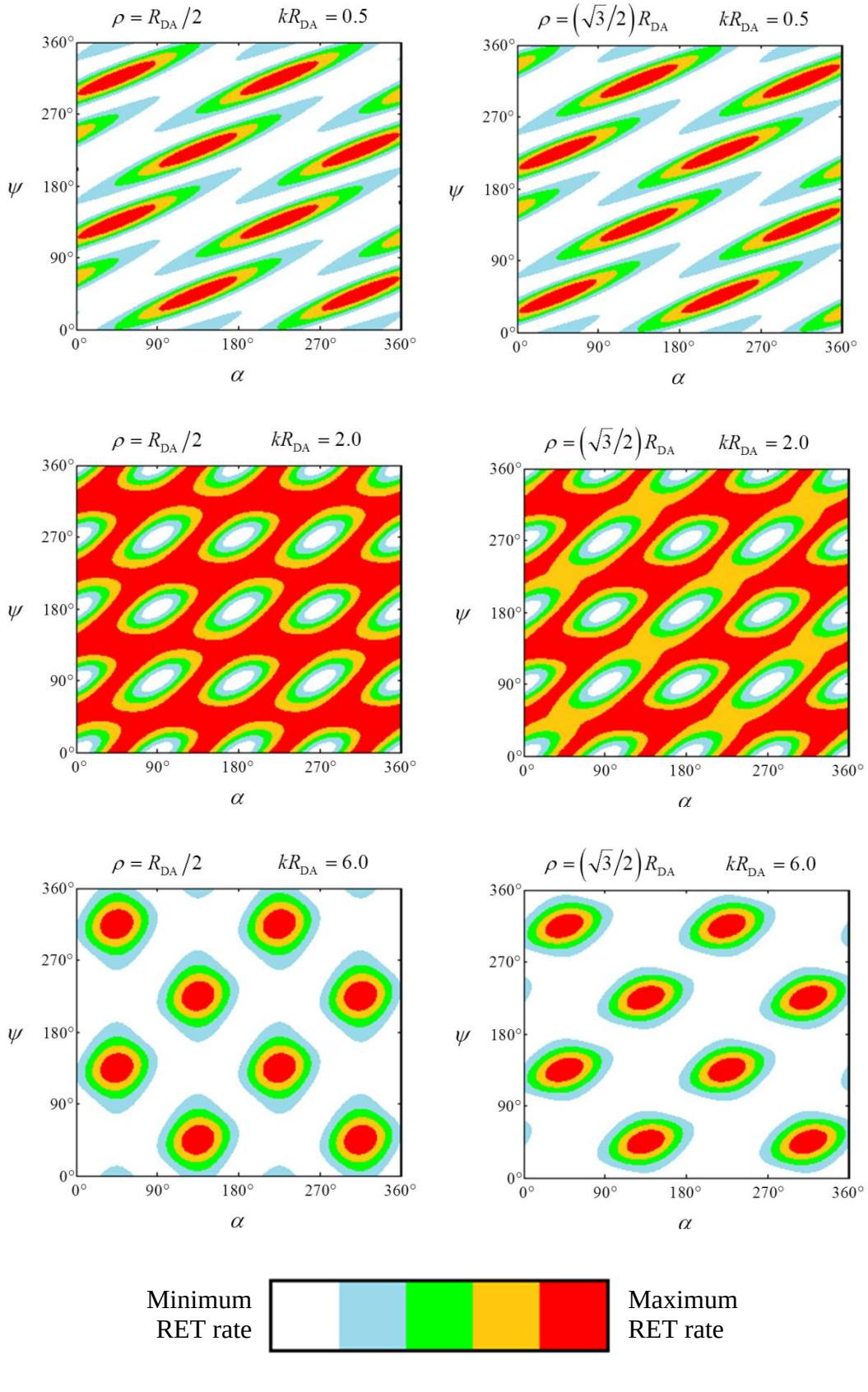

Figure 3b.4: Colour-spectrum plots of mediated-RET rate, plotted as a function of M's azimuthal position ψ and azimuthal orientation α, for choice values of the distance ρ and the dimensionless scalar kR_{DA}. At left, $\rho = R_{DA}/2$, plotting equation (3b.45); at right, $\rho = (\sqrt{3}/2)R_{DA}$, plotting equation (3b.39).

Chapter 4: **Emission by multi-chromophore complexes**

4a: **Excitation delocalised between a pair of emitters**

1. Introduction

The MQED theory and calculation-methods used throughout this thesis are of general application, such that the electrodynamical behaviour of metal nanoantennas may be validly approximated as the photonic interactions of chromophores. Nanoparticles may become emitters or detectors of radiation due to the attachment of fluorescent molecules, or the excitation of plasmon resonances on the metal surface, and a close pair of nanoemitters may be expected to exhibit special QED effects.[1] This chapter explores the properties of emitted radiation from such a pair, in particular investigating the distinctive features attributable to electromagnetic coupling between them and with the photodetector.

The advanced features of coupled emitter pairs is a question of current research interest.[2–4] Metal nanoantenna technology underpins miniaturised radio-frequency antenna,[5–7] enhancement of fluorescence[8–10] and resonance energy transfer (RET)[9,11], and optimising data yield in fluorescence microscopy.[12] The conventional approach has focused on either detailed modelling of a single antenna, or the emergent activity of an ordered array.[13–15] This chapter specifically concerns a pair of coupled emitters, such that the inter-emitter interactions are significant but do not comprise the kind of mass cooperation found in an array.[16]

By treating the emitters and detector as a three-chromophore photonic system, advanced quantum effects arise from the electromagnetic coupling between emitter and detector. An important property of modern gold nanoantenna systems is their ability to modify the directionality of their emission based on emitter-detector coupling strength.[17–22] The MQED analysis of this chapter delivers robust predictions of detected signal intensity and phase, at close range (as detected by a near-field microscope) or in the wave zone (as detected by a remote photodetector).[23,24]

2. System Specification

The system under consideration in this chapter consists of two emitter chromophores, herein labelled A and B, and a detector (energy acceptor) chromophore labelled D. The MQED framework is compatible with a variety of very different physical systems, and this versatility allows the results from this chapter's simplified calculations to be applied to arbitrary nanoemitters and photodetectors.

The emission and detection of radiation is equivalent to the radiative transfer of energy from the emitter pair to D. The initial state I with the energy on the emitters depends on whether this excitation is localised on one of them, or shared between both – the following sections explore these two possibilities separately. Regardless, the process of emission and detection ends with a final state F, where A and B are both relaxed to their ground states 0, and D is excited (however briefly) to a higher-energy state labelled γ.

$$\left|F\right\rangle = \left|A_0, B_0\right\rangle \left|D_\gamma\right\rangle \tag{4a.1}$$

Overall energy conservation, $E_\mathrm{I} = E_\mathrm{F}$, demands that the energy given up by the emitters must be equal to the relative energy of the detector's excited state γ, and this quantity defines the ideal wavevector magnitude k:

$$\hbar ck = E_\gamma^D - E_0^D \tag{4a.2}$$

If the transferred energy $\hbar ck$ is considered to be the emission and reception of real radiation, then it shall have wavelength $2\pi k^{-1}$. The requirement that D is capable of absorbing such radiation is equivalent to assuming the existence of a molecular stationary state γ, even if it is short-lived.

The Cartesian coordinate system's origin is chosen to be at the point midway between A and B; the x-axis passes through both A and B; the z-axis passes through D. The two emitters are thus assumed to be equidistant from D, but this distance R_AD and the separation between the pair, R_AB, are unspecified variables relative to the ideal wavelength $2\pi k^{-1}$. The relevant transition dipole moments of the emitters, $\boldsymbol{\mu}^\mathrm{A}$ and $\boldsymbol{\mu}^\mathrm{B}$, are assumed to be parallel, and oriented according to polar angle θ and azimuth ϕ. The dipole moment of the detector, $\boldsymbol{\mu}^\mathrm{D}$, is limited to the horizontal xy plane with azimuth ψ, consistent with a feasible experimental

setup involving a polarized photodetector lowered from above. Figure 4a.1 illustrates this system geometry.

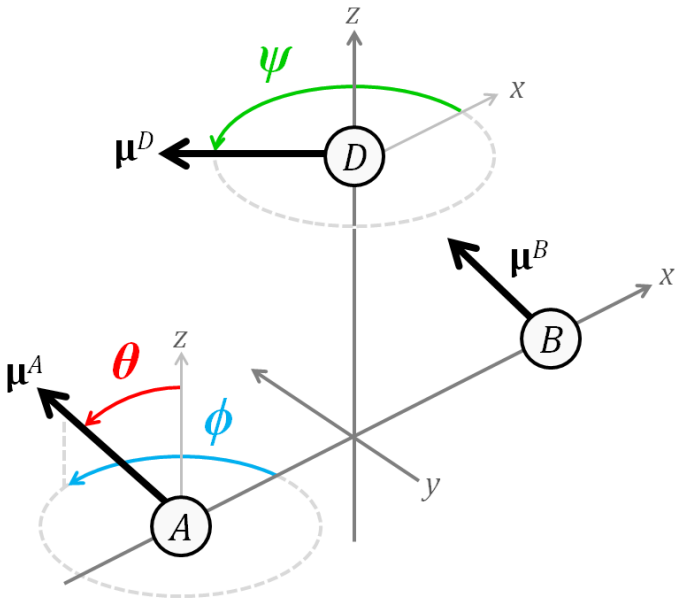

Figure 4a.1: The geometric variables R_{AB}, R_{OD}, ψ, θ, and ϕ define the relative position and orientations of the emitters A and B and the detector D. The Cartesian coordinate system is fixed accordingly.

The assumptions of parallel emitter dipoles and the emitters being equally distant from D are both intended to maximise pairwise coupling so that novel quantum effects will be most apparent, and to increase the system's symmetry for ease of calculation. In particular, it must be considered that the distance $R_{AD} = R_{BD}$ and this crucial coupling variable may be controlled by direct experimental manipulation of the *z*-coordinate (altitude) of D, labelled R_{OD}.

The first part of this chapter concerns the simple transfer of excitation from chromophore A to chromophore D, modified by the nearby third body B – this is directly equivalent to the three-body RET of chapters 3a and 3b, but the focus here is on making the theory applicable to a system of real nanoemitters and a photodetector. Completely unrelated quantum mechanical features appear when the emitter pair is instead treated as one unit, with the individual states of A and B left unspecified.[25] The framing of the Dirac kets in equation (4a.1) is intended to facilitate this analysis.

This chapter does not directly address cases with both emitters being initially excited, $|A_m, B_m\rangle$. In brief, the emission-and-detection process involves transfer of $\hbar ck$ energy from A to B and transfer of $2\hbar ck$ from A to D; or the same with A and B reversed; or simultaneous transfer of $\hbar ck$ to D from each emitter. The latter coupling configuration is equivalent to energy pooling.[26–29]

3. Excitation localized on one emitter

3.1 Quantum amplitudes

If excitation is localized on one of the emitters, the system's initial state I is as follows. In the language of energy transfer employed in the previous chapters, one emitter – in this example, A – must initially occupy an excited state labelled *m*, while the second emitter and D are each in a ground state labelled 0.

$$|I\rangle = |D_0\rangle |A_m, B_0\rangle \tag{4a.3}$$

$$\hbar ck = E_m^A - E_0^A \tag{4a.4}$$

Equations (4a.2) and (4a.4) together ensure overall energy conservation. The quantum amplitude of the A-to-D energy transfer process is given by the same sum-over-mechanisms explained in chapter 3a of this thesis, and in ref. [30]. This amplitude is labeled M_{A}, whereas M_{B} would be the amplitude for the identical B-to-D transfer process.

$$M_{\mathrm{A}} = M_{\mathrm{DA}} + M_{\mathrm{DAB}} + M_{\mathrm{DBA}} + M_{\mathrm{BDA}} \tag{4a.5}$$

There are four coupling configurations, each connecting the same initial state I to the final state F, defined in both parts of chapter 3. Selection rules for the electronic transitions may forbid certain mechanisms, in which case those components will be vanishing. The first and leading term is the amplitude of direct RET-like coupling. In this application, it is written as:

$$M_{\mathrm{DA}} = \mu_i^{D_\gamma D_0}\, V_{ij}\left(k; \mathbf{R}_{\mathrm{DA}}\right) \mu_j^{A_0 A_m} \tag{4a.6}$$

The other three terms are fourth-order amplitudes for mechanisms involving coupling to B. These are the lowest-order of the many possible amplitude contributions that depend on the relative position and orientation of B.

$$
\begin{aligned}
M_{\mathrm{DAB}} &= \mu_i^{D_\gamma D_0}\, V_{ij}\left(k;\mathbf{R}_{\mathrm{DA}}\right)\, \alpha_{jk}^{A_0 A_m}(-k;0)\, V_{kl}\left(0;\mathbf{R}_{\mathrm{AB}}\right)\, \mu_l^{B_0 B_0} \\
M_{\mathrm{DBA}} &= \mu_i^{D_\gamma D_0}\, V_{ij}\left(k;\mathbf{R}_{\mathrm{DB}}\right)\, \alpha_{jk}^{B_0 B_0}(-k;k)\, V_{kl}\left(k;\mathbf{R}_{\mathrm{AB}}\right)\, \mu_l^{A_0 A_m} \\
M_{\mathrm{BDA}} &= \mu_i^{B_0 B_0}\, V_{ij}\left(0;\mathbf{R}_{\mathrm{DB}}\right)\, \alpha_{jk}^{D_\gamma D_0}(k;0)\, V_{kl}\left(k;\mathbf{R}_{\mathrm{DA}}\right)\, \mu_l^{A_0 A_m}
\end{aligned}
\qquad (4a.7)
$$

The transition polarizabilities $\boldsymbol{\alpha}$ are defined by equation 5.2.7 of ref. [31], or in more detail by equation (3a.6) of this thesis. The general intermolecular coupling tensor, **V**, is defined as in chapters 3a and 3b. If the wavevector argument is zero, such that zero real energy is exchanged, this is described as static coupling.

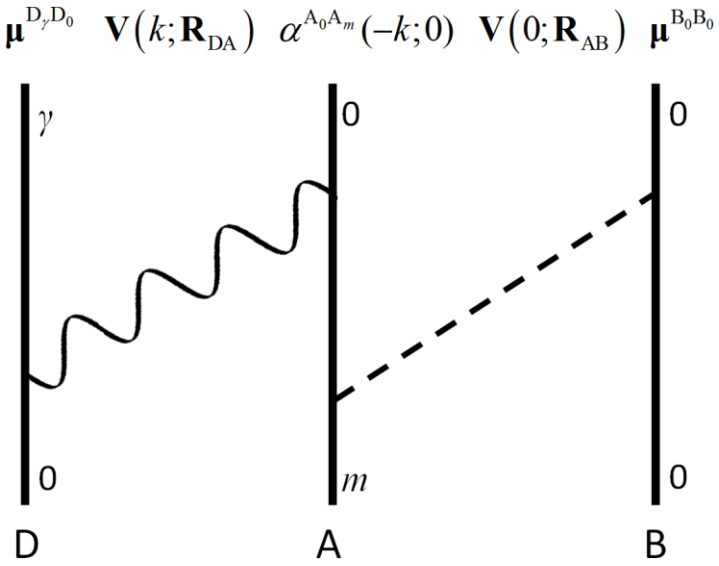

Figure 4a.2: The DAB coupling configuration. Emitter B does not transition, so M_{DAB} involves static A-B coupling, such that A is perturbed by the *permanent* dipole of B and undergoes an $\mathrm{E1}^2$ relaxation.

3.2 Leading signal terms

By the Fermi rule, the rate of energy transfer (in this scenario, the signal strength of detected fluorescence) is proportional to the square modulus of M_{A}. The four amplitude terms thus expand into ten rate (signal) terms as per equation (2a.12), and the leading rate term will be the square modulus of the dominant amplitude, M_{DA}. Of the remaining nine signal terms, the dominant three shall be the quantum interference involving M_{DA}.

$$\begin{aligned}\Gamma_{FI} \propto \left|M_{\mathrm{A}}\right|^2 = \quad & \left|M_{\mathrm{DA}}\right|^2 + 2\,\mathrm{Re}\left(\bar{M}_{\mathrm{DA}} M_{\mathrm{DAB}}\right) \\ & + 2\,\mathrm{Re}\left(\bar{M}_{\mathrm{DA}} M_{\mathrm{DBA}}\right) + 2\,\mathrm{Re}\left(\bar{M}_{\mathrm{DA}} M_{\mathrm{BDA}}\right) + \ldots\end{aligned} \tag{4a.8}$$

The lead term is the square modulus of equation (4a.6).

$$\left|M_{\mathrm{DA}}\right|^2 = \left(4\pi\varepsilon_0\right)^{-2} \left|\boldsymbol{\mu}^{D_\gamma D_0}\right|^2 \left|\boldsymbol{\mu}^{A_0 A_m}\right|^2 \left[\tfrac{1}{4} R_{\mathrm{AB}}^2 + R_{\mathrm{OD}}^2\right]^{-3} \left|S\right|^2 \tag{4a.9}$$

The complex dimensionless scalar labelled *S* is shorthand for the detailed geometric function:

$$\begin{aligned} S = \sin\theta\cos\varphi\cos\psi \Big(& \quad k^2\left[\tfrac{1}{4}R_{AB}^2 + R_{OD}^2\right]\left\{R_{AB}^2\left[R_{AB}^2 + 4R_{OD}^2\right]^{-1} - 1\right\} \\ & + \left\{1 - i\,k\sqrt{\tfrac{1}{4}R_{AB}^2 + R_{OD}^2}\right\}\left\{1 - 3R_{AB}^2\left[R_{AB}^2 + 4R_{OD}^2\right]^{-1}\right\}\Big) \\ & + \sin\theta\sin\varphi\sin\psi\left(1 - k^2\left[\tfrac{1}{4}R_{AB}^2 + R_{OD}^2\right] - i\,k\sqrt{\tfrac{1}{4}R_{AB}^2 + R_{OD}^2}\right) \\ & + \cos\theta\cos\psi\, R_{AB}R_{OD}\left[R_{AB}^2 + 4R_{OD}^2\right]^{-1} \\ & \times\left(k^2\left[\tfrac{1}{4}R_{AB}^2 + R_{OD}^2\right] - 3 + 3i\,k\sqrt{\tfrac{1}{4}R_{AB}^2 + R_{OD}^2}\right) \end{aligned} \tag{4a.10}$$

The variable R_{AD} has been subsumed into R_{OD} and R_{AB}, to reduce redundancy and because these are the length parameters most likely to be readily measurable. Equation (4a.9) is plotted in the upper half of figure 4a.3, in the near-zone, $R_{\mathrm{AB}} << k^{-1}$. With dipoles aligned $\theta = 90°$ and $\phi = \psi = 51.7°$, there is an interesting dependence on R_{OD} that predicts zero signal contribution at $R_{OD} \approx 0.019 k^{-1}$.

The relative magnitudes of the three quantum interference terms of equation (4a.8) will be determined by the same geometric variables as the lead term, but also by the molecule's selection rules for one-photon and two-photon transitions. In equations (4a.6) and (4a.7), the single-photon transition (E1) allowedness is represented by the transition dipole moment **μ**; the two-photon transition ($\mathrm{E1}^2$) allowedness is represented by the transition polarisability **α**.

As an example, if a relaxation process involving two photons is forbidden for emitter A ($\boldsymbol{\alpha}^{A_0 A_m} = 0$) and static coupling is forbidden for emitter B ($\boldsymbol{\mu}^{B_0 B_0} = 0$, i.e. B is nonpolar in its ground state), then M_{DAB} and M_{BDA} will vanish according to equations (4a.7). In this case, the leading signal contribution in rate equation (4a.8) that involves B in any way will be:

$$\begin{aligned} 2\,\mathrm{Re}\left(\bar{M}_{\mathrm{DA}} M_{\mathrm{DBA}}\right) = \quad & 2\left(4\pi\varepsilon_0\right)^{-3} \left|\boldsymbol{\mu}^{D_\gamma D_0}\right|^2 \left|\boldsymbol{\mu}^{A_0 A_m}\right|^2 \left[\tfrac{1}{4} R_{AB}^2 + R_{OD}^2\right]^{-3} R_{AB}^{-3} \\ & \times \mathrm{Re}\left[\exp\left(ikR_{AB}\right) W\ T_j\, U_k\, \alpha_{jk}^{B_0 B_0}\left(-k;k\right)\right] \end{aligned} \tag{4a.11}$$

The complex dimensionless scalar labelled *W* and the complex vectors **T** and **U** are shorthand for detailed geometric functions:

$$\begin{aligned} W &= T_x \sin\theta\cos\phi + T_y \sin\theta\sin\phi - T_z\cos\theta \\ T_x &= \cos\psi\Bigg(\quad k^2\left[\tfrac{1}{4}R_{AB}^2 + R_{OD}^2\right]\left\{R_{AB}^2\left[R_{AB}^2 + 4R_{OD}^2\right]^{-1} - 1\right\} \\ &\qquad + \left\{1 - ik\sqrt{\tfrac{1}{4}R_{AB}^2 + R_{OD}^2}\right\}\left\{1 - 3R_{AB}^2\left[R_{AB}^2 + 4R_{OD}^2\right]^{-1}\right\}\Bigg) \\ T_y &= \sin\psi\left(1 - k^2\left[\tfrac{1}{4}R_{AB}^2 + R_{OD}^2\right] - ik\sqrt{\tfrac{1}{4}R_{AB}^2 + R_{OD}^2}\right) \\ T_z &= \cos\psi\, R_{AB} R_{OD}\left[R_{AB}^2 + 4R_{OD}^2\right]^{-1}\left(3 - k^2\left[\tfrac{1}{4}R_{AB}^2 + R_{OD}^2\right] - 3ik\sqrt{\tfrac{1}{4}R_{AB}^2 + R_{OD}^2}\right) \\ U_x &= \sin\theta\cos\phi\left(-2 + 2ikR_{AB}\right) \\ U_y &= \sin\theta\sin\phi\left(1 - k^2 R_{AB}^2 - ikR_{AB}\right) \\ U_z &= \cos\theta\left(1 - k^2 R_{AB}^2 - ikR_{AB}\right) \end{aligned} \tag{4a.12}$$

Equation (4a.11) is plotted in the lower half of figure 4a.3, with the same abscissa and angles as the upper half. Each coloured curve is the result for a given component of $\boldsymbol{\alpha}^{B_0 B_0}\left(-k;k\right)$. All five components in *z* give a result of zero – this is a consequence of $\theta = 90°$, as induced-dipoles of B oriented in the z-direction produce a $\kappa = 0$ geometry (explained in chapter 3b). The total zero at $R_{\mathrm{OD}} \approx 0.02\,k^{-1}$ arises for the same reasons as in the upper graph, as M_{DA} is of course a factor of $M_{\mathrm{DA}} M_{\mathrm{DBA}}$.

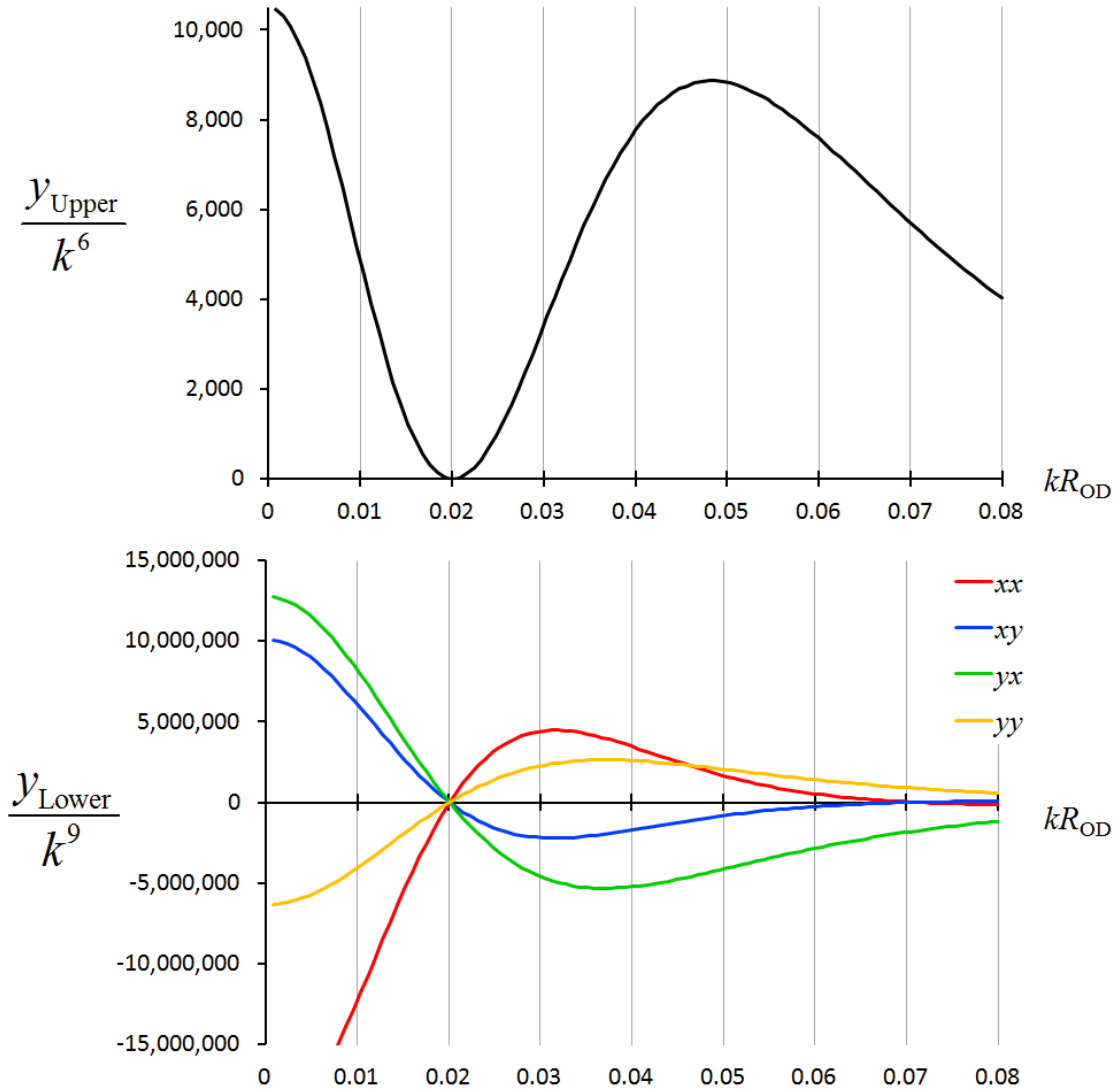

Figure 4a.3:

$$y_{\text{Upper}} = (4\pi)^{-2}\left[\tfrac{1}{4}R_{\text{AB}}^2 + R_{\text{OD}}^2\right]^{-3}\left|S\right|^2$$

$$y_{\text{Lower}} = 2(4\pi)^{-3}\left[\tfrac{1}{4}R_{AB}^2 + R_{OD}^2\right]^{-3} R_{AB}^{-3}\,\text{Re}\left[\exp(ikR_{AB})\,W\,T_j\,U_k\right]$$

The upper graph plots the results of equation (4a.9); the lower graph plots the results of equation (4a.11) for the four nonzero tensor components *jk*. The reduced wavelength k^{-1} is used as the unit of length. The two graphs' shared abscissa illustrates the common zero at $R_{\text{OD}} \approx 0.02\,k^{-1}$.

Both graphs use the values $R_{\text{AB}} = 0.1k^{-1}$; $\theta = 90°$; $\phi = \psi = 51.7°$.

4. Excitation delocalized across the pair

4.1 Combination states

In cases where the coupling between A and B described by tensor $\mathbf{V}(k;R_{AB})$ favours unobserved transfer of excitation prior to the emission-and-detection process, then in the system's initial state I the emitter pair may already be sharing the excitation $\hbar ck$.

An initial state I in which excitation is delocalised between A and B is some superposition combining the state in which m is localised on A (described in the previous section) and the counterpart state in which m is localised on B. The Dirac ket for such an initial state I is found by adding or subtracting the kets of the two component states, and normalising. Addition produces the symmetric exciton, labelled $|I^+\rangle$; subtraction produces the antisymmetric exciton, labelled $|I^-\rangle$.

$$|I^{\pm}\rangle = 2^{-1/2}\,|D_0\rangle\big(\,|A_m,B_0\rangle \pm |A_0,B_m\rangle\,\big) \qquad \text{(4a.13)}$$

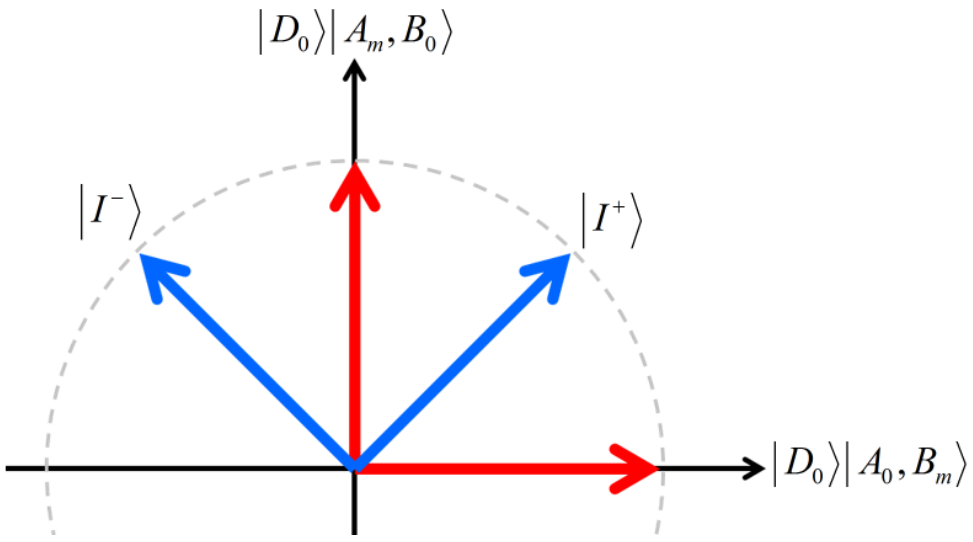

Figure 4a.4: Construction of symmetric (+) and antisymmetric (-) exciton states (blue) as combinations of the localised-excitation states (red). The red vertical arrow is the initial state used in M^A; the horizontal red arrow is the counterpart state with excited B.

Note that these excitons are combination states produced by a superposition of two localised-excitation base states, and are thus an example of *entangled* states. If the two-emitter subsystem is disturbed by a direct measurement of the energy state of A (either A_0 or A_m), then B will necessarily be in the opposite energy state (B_m or B_0, respectively). See ref.[32] and appendix 8d of this thesis for further discussion of the superposition principle at work here.

The emission-and-detection process may proceed from either of the starting points $\left|I^{\pm}\right\rangle$, with the emitter pair initially in an exciton state. The quantum amplitude of such a process, M_+ or M_-, may be derived from equation (4a.13):

$$\begin{aligned} M_{\pm} &= 2^{-1/2}\left\langle D_\gamma\middle|\langle A_0,B_0|\ \{\ldots\}\ |D_0\rangle\right(\left|A_m,B_0\right\rangle \pm \left|A_0,B_m\right\rangle\left) \\ &= 2^{-1/2}\left(\left\langle D_\gamma\middle|\langle A_0,B_0|\ \{\ldots\}\ |D_0\rangle\middle|A_m,B_0\right\rangle \pm \left\langle D_\gamma\middle|\langle A_0,B_0|\ \{\ldots\}\ |D_0\rangle\middle|A_0,B_m\right\rangle\right) \\ &= 2^{-1/2}\left(M_{\mathrm{A}} \pm M_{\mathrm{B}}\right) \end{aligned} \qquad (4a.14)$$

Here, the missing details $\{\ldots\}$ are the rest of the fourth-order term of the perturbative expansion given by equation (2a.13), as only the $\langle F|$ bra and $|I\rangle$ ket have been shown explicitly. Amplitude M_{A} is the result from equation (4a.5) and M_{B} is the amplitude for the counterpart process that begins with excitation localised on B. The latter has exactly the same form as the results of the previous section, only differing in the particular values of $\boldsymbol{\alpha}^{B_0B_m}$ and $\boldsymbol{\mu}^{B_0B_m}$ compared to A's molecular response tensors – and this difference vanishes if the two emitters are chemically similar.

4.2 Degeneracy splitting

Coupling between the two emitters will lead to degeneracy splitting of the symmetric and antisymmetric excitons. The two initial states $\left|I^{+}\right\rangle$ and $\left|I^{-}\right\rangle$ differ in total energy by $2M_{\mathrm{AB}}$, where M_{AB} is the quantum amplitude for RET between A and B. See appendix 8d for a quantum-mechanical justification for this prediction.

$$\begin{aligned} M_{\mathrm{AB}} &= \mu_i^{A_mA_0} V_{ij}\left(k;\mathbf{R}_{AB}\right)\mu_j^{B_0B_m} \\ &= \left(4\pi\varepsilon_0\right)^{-1} R_{AB}^{-3}\exp\left(ikR_{AB}\right)\left|\boldsymbol{\mu}^{A_mA_0}\right|\left|\boldsymbol{\mu}^{B_0B_m}\right| \\ &\quad\times\left\{2\left[ikR_{AB}-1\right]\sin^2\theta\cos^2\phi+\left[1-ikR_{AB}-k^2R_{AB}^2\right]\left(\sin^2\theta\sin^2\phi+\cos^2\theta\right)\right\} \end{aligned} \qquad (4a.15)$$

Recall that equations (4a.2) and (4a.4) define the wavenumber variable *k*. The loss of energy by the emitters is overall equal to the photon energy $\hbar ck$, and to the energy gained by the detector, $E_\gamma^D - E_0^D$.

The difference in energy between symmetric and antisymmetric initial states implies two distinct values of E_γ^D differing by $2M_{\mathrm{AB}}$, and two distinct wavelengths of radiation $2\pi k^{-1}$ because *k* has two values differing by $2M_{\mathrm{AB}}/\hbar c$. It may or may not be possible to experimentally resolve the two different fluorescence signals produced by an emitter pair in these two exciton states. If the energy gap $2M_{\mathrm{AB}}$ is too small to enable resolution of the two signals, then the detected emission rate will be a simple sum of the two indistinguishable emission processes, which reduces to the sum of uncoupled-emission signals from the two individual emitters:

$$\Gamma_{FI} \propto \left|M_+\right|^2 + \left|M_-\right|^2 = \left|M_{\mathrm{A}}\right|^2 + \left|M_{\mathrm{B}}\right|^2 \qquad \text{(4a.16)}$$

But if the detector is capable of distinguishing between emission from the symmetric and antisymmetric excitons, then the two observed signals will be proportional to $\left|M_+\right|^2$ and $\left|M_-\right|^2$ respectively.

4.3 Intensity distribution of antisymmetric emission

Consider the third line of equation (4a.14), in the minus case.

$$\begin{aligned} M_- &= 2^{-1/2}\left(M_{\mathrm{A}} - M_{\mathrm{B}}\right) \\ &= 2^{-1/2}\left[M_{\mathrm{A}} + \exp\left(i\pi\right)M_{\mathrm{B}}\right] \end{aligned} \qquad \text{(4a.17)}$$

If detector D is located equidistant from the two emitters, emitters A and B are chemically similar, and there is a symmetric geometry obeying $\phi \in \{\pi/2,\, 3\pi/2\}$ or $\theta \in \{0,\, \pi\}$, it follows that $M_{\mathrm{A}} = M_{\mathrm{B}}$. Therefore $M_- = 0$, meaning that the emission-and-detection process from the antisymmetric initial state is forbidden. In an experiment that systematically varies the position of D, the existence of this plane of zero detectable signal is diagnostic of the antisymmetric exciton.

This accords with a semiclassical analysis of real dipolar emission by the nanoemitter pair.[1,33] The minus sign in equation (4a.17) may be written as $+e^{i\pi}$ according to Euler's identity, and this can be interpreted to determine the structural character of the real radiation emitted by the pair: in the symmetric exciton state, the two emitters emit waves that are in phase; in the antisymmetric exciton state, the two emitters emit waves with a phase difference of π. It follows from the system's symmetry that if $\phi \in \{\pi/2, 3\pi/2\}$ or $\theta \in \{0, \pi\}$, then symmetry dictates total wave cancellation at the plane of equidistance, so no signal will be received by a detector in this plane.

5. Discussion

The calculations in this chapter show the conditions under which effects of back-coupling and degeneracy splitting may appear in the emission profile of coupled nanoemitters. The inclusion of the fluorescence detector as a "third chromophore", as part of a closed QED system, is necessary to elucidate these pure quantum features of cooperative emission behaviour. This demonstrates the utility of such a rigorous applied-MQED analysis.

If $\phi \in \{\pi/2, 3\pi/2\}$ or $\theta \in \{0, \pi\}$, the emitter pair is symmetric about the $x = 0$ plane (see figure 4a.1). Intuitively, a mirror surface on this plane could produce equivalent emission behaviour with just one emitter interacting with its own reflected image. But the excitation-sharing physics of sections 3 and 4 cannot occur if the state of chromophore B is limited to the reflected image of the state of A, and so the emission profile will not exhibit the quantum features predicted by this chapter. In constructing an MQED model of this mirror-modified emission process, the reflected image of the actual chromophore "A" cannot simply be included as a "chromophore B" because the minimum-interaction description of this process has A coupled to the actual atoms of the mirror.

Each of the four initial excitation states of the emitter pair produces radiation with distinctive characteristics. With excitation localised on a single nanoemitter, electromagnetic coupling with the second unit and the detector results in a fluorescence signal with a particular dependence on the positions, orientations, and static polarizabilities of the three components. With excitation delocalised

across the pair, the result is a signal with wavelength, intensity distribution and phase profile that are all characteristic of an exciton doublet, distinct from single-centre emission.[33]

These results may inform the design of measurements to discriminate between the unique excitation states of a pair of nanoantennas, enabling more precise control in the construction and operation of nano-component systems.

[1] E.M. Rice and D.L. Andrews, "Optical Emission of a Molecular Nanoantenna Pair": *J. Chem. Phys.* **136**, (2012).
[2] J. Evers, M. Kiffner, M. Macovei, and C.H. Keitel, "Geometry-Dependent Dynamics of Two Lambda-Type Atoms via Vacuum-Induced Coherences": *Phys Rev A* **73**, 023804 (2006).
[3] S.I. Schmid and J. Evers, "Dipole-Dipole Interaction between Orthogonal Dipole Moments in Time-Dependent Geometries": *Phys Rev A* **77**, 013822 (2008).
[4] S.I. Schmid and J. Evers, "Interplay of Vacuum-Mediated Inter- and Intra-Atomic Couplings in a Pair of Atoms": *Phys Rev A* **81**, 063805 (2010).
[5] P. Anger, P. Bharadwaj, and L. Novotny, "Enhancement and Quenching of Single-Molecule Fluorescence": *Phys Rev Lett* **96**, 113002 (2006).
[6] L. Novotny, "Effective Wavelength Scaling for Optical Antennas": *Phys Rev Lett* **98**, 266802 (2007).
[7] P. Biagioni, J.-S. Huang, and B. Hecht, "Nanoantennas for Visible and Infrared Radiation": *Rep. Prog. Phys.* **75**, 024402 (2012).
[8] X. Li, F.-J. Kao, C.-C. Chuang, and S. He, "Enhancing Fluorescence of Quantum Dots by Silica-Coated Gold Nanorods under One- and Two-Photon Excitation": *Opt Express* **18**, 11335 (2010).
[9] M. Schmelzeisen, Y. Zhao, M. Klapper, K. Müllen, and M. Kreiter, "Fluorescence Enhancement from Individual Plasmonic Gap Resonances": *ACS Nano* **4**, 3309 (2010).
[10] V.J. Sorger, N. Pholchai, E. Cubukcu, R.F. Oulton, P. Kolchin, C. Borschel, M. Gnauck, C. Ronning, and X. Zhang, "Strongly Enhanced Molecular Fluorescence inside a Nanoscale Waveguide Gap": *Nano Lett.* **11**, 4907 (2011).

[11] S. Batabyal, T. Mondol, K. Das, and S.K. Pal, "Förster Resonance Energy Transfer in a Nanoscopic System on a Dielectric Interface": *Nanotechnology* **23**, 495402 (2012).

[12] D.S. Bradshaw, J.M. Leeder, and D.L. Andrews, "Nonlinear Optical Techniques for Improved Data Capture in Fluorescence Microscopy and Imaging": *Proc. SPIE*, **7571** (2010), p. 0B.

[13] K. Leong, Y. Chen, D.J. Masiello, M.T. Zin, M. Hnilova, H. Ma, C. Tamerler, M. Sarikaya, D.S. Ginger, and A.K.-Y. Jen, "Cooperative Near-Field Surface Plasmon Enhanced Quantum Dot Nanoarrays": *Adv. Funct. Mater.* **20**, 2675 (2010).

[14] J. Abramson, M. Palma, S.J. Wind, and J. Hone, "Quantum Dot Nanoarrays: Self-Assembly With Single-Particle Control and Resolution": *Adv. Mater.* **24**, 2207 (2012).

[15] V.A.G. Rivera, Y. Ledemi, M. El-Amraoui, Y. Messaddeq, and E. Marega, "Resonant near-Infrared Emission of Er3+ Ions in Plasmonic Arrays of Subwavelength Square Holes": *Proc. SPIE*, **8632** (2013), p. 25.

[16] V.E. Lembessis, A. Lyras, A.A. Rsheed, O.M. Aldossary, and Z. Ficek, "Radiation Pattern of Two Identical Emitters Driven by a Laguerre-Gaussian Beam: An Atom Nanoantenna": *Phys Rev A* **92**, 023850 (2015).

[17] G. Vecchi, V. Giannini, and J. Gómez Rivas, "Shaping the Fluorescent Emission by Lattice Resonances in Plasmonic Crystals of Nanoantennas": *Phys Rev Lett* **102**, 146807 (2009).

[18] A.G. Curto, G. Volpe, T.H. Taminiau, M.P. Kreuzer, R. Quidant, and N.F. van Hulst, "Unidirectional Emission of a Quantum Dot Coupled to a Nanoantenna": *Science* **329**, 930 (2010).

[19] A. Devilez, B. Stout, and N. Bonod, "Compact Metallo-Dielectric Optical Antenna for Ultra Directional and Enhanced Radiative Emission": *ACS Nano* **4**, 3390 (2010).

[20] H. Aouani, O. Mahboub, E. Devaux, H. Rigneault, T.W. Ebbesen, and J. Wenger, "Plasmonic Antennas for Directional Sorting of Fluorescence Emission": *Nano Lett.* **11**, 2400 (2011).

[21] Lee K. G., Chen X. W., Eghlidi H., Kukura P., Lettow R., Renn A., Sandoghdar V., and Gotzinger S., "A Planar Dielectric Antenna for Directional Single-Photon Emission and near-Unity Collection Efficiency": *Nat Photon* **5**, 166 (2011).

[22] B. Rolly, B. Stout, and N. Bonod, "Boosting the Directivity of Optical Antennas with Magnetic and Electric Dipolar Resonant Particles": *Opt Express* **20**, 20376 (2012).

[23] D.S. Bradshaw, J.S. Ford, and D.L. Andrews, "On the Detection of Characteristic Optical Emission from Electronically Coupled Nanoemitters": *Proc. SPIE*, **8807** (2013), p. 03.

[24] J.S. Ford, D.S. Bradshaw, and D.L. Andrews, "Signatures of Exciton Coupling in Paired Nanoemitters": *J. Phys. Chem. C* **117**, 12393 (2013).

[25] G. D. Scholes and G. Rumbles, "Excitons in Nanoscale Systems": *Nat. Mater.* **5**, 683 (2006).

[26] D.L. Andrews and R.D. Jenkins, "A Quantum Electrodynamical Theory of Three-Center Energy Transfer for Upconversion and Downconversion in Rare Earth Doped Materials": *J. Chem. Phys.* **114**, 1089 (2001).

[27] C. Hettich, C. Schmitt, J. Zitzmann, S. Kühn, I. Gerhardt, and V. Sandoghdar, "Nanometer Resolution and Coherent Optical Dipole Coupling of Two Individual Molecules": *Science* **298**, 385 (2002).

[28] D.L. Andrews and D.S. Bradshaw, "Optically Nonlinear Energy Transfer in Light-Harvesting Dendrimers": *J. Chem. Phys.* **121**, 2445 (2004).

[29] M.D. LaCount, D. Weingarten, N. Hu, S.E. Shaheen, J. van de Lagemaat, G. Rumbles, D.M. Walba, and M.T. Lusk, "Energy Pooling Upconversion in Organic Molecular Systems": *J. Phys. Chem. A* **119**, 4009 (2015).

[30] Daniels, Gareth J. and Andrews, David L., "The Electronic Influence of a Third Body on Resonance Energy Transfer (Corrected Article)": *J. Chem. Phys.* **117**, 6882 (2002).

[31] D. P. Craig and T. Thirunamachandran, *Molecular Quantum Electrodynamics*, 2nd ed. (Dover Publications, Mineola, New York, 1998).

[32] M. Kasha, H. R. Rawls, and M. Ashraf El-Bayoumi, "The Exciton Model in Molecular Spectroscopy": *Pure Appl. Chem.* **11**, 371 (1965).

[33] E.M. Rice, D.S. Bradshaw, K. Saadi, and D.L. Andrews, "Identifying the Development in Phase and Amplitude of Dipole and Multipole Radiation": *Eur. J. Phys.* **33**, 345 (2012).

–

Chapter 4: **Emission by multi-chromophore complexes**

4b: **Anisotropy of fluorescence in solution**

1. Introduction

For molecules with more than one chromophore, interactions such as fluorescence or RET are complicated by internal dynamics – the exchange or sharing of energy between the constituent chromophores.[1] In addition to the exciton scenario of the previous chapter, a more direct effect of quantum mechanics allows the position of excitation to be physically undetermined *without* explicit delocalisation: the chromophores may share in the probability distribution of not just the excitation location, but of the location of the whole two-interaction fluorescence process.

This chapter concerns single-photon fluorescence, a process whose elementary microscopic description is a one-photon absorption event quickly followed by the emission of one photon from the same chromophore. The analysis is tailored for application to a molecule containing N chemically-identical chromophores in the solution phase, yielding predictions of fluorescence rate and anisotropy. Fluorescence anisotropy values outside the range -0.2 – 0.4 are predicted under certain conditions, which is novel for single-photon fluorescence in an isotropic solution.

2. MQED of fluorescence

The absorption and the re-emission of light are discrete photon-molecule interactions that together comprise the fluorescence mechanism. The MQED description is identical to Rayleigh scattering if no overall molecular transition is described. The effective quantum amplitude of such a two-interaction process is delivered by the second term of equation (2a.13).

$$M_{FI} = \sum_R \frac{\langle F | H_{\text{int}} | R \rangle \langle R | H_{\text{int}} | I \rangle}{E_I - E_R} \tag{4b.1}$$

The double Dirac bracket is evaluated, using an E1 (electric dipole) approximation, as the scalar product of a linear electric displacement with the relevant molecular response:

$$\langle F|H_{int}|R\rangle\langle R|H_{int}|I\rangle = \varepsilon_0^{-2}\left(\mathbf{d}^{1'0}\cdot\boldsymbol{\mu}^{fr}\right)\left(\mathbf{d}^{01}\cdot\boldsymbol{\mu}^{r0}\right) \tag{4b.2}$$

The molecular response $\boldsymbol{\mu}^{r0}$ is the chromophore's transition dipole moment for the transition between those states indicated by symbols in superscript; each electric displacement **d** is associated with a transition involving a change of the occupation number of a specific radiation mode.[2] A prime mark (ʻ) indicates the mode of the output photon(s), **k'** ; unprimed symbols denote properties of the input mode **k**. So the superscript 01 signifies a transition in which the radiation state reduces from one input photon to none; the superscript 1ʻ0 signifies an increase from zero to one output photon. Evaluating the Dirac brackets according to equations (2a.4-9) yields:

$$M_{FI} = \frac{\hbar c}{2\varepsilon_0 V}\sqrt{kk'}\;\vec{e}_i'e_j\sum_r\frac{\mu_i^{fr}\mu_j^{r0}}{E_{0r}+\hbar ck+i\hbar c\gamma_r} \tag{4b.3}$$

Here, the symbol E_{0r} refers to the energy of the molecule in initial state 0 minus its energy when in state *r*. The volume of quantization *V*, which represents the average volume containing exactly one photon, can be explained as the irradiance of a beam being proportional to $\hbar ck/V$. In equation (4b.2), an imaginary part $\hbar c\gamma_r$ has been added to the energy denominator: this is the *damping* discussed in chapter 2a section 6.

The summation over *r* in equation (4b.3) yields just one term, as the fluorescence process entails excitation of the molecule to occupy one definite electronic state *r* during the process' intermediate era R. Thus the basic quantum amplitude consists of a single term that may be decomposed into scalar and tensor parts:

$$M_{FI} = \frac{1}{2\varepsilon_0}\left[\frac{k^{1/2}\,k'^{1/2}\,V^{-1}}{k+E_{0r}/\hbar c+i\gamma_r}\right]e_i'\,e_j\,\mu_i^{fr}\mu_j^{r0} \tag{4b.4}$$

Note that the molecular parts of equation (4b.4) are equivalent to a damped transition polarisability ($E1^2$ response) tensor given by equation (3a.6), with only one state *r* and the "anti-resonant" term omitted as it is insignificant near resonance.[3,4]

$$\alpha_{ij}^{f0}(-k';k) = \frac{1}{\hbar c}\sum_r \left[\frac{\mu_i^{fr}\mu_j^{r0}}{k + E_{0r}/\hbar c + i\gamma_r} + \frac{\mu_j^{fr}\mu_i^{r0}}{-k' + E_{0r}/\hbar c \pm i\gamma_r} \right]$$
$$\approx \frac{1}{\hbar c}\left[\frac{1}{k + E_{0r}/\hbar c + i\gamma_r} \right] \mu_i^{fr}\mu_j^{r0} \qquad (4b.5)$$

A field-centric "radiation reaction" formulation produces an equivalent polarisability derivation.[5]

3. Quantum interference

For a multichromophore molecule, it should be understood that absorption of the input photon is associated with distinct quantum amplitudes M_{FI} for each of its N chemically-identical chromophores. The subsequent emission event may originate from any of those chromophores, and emissions from each of them are indistinguishable – the identity of the individual chromophore engaged in a particular fluorescence process is unobservable.

The underlying reason is that, since no measurement is made on the system's intermediate state R, the molecular wavefunction Ψ_R does not collapse in a way that could localise the excitation on any one chromophore unit. This superposition is consistent with the wavefunction:

$$\Psi_R = N^{-1/2}\sum_A^N \phi_A \qquad (4b.6)$$

Here, ϕ_A is the wavefunction for the molecule with all chromophores unexcited except for *A*, which is the one excited to its higher stationary state *r*.

As always, the quantum amplitude for the overall process, as observed, consists of a sum of amplitudes for all mechanisms consistent with the observation. Here, the identity of the active chromophore is part of this unspecified mechanistic information. Phase issues connected to this summation are discussed in section 6 of this chapter.

The observable rate of fluorescence is now given by application of the Fermi rule:

$$\begin{aligned}\Gamma &= 2\pi\hbar^{-1}\rho_f\left|\sum_A^N M_{FI}^A\right|^2 \\ &= \frac{\pi}{2\hbar\varepsilon_0^2}\left[\frac{\rho_f\, k\, k' V^{-2}}{\left(k + E_{0r}/\hbar c\right)^2 + \gamma_r^2}\right] \\ &\quad \times e_i' e_j' e_k' e_l \left(\sum_A^N \mu_i^{Afr}\mu_j^{Ar0}\mu_k^{Afr}\mu_l^{Ar0} + 2\sum_{A\neq B}^{N(N-1)/2}\mu_i^{Afr}\mu_j^{Ar0}\mu_k^{Bfr}\mu_l^{Br0}\right)\end{aligned} \tag{4b.7}$$

The first N terms of this rate equation represent the combined fluorescence from the N individual chromophores – this fluorescence rate is what may be predicted if the Fermi rule is applied separately to each chromophore's fluorescence. The additional $N(N-1)/2$ terms are the quantum interference that arise from the position of the fluorescence process being unspecified.

Although the quantum interference terms describe a certain sharing of fluorescence activity between chromophores, this formulation does **not** entail excitation delocalisation via any exciton or FRET effect – the analysis here is thus distinct from theories based on inter-chromophore coupling.[6] Microscopically, the fluorescence mechanism is itself single-centre. Quantum interference in the observable rate of fluorescence is a quantum measurement phenomenon, not evidence for real mixing-of-states between chromophores.

4. Rotational average

To describe the fluorescence of a molecule in solution, an isotropic average must be applied to the molecular response tensors. The field vectors are unaffected, as the input light is presumed to be from a source fixed in the laboratory reference frame, and the observed output photons must have polarisation aligned to the receiving spectrometer. With chevron brackets indicating a continuous integration over the three Euler angles of molecular orientation,[7] the rate result averages as follows according to the method outlined in chapter 2b:

$$\begin{aligned}\left\langle\Gamma\right\rangle &= \frac{\pi}{2\hbar\varepsilon_0^2}\left[\frac{\rho_f\, k\, k' V^{-2}}{\left(k + E_{0r}/\hbar c\right)^2 + \gamma_r^2}\right] \\ &\quad \times e_i' e_j' e_k' e_l \left(\sum_A^N \mu_\lambda^{Afr}\mu_\mu^{Ar0}\mu_\nu^{Afr}\mu_\xi^{Ar0} + 2\sum_{A\neq B}^{N(N-1)/2}\mu_\lambda^{Afr}\mu_\mu^{Ar0}\mu_\nu^{Bfr}\mu_\xi^{Br0}\right) I^{(4)}_{ijkl;\lambda\mu\nu\xi}\end{aligned} \tag{4b.8}$$

This averaged-rate result may apply to the fluorescence of a solute molecule rotating stochastically with no well-defined orientation, or alternatively an ensemble average of the fluorescence from many randomly-oriented molecules, which individually do not exhibit any appreciable rotation.[8] The chromophores within the molecule are also not necessarily fixed in orientation relative to each other.

The $I^{(4)}$ double-tensor is reported in appendix 8b. Applying the Kronecker deltas, the tensor parts of each of the $N(N+1)/2$ rate terms thus acquire the following general form:

$$\begin{aligned} & e'_i e_j e'_k e_l \, \mu_\lambda^{A\,fr} \mu_\mu^{Ar0} \mu_\nu^{B\,fr} \mu_\xi^{Br0} I^{(4)}_{ijkl;\lambda\mu\nu\xi} \\ & \quad = \frac{\left(\mu^{fr}\mu^{r0}\right)^2}{30} \Big\{ \quad \left[3\left(\mathbf{e}'\cdot\mathbf{e}\right)^2 - 1\right]\left(\hat{\boldsymbol{\mu}}^{A\,fr}\cdot\hat{\boldsymbol{\mu}}^{Ar0}\right)\left(\hat{\boldsymbol{\mu}}^{B\,fr}\cdot\hat{\boldsymbol{\mu}}^{Br0}\right) \\ & \qquad + \left[4 - 2\left(\mathbf{e}'\cdot\mathbf{e}\right)^2\right] \left(\hat{\boldsymbol{\mu}}^{A\,fr}\cdot\hat{\boldsymbol{\mu}}^{B\,fr}\right)\left(\hat{\boldsymbol{\mu}}^{Ar0}\cdot\hat{\boldsymbol{\mu}}^{Br0}\right) \\ & \qquad + \left[3\left(\mathbf{e}'\cdot\mathbf{e}\right)^2 - 1\right]\left(\hat{\boldsymbol{\mu}}^{A\,fr}\cdot\hat{\boldsymbol{\mu}}^{Br0}\right)\left(\hat{\boldsymbol{\mu}}^{Ar0}\cdot\hat{\boldsymbol{\mu}}^{B\,fr}\right) \Big\} \end{aligned} \tag{4b.9}$$

The magnitudes of each chromophore's absorption and emission dipoles will all be equal provided they are chemically similar, permitting the factorisation above. Each of the bracketed dot-products corresponds to a physical angle in the system:

- $\zeta \equiv \cos^{-1}\left(\mathbf{e}'\cdot\mathbf{e}\right)$ is the angle between the polarisation vectors of the input absorbed light and the emitted light. Parallel fluorescence is the $\zeta = 0°$ case; perpendicular fluorescence is the $\zeta = 90°$ case.
- $\theta_A \equiv \cos^{-1}\left(\hat{\boldsymbol{\mu}}^{A\,fr}\cdot\hat{\boldsymbol{\mu}}^{Ar0}\right)$ is the angle between the absorption and emission dipoles for chromophore *A*. Each chromophore's θ angle represents some undetermined combination of molecular rotation (during the state *r* lifetime), and a natural difference in the orientation of the two dipoles relative to the molecule. If the intrinsic physical properties of chromophore species *A* dispose it to have emission and absorption dipoles that are parallel, then the reorientation θ_A must be entirely due to molecular rotation – with sufficient stochastic rotation, this averages to $\theta_A = 90°$. The opposite limit is where molecular rotation is negligible (due to the lifetime of state *r* being vanishingly short, or the molecule being trapped in a cold and viscous solvent), such that the value of θ_A is wholly set by intrinsic chromophore properties.

- $\psi_{AB}^{Abs} \equiv \cos^{-1}\left(\hat{\boldsymbol{\mu}}^{Ar0} \cdot \hat{\boldsymbol{\mu}}^{Br0}\right)$ is the angle between the absorption dipoles for chromophores *A* and *B*. This is the difference in orientation between *A* and *B* at the time of absorption. Likewise, $\psi_{AB}^{Em} \equiv \cos^{-1}\left(\hat{\boldsymbol{\mu}}^{A\,fr} \cdot \hat{\boldsymbol{\mu}}^{B\,fr}\right)$ is the angle at the time of emission. The ψ angles describe the shape of the multi-chromophore molecule at the two transition times. Note that $\psi_{AA}^{Abs} = \psi_{AA}^{Em} = 0°$.
- Lastly, $\chi_{A;B} \equiv \cos^{-1}\left(\hat{\boldsymbol{\mu}}^{Ar0} \cdot \hat{\boldsymbol{\mu}}^{B\,fr}\right)$ is the angle between the dipole of *A*'s absorption and the dipole of *B*'s emission. Each χ angle represents some undetermined combination of the relevant ψ and θ angles, determined by the precise configuration and dynamics of the multi-chromophore system. Note that $\chi_{B;A}$ is distinct from $\chi_{A;B}$, and that $\chi_{A;A} = \theta_A$.

All of the above angles are required to have definite values between 0° and 180°. With this angular nomenclature, our $N(N+1)/2$ rate terms each become

$$\begin{aligned} & e'_i e_j e'_k e_l \left\langle I^{(4)} \right\rangle \mu_\lambda^{A\,fr} \mu_\mu^{Ar0} \mu_\nu^{B\,fr} \mu_\xi^{Br0} \\ & \quad = \frac{\left(\mu^{fr}\mu^{r0}\right)^2}{30} \Big\{ \quad \left[3\cos^2\zeta - 1\right]\cos\theta_A \cos\theta_B \\ & \qquad\qquad + \left[4 - 2\cos^2\zeta\right] \cos\psi_{AB}^{Abs} \cos\psi_{AB}^{Em} \\ & \qquad\qquad + \left[3\cos^2\zeta - 1\right]\cos\chi_{A;B} \cos\chi_{B;A} \Big\} \end{aligned} \tag{4b.10}$$

Resubstituting these results into the rate equation (4b.8) yields the rotationally-averaged rate;

$$\begin{aligned} \left\langle \Gamma \right\rangle = & \frac{\pi}{30\hbar\varepsilon_0^2} \left[\frac{\rho_f \, k\, k' V^{-2}}{\left(k + E_{0r}/\hbar c\right)^2 + \gamma_r^2} \right] \left(\mu^{fr}\mu^{r0}\right)^2 \\ & \times \Bigg\{ 2N - N\cos^2\zeta + \left(3\cos^2\zeta - 1\right)\sum_A^N \cos^2\theta_A \\ & \quad + \sum_{A\neq B}^{N(N-1)/2} \Big[\quad \left(3\cos^2\zeta - 1\right)\cos\theta_A \cos\theta_B \\ & \qquad\qquad + \left(4 - 2\cos^2\zeta\right)\cos\psi_{AB}^{Abs} \cos\psi_{AB}^{Em} \\ & \qquad\qquad + \left(3\cos^2\zeta - 1\right)\cos\chi_{A;B} \cos\chi_{B;A} \Big] \Bigg\} \end{aligned} \tag{4b.11}$$

Recall that the first line is equivalent to a transition polarisability, **α**. This formula allows us to predict the observable rate of fluorescence for any particular multi-chromophore system in solution, in terms of its internal angles and dynamics.

5. Fluorescence anisotropy

The anisotropy of fluorescence is a readily-measured observable, offering a reliable means of examining the detailed fluorescence behaviour of molecules in solution. It is quantified as a function of the relative rates of emission with polarization that is parallel or perpendicular to the input mode, which must be measured separately:[9,10]

$$r = \frac{\Gamma_{\zeta=0^\circ} - \Gamma_{\zeta=90^\circ}}{\Gamma_{\zeta=0^\circ} + 2\Gamma_{\zeta=90^\circ}} \tag{4b.12}$$

The theoretical maximum anisotropy of r =1.0 indicates zero perpendicular fluorescence; the minimum of $r = -0.5$ indicates zero parallel fluorescence; *isotropy*, indicated by $r = 0$, results from fluorescence that is independent of ζ. Anisotropy is also commonly formulated as the equivalent quantity called polarization ratio, P, straightforwardly related to r as:[9]

$$P = \frac{3r}{2+r} \tag{4b.13}$$

Substitution of the solution-phase predictions of equation (4b.11) as the arguments of equation (4b.12) yields a testable formula for r:

$$r = \frac{-N + 3\sum_{A}^{N} \cos^2\theta_A + \sum_{A\neq B}^{N(N-1)/2} \left[3\cos\theta_A \cos\theta_B - 2\cos\psi_{AB}^{Abs} \cos\psi_{AB}^{Em} + 3\cos\chi_{A;B} \cos\chi_{B;A} \right]}{5N + 10 \sum_{A\neq B}^{N(N-1)/2} \cos\psi_{AB}^{Abs} \cos\psi_{AB}^{Em}} \tag{4b.14}$$

For any molecule of interest whose internal structure is known, equation (4b.14) may be directly applied. There are too many uncorrelated variables for a generic analysis, so what follows in this section is an overview of the results for certain limiting cases.

Firstly, the case of $\psi_{AB}^{Abs} = \psi_{AB}^{Em} = 0^\circ$ for each pair $A \neq B$. This represents a condition where all of the absorption dipoles are parallel, and all of the emission dipoles are also parallel. This constrains the values for all θ_A and $\chi_{A;B}$ angles to one angle for the absorption-emission orientation difference, labelled θ. The anisotropy result is independent of N:

$$r_{\psi=0°} = \frac{3\cos^2\theta - 1}{5} \tag{4b.15}$$

This is well known to be true for $N = 1$, and for a parallel ensemble of arbitrary N. See equation 10.20 of ref.[9]. The maximum and minimum anisotropy values are 0.4 (at $\theta = 0°$ or 180°) and –0.2 (at $\theta = 90°$), consistent with single-photon fluorescence in an isotropic solution. A prediction of MQED theory via Fermi rate equations has re-derived a result that is familiar to fluorescence spectroscopy.

Next, consider the case of $\theta_A = 0°$ for all chromophores, which specifies that each individual chromophore's absorption dipole and emission dipole are parallel in space (the molecule is rigid and fixed in orientation). This implies the equalities $\psi_{AB}^{Abs} = \psi_{AB}^{Em} = \chi_{A;B} = \chi_{B;A}$ for each pair $A \neq B$, so all those angles are subsumed into a single variable labelled ψ_{AB}.

$$r_{\theta=0°} = \frac{3N^2 + N + 2\sum_{A\neq B}^{N(N-1)/2} \cos^2\psi_{AB}}{10N + 20\sum_{A\neq B}^{N(N-1)/2} \cos^2\psi_{AB}} \tag{4b.16}$$

This yields a maximum anisotropy value of 1.0, for a N=3 molecule whose chromophores are mutually orthogonal, and for any configuration of chromophores whose dipoles all point toward or away from a common centre and are positioned at the vertices of a Platonic solid. Here, it is the *minimum* of anisotropy that takes the value of 0.4, when all angles $\psi_{AB} = 0°$ or 180°.

Equation (4b.16) is further analysed in figure 4b.1.

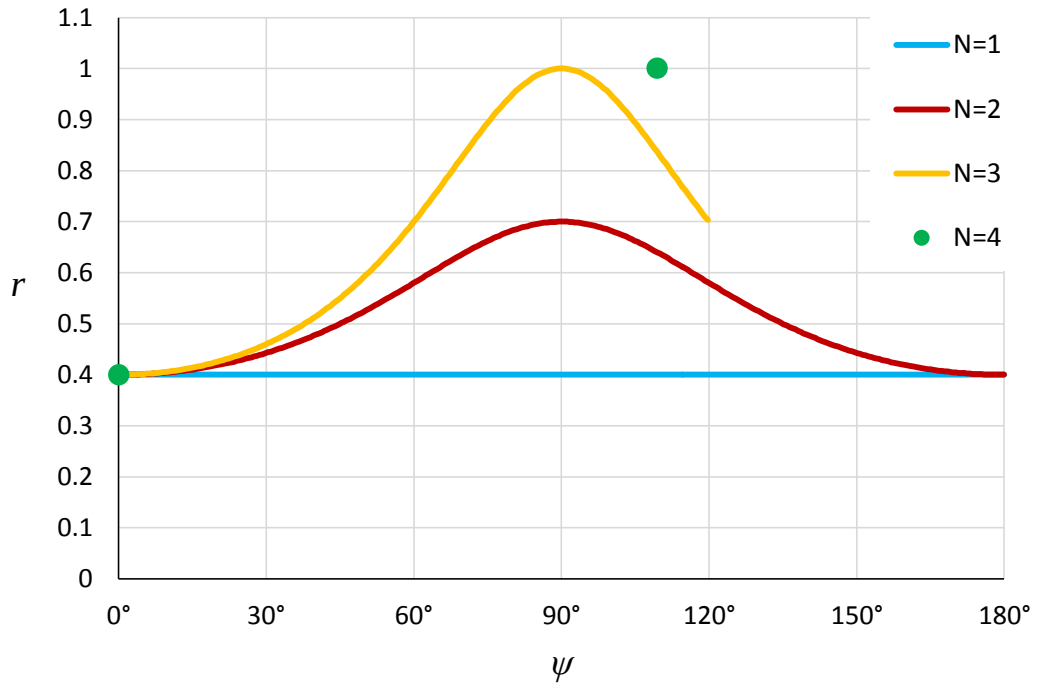

Figure 4b.1: Plot of equation (4b.16) with the assumption that all angles ψ_{AB} are equal, subsumed into a single abscissa ψ. The N=3 curve represents a trigonal pyramidal molecule, approaching a trigonal-planar geometry at ψ =120°. With N=4, it is not possible to have all six angles ψ_{AB} be equal unless ψ =0° or ψ =109.47° (a tetrahedral molecule).

It is known that a tetraphenylporphyrin molecule with square planar symmetry (and corresponding fourfold degeneracy in its excited state) may exhibit $r \geq 0.7$.[11] The conjugated bonds of this system hold the component groups together inflexibly – therefore, if molecular rotation is controlled, equation (4b.16) will be applicable as the correct anisotropy equation. If the four phenyl branches are treated as separate dipolar chromophores, then according to equation (4b.16):

$$\begin{aligned} &N = 4 \\ &\psi_{AB} = \psi_{BC} = \psi_{CD} = \psi_{AD} = 90° \\ &\psi_{AC} = \psi_{BD} = 180° \\ &\therefore r_{\theta=0°} = 0.7 \end{aligned} \qquad (4b.17)$$

The experiment in ref.[11] observed anisotropy values in exactly this region with ultrafast measurements, such that the intermediate state lifetime was vanishingly short and thus $\theta \approx 0°$.

6. Discussion

The issue of quantum uncertainty in the intermediate state between absorption and emission deserves further comment. The results of this chapter rest on a certain coherence being retained by the system, described as a superposition of states by equation (4b.6). It is important to recognise that the selection of a specific superposition state, in which the phases of each ϕ_A are equal, is the origin of equation (4b.7) having identical (unweighted, unphased) contributions from each fluorescent chromophore. This condition is physically consistent with each chromophore experiencing input radiation with nearly the same optical phase, because the dimensions of the molecule will usually be much smaller than the optical wavelength. Alternative molecule states, with different relative phase factors, would constitute another acceptable basis set – summation over which would lead to statistically-weighted results.

This formulation of fluorescence theory, incorporating quantum interference between chromophores, should more fully capture the advanced geometric effects governing the fluorescence behaviour of multi-component molecules. Insofar that the fluorescence behaviour of a multi-chromophore system is related to its capacity for electronic energy exchange or RET, the analysis developed here may also be adapted to contribute to optimisation of RET efficiency in light-harvesting compounds.[12]

There is relatively little existing theoretical work describing the basis for a range of r values beyond the limits of equation (4b.15), with the most-cited theories often appealing to the possibility of complex effects of coherence in systems of multiple energy levels.[13] The anisotropy derivations of this chapter can explain and predict such observations based only on the assumptions of the MQED framework.

[1] A.A. Demidov and D.L. Andrews, "Determination of Fluorescence Polarization and Absorption Anisotropy in Molecular Complexes Having Threefold Rotational Symmetry": *Photochem. Photobiol.* **63**, 39 (1996).

[2] D. P. Craig and T. Thirunamachandran, *Molecular Quantum Electrodynamics*, 2nd ed. (Dover Publications, Mineola, New York, 1998).

[3] D. L. Andrews, S. Naguleswaran, and G. E. Stedman, "Phenomenological Damping of Nonlinear-Optical Response Tensors": *Phys Rev A* **57**, 4925 (1998).

[4] D.L. Andrews and J.S. Ford, "Resonance Energy Transfer: Influence of Neighboring Matter Absorbing in the Wavelength Region of the Acceptor": *J. Chem. Phys.* **139**, (2013).

[5] R. Carminati, J.-J. Greffet, C. Henkel, and J.M. Vigoureux, "Radiative and Non-Radiative Decay of a Single Molecule close to a Metallic Nanoparticle": *Opt. Commun.* **261**, 368 (2006).

[6] T.S. Rahman, R.S. Knox, and V.M. Kenkre, "Theory of Depolarization of Fluorescence in Molecular Pairs": *Chem. Phys.* **44**, 197 (1979).

[7] D. P. Craig and T. Thirunamachandran, "Rotational Averaging of Tensors": *Mol. Quantum Electrodyn.*, Dover Paperback (Dover Publications, Mineola, New York, 1998), pp. 310–315.

[8] R.G. Bray and R.M. Hochstrasser, "Two-Photon Absorption by Rotating Diatomic Molecules": *Mol. Phys.* **31**, 1199 (1976).

[9] J. Lakowicz, "Fluorescence Anisotropy": *Princ. Fluoresc. Spectrosc.*, 2nd ed. (Kluwer Academic Plenum, New York, 1999), p. 291.

[10] B. Valeur, "Vertically Polarized Excitation": *Mol. Fluoresc.* (Weinheim, 2002), p. 129.

[11] G.G. Gurzadyan, T.-H. Tran-Thi, and T. Gustavsson, "Time-Resolved Fluorescence Spectroscopy of High-Lying Electronic States of Zn-Tetraphenylporphyrin": *J. Chem. Phys.* **108**, 385 (1998).

[12] G.D. Scholes, G.R. Fleming, A. Olaya-Castro, and R. van Grondelle, "Lessons from Nature about Solar Light Harvesting": *Nat Chem* **3**, 763 (2011).

[13] K. Wynne and R.M. Hochstrasser, "Coherence Effects in the Anisotropy of Optical Experiments": *Chem. Phys.* **171**, 179 (1993).

–

Chapter 5: **Effects of non-resonant light on one- and two-photon absorption**

1. Introduction

The multi-order theory of molecule-light interactions can include the interactions of photons that are not resonant with a molecular transition.[1] Off-resonant laser light is known to physically interfere with elementary absorption and two-photon absorption processes, passively interacting with the molecule and thus observably modifying the absorption intensity.[2] In principle, the fields attributable to vacuum modes could perform the same passive interactions, but analysis suggests that the resulting modifications would be negligible. The optically-modified process is a higher-order mechanism, which may allow molecular transitions that are formally forbidden for unmodified absorption.[3] The theoretical treatment of such a high-order multiphoton transition is familiar from descriptions of multiphoton fluorescence and the optical Kerr effect. [4–6]

This chapter deals with one- and two-photon absorption rates and predicts how they may be modified by the passive influence of an auxiliary non-resonant light source.[7] The calculations here are tailored to the scenario of a single molecule in solution, as this describes systems of practical interest and simple experiment design.[8] The rate of absorption may be derived from the measured fluorescence of a sample through which a resonant beam and a non-resonant beam cross.

The physical character of photons is affected by the refractive properties of the liquid medium through which they propagate, so the MQED of interactions must accommodate the modification of electric displacement by the medium's refractive index. Additionally, the orientation of a solution-phase molecule is randomised by thermal agitation between each absorption event, so the observed rate of absorption will be an average of the theoretical static-molecule rate results at all possible orientations. In sections 4 and 5, the rotationally-averaged rates of optically-modified one- and two-photon absorption are calculated using advanced methods for high-rank tensor isotropic averages. The outcome is a rigorous analysis of the correspondence between details of the molecule's electronic response and the polarisation states of the two beams.

2. MQED model of absorption

This chapter focuses on the excitation of a molecule in solution by a process of either single-photon absorption or two-photon absorption. The absorbed photons implicate the presence of an input light source (ideally a paraxial laser beam) whose wavelength is resonant with the molecule's stationary state gaps. Simultaneously, an auxiliary off-resonant beam is introduced – this cannot excite the molecule, but may passively interact in a way that modifies the absorption processes. Specifying the auxiliary beam radiation as "off-resonant" means that neither a single photon nor two photons have sufficient energy to excite the molecule to its higher state, and therefore the molecule is transparent to this light.

The throughput of off-resonant light becomes a part of the absorption process. As shown in figures 5.2 and 5.4, the following interaction events occur: one or two resonant absorptions, annihilation of one off-resonant photon, and the creation of one off-resonant photon. The absorption of the excitation beam and the (elastic Rayleigh) forward-scattering of the auxiliary beam are effectively instantaneous and cannot be meaningfully separated. Lower-case state labels *r*, *s*, *t* denote the state of the molecule within the respective intermediate system states *R*, *S* and *T*. The molecule is in ground state 0 within the initial system state (*I*), and in excited state α within the final state (*F*). In this nomenclature, it is the second-in-time interaction event which transitions the whole system from *R* to *S*.

Even though these processes involve multiple photonic interactions, the overall molecular response tensors are constructed from combinations of transition dipole moments: a two-event transition is modelled as two dipolar interactions ($E1^2$) that comprise a transition polarizability tensor, $\boldsymbol{\alpha}$; a three-event transition is modelled as three dipoles ($E1^3$) that comprise a hyperpolarisability tensor, $\boldsymbol{\beta}$; four events are $E1^4$, comprising a "second" hyperpolarisability, $\boldsymbol{\chi}$.[9] Each of these response tensors has its own symmetry features and selection rules.[3]

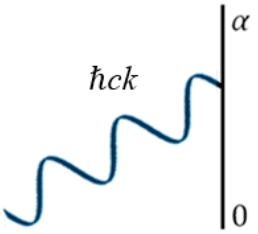

Figure 5.1

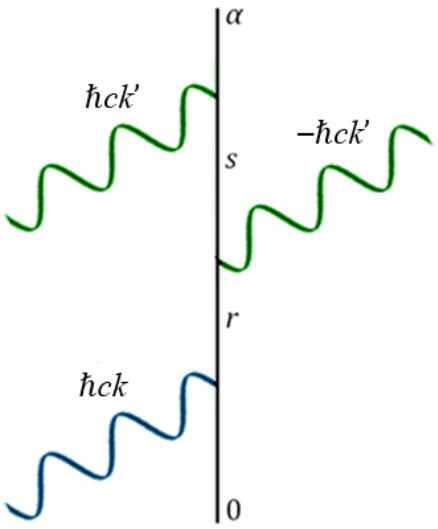

Figure 5.2

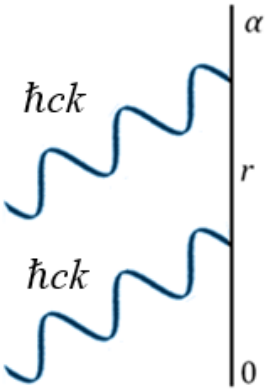

Figure 5.3

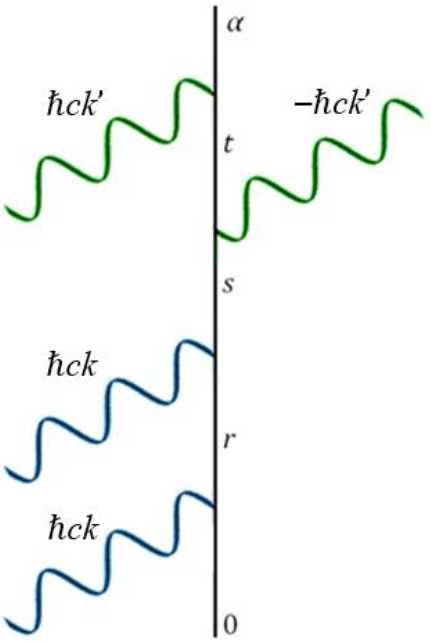

Figure 5.4

Figures 5.1-4: Feynman diagrams for: (**5.1**) elementary one-photon absorption; (**5.2**) one-photon absorption engaging with forward scattering of a passive beam, showing one of six time orderings; (**5.3**) two-photon absorption; (**5.4**) two-photon absorption engaging with forward scattering of a passive beam, showing one of 24 time orderings. In all these cases, the molecule is excited $\alpha \leftarrow 0$. The excitation beam is shown as blue and the auxiliary beam shown as green (the implication that the auxiliary wavelength is longer than the excitation wavelength is consistent with the photon energy inequalities in section 2).

The auxiliary light is distinguished from the absorbed photons by a prime mark on all variables associated with it. The absorbed photons have energy $\hbar ck = E_{\alpha 0}^{\mathrm{Mol}}$ for one-photon absorption, and $2\hbar ck = E_{\alpha 0}^{\mathrm{Mol}}$ for two-photon absorption; the requirement of the auxiliary beam to be off-resonant is written as $\hbar ck' < E_{\alpha 0}^{\mathrm{Mol}}$ for one-photon absorption, and $2\hbar ck' < E_{\alpha 0}^{\mathrm{Mol}}$ for two-photon absorption.

For a molecule in solution, the surrounding matter can be expected to modify the electric field properties of radiation, which affects the character of all interactions. In a solid matrix, it would be correct to invoke a polariton formulation, but for an essentially-transparent liquid medium, all media effects may be approximated as an electronic "field dressing".[10] For each radiation mode, the dressing is quantified as the medium's refractive index *n*, whose definition involves the angular frequency ω, wavevector magnitude *k*, and group velocity v_g: [11]

$$\omega n_{(\omega)} = ck \;; \qquad v_g \equiv \frac{\partial \omega}{\partial k} = \frac{c}{n_{(\omega)}} \tag{5.1}$$

This formulation of dressed fields in the condensed-phase renders the quantum description of radiation as intermediate between photon and polariton.[11,12] The result is a modified form for the electric displacement experienced by the molecule, such that equation (2a.4) is changed to:

$$\mathbf{d}^{\perp} = i\left(\frac{\hbar \varepsilon_0 v_g \omega}{2cV}\right)^{1/2} \left(\frac{n_{(\omega)}^2 + 2}{3n_{(\omega)}^{1/2}}\right)\left[\mathbf{e}_{(\eta,\mathbf{k})} a_{(\eta,\mathbf{k})} - \overline{\mathbf{e}}_{(\eta,\mathbf{k})} a_{(\eta,\mathbf{k})}^{\dagger}\right] \tag{5.2}$$

This once again implies a mode expansion over transverse plane waves – each mode is defined by a polarization state η and wavevector $\mathbf{k}$; the vector $\mathbf{e}_{(\eta,\mathbf{k})}$ is the electric field unit-vector of such a wave (overbar indicates complex conjugation). This calculation describes a single-centre process, with all events occurring at the one molecule's position, so there are no phase factors dependent on relative displacement.

Additional background information for this absorption model is detailed in ref.[2], but without accommodating local solvent effects. Section 3 of this chapter applies the MQED analysis to the auxiliary-beam-modified absorption behaviour of a single molecule that is fixed in some static orientation.

3. Rate equations

3.1 Dirac brackets

The rate of a multi-interaction-event process is given by equation (2a.5) in terms of Dirac brackets for each interaction. Using equation (5.2) instead of equation (2a.4), each interaction event is either a photon annihilation:

$$\left\langle S\left|H_{\text{int}}\right|R\right\rangle = -i\left(\frac{\hbar}{2\varepsilon_0 V}\right)^{1/2}\sum_{\eta,\mathbf{k}}\omega_{\mathbf{k}}^{1/2}\left(\frac{n_{\mathbf{k}}^2+2}{3n_{\mathbf{k}}}\right)\left(\boldsymbol{\mu}^{sr}\cdot\mathbf{e}_{(\eta,\mathbf{k})}\right)\left\langle \text{Rad}_S\left|a_{(\eta,\mathbf{k})}\right|\text{Rad}_R\right\rangle \tag{5.3}$$

Or it is a photon creation:

$$\left\langle S\left|H_{\text{int}}\right|R\right\rangle = +i\left(\frac{\hbar}{2\varepsilon_0 V}\right)^{1/2}\sum_{\eta,\mathbf{k}}\omega_{\mathbf{k}}^{1/2}\left(\frac{n_{\mathbf{k}}^2+2}{3n_{\mathbf{k}}}\right)\left(\boldsymbol{\mu}^{sr}\cdot\bar{\mathbf{e}}_{(\eta,\mathbf{k})}\right)\left\langle \text{Rad}_S\left|a^{\dagger}_{(\eta,\mathbf{k})}\right|\text{Rad}_R\right\rangle \tag{5.4}$$

The operators $a_{(\eta,\mathbf{k})}$ and $a^{\dagger}_{(\eta,\mathbf{k})}$ each apply to either photon creation or annihilation, with quantum algebra as in equations (2a.5-9). In the following subsections, the symbol q is again used to represent the number of photons within the system volume V that have polarization state η and wavevector $\mathbf{k}$. In the initial radiation state $\left|\text{Rad}_I\right\rangle$, the excitation beam and auxiliary beam are both present in their initial states: there are q photons in volume V that have polarization state η and wavevector $\mathbf{k}$ corresponding to angular frequency ω, associated with electric fields $\mathbf{e}$ and refractive index n; there are also q' photons in volume V that have polarization state η' and wavevector $\mathbf{k}'$ corresponding to angular frequency ω', associated with electric fields $\mathbf{e}'$ and refractive index n'.

3.2 One-photon absorption

Elementary single-photon absorption, illustrated by figure 5.1, is a single photon-annihilation event whose quantum amplitude is given by a single Dirac bracket. Using the dressed-field E1 approximation of section 2, this evaluates as:

$$\left\langle F\left|H_{\text{int}}\right|I\right\rangle = -i\left[\frac{q\hbar\omega}{2\varepsilon_0 V}\right]^{1/2}\left(\frac{n^2+2}{3n}\right)\left(\boldsymbol{\mu}^{\alpha 0}\cdot\mathbf{e}\right) \tag{5.5}$$

Absorption combined with forward-scattering of auxiliary light, illustrated by figure 5.2, is a three-interaction process whose quantum amplitude is given by the

third-order term of equation (2a.13). No other terms need to be considered – the three-event process represents the leading modification to simple absorption.

$$\begin{aligned}\sum_{R,S}&\frac{\langle F|H_{\text{int}}|S\rangle\langle S|H_{\text{int}}|R\rangle\langle R|H_{\text{int}}|I\rangle}{(E_I-E_S)(E_I-E_R)}\\ &=-i\,q^{1/2}q'\left[\frac{\hbar}{2\varepsilon_0 V}\right]^{3/2}\omega^{1/2}\omega'\left(\frac{n^2+2}{3n}\right)\left(\frac{n'^2+2}{3n'}\right)^2\\ &\quad\times e_i\,e'_j\,\bar{e}'_k\sum_{R,S}\frac{\mu_a^{\alpha s}\mu_b^{sr}\mu_c^{r0}}{\left(E_{0s}^{\text{Mol}}+E_{IS}^{\text{Rad}}\right)\left(E_{0r}^{\text{Mol}}+E_{IR}^{\text{Rad}}\right)}\end{aligned}\qquad(5.6)$$

The assumption of high irradiance in the auxiliary beam justifies the approximation $q'/V\approx(q'+1)/V$, which leads to the appearance of *q'* as the auxiliary intensity factor. The sum-over-states for all *R* and *S* includes a sum over six time-orderings of the three events and over all possible molecular states *r* and *s*. In each time-ordering, the dipole component indices {*a*,*b*,*c*} are a unique permutation of {*i*,*j*,*k*}, such that contraction with the electric field vector components results in a set of scalar products. The complete result of the sum-over-states is a tensor that encapsulates the molecule's $E1^3$ response to microscopic electric fields, so the molecular part of equation (5.6) (the dipole moments and energy differences) is a form of transition hyperpolarisability tensor, labelled $\beta_{ijk}^{\alpha 0}$.[9]

Following the Fermi rule, the overall quantum amplitude of single-photon absorption is the sum of the above two amplitudes (combining the modified and unmodified mechanisms), and the observable rate is calculated according to equation (2a.12):

$$\begin{aligned}\Gamma_{1\phi}=\frac{\pi\rho_F}{\hbar}\left[\frac{I}{c\varepsilon_0}\right]\left(\frac{n^2+2}{3n}\right)^2 e_i\bar{e}_j\Big\{&\mu_i^{\alpha 0}\bar{\mu}_j^{\alpha 0}\\ &+\left[\frac{I'}{c\varepsilon_0}\right]\left(\frac{n'^2+2}{3n'}\right)^2\bar{e}'_k e'_l\,\mu_i^{\alpha 0}\bar{\beta}_{jkl}^{\alpha 0}\\ &+\frac{1}{4}\left[\frac{I'}{c\varepsilon_0}\right]^2\left(\frac{n'^2+2}{3n'}\right)^4 e'_k\bar{e}'_l\bar{e}'_m e'_n\beta_{ikl}^{\alpha 0}\bar{\beta}_{jmn}^{\alpha 0}\Big\}\end{aligned}\qquad(5.7)$$

The "photon density" *q /V* is not directly measurable, but beam irradiance is, so this rate equation has been expressed in terms of excitation beam irradiance

$I \equiv \hbar cq\omega/V$ and auxiliary beam irradiance $I' \equiv \hbar cq'\omega'/V$. The second term of equation (5.7), which is linear in I', is quantum interference between the two absorption mechanisms.

3.3 Two-photon absorption

The process of two-photon absorption entails either exactly two annihilation events, illustrated by figure 5.3, or two annihilations combined with forward-scattering of auxiliary light, illustrated by figure 5.4. The quantum amplitude is given as the sum of a second-order term of equation (2.13) for the former and a fourth-order term for the latter.

In the second-order mechanism, the two absorbed photons are in principle indistinguishable which means there is only one unique time-ordering of the two events. This may be thought of as two combined single-photon absorptions from different excitation beams, at the limit of the two beams becoming equal in wavelength and parallel in polarisation. If each fictitious beam is at half the intensity of the actual excitation beam (ergo, photon density = $q/2V$), then the quantum amplitude becomes:

$$\sum_R \frac{\langle F|H_{\text{int}}|R\rangle\langle R|H_{\text{int}}|I\rangle}{(E_I - E_R)} = -\left(\frac{\hbar}{4\varepsilon_0}\right)\frac{q}{V}\left[\frac{q-1}{q}\right]^{1/2}\omega\left(\frac{n^2+2}{3n}\right)^2 e_i e_j \sum_r \frac{\mu_i^{\alpha r}\mu_j^{r0} + \mu_j^{\alpha r}\mu_i^{r0}}{E_{0r}^{\text{Mol}} + \hbar\omega} \tag{5.8}$$

The $E1^2$ molecular response tensor may be constructed from the normalised and index-symmetrised sum of the two time-order-dependent double-absorption molecular responses – i.e. the mean of the two absorption dipole pairs. This demonstrates that the E1 approximation accommodates transitions that entail a shift in permanent dipole and those that do not.[13]

$$\alpha_{ij}^{\alpha 0} \equiv \frac{1}{2}\sum_r \frac{\mu_i^{\alpha r}\mu_j^{r0} + \mu_j^{\alpha r}\mu_i^{r0}}{E_{0r}^{\text{Mol}} + \hbar\omega} \tag{5.9}$$

The auxiliary-modified mechanism involves four interaction events, and is evaluated via the same method:

$$\sum_{R,S,T} \frac{\langle F|H_{\text{int}}|T\rangle\langle T|H_{\text{int}}|S\rangle\langle S|H_{\text{int}}|R\rangle\langle R|H_{\text{int}}|I\rangle}{(E_I-E_T)(E_I-E_S)(E_I-E_R)}$$
$$= -\left(\frac{\hbar}{2\varepsilon_0}\right)^2 \frac{q\,q'}{V^2}\left[\frac{q-1}{q}\right]^{1/2} \omega\omega' \left(\frac{n^2+2}{3n}\right)^2 \left(\frac{n'^2+2}{3n'}\right)^2 e_i e_j e'_k \bar{e}'_l \qquad (5.10)$$
$$\times \sum_{R,S,T} \frac{\mu_d^{\alpha t}\mu_c^{ts}\mu_b^{sr}\mu_a^{r0}}{(E_I-E_T)(E_I-E_S)(E_I-E_R)}$$

Once again, the approximation $q'/V \approx (q'+1)/V$ is employed. The sum-over-states includes a sum over 24 time-orderings, and in each time-ordering the indices $\{a,b,c,d\}$ are a different permutation of $\{i,j,k,l\}$. The complete result of the sum-over-states is an $E1^4$ molecular response tensor, so the molecular part of equation (5.10) is a second-hyperpolarisability tensor, labelled $\chi^{\alpha 0}_{ijkl}$. Ref.[3] discusses the selection rule implications of this. The indistinguishability of the two absorbed photons implies that only half of the 24 time-orderings are truly distinct – this degeneracy has been hidden within the structure of the χ tensor, and will reappear as a certain index-symmetry.

The Fermi rule rate of two-photon absorption, combining the modified and unmodified mechanisms, is likewise calculated according to equation (2a.12):

$$\Gamma_{2\phi} = \frac{\pi\rho_F}{2\hbar}\left[\frac{I}{c\varepsilon_0}\right]^2 \left(\frac{n^2+2}{3n}\right)^4 e_i e_j \bar{e}_k \bar{e}_l \left\{ \alpha^{\alpha 0}_{ij}\,\bar{\alpha}^{\alpha 0}_{kl} \right.$$
$$+ \left[\frac{I'}{c\varepsilon_0}\right]\left(\frac{n'^2+2}{3n'}\right)^2 \bar{e}'_m e'_n\, \alpha^{\alpha 0}_{ij}\,\bar{\chi}^{\alpha 0}_{klmn} \qquad (5.11)$$
$$\left. + \frac{1}{4}\left[\frac{I'}{c\varepsilon_0}\right]^2 \left(\frac{n'^2+2}{3n'}\right)^4 e'_m \bar{e}'_n\, \bar{e}'_o e'_p\, \chi^{\alpha 0}_{ijmn}\bar{\chi}^{\alpha 0}_{klop} \right\}$$

Again, photon density has been expressed as irradiances I and I'. In the case of the excitation beam, using a single value for I implies that the photon-density is not significantly diminished by the first absorption event. Explicitly, the approximation $(q-1)/V \approx q/V$ has been employed, which assumes constant high beam intensity. The appearance of the factor $\left[(q-1)/q\right]^{1/2}$ in equations (5.8) and (5.10) has been deliberately ignored – this contains information on the beam's second-order coherence,[14] and may be replaced by a rate factor $g^{(2)}$.

Within any finite system volume at any one time (absent any special boundary conditions), the number of vacuum fluctuation photons with any *specific* polarization state and wavevector will be very small.[14] So if the auxiliary light is not a coherent beam but merely a vacuum mode whose photons *q'* are transient quantum fluctuations, then $q'/V \approx 0$. This will give rise to no observable modification to absorption – an auxiliary *beam* of definite irradiance I' is needed.

4. Tensor contractions

4.1 Scalar rate factors

In each of the quantum amplitudes expressed by equations (5.5), (5.6), (5.8) and (5.10), the tensor parts consist of *N* field vectors **e** contracted with the *N*th-order molecular response tensor. Each thus forms a scalar inner-product. The indices *i*, *j*, *k*, etc. represent Cartesian components of the tensors in a laboratory-fixed frame, as the molecule and beams are in fixed orientations in space.

The six rate terms are therefore each expressible as a tensor contraction between a set of field vectors and a composite molecular response tensor for the $0 \leftarrow \alpha$ transition. Equations (5.7) and (5.11) are re-written in concise form to isolate these orientation-dependent tensor contraction parts:

$$\Gamma_{1\phi} = \frac{\pi \rho_F}{\hbar}\left[\frac{I}{c\varepsilon_0}\right]\left(\frac{n^2+2}{3n}\right)^2 \times\left\{C_1^{1\phi} + \left[\frac{I'}{c\varepsilon_0}\right]\left(\frac{n'^2+2}{3n'}\right)^2 C_2^{1\phi} + \frac{1}{4}\left[\frac{I'}{c\varepsilon_0}\right]^2\left(\frac{n'^2+2}{3n'}\right)^4 C_3^{1\phi}\right\} \tag{5.12}$$

$$\Gamma_{2\phi} = \frac{\pi \rho_F}{2\hbar}\left[\frac{I}{c\varepsilon_0}\right]^2\left(\frac{n^2+2}{3n}\right)^4 \times\left\{C_1^{2\phi} + \left[\frac{I'}{c\varepsilon_0}\right]\left(\frac{n'^2+2}{3n'}\right)^2 C_2^{2\phi} + \frac{1}{4}\left[\frac{I'}{c\varepsilon_0}\right]^2\left(\frac{n'^2+2}{3n'}\right)^4 C_3^{2\phi}\right\} \tag{5.13}$$

The label $C_B^{A\phi}$ is used for the tensor contraction that appears in the *B*th term of the *A*-photon absorption rate equation. The values of *N* in each of these contractions is the sum of the *N*s for the two quantum amplitudes that interfere to produce this rate term.

In this formulation, selection rules (i.e. a molecule intrinsically forbidding certain kinds of excitation interaction) are represented by certain molecular response tensors having zero magnitude: If one unmodified single-photon absorption is forbidden, this means $\boldsymbol{\mu}^{\alpha 0} = 0$, and thus $C_1^{1\phi}$ and $C_2^{1\phi}$ disappear; if one unmodified two-photon absorption is forbidden, this means $\boldsymbol{\alpha}^{\alpha 0} = 0$, and thus $C_1^{2\phi}$ and $C_2^{2\phi}$ disappear.

4.2 Rotational average

If the molecule is strongly aligned to the beam, such that molecular orientation is static in the reference frame of the fields, then equations (5.7) and (5.11) are the complete results for absorption rate. Such alignment may be forced by a molecule that preferentially orients its response dipoles to the auxiliary beam polarization vector – then if this direction is defined as the *z* axis, the indices *k*, *l*, *m*, *n* in equation (5.7) become limited to *z*; and the indices *m*, *n*, *o*, *p* in equation (5.11) become limited to *z*.

But for the case of a molecule rotating freely in solution, the rotational-average of these results must be calculated. This average, denoted by chevron brackets, is a continuous integration over the three Euler angles which relate the molecule's orientation to the laboratory-fixed frame. See chapter 2b for a full explanation of this calculation and the standard evaluation method based on $I^{(N)}$.

The two beams are assumed to be fixed in space, their sources at rest in the laboratory frame. This means the field vectors have well-defined components fixed in this frame, so their indices *i*, *j*, *k*… belong to the set {*x*,*y*,*z*}. The right-hand factors in equations (5.7) and (5.11) are components of the molecular response tensors in that same frame. It is necessary to express the response tensor components in terms of a molecule-fixed frame, with indices *λ*, *γ*, *ζ*… that instead belong to the set of unit vectors that are the natural orthogonal triad for the molecule's structure.

In the fluid phase, the six contractions that appear in equations (5.12) and (5.13) average to:

$$\left\langle C_1^{1\phi} \right\rangle = e_{i1}\bar{e}_{i2}\, I^{(2)}\, \mu_{\lambda 1}\bar{\mu}_{\lambda 2} \tag{5.14}$$

$$\left\langle \mathrm{C}_2^{1\phi} \right\rangle = e_{i1}\bar{e}_{i2}\bar{e}'_{i3}e'_{i4}\ I^{(4)}\ \mu_{\lambda 1}\bar{\beta}_{\lambda 234} \tag{5.15}$$

$$\left\langle \mathrm{C}_3^{1\phi} \right\rangle = e_{i1}\bar{e}_{i2}e'_{i3}\bar{e}'_{i4}\bar{e}'_{i5}e'_{i6}\ I^{(6)}\ \beta_{\lambda 134}\bar{\beta}_{\lambda 256} \tag{5.16}$$

$$\left\langle \mathrm{C}_1^{2\phi} \right\rangle = e_{i1}e_{i2}\bar{e}_{i3}\bar{e}_{i4}\ I^{(4)}\ \alpha_{\lambda 12}\bar{\alpha}_{\lambda 34} \tag{5.17}$$

$$\left\langle \mathrm{C}_2^{2\phi} \right\rangle = e_{i1}e_{i2}\bar{e}_{i3}\bar{e}_{i4}\bar{e}'_{i5}e'_{i6}\ I^{(6)}\ \alpha_{\lambda 12}\ \bar{\chi}_{\lambda 3456} \tag{5.18}$$

$$\left\langle \mathrm{C}_3^{2\phi} \right\rangle = e_{i1}e_{i2}\bar{e}_{i3}\bar{e}_{i4}e'_{i5}\bar{e}'_{i6}\bar{e}'_{i7}e'_{i8}\ \ I^{(8)}\ \chi_{\lambda 1256}\bar{\chi}_{\lambda 3478} \tag{5.19}$$

These are then evaluated according to $I^{(N)} = f^{(N)}_{r;\,i123\cdots N}\, m^{(N)}_{rs} g^{(N)}_{s;\,\lambda 123\cdots N}$, as outlined in chapter 2b.[15]

If the beams are plane waves, the field vectors have no imaginary part, so $(\mathbf{e}\cdot\mathbf{e}) = (\mathbf{e}\cdot\bar{\mathbf{e}}) = 1$ and $(\mathbf{e}'\cdot\mathbf{e}') = (\mathbf{e}'\cdot\bar{\mathbf{e}}') = 1$. Therefore, every Kronecker delta in the tensor $f^{(N)}_{r;\,i123\cdots N}$ contracting with field vectors will yield either 1 or $(\mathbf{e}\cdot\mathbf{e}')$. Similar degeneracy effects in the contraction with $g^{(N)}_{s;\,\lambda 123\cdots N}$ cause the molecular response tensor components to be reduced to a set of the natural invariant scalars.

4.3 Unmodified absorption

The *B*=1 terms give the rate of absorption via a mechanism with no auxiliary beam involvement, as illustrated by figures 5.1 and 5.3. They are independent of $\mathbf{e}'$, so may be evaluated straightforwardly without any reference to the polarisation vector angles that dominate the calculations of the following section.

$$\left\langle \mathrm{C}_1^{1\phi} \right\rangle = \frac{1}{3}(\boldsymbol{\mu}\cdot\bar{\boldsymbol{\mu}}) \tag{5.20}$$

$$\left\langle \mathrm{C}_1^{2\phi} \right\rangle = \frac{1}{15}\left(\alpha_{\lambda\lambda}\bar{\alpha}_{\zeta\zeta} + 2\alpha_{\lambda\zeta}\bar{\alpha}_{\lambda\zeta}\right) \tag{5.21}$$

Every field vector is the same **e**, so every Kronecker delta in the tensor $f^{(N)}_{r;\,i123\cdots N}$ yields a contraction equal to 1. Therefore, the results are a sum of every natural invariant ($\mathrm{C}_1^{1\phi}$ has only one, $\mathrm{C}_1^{2\phi}$ has two) multiplied by a coefficient derived from $m^{(N)}_{rs}$, and the sum of all coefficients comes to $(N+1)^{-1}$.

5 Dependence on beam polarisation geometry

5.1 Inter-polarisation angle

The scalar $(\mathbf{e}\cdot\mathbf{e}')$ is under direct experimental control, as the angle $\cos^{-1}(\mathbf{e}\cdot\mathbf{e}')$ is simply the difference in polarisation orientation for the absorbed and auxiliary beams at the molecule's position. The implication is that apart from irradiances *I* and *I′* and coherence, this angle is the only property of the pair of beams to determine the absorption rate in rotationally-averaged cases. The direction of the Poynting vectors **S** & **S** or wavevectors **k** & **k′** are *not* relevant.

An experiment designed to interrogate molecular behaviour, extracting maximum information concerning the magnitudes of molecular response tensor natural invariants, should measure absorption rates with different values for $\cos^{-1}(\mathbf{e}\cdot\mathbf{e}')$. The following subsections predict the results for the two extreme cases: choosing $\cos^{-1}(\mathbf{e}\cdot\mathbf{e}')=0°$ represents a case of *parallel* polarisations, denoted $\mathbf{e}\|\mathbf{e}'$, which results in $(\mathbf{e}\cdot\mathbf{e}')=1$; choosing $\cos^{-1}(\mathbf{e}\cdot\mathbf{e}')=90°$ represents a case of *perpendicular* polarisations, denoted $\mathbf{e}\perp\mathbf{e}'$, which results in $(\mathbf{e}\cdot\mathbf{e}')=0$. The results (5.20-29) may be directly substituted into equations (5.12) and (5.13), giving the one- or two-photon absorption rate for the fluid phase, for a given polarisation geometry.

5.2 Parallel polarisations, $\mathbf{e}\|\mathbf{e}'$

With parallel polarisations, every Kronecker delta in the tensor $f^{(N)}_{r;\,i123\cdots N}$ yields a contraction equal to 1, just like in the *B*=1 rate terms. Each rotationally-averaged *C* becomes a sum of all natural invariants multiplied by a coefficient $\sum_{r;\,s\in S'} m^{(N)}_{rs}$, where the set S' is defined as all *s* values that yield the chosen natural invariant from the contraction of molecular response tensors with $g^{(N)}_{s;\,\lambda123\cdots N}$.

$$\left\langle \mathrm{C}_2^{1\phi}\right\rangle^{\mathbf{e}\|\mathbf{e}'} = \frac{1}{15}\left(\mu_\lambda\bar{\beta}_{\lambda\zeta\zeta}+2\mu_\lambda\bar{\beta}_{\zeta\lambda\zeta}\right) \tag{5.22}$$

$$\begin{aligned}\left\langle \mathrm{C}_3^{1\phi}\right\rangle^{\mathbf{e}\|\mathbf{e}'} = \frac{1}{105}\big(\;& 2\beta_{\lambda\lambda\gamma}\bar{\beta}_{\gamma\zeta\zeta}+2\beta_{\lambda\lambda\gamma}\bar{\beta}_{\zeta\zeta\gamma}+2\beta_{\lambda\lambda\zeta}\bar{\beta}_{\gamma\zeta\gamma}+2\beta_{\lambda\zeta\gamma}\bar{\beta}_{\lambda\zeta\gamma}\\ &+2\beta_{\lambda\zeta\zeta}\bar{\beta}_{\gamma\lambda\gamma}+2\beta_{\lambda\zeta\gamma}\bar{\beta}_{\zeta\lambda\gamma}+2\beta_{\lambda\zeta\gamma}\bar{\beta}_{\gamma\lambda\zeta}+\beta_{\lambda\zeta\zeta}\bar{\beta}_{\lambda\gamma\gamma}\;\big)\end{aligned} \tag{5.23}$$

$$\left\langle \mathrm{C}_2^{2\phi} \right\rangle^{\mathbf{e}\parallel\mathbf{e}'} = \frac{1}{105}\left(\alpha_{\lambda\lambda}\bar{\chi}_{\gamma\gamma\zeta\zeta} + 2\alpha_{\lambda\lambda}\bar{\chi}_{\zeta\gamma\zeta\gamma} + 2\alpha_{\lambda\zeta}\bar{\chi}_{\lambda\zeta\gamma\gamma} + 2\alpha_{\lambda\zeta}\bar{\chi}_{\gamma\gamma\lambda\zeta} + 8\alpha_{\lambda\zeta}\bar{\chi}_{\lambda\gamma\zeta\gamma}\right) \tag{5.24}$$

$$\begin{aligned}\left\langle \mathrm{C}_3^{2\phi} \right\rangle^{\mathbf{e}\parallel\mathbf{e}'} = \frac{1}{945}\Big(& \chi_{\lambda\lambda\zeta\zeta}\bar{\chi}_{\gamma\gamma\varepsilon\varepsilon} + 2\chi_{\lambda\lambda\zeta\varepsilon}\bar{\chi}_{\gamma\gamma\zeta\varepsilon} + 2\chi_{\lambda\lambda\gamma\zeta}\bar{\chi}_{\gamma\zeta\varepsilon\varepsilon} + 2\chi_{\lambda\lambda\varepsilon\varepsilon}\bar{\chi}_{\gamma\zeta\gamma\zeta} \\ & + 8\chi_{\lambda\lambda\gamma\varepsilon}\bar{\chi}_{\gamma\zeta\zeta\varepsilon} + 2\chi_{\lambda\gamma\zeta\zeta}\bar{\chi}_{\lambda\gamma\varepsilon\varepsilon} + 4\chi_{\lambda\gamma\zeta\varepsilon}\bar{\chi}_{\lambda\gamma\zeta\varepsilon} + 8\chi_{\lambda\gamma\gamma\zeta}\bar{\chi}_{\lambda\zeta\varepsilon\varepsilon} \\ & + 8\chi_{\lambda\gamma\varepsilon\varepsilon}\bar{\chi}_{\lambda\zeta\gamma\zeta} + 16\chi_{\lambda\gamma\gamma\varepsilon}\bar{\chi}_{\lambda\zeta\zeta\varepsilon} + 16\chi_{\lambda\gamma\zeta\varepsilon}\bar{\chi}_{\lambda\zeta\gamma\varepsilon} + 2\chi_{\lambda\gamma\lambda\gamma}\bar{\chi}_{\zeta\zeta\varepsilon\varepsilon} \\ & + 2\chi_{\lambda\gamma\varepsilon\varepsilon}\bar{\chi}_{\zeta\zeta\lambda\gamma} + 8\chi_{\lambda\gamma\lambda\varepsilon}\bar{\chi}_{\zeta\zeta\gamma\varepsilon} + 4\chi_{\lambda\gamma\lambda\gamma}\bar{\chi}_{\zeta\varepsilon\zeta\varepsilon} + 4\chi_{\lambda\gamma\zeta\varepsilon}\bar{\chi}_{\zeta\varepsilon\lambda\gamma} + 16\chi_{\lambda\gamma\lambda\zeta}\bar{\chi}_{\zeta\varepsilon\gamma\varepsilon}\Big)\end{aligned} \tag{5.25}$$

Every element in the $m^{(N)}$ matrix contributes once to the coefficients, so in each averaged C the sum of all coefficients comes to $(N+1)^{-1}$.

5.3 Perpendicular polarisations, $\mathbf{e} \perp \mathbf{e}'$

With perpendicular polarizations, every contraction of the field vectors with $f^{(N)}_{r;\,i123\cdots N}$ yields 0 if the factor $(\mathbf{e}\cdot\mathbf{e}')$ appears, or 1 if it does not. So each rate term becomes a sum of all natural invariants, each multiplied by a coefficient $\sum_{\substack{r\in R'\\ s\in S'}} m^{(N)}_{rs}$, where the set R' is defined as all r values for which the $f^{(N)}_{r;\,i123\cdots N}$ contraction result is 1, and the set S' is again defined as all s values that yield the chosen natural invariant.

$$\left\langle \mathrm{C}_2^{1\phi} \right\rangle^{\mathbf{e}\perp\mathbf{e}'} = \frac{1}{15}\left(2\mu_\lambda\bar{\beta}_{\lambda\zeta\zeta} - \mu_\lambda\bar{\beta}_{\zeta\lambda\zeta}\right) \tag{5.26}$$

$$\begin{aligned}\left\langle \mathrm{C}_3^{1\phi} \right\rangle^{\mathbf{e}\perp\mathbf{e}'} = \frac{1}{210}\Big(& 5\beta_{\lambda\lambda\gamma}\bar{\beta}_{\gamma\zeta\zeta} + 12\beta_{\lambda\lambda\gamma}\bar{\beta}_{\zeta\zeta\gamma} - 2\beta_{\lambda\lambda\zeta}\bar{\beta}_{\gamma\zeta\gamma} - 2\beta_{\lambda\zeta\gamma}\bar{\beta}_{\lambda\zeta\gamma} \\ & - 2\beta_{\lambda\zeta\zeta}\bar{\beta}_{\gamma\lambda\gamma} - 2\beta_{\lambda\zeta\gamma}\bar{\beta}_{\zeta\lambda\gamma} - 2\beta_{\lambda\zeta\gamma}\bar{\beta}_{\gamma\lambda\zeta} - \beta_{\lambda\zeta\zeta}\bar{\beta}_{\lambda\gamma\gamma}\Big)\end{aligned} \tag{5.27}$$

$$\left\langle \mathrm{C}_2^{2\phi} \right\rangle^{\mathbf{e}\perp\mathbf{e}'} = \frac{1}{105}\left(3\alpha_{\lambda\lambda}\bar{\chi}_{\gamma\gamma\zeta\zeta} - \alpha_{\lambda\lambda}\bar{\chi}_{\zeta\gamma\zeta\gamma} + 6\alpha_{\lambda\zeta}\bar{\chi}_{\lambda\zeta\gamma\gamma} - \alpha_{\lambda\zeta}\bar{\chi}_{\gamma\gamma\lambda\zeta} - 4\alpha_{\lambda\zeta}\bar{\chi}_{\lambda\gamma\zeta\gamma}\right) \tag{5.28}$$

$$\begin{aligned}\left\langle \mathrm{C}_3^{2\phi} \right\rangle^{\mathbf{e}\perp\mathbf{e}'} = \frac{1}{630}\Big(& 4\chi_{\lambda\lambda\zeta\zeta}\bar{\chi}_{\gamma\gamma\varepsilon\varepsilon} + 8\chi_{\lambda\lambda\zeta\varepsilon}\bar{\chi}_{\gamma\gamma\zeta\varepsilon} - \chi_{\lambda\lambda\gamma\zeta}\bar{\chi}_{\gamma\zeta\varepsilon\varepsilon} - \chi_{\lambda\lambda\varepsilon\varepsilon}\bar{\chi}_{\gamma\zeta\gamma\zeta} \\ & - 4\chi_{\lambda\lambda\gamma\varepsilon}\bar{\chi}_{\gamma\zeta\zeta\varepsilon} + 8\chi_{\lambda\gamma\zeta\zeta}\bar{\chi}_{\lambda\gamma\varepsilon\varepsilon} + 16\chi_{\lambda\gamma\zeta\varepsilon}\bar{\chi}_{\lambda\gamma\zeta\varepsilon} - 4\chi_{\lambda\gamma\gamma\zeta}\bar{\chi}_{\lambda\zeta\varepsilon\varepsilon} \\ & - 4\chi_{\lambda\gamma\varepsilon\varepsilon}\bar{\chi}_{\lambda\zeta\gamma\zeta} - 8\chi_{\lambda\gamma\gamma\varepsilon}\bar{\chi}_{\lambda\zeta\zeta\varepsilon} - 8\chi_{\lambda\gamma\zeta\varepsilon}\bar{\chi}_{\lambda\zeta\gamma\varepsilon} - \chi_{\lambda\gamma\lambda\gamma}\bar{\chi}_{\zeta\zeta\varepsilon\varepsilon} \\ & - \chi_{\lambda\gamma\varepsilon\varepsilon}\bar{\chi}_{\zeta\zeta\lambda\gamma} - 4\chi_{\lambda\gamma\lambda\varepsilon}\bar{\chi}_{\zeta\zeta\gamma\varepsilon} + \chi_{\lambda\gamma\lambda\gamma}\bar{\chi}_{\zeta\varepsilon\zeta\varepsilon} + \chi_{\lambda\gamma\zeta\varepsilon}\bar{\chi}_{\zeta\varepsilon\lambda\gamma} + 4\chi_{\lambda\gamma\lambda\zeta}\bar{\chi}_{\zeta\varepsilon\gamma\varepsilon}\Big)\end{aligned} \tag{5.29}$$

If a certain natural invariant's coefficient is zero, $\sum_{\substack{r\in R' \\ s\in S'}} m_{rs}^{(N)} = 0$, this implies that the absorption interaction process does not engage with that particular form of molecular electronic response.

5.4 Depolarisation ratio

The scale of the effect on absorption of choosing $\cos^{-1}(\mathbf{e}\cdot\mathbf{e}')$ may be quantified by the ratio of the $\mathbf{e}\parallel\mathbf{e}'$ and $\mathbf{e}\perp\mathbf{e}'$ rate results. The value of this ratio indicates the range of absorption rates that are under experimental control via manipulation of beam polarisation. This is equivalent in definition and analytic role to the Raman spectroscopy concept of *depolarization ratio*.[16]

It must be noted that each of the second-term contractions $\mathrm{C}_2^{A\phi}$ are derived from the product of two different quantum amplitudes (either expressions (5.5) and (5.6) for single-photon absorption, or (5.8) and (5.10) for two-photon absorption), while the corresponding $\mathrm{C}_1^{A\phi}$ and $\mathrm{C}_3^{A\phi}$ are each derived from the square of one of them. This implies that if $\mathrm{C}_1^{A\phi} = 0$ (*un*modified absorption is forbidden) or $\mathrm{C}_3^{A\phi} = 0$ (*modified* absorption is forbidden), this is because one of the quantum amplitudes has zero magnitude, and ergo $\mathrm{C}_2^{A\phi} = 0$.

If absorption in the fluid phase is only possible with auxiliary beam involvement, the $\left\langle \mathrm{C}_1^{A\phi} \right\rangle = 0$ case, then it follows that $\Gamma_{A\phi} \propto \left\langle \mathrm{C}_3^{A\phi} \right\rangle$. So the depolarisation ratios are expressible as:

$$\frac{\Gamma_{A\phi}^{\mathbf{e}\perp\mathbf{e}'}}{\Gamma_{A\phi}^{\mathbf{e}\parallel\mathbf{e}'}} = \frac{\left\langle \mathrm{C}_3^{A\phi} \right\rangle^{\mathbf{e}\perp\mathbf{e}'}}{\left\langle \mathrm{C}_3^{A\phi} \right\rangle^{\mathbf{e}\parallel\mathbf{e}'}} \tag{5.30}$$

For single-photon absorption (A=1), the results of expressions (5.23) and (5.27) apply here. If all eight of the $\beta\overline{\beta}$ natural invariants are taken to be approximately equal, then the ratio will evaluate as 1/5. The maximum possible value is 3, in the case of the natural invariant $\beta_{\lambda\lambda\gamma}\overline{\beta}_{\zeta\zeta\gamma}$ being far greater than the other seven. For two-photon absorption (A=2), expressions (5.25) and (5.29) apply. If all 17 of the $\chi\overline{\chi}$ natural invariants are equal, then the ratio will evaluate as 3/35. The

maximum possible value is 6, achieved when $\chi_{\lambda\lambda\zeta\zeta}\overline{\chi}_{\gamma\gamma\varepsilon\varepsilon}$, $\chi_{\lambda\lambda\zeta\varepsilon}\overline{\chi}_{\gamma\gamma\zeta\varepsilon}$, $\chi_{\lambda\gamma\zeta\zeta}\overline{\chi}_{\lambda\gamma\varepsilon\varepsilon}$, or $\chi_{\lambda\gamma\zeta\varepsilon}\overline{\chi}_{\lambda\gamma\zeta\varepsilon}$ is dominant.

If fluid-phase absorption is not modified by the auxiliary beam, the case of $\left\langle \mathrm{C}_3^{A\phi} \right\rangle = 0$, then the beam's polarisation geometry is irrelevant. The ratio will have a default value of 1.

6 Discussion

The absorption processes analysed in this chapter may be nonlinear and include annihilation and re-creation of coherent photons, but they are fundamentally distinct (and experimentally distinguishable) from even-order transitions of no net excitation, such as the optical Kerr effect.[17–19] That said, it is possible that a high-order multiphoton interaction (such as four- or six-wave mixing) may lose its character of a coherent parametric process by resonant absorption at an intermediate state: The absorption would then become identifiable as a discrete process, physically distinct from the other interaction events, as it would be separated by a definite time delay and possibly a Stokes frequency shift.

In the fluid phase, with molecules freely rotating, the correct basis set for the molecular electronic response to absorption transitions is formed by the natural invariants that appear in equations (5.20-29). Their magnitudes contain all information regarding the relevant molecular responses. The natural invariant values are in large part determined by molecular structure, with the self-index-contraction pattern related to molecular symmetries. The results of sections 4 and 5 offer insights concerning the interplay of field geometry, molecular orientation and the symmetry of the molecule's structure. The variation of molecular response with beam polarisation and molecular orientation allows for straightforward measurement of interactions that are sensitive to such geometric considerations.[20]

In cases where the conventional single-photon or two-photon absorption mechanism is forbidden, an auxiliary-beam-modified absorption mechanism becomes necessary for any measurable absorption to occur. The results of section 5, which require high-order (up to N=8) rotational averaging methods, show some of the symmetry considerations that become important in such cases. These results

may be of particular interest to application in fluorescence spectroscopy experiments, as they permit information to be gained from manipulation of the easily-controllable beam parameters of intensity and polarisation direction. The depolarisation ratio defines the range of absorption-rate variation that is under the control of auxiliary beam polarisation.

In the vacuum case ($n = 1$), the results of section 5 here exactly reduce to a rotational average of the results reported by ref.[2] – the advanced symmetry selection-rule discussion in that paper also applies to these results. The depolarization measurement detailed in section 5 of this chapter is another tool for the analysis of symmetry rules, as it is a straightforward measurement that may be related to natural invariant magnitudes. These analytical methods should be useful for better understanding some of the advanced symmetry effects that arise in nonlinear solution-phase interactions.

As outlined in section 2, this chapter has employed a "dressed-field" formulation of molecular QED, with functions of refractive index n involved in the fundamental equations. This formulation differs from the media-modified MQED theory employed in chapter 3a and refs.[21,22], being more appropriate to this single-molecule problem.

Interpretation of equations (5.7) and (5.11) show that if an absorption process requires the involvement of an auxiliary beam, then the rate's proportionality to the square of auxiliary beam intensity I'^2 helps to identify the observed process as optically-modified absorption as opposed to sum-frequency absorption or similar. The depolarisation ratio measurement is a further means of verification.

Practically, nonlinearity in the auxiliary beam implies a need to use intense lasers as the beam source, as implied by the comments in section 3 regarding photon density q'/V. This may suggest that complicating effects of molecular re-alignment could arise, as the molecule might preferentially orient itself according to the auxiliary beam polarization. However, thermal agitation (Brownian motion, etc.) will usually overcome any such orientation-forcing.

The auxiliary beam has been described as undergoing forward scattering, such that the output photons experience no change in physical state. In principle, it is therefore possible for the observation of modified-absorption to serve as proof of

the involvement of these photons without their explicit annihilation. This constitutes a form of weak measurement of the auxiliary photon state. New kinds of weak-measurement experiment may be imagined from this basis.[23,24]

[1] D.L. Andrews, "Anomalous Absorption of the Ultrafast-Laser Supercontinuum": *Phys Rev A* **38**, 5129 (1988).

[2] D.S. Bradshaw and D.L. Andrews, "Laser-Modified One- and Two-Photon Absorption: Expanding the Scope of Optical Nonlinearity": *Phys Rev A* **88**, 033807 (2013).

[3] D.L. Andrews and D.S. Bradshaw, "Optically Tailored Access to Metastable Electronic States": *Chem. Phys. Lett.* **590**, 235 (2013).

[4] D.S. Bradshaw and D.L. Andrews, "Mechanism for Optical Enhancement and Suppression of Fluorescence": *J. Phys. Chem. A* **113**, 6537 (2009).

[5] D.S. Bradshaw and D.L. Andrews, "All-Optical Control of Molecular Fluorescence": *Phys Rev A* **81**, 013424 (2010).

[6] J.M. Leeder, D.S. Bradshaw, and D.L. Andrews, "Laser-Controlled Fluorescence in Two-Level Systems": *J. Phys. Chem. B* **115**, 5227 (2011).

[7] J.S. Ford and D.L. Andrews, "One- and Two-Photon Absorption in Solution: The Effects of a Passive Auxiliary Beam": *J. Chem. Phys.* **141**, (2014).

[8] Alberto Diaspro, Paolo Bianchini, Giuseppe Vicidomini, Mario Faretta, Paola Ramoino, and Cesare Usai, "Multi-Photon Excitation Microscopy": *Biomed. Eng. OnLine* **5**, 36 (2006).

[9] M.G. Kuzyk, K.D. Singer, and G.I. Stegeman, "Theory of Molecular Nonlinear Optics": *Adv Opt Photon* **5**, 4 (2013).

[10] D. L. Andrews and P. Allcock, *Optical Harmonics in Molecular Systems* (Wiley-VCH, Weinheim, 2002).

[11] G. Juzeliūas, "Microscopic Theory of Quantization of Radiation in Molecular Dielectrics: Normal-Mode Representation of Operators for Local and Averaged (macroscopic) Fields": *Phys Rev A* **53**, 3543 (1996).

[12] P.W. Milonni, "Field Quantization and Radiative Processes in Dispersive Dielectric Media": *J. Mod. Opt.* **42**, 1991 (1995).

[13] W.J. Meath and B.N. Jagatap, "On the Effects of Permanent Molecular Dipoles in the Simultaneous Absorption of Two Photons: Full Generalized Rotating Wave Approximation versus Analytical Results": *J. Chem. Phys.* **139**, (2013).

[14] R. Loudon, *The Quantum Theory of Light*, 3rd ed. (Oxford Science Publications, Oxford, 2000).

[15] D. P. Craig and T. Thirunamachandran, "Rotational Averaging of Tensors": *Mol. Quantum Electrodyn.*, Dover Paperback (Dover Publications, Mineola, New York, 1998), pp. 310–315.

[16] C.D. Allemand, "Depolarization Ratio Measurements in Raman Spectrometry": *Appl. Spectrosc.* **24**, 348 (1970).

[17] R. W. Boyd, *Nonlinear Optics*, 2nd ed. (Academic Press, San Diego, CA, 2003).

[18] S.R. Vigil and M.G. Kuzyk, "Absolute Molecular Optical Kerr Effect Spectroscopy of Dilute Organic Solutions and Neat Organic Liquids": *J Opt Soc Am B* **18**, 679 (2001).

[19] K. Mazur, I.A. Heisler, and S.R. Meech, "Water Dynamics at Protein Interfaces: Ultrafast Optical Kerr Effect Study": *J. Phys. Chem. A* **116**, 2678 (2012).

[20] V. Le Floc'h, S. Brasselet, J.-F. Roch, and J. Zyss, "Monitoring of Orientation in Molecular Ensembles by Polarization Sensitive Nonlinear Microscopy": *J. Phys. Chem. B* **107**, 12403 (2003).

[21] D.L. Andrews and J.S. Ford, "Resonance Energy Transfer: Influence of Neighboring Matter Absorbing in the Wavelength Region of the Acceptor": *J. Chem. Phys.* **139**, (2013).

[22] Z.-Q. You and C.-P. Hsu, "Theory and Calculation for the Electronic Coupling in Excitation Energy Transfer": *Int. J. Quantum Chem.* **114**, 102 (2014).

[23] P. Grangier, J.A. Levenson, and J.-P. Poizat, "Quantum Non-Demolition Measurements in Optics": *Nature* **396**, 537 (1998).

[24] W.J. Munro, K. Nemoto, R.G. Beausoleil, and T.P. Spiller, "High-Efficiency Quantum-Nondemolition Single-Photon-Number-Resolving Detector": *Phys Rev A* **71**, 033819 (2005).

–

Chapter 6: **Hyper-Rayleigh scattering including multipolar contributions**

1. Introduction

Rayleigh scattering, well-known as the cause of the atmosphere's light blue colour, is a photonic process consisting of single-photon absorption, concerted with one emission. The output photon is of equal wavelength and in a random direction, and the molecule returns to its initial state.[1] It is favourable at low luminosity, and is allowed by all atoms and molecules – scattering rate is determined by the $E1^2$ response tensor, polarisability $\boldsymbol{\alpha}$, which is finite for all matter due to its spatially-even optical-susceptibility parity.

A higher intensity of light input leads to related processes that involve more photon-absorption interaction events. The scattering process in which a molecule absorbs two photons and emits a second-harmonic is called hyper-Rayleigh scattering (HRS).[2] Note that the term "second harmonic generation" conventionally refers to a different process – a beam interacting with a solid material, generating coherent half-wavelength emission in the same direction as the input mode, not the *scattering* of photons described here.

The HRS process has applications in the spectroscopic analysis of minerals and condensed-phase nanoparticles.[3–5] The rate of HRS is determined by the $E1^3$ response tensor, hyperpolarisability $\boldsymbol{\beta}$.[1,6,7] Simplified "push-pull" models of molecular dynamics have been developed for predicting the principal $\boldsymbol{\beta}$ components of molecules,[8–10] often using a two-level approximation,[11–13] whose limitations have been identified and much discussed.[14–18]

For centrosymmetric molecules, all molecular state wavefunctions ψ have a parity that is either gerade (*symmetric* with respect to spatial inversion) or ungerade (antisymmetric). Consider the full integral form of the Dirac bracket that describes the molecular transition in an E1 interaction, such as in equation (2a.3):

$$\langle f|\boldsymbol{\mu}|i\rangle = \int \overline{\psi}_f \,\hat{\boldsymbol{\mu}}\, \psi_i \, d\tau \tag{6.1}$$

The integration is over all of three-dimensional space, so if the integrand is overall ungerade then the result will be zero. An electric dipole $\hat{\boldsymbol{\mu}}$ is naturally ungerade, as it consists of opposing positive and negative electric poles. According to the rules for combining gerade and ungerade (equivalent to multiplying +1 and –1), the integrand will thus be ungerade unless the molecule's initial and final state wavefunctions are of opposite parity. Therefore, an E1 interaction must impose a parity reversal on a centrosymmetric molecule, or else be forbidden. This is the Laporte selection rule.[19]

In a process of scattering there is no net molecular transition, such that the molecule's final state is also its initial state. In figure 6.1, this is shown as $|f\rangle = |i\rangle = |0\rangle$. In particular, scattering preserves the spatial parity of the molecule's state, and so the Laporte rule forbids a scattering process for centrosymmetric molecules that consists of an odd number of interactions. It follows that HRS, entailing three interactions and no overall molecular state change, is forbidden for molecules of sufficiently high symmetry. But second-harmonics may still be generated by such media – this chapter provides an explanation for this observation.

Going beyond the E1 approximation, considering additional terms of equation (2a.2), allows for additional multipolar interaction mechanisms, which may be immune to the symmetry arguments above which forbid HRS.[20] This chapter describes mechanisms that enable conventionally-forbidden HRS, using a QED derivation with an extended interaction Hamiltonian to calculate a more complete rate equation for HRS.

2. Process specification

Hyper-Rayleigh scattering is a photonic process of one molecule undergoing three photonic interaction events: two input photons are annihilated, and one second-harmonic output photon is created with unspecified direction of propagation. Observations of HRS are typically made on a sample of the molecule-of-interest in liquid solution. This chapter will not consider resonance effects – the two intermediate molecular states (labelled *r* and *s* as usual) must be presumed non-stationary.

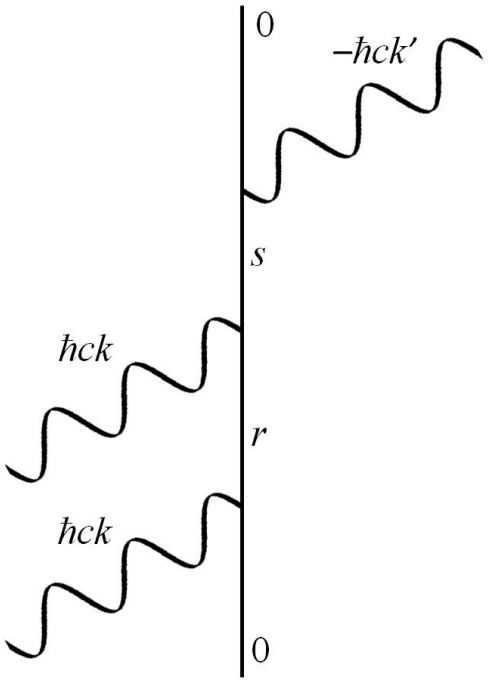

Figure 6.1: Molecular Feynman diagram for hyper-Rayleigh scattering, showing one of three (or six) time-orderings. The molecule finally returns to its initial state 0. The output photon, whose properties are denoted by labels bearing a prime mark (′), is a second-harmonic of the input light, such that $\hbar ck' = \hbar ck + \hbar ck$.

The HRS process is incoherent, such that each individual occurrence is unconnected and singular. The total HRS rate is thus a simple sum of the HRS rate for every molecule in the sample. This is in contrast to the multi-chromophore fluorescence described in chapter 4b, where the identity of the active chromophore is undetermined. For coherent second-harmonic-generating processes in fluid media, the M1 and E2 interactions are forbidden.[21,22]

The "E1 approximation" is the case where all interaction events are describable with an interaction Hamiltonian of purely electric dipole character – only the first term of equation (2a.2). The electric quadrupole (E2) and the magnetic dipole (M1) are jointly the next-leading interaction Hamiltonian terms, as they both arise from the multipolar transformation of the second order of the minimal coupling interaction.[23–25] Thus, the leading corrections to the E1 approximation of HRS will be where one of the three interactions has M1 character or E2 character. This choice of multipolar description is more fully explained in the next section.

The output photon and the interaction which creates it are distinguished from the absorptions by the presence of a prime mark (′). This chapter considers five possible HRS mechanisms:

- ($E1^3$) is the HRS mechanism conforming to the E1 approximation. The label indicates that there are three E1 interactions. A more systematic label might be ($E1^2E1'$).
- (E1M1E1′) is where one absorption event is an M1 interaction. The label indicates that the other absorption event and the emission event are both E1.
- (E1E2E1′) is where one absorption event is E2.
- ($E1^2M1'$) is where both absorption events are E1 interactions but the emission is M1.
- ($E1^2E2'$) is where the emission is E2.

Where M_{FI} is the quantum amplitude for a certain HRS mechanism, the following form of the Fermi rule gives the rate of the HRS process for a sample of N randomly-oriented molecules that are chemically similar. Chevron brackets denote an isotropic average over all molecular orientations.

$$\begin{aligned}\Gamma_{FI} &= \left\langle 2\pi\hbar^{-1}\rho_F \sum_{\text{Molecules}}^{N} \left| \sum_{\text{Mechanisms}}^{5} M_{FI} \right|^2 \right\rangle \\ &= 2\pi N \hbar^{-1}\rho_F \left\langle \left| M_{FI}^{(E1^3)} + M_{FI}^{(E1M1E1')} + M_{FI}^{(E1E2E1')} + M_{FI}^{(E1^2M1')} + M_{FI}^{(E1^2E2')} \right|^2 \right\rangle\end{aligned} \tag{6.2}$$

According to the pattern of equation (2a.12), this rate equation expands into 15 terms, for which the rotational average must be calculated separately.

$$\begin{aligned}\Gamma_{FI} &= 2\pi N \hbar^{-1}\rho_F \\ &\times \Big\{ \left\langle \left| M_{FI}^{(E1^3)} \right|^2 \right\rangle + 2\,\mathrm{Re}\left\langle M_{FI}^{(E1^3)} \bar{M}_{FI}^{(E1M1E1')} \right\rangle + \left\langle \left| M_{FI}^{(E1M1E1')} \right|^2 \right\rangle \\ &\quad + 2\,\mathrm{Re}\left\langle M_{FI}^{(E1^3)} \bar{M}_{FI}^{(E1E2E1')} \right\rangle + 2\,\mathrm{Re}\left\langle M_{FI}^{(E1M1E1')} \bar{M}_{FI}^{(E1E2E1')} \right\rangle + \left\langle \left| M_{FI}^{(E1E2E1')} \right|^2 \right\rangle \\ &\quad + 2\,\mathrm{Re}\left\langle M_{FI}^{(E1^3)} \bar{M}_{FI}^{(E1^2M1')} \right\rangle + 2\,\mathrm{Re}\left\langle M_{FI}^{(E1M1E1')} \bar{M}_{FI}^{(E1^2M1')} \right\rangle + 2\,\mathrm{Re}\left\langle M_{FI}^{(E1E2E1')} \bar{M}_{FI}^{(E1^2M1')} \right\rangle \\ &\quad + \left\langle \left| M_{FI}^{(E1^2M1')} \right|^2 \right\rangle + 2\,\mathrm{Re}\left\langle M_{FI}^{(E1^3)} \bar{M}_{FI}^{(E1^2E2')} \right\rangle + 2\,\mathrm{Re}\left\langle M_{FI}^{(E1M1E1')} \bar{M}_{FI}^{(E1^2E2')} \right\rangle \\ &\quad + 2\,\mathrm{Re}\left\langle M_{FI}^{(E1E2E1')} \bar{M}_{FI}^{(E1^2E2')} \right\rangle + 2\,\mathrm{Re}\left\langle M_{FI}^{(E1^2M1')} \bar{M}_{FI}^{(E1^2E2')} \right\rangle + \left\langle \left| M_{FI}^{(E1^2E2')} \right|^2 \right\rangle \Big\}\end{aligned} \tag{6.3}$$

3. Quantum amplitudes

The five quantum amplitudes M_{FI} are each given by the three-interaction term of equation (2a.13).

$$M_{FI} = \sum_{R,S} \frac{\langle F|H_{\text{int}}|S\rangle\langle S|H_{\text{int}}|R\rangle\langle R|H_{\text{int}}|I\rangle}{(E_I - E_R)(E_I - E_S)} \tag{6.4}$$

For each interaction event, equation (2a.2) gives the complete interaction Hamiltonian, H_{int}. In the previous section, the sum over various multipolar Hamiltonian terms has been subsumed into the sum of five quantum amplitudes for the five mechanisms – these are two complementary forms of the sum-over-mechanisms discussed in section 5 of chapter 2a. In this analysis, with five distinct mechanisms identified, each interaction event is described as either purely an E1 interaction, or purely an M1 interaction, or purely an E2 interaction. The relevant interaction Hamiltonian will thus be the single scalar-product found in the term of equation (2a.2) that corresponds to the type of interaction being described:

$$H_{\text{int}}^{(\text{E1})} = -\varepsilon_0^{-1}\,\boldsymbol{\mu}\cdot\mathbf{d}^{\perp} \tag{6.5}$$

$$H_{\text{int}}^{(\text{M1})} = -\mathbf{m}\cdot\mathbf{b} \tag{6.6}$$

$$H_{\text{int}}^{(\text{E2})} = -\varepsilon_0^{-1} Q_{ij}\nabla_j d_i^{\perp} \tag{6.7}$$

The relevant electric and magnetic fields are given in photonic form as mode expansions:

$$\mathbf{d}^{\perp} = i\sum_{\mathbf{k},\eta}\sqrt{\frac{\hbar ck\varepsilon_0}{2V}}\left[\mathbf{e}^{(\eta,\mathbf{k})}a^{(\eta,\mathbf{k})}e^{i\mathbf{k}.\mathbf{r}} - \overline{\mathbf{e}}^{(\eta,\mathbf{k})}a^{\dagger(\eta,\mathbf{k})}e^{-i\mathbf{k}.\mathbf{r}}\right] \tag{6.8}$$

$$\mathbf{b} = i\sum_{\mathbf{k},\eta}\sqrt{\frac{\hbar k}{2c\varepsilon_0 V}}\left[\mathbf{b}^{(\eta,\mathbf{k})}a^{(\eta,\mathbf{k})}e^{i\mathbf{k}.\mathbf{r}} - \overline{\mathbf{b}}^{(\eta,\mathbf{k})}\overline{a}^{\dagger(\eta,\mathbf{k})}e^{-i\mathbf{k}.\mathbf{r}}\right] \tag{6.9}$$

The partial-del operator in $H_{\text{int}}^{(\text{E2})}$ evaluates as:

$$\nabla_j e^{\pm i\mathbf{k}.\mathbf{r}} = \frac{d}{dr_j}e^{\pm ik_j r_j} = \pm i\,k_j\,e^{\pm i\mathbf{k}.\mathbf{r}} \tag{6.10}$$

HRS is a single-position process, so **r**=0 in all of the above equations. The operators a and $a^{\dagger}$ each apply to either photon creation or annihilation, with quantum algebra as in equations (2a.6-7). The three Dirac brackets of the M_{FI} numerator will therefore each be one of the following six results:

- The Dirac bracket for an E1 absorption event:

$$\left\langle S\left|H_{\text{int}}^{(\text{E1})}\right|R\right\rangle = -\left(i\sqrt{\frac{\hbar c}{2\varepsilon_0 V}}\right)\sqrt{q_R k}\ \mu_i^{sr}\ e_i^{(\mathbf{k},\eta)} \tag{6.11}$$

- The Dirac bracket for an E1 emission event:

$$\left\langle S\left|H_{\text{int}}^{(\text{E1})}\right|R\right\rangle = \left(i\sqrt{\frac{\hbar c}{2\varepsilon_0 V}}\right)\sqrt{(q'_R+1)k'}\ \mu_i^{sr}\ \bar{e}_i^{(\mathbf{k}',\eta')} \tag{6.12}$$

- The Dirac bracket for an M1 absorption event:

$$\left\langle S\left|H_{\text{int}}^{(\text{M1})}\right|R\right\rangle = \left(-i\sqrt{\frac{\hbar}{2c\varepsilon_0 V}}\right)\sqrt{q_R k}\ m_i^{sr}\ b_i^{(\mathbf{k},\eta)} \tag{6.13}$$

- The Dirac bracket for an M1 emission event:

$$\left\langle S\left|H_{\text{int}}^{(\text{M1})}\right|R\right\rangle = \left(-i\sqrt{\frac{\hbar}{2c\varepsilon_0 V}}\right)\sqrt{(q'_R+1)k'}\ m_i^{sr}\ \bar{b}_i^{(\mathbf{k}',\eta')} \tag{6.14}$$

- The Dirac bracket for an E2 absorption event:

$$\left\langle S\left|H_{\text{int}}^{(\text{E2})}\right|R\right\rangle = \sqrt{\frac{\hbar c}{2\varepsilon_0 V}}\sqrt{q_R k}\ \ Q_{ij}^{sr} e_i^{(\mathbf{k},\eta)} k_j \tag{6.15}$$

- The Dirac bracket for an E2 emission event:

$$\left\langle S\left|H_{\text{int}}^{(\text{E2})}\right|R\right\rangle = \sqrt{\frac{\hbar c}{2\varepsilon_0 V}}\sqrt{(q'_R+1)k'}\ \ Q_{ij}^{sr}\ \bar{e}_i^{(\mathbf{k}',\eta')}\ k'_j \tag{6.16}$$

Throughout this chapter, the unprimed symbol q refers to the average number of input photons occupying volume V before the first absorption event. The volume V is defined as the average volume that contains one output photon ($\hbar ck'$ of energy) after HRS. The input beam irradiance may be expressed as $I = \hbar c^2 qk/V$, with number-density q/V representing the average number of input photons

occupying a unit volume. Each absorption interaction is the annihilation of one input photon $(q_S = q_R - 1)$; each emission interaction is the creation of one output photon $(q'_S = q'_R + 1)$. The initial system state *I* has no radiation of the output mode $(q'_I = 0)$, but there is some flux of the input mode, such that volume *V* contains q_I photons. These equations have used the approximation of high input flux, $q \approx \sqrt{q(q-1)}$; but as HRS is an optically nonlinear process, a $g^{(2)}$ factor should in general be included to describe beam coherence.

In general, with six time-orderings for each HRS mechanism, the distinguishability of the three interaction events creates six potentially-distinct amplitude terms. But for the HRS mechanisms where the two absorption events are **in**distinguishable, there are only three distinct time-orderings and so the amplitude has only three unique terms.

What follows are the complete derivations of the five quantum amplitudes, with the molecular response tensor assigned a single symbol.

$$\begin{aligned} M_{FI}^{(\mathrm{E1^3})} &= -i\,q\left(\frac{\hbar ck}{\varepsilon_0 V}\right)^{\frac{3}{2}} e_i\, e_j\, \overline{e}'_k \\ &\quad \times \sum_{r,s}\left\{ \frac{\mu_i^{r0}\,\mu_j^{sr}\,\mu_k^{0s}}{\left(E_{0r}-\hbar ck\right)\left(E_{0s}-2\hbar ck\right)} \right. \\ &\qquad \left. + \frac{\mu_i^{r0}\,\mu_k^{sr}\,\mu_j^{0s}}{\left(E_{0r}-\hbar ck\right)\left(E_{0s}+\hbar ck\right)} + \frac{\mu_k^{r0}\,\mu_j^{sr}\,\mu_i^{0s}}{\left(E_{0r}+2\hbar ck\right)\left(E_{0s}+\hbar ck\right)} \right\} \\ &= -i\,q\left(\frac{\hbar ck}{\varepsilon_0 V}\right)^{\frac{3}{2}} e_i\, e_j\, \overline{e}'_k\, \beta_{(ij)k} \end{aligned} \tag{6.17}$$

$$\begin{aligned} M_{FI}^{(\mathrm{E1M1E1'})} &= -\frac{i}{2}\,q\,c^{1/2}\left(\frac{\hbar k}{\varepsilon_0 V}\right)^{\frac{3}{2}} e_i\, b_j\, \overline{e}'_k \\ &\quad \times \sum_{r,s}\left\{ \frac{\left(\mu_i^{r0}\,m_j^{sr}\,\mu_k^{0s} + m_j^{r0}\,\mu_i^{sr}\,\mu_k^{0s}\right)}{\left(E_{0r}-\hbar ck\right)\left(E_{0s}-2\hbar ck\right)} \right. \\ &\qquad \left. + \frac{\left(\mu_i^{r0}\,\mu_k^{sr}\,m_j^{0s} + m_j^{r0}\,\mu_k^{sr}\,\mu_i^{0s}\right)}{\left(E_{0r}-\hbar ck\right)\left(E_{0s}+\hbar ck\right)} + \frac{\left(\mu_k^{r0}\,\mu_i^{sr}\,m_j^{0s} + \mu_k^{r0}\,m_j^{sr}\,\mu_i^{0s}\right)}{\left(E_{0r}+2\hbar ck\right)\left(E_{0s}+\hbar ck\right)} \right\} \\ &= -\frac{i}{2}\,q\,c^{1/2}\left(\frac{\hbar k}{\varepsilon_0 V}\right)^{\frac{3}{2}} e_i\, b_j\, \overline{e}'_k\, J_{ijk} \end{aligned} \tag{6.18}$$

$$
\begin{aligned}
M_{FI}^{(\mathrm{E1E2E1'})} &= \frac{1}{2}k^{\frac{5}{2}}q\left(\frac{\hbar c}{\varepsilon_0 V}\right)^{\frac{3}{2}} e_i\, e_j\, \hat{k}_k \vec{e}'_l \\
&\quad \times \sum_{r,s}\left\{ \frac{\left(\mu_i^{r0}\, Q_{jk}^{sr}\, \mu_l^{0s} + Q_{jk}^{r0}\, \mu_i^{sr}\, \mu_l^{0s}\right)}{\left(E_{0r} - \hbar ck\right)\left(E_{0s} - 2\hbar ck\right)} \right. \\
&\qquad \left. + \frac{\left(\mu_i^{r0}\, \mu_l^{sr}\, Q_{jk}^{0s} + \mu_l^{r0}\, \mu_i^{sr}\, Q_{jk}^{0s}\right)}{\left(E_{0r} - \hbar ck\right)\left(E_{0s} + \hbar ck\right)} + \frac{\left(Q_{jk}^{r0}\, \mu_l^{sr}\, \mu_i^{0s} + \mu_l^{r0}\, Q_{jk}^{sr}\, \mu_i^{0s}\right)}{\left(E_{0r} + 2\hbar ck\right)\left(E_{0s} + \hbar ck\right)} \right\} \\
&= \frac{1}{2}k^{\frac{5}{2}}q\left(\frac{\hbar c}{\varepsilon_0 V}\right)^{\frac{3}{2}} e_i\, e_j\, \hat{k}_k \vec{e}'_l\; K_{(ij)kl}
\end{aligned}
\tag{6.19}
$$

$$
\begin{aligned}
M_{FI}^{\left(\mathrm{E1^2M1'}\right)} &= i\, q\, c^{1/2}\left(\frac{\hbar k}{\varepsilon_0 V}\right)^{\frac{3}{2}} e_i\; e_j\, \bar{b}'_k \\
&\quad \times \sum_{r,s}\left\{ \frac{\mu_i^{r0}\, \mu_j^{sr}\, m_k^{0s}}{\left(E_{0r} - \hbar ck\right)\left(E_{0s} - 2\hbar ck\right)} \right. \\
&\qquad \left. + \frac{\mu_i^{r0}\, m_k^{sr}\, \mu_j^{0s}}{\left(E_{0r} - \hbar ck\right)\left(E_{0s} + \hbar ck\right)} + \frac{m_k^{r0}\, \mu_j^{sr}\, \mu_i^{0s}}{\left(E_{0r} + 2\hbar ck\right)\left(E_{0s} + \hbar ck\right)} \right\} \\
&= i\, q\, c^{1/2}\left(\frac{\hbar k}{\varepsilon_0 V}\right)^{\frac{3}{2}} e_i\; e_j\, \bar{b}'_k\; J'_{(ij)k}
\end{aligned}
\tag{6.20}
$$

$$
\begin{aligned}
M_{FI}^{\left(\mathrm{E1^2E2'}\right)} &= -2k^{\frac{5}{2}}q\left(\frac{\hbar c}{\varepsilon_0 V}\right)^{\frac{3}{2}} e_i\, e_j\, \vec{e}'_k\; \hat{k}'_l \\
&\quad \times \sum_{r,s}\left\{ \frac{\mu_i^{r0}\, \mu_j^{sr}\, Q_{kl}^{0s}}{\left(E_{0r} - \hbar ck\right)\left(E_{0s} - 2\hbar ck\right)} \right. \\
&\qquad \left. + \frac{\mu_i^{r0}\, Q_{kl}^{sr}\, \mu_j^{0s}}{\left(E_{0r} - \hbar ck\right)\left(E_{0s} + \hbar ck\right)} + \frac{Q_{kl}^{r0}\, \mu_j^{sr}\, \mu_i^{0s}}{\left(E_{0r} + 2\hbar ck\right)\left(E_{0s} + \hbar ck\right)} \right\} \\
&= -2k^{\frac{5}{2}}q\left(\frac{\hbar c}{\varepsilon_0 V}\right)^{\frac{3}{2}} e_i\, e_j\, \vec{e}'_k\; \hat{k}'_l\, K'_{(ij)kl}
\end{aligned}
\tag{6.21}
$$

4. General rate equation

Substituting-in the quantum amplitude results (6.17-21) above into equation (6.3), the rate equation for HRS becomes:

$$\begin{aligned}\Gamma_{FI} = 2\pi\hbar^2\varepsilon_0^{-3} N\rho_F\ q^2 V^{-3}\Big\{ \quad & c^3k^3 \left\langle e_i\, e_j\, \overline{e}'_k \overline{e}_l\, \overline{e}_m\, e'_n \beta_{(ij)k} \overline{\beta}_{(lm)n} \right\rangle \\ & + c^2k^3\, \mathrm{Re}\left\langle e_i\, e_j\, \overline{e}'_k\, \overline{e}_l\, \overline{b}_m e'_n\, \beta_{(ij)k}\, \overline{J}_{lmn} \right\rangle \\ & + \frac{1}{4}\, c\, k^3 \left\langle e_i\, b_j \overline{e}'_k\, \overline{e}_l\, \overline{b}_m e'_n\, J_{ijk} \overline{J}_{lmn} \right\rangle \\ & - c^3k^4\, \mathrm{Im}\left\langle e_i\, e_j\, \overline{e}'_k\, \overline{e}_l\, \overline{e}_m \hat{k}_n e'_o\, \beta_{(ij)k} \overline{K}_{(lm)no} \right\rangle \\ & + \frac{1}{2} c^2k^4\, \mathrm{Im}\left\langle e_i\, e_j \hat{k}_k \overline{e}'_l\, \overline{e}_m \overline{b}_n\, e'_o\, K_{(ij)kl} \overline{J}_{mno} \right\rangle \\ & + \frac{1}{4} c^3k^5 \left\langle e_i\, e_j \hat{k}_k \overline{e}'_l\, \overline{e}_m \overline{e}_n\, \hat{k}_o e'_p\, K_{(ij)kl} \overline{K}_{(mn)op} \right\rangle \\ & - 2c^2\, k^3\ \mathrm{Re}\left\langle e_i\, e_j\, \overline{e}'_k\, \overline{e}_l\ \overline{e}_m\, b'_n\, \beta_{(ij)k} \overline{J}'_{(lm)n} \right\rangle \\ & - c\, k^3\, \mathrm{Re}\left\langle e_i\ e_j\, \overline{b}'_k\, \overline{e}_l\, \overline{b}_m e'_n\, J'_{(ij)k}\, \overline{J}_{lmn} \right\rangle \\ & + c^2\, k^4\, \mathrm{Im}\left\langle e_i\, e_j \hat{k}_k \overline{e}'_l\ \overline{e}_m\, \overline{e}_n\ b'_o\ K_{(ij)kl} \overline{J}'_{(mn)o} \right\rangle \\ & + c\, k^3 \left\langle e_i\ e_j\, \overline{b}'_k\, \overline{e}_l\ \overline{e}_m\, b'_n\ J'_{(ij)k} \overline{J}'_{(lm)n} \right\rangle \\ & + 4c^3k^4\, \mathrm{Im}\left\langle e_i\, e_j\, \overline{e}'_k\, \overline{e}_l\, \overline{e}_m e'_n\, \hat{k}'_o\, \beta_{(ij)k} \overline{K}'_{(lm)no} \right\rangle \\ & - 2c^2\, k^4\, \mathrm{Im}\left\langle e_i\, e_j \overline{e}'_k\, \hat{k}'_l\, \overline{e}_m \overline{b}_n\, e'_o\, K'_{(ij)kl} \overline{J}_{mno} \right\rangle \\ & - 2c^3k^5\, \mathrm{Re}\left\langle e_i\, e_j \overline{e}'_k\, \hat{k}'_l\, \overline{e}_m \overline{e}_n\, \hat{k}_o e'_p\, K'_{(ij)kl} \overline{K}_{(mn)op} \right\rangle \\ & - 4c^2k^4\, \mathrm{Im}\left\langle e_i\, e_j \overline{e}'_k\, \hat{k}'_l \overline{e}_m\ \overline{e}_n\ b'_o\, K'_{(ij)kl} \overline{J}'_{(mn)o} \right\rangle \\ & + 4c^3k^5 \left\langle e_i\, e_j \overline{e}'_k\, \hat{k}'_l \overline{e}_m \overline{e}_n\, e'_o\, \hat{k}'_p\, K'_{(ij)kl} \overline{K}'_{(mn)op} \right\rangle \quad \Big\} \end{aligned} \tag{6.22}$$

The second-"order" interaction Hamiltonians $H_{\mathrm{int}}^{(\mathrm{E2})}$ and $H_{\mathrm{int}}^{(\mathrm{M1})}$ are typically weaker than $H_{\mathrm{int}}^{(\mathrm{E1})}$ by a ratio of approximately the fine structure constant (≈137).[24] Thus the higher-order tensors **J**, **J'**, **K**, and **K'** will be similarly lesser in magnitude relative to **β**, if the latter is not reduced to zero by symmetry considerations: For a centrosymmetric molecule, it is known that **β**=0. The tensors **J**, **J'**, **K**, and **K'** describe even-order molecular susceptibilities, so the very same symmetry arguments suggest that these are nonzero for all molecules.

The first rate term, $\left|M_{FI}^{(\mathrm{E1}^3)}\right|^2$, would normally dominate the HRS process due to its $\beta\overline{\beta}$ dependence on molecular response – but centrosymmetry causes the ($\mathrm{E1}^3$)

mechanism to be forbidden. The four terms of quantum interference between ($E1^3$) and the higher-multipole mechanisms (i.e. the rate terms with a single β factor) are largely irrelevant: with a finite **β** they are insignificant compared to the $\left|M_{FI}^{(E1^3)}\right|^2$ term; and in the **β**=0 case they vanish along with it.[26] The 10 rate terms not involving ($E1^3$) only become significant under the **β**=0 condition.

This means that normally only the first line of equation (6.22) is significant; but in the centrosymmetric case, the 10 terms with no **β** factor will dominate the HRS rate.[27] What follows are the full calculations for these ten multipolar rate terms.

5. Rotational averages and experimental setups

Moving from static results to fluid, the rate terms of equation (6.22) are each rotationally-averaged according to the standard method outlined in chapter 2b.

$$\begin{aligned}\left\langle v_{i1}\ldots v_{iN}T_{i1\ldots iN}\right\rangle &= f_r\, v_{i1}\ldots v_{iN}\, m_{rs}\, g_s\, T_{\lambda 1\ldots\lambda N}\\ &= \left\{ f\, v_{i1}\ldots v_{iN}\right\}_r m_{rs} \left\{ g\, T_{\lambda 1\ldots\lambda N}\right\}_s\end{aligned} \qquad (6.23)$$

This is an Einstein index-summation of scalar factors: *r* is the index of experiment-specific radiation scalars, produced by applying Kronecker deltas *f* to the radiation vectors *v* (which in each rate term is a product of **e**, **ē**, **b**, **b̄**, and $\hat{\mathbf{k}}$ variants); *s* is the index of natural-invariant molecular scalars, produced by applying Kronecker deltas *g* to the two-factor molecular response tensors *T*; m_{rs} is a dimensionless number given in appendix 8b.

Information about the structure of the input and output radiation modes is required in order to evaluate the radiation scalars $\left\{ f\, v_{i1}\ldots v_{in}\right\}_r$. This chapter considers four choices of experimental setup:

- "Parallel": Linearly-polarised light is input; light of parallel polarisation is detected from an orthogonal position.
- "Perpendicular": Linearly-polarised light is input; light of perpendicular polarisation is detected from an orthogonal position.
- "Preserved": Circularly-polarised light is input; light of preserved left-polarisation is detected from a forward position.

- "Flipped": Circularly-polarised light is input; light of reversed polarisation (left to right) is detected from a forward position.

These are illustrated in figure 6.2. The "parallel" and "perpendicular" HRS experiments may be compared in order to determine the depolarisation ratio of scattered radiation – simply take the ratio of the parallel and perpendicular HRS rate values. The same is true for the "preserved" and "flipped" setups – the ratio of their rates gives the reversal ratio of HRS.[27]

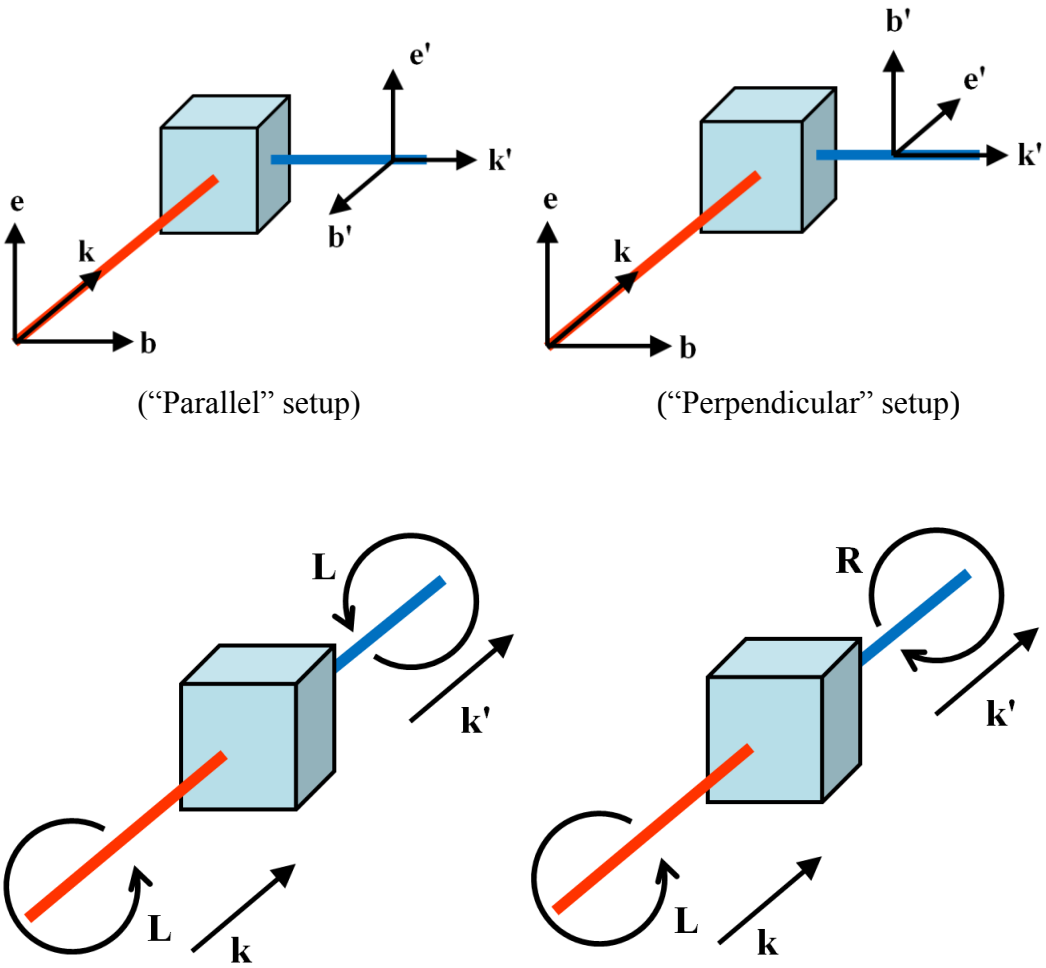

Figure 6.2: Illustrations of the four example experimental setups. The cube represents a sample of *N* condensed-phase molecules, each of which is an individual HRS system. Input light is shown in orange with wavevector **k**; output light in blue with wavevector **k'**.

The choice of experimental setup specifies the orientation of the radiation vectors **e**, **ē**, **b**, **b̄**, and **k** in the input and output modes. These ten vectors each have a magnitude of unity (note the carat on the **k** vectors appearing in the rate equation). Accordingly, each is expressible as a combination of the standard-basis Cartesian unit vectors $\{\hat{\mathbf{x}}, \hat{\mathbf{y}}, \hat{\mathbf{z}}\}$.

	P. or P. input	Parallel output	Perpendicular output	Left-circular polarisation	Right-circular polarisation
e =	$\hat{\mathbf{x}}$	$\hat{\mathbf{x}}$	$\hat{\mathbf{z}}$	$\frac{1}{\sqrt{2}}(\hat{\mathbf{x}}+i\,\hat{\mathbf{y}})$	$\frac{1}{\sqrt{2}}(\hat{\mathbf{x}}-i\,\hat{\mathbf{y}})$
ē =	$\hat{\mathbf{x}}$	$\hat{\mathbf{x}}$	$\hat{\mathbf{z}}$	$\frac{1}{\sqrt{2}}(\hat{\mathbf{x}}-i\,\hat{\mathbf{y}})$	$\frac{1}{\sqrt{2}}(\hat{\mathbf{x}}+i\,\hat{\mathbf{y}})$
b =	$\hat{\mathbf{y}}$	$-\hat{\mathbf{z}}$	$\hat{\mathbf{x}}$	$\frac{-i}{\sqrt{2}}(\hat{\mathbf{x}}+i\,\hat{\mathbf{y}})$	$\frac{i}{\sqrt{2}}(\hat{\mathbf{x}}-i\,\hat{\mathbf{y}})$
b̄ =	$\hat{\mathbf{y}}$	$-\hat{\mathbf{z}}$	$\hat{\mathbf{x}}$	$\frac{i}{\sqrt{2}}(\hat{\mathbf{x}}-i\,\hat{\mathbf{y}})$	$\frac{-i}{\sqrt{2}}(\hat{\mathbf{x}}+i\,\hat{\mathbf{y}})$
k =	$\hat{\mathbf{z}}$	$\hat{\mathbf{y}}$	$\hat{\mathbf{y}}$	$\hat{\mathbf{z}}$	$\hat{\mathbf{z}}$

Table 6.1: Evaluation of the field vectors in equation (6.22).

The values of their dot products are hence derived by straightforward comparison of their Cartesian components listed here – e.g. in the "parallel" experiment, $(\mathbf{k}\cdot\mathbf{b}') = \hat{\mathbf{z}}\cdot(-\hat{\mathbf{z}}) = -1$; and in the "perpendicular" experiment, $(\bar{\mathbf{e}}\cdot\mathbf{b}') = \hat{\mathbf{x}}\cdot\hat{\mathbf{x}} = 1$. The constituent factors of any radiation scalar $\{f\, v_{i1}\ldots v_{in}\}_r$ may be easily derived from table 6.1 in this way.

For example, consider the rate term arising from the square of the ($E1^2E2'$) mechanism:

$$\left\langle \left| M_{FI}^{\left(E1^2E2'\right)} \right|^2 \right\rangle \propto \left\langle e_i\, e_j \bar{e}'_k\, \hat{k}'_l\, \bar{e}_m \bar{e}_n\, e'_o\, \hat{k}'_p\, K'_{(ij)kl} \bar{K}'_{(mn)op} \right\rangle \tag{6.24}$$

The field tensor $e_i\, e_j \bar{e}'_k\, \hat{k}'_l \bar{e}_m \bar{e}_n\, e'_o\, \hat{k}'_p$ is contracted by application of Kronecker deltas f to produce a set of radiation scalars $\left\{ f\, e_i\, e_j \bar{e}'_k\, \hat{k}'_l \bar{e}_m \bar{e}_n\, e'_o\, \hat{k}'_p \right\}_r$. According to equation (2b.7), the set of *r* values has cardinality of 105. But because the vectors

e, $\overline{\mathbf{e}}$ and **k'** each appear twice, degeneracy ensures that there are only 23 distinct scalars. As this rate term is an eighth-rank rotational average, each of the scalars has four dot-product factors, which can be derived from table 6.1. The radiation scalars $\left\{ f\, e_i e_j \vec{e}'_k \hat{k}'_l \bar{e}_m \bar{e}_n e'_o \hat{k}'_p \right\}_r$ are evaluated in table 6.3 at the end of this chapter.

The other 14 terms of rate equation (6.22) have their own set of radiation scalars, which likewise evaluate as dimensionless numbers in each setup. These numbers may be complex, but the Fermi rule keeps the rate result real.

Each rate term also has its own set of molecular scalars $\{g\, T_{\lambda 1 \ldots \lambda n}\}_s$. Each of these is a natural invariant of the molecule's intrinsic electronic behaviour, as discussed in chapter 2b.

For the rate term arising from the square of the ($E1^2E2'$) mechanism, the molecular response tensor $K'_{(ij)kl}\bar{K}'_{(mn)op}$ is contracted by application of Kronecker deltas *g* to produce a set of molecular scalars $\left\{g\, K'_{(ij)kl}\bar{K}'_{(mn)op}\right\}_s$. The bracketed subscript indices indicate index-symmetry, and this implies degeneracy which reduces the set of 105 independent *s* values to just 36 distinct natural invariants. The molecular scalars $\left\{g\, K'_{(ij)kl}\bar{K}'_{(mn)op}\right\}_s$ are evaluated in table 6.4 at the end of this chapter.

Each of the other 14 rate terms has a two-factor molecular response tensor (arising from a combination of two HRS mechanisms) which likewise evaluates as a set of natural invariant scalars. Any real molecule will have in-principle-measurable values for each of its natural invariants.

With the radiation scalars $\{ f\, v_{i1} \ldots v_{in} \}_r$ and molecular scalars $\{g\, T_{\lambda 1 \ldots \lambda n}\}_s$ each derived for all possible values of *r* and *s*, it is possible to calculate the rotationally-averaged rate term as a simple unweighted sum of 15^2 or 105^2 terms, according to equation (6.23).[28–30] The radiation scalars and the m_{rs} elements are each dimensionless numbers that can be precisely known for each experimental setup, but the molecular scalars are unknown properties of the molecule, the natural invariants of its interactions, and must remain as labelled variables. In calculating the sum over *r* and *s*, the final result is a weighted sum over the set of these natural invariants.

For our example rate term, equation (6.23) becomes:

$$\begin{aligned}&\left\langle e_i\, e_j \bar{e}'_k\; \hat{k}'_l \bar{e}_m \bar{e}_n\, e'_o\; \hat{k}'_p\; K'_{(ij)kl} \bar{K}'_{(mn)op} \right\rangle \\ &\quad = \left\{ f\, e_i\, e_j \bar{e}'_k\; \hat{k}'_l \bar{e}_m \bar{e}_n\, e'_o\; \hat{k}'_p \right\}_r m^{(8)}_{rs} \left\{ g\, K'_{(ij)kl} \bar{K}'_{(mn)op} \right\}_s\end{aligned} \tag{6.25}$$

The values of the three scalar factors in each of the 11025 terms are given in table 6.3, table 6.4, and tables 8b.3-8. The radiation scalars and $m^{(8)}$ elements are numbers, so the 36 natural invariants can factorise out. Thus for each experimental setup, the predicted value of this averaged-tensor is a weighted sum of the 36 natural invariants, each multiplied by a number coefficient.

The outcome of equation (6.25) is reported in table 6.5 at the end of this chapter. This is the most succinct statement of the rate term that is possible without making additional assumptions about the molecular properties. The equivalent data derived for the other nine non-($E1^3$) rate terms can be found in the supplementary material of ref.[31].

6. Simple case

An assumption of ideal molecular symmetry lets us set all of the natural invariants in each rate term to be equal. This means total degeneracy in the index *s*, so we may define a single molecular scalar $T \equiv \left\{ g\, T_{\lambda 1 \ldots \lambda n} \right\}_s$ that is the same for all *s*. Then, in the final rate equation for each experimental setup, each averaged-tensor is reduced to a single molecular scalar *T* multiplied by a single dimensionless coefficient, $x_T \equiv \sum_{r,s} \left\{ f\, v_{i1} \ldots v_{in} \right\}_r m_{rs}$.

$$\therefore \;\; \left\langle v_{i1} \ldots v_{in} T_{i1 \ldots in} \right\rangle = x_T\, T \tag{6.26}$$

So the complete 10-term (**β**=0) version of rate equation (6.22) becomes:

$$\begin{aligned}\Gamma_{FI} &= 2\pi\hbar^2 \varepsilon_0^{-3} N \rho_F\, q^2 V^{-3} \\ &\quad \times \Big\{ \quad c\, k^3 \Big[\; 2^{-2}\, x_{J\bar{J}} \left| J\, \bar{J} \right| - x_{J'\bar{J}} \, \mathrm{Re}\left(J'\, \bar{J} \right) + x_{J'\bar{J}'} \left| J'\, \bar{J}' \right| \; \Big] \\ &\qquad + c^2 k^4 \Big[\; -2^{-1}\, x_{K\bar{J}} \; \mathrm{Im}\left(K\, \bar{J} \right) + x_{K\bar{J}'} \; \mathrm{Im}\left(K\, \bar{J}' \right) \\ &\qquad\qquad -2 x_{K'\bar{J}} \; \mathrm{Im}\left(K'\, \bar{J} \right) - 4 x_{K'\bar{J}'} \; \mathrm{Im}\left(K'\, \bar{J}' \right) \; \Big] \\ &\qquad + c^3 k^5 \Big[\; 2^{-2}\, x_{K\bar{K}} \left| K\, \bar{K} \right| - 2 x_{K'\bar{K}} \; \mathrm{Re}\left(K'\, \bar{K} \right) + 4\, x_{K'\bar{K}'} \left| K'\, \bar{K}' \right| \; \Big] \; \Big\}\end{aligned} \tag{6.27}$$

x_T	Parallel	Perpendicular	Preserved	Reversed
$J\,\bar{J}$	1/35	1/105	2/35	2/35
$J'\,\bar{J}$	0	0	−4/35	4/35
$J'\,\bar{J}'$	−2/105	1/7	2/35	2/35
$K\,\bar{J}$	0	0	2/35	0
$K\,\bar{J}'$	1/35	−1/105	2/35	0
$K'\,\bar{J}$	−1/35	1/105	−2/35	−44/105
$K'\,\bar{J}'$	0	0	2/35	−4/15
$K\,\bar{K}$	1/63	1/105	2/315	2/315
$K'\,\bar{K}$	0	0	4/315	4/315
$K'\,\bar{K}'$	1/63	1/315	2/315	2/315

Table 6.2: Values of x_T for use in equation (6.27). Many thanks to Matthew D. Williams for calculating the first seven rows, which require 6th- and 7th-order rotational averages.

To continue the worked example of the previous section, the values of $x_{K'\bar{K}'}$ for each experimental setup (the final row of table 6.2) are calculated by simply adding all 23 of the coefficients in the relevant column of table 6.5.[31]

7. Discussion

The higher-multipolar interaction moments **m** and **Q** are usually ignored as negligible, but if the ($E1^3$) HRS mechanism is forbidden by symmetry, then they become necessary for the HRS process. The four mechanisms involving M1 and E2 interactions are allowed for all molecules, and the rate of HRS arising therefrom should be non-negligible. The nonzero rate results of this chapter lead to the conclusion that HRS is universally allowed. Centrosymmetric HRS should be weaker than conventional HRS by a factor in the ballpark of 137^2. Use of near-resonant wavelengths, such that $\hbar ck$ or $\hbar ck$' is chosen to be near to an energy gap

for the molecule's ground state, may enhance the tensors **J**, **J'**, **K**, or **K'** by a much greater degree,[32] turning the "forbidden" HRS process into a measurable signal.

The depolarisation and reversal ratios of HRS provide a new method for uniquely characterising different molecules. Experimental equipment that automatically switches between the detection of different polarisation states may be used, combining two setups into one experiment that can directly test the results of this chapter.[27,33]

One notable prediction of these results comes from comparing the preserved and flipped rates in the case of **J** and **J'** tensors being negligible compared to the **K** and **K'** (i.e. the M1-involving mechanisms are near-forbidden). This reversal ratio evaluates as 1, indicating total reversal of circularity for forward emission of second-harmonic photons. The powers of *k* in equation (6.27) suggest that this observation will be most likely at shorter wavelengths.

[1] D. L. Andrews and P. Allcock, *Optical Harmonics in Molecular Systems* (Wiley-VCH, Weinheim, 2002).
[2] S. Kielich, J.R. Lalanne, and F.B. Martin, "Double-Photon Elastic Light Scattering by Liquids Having Centrosymmetric Molecules": *Phys Rev Lett* **26**, 1295 (1971).
[3] David B. Hollis, "Review of Hyper-Rayleigh and Second Harmonic Scattering in Minerals and Other Inorganic Solids": *Am. Mineral.* **73**, 701 (1988).
[4] G. Revillod, J. Duboisset, I. Russier-Antoine, E. Benichou, G. Bachelier, C. Jonin, and P.-F. Brevet, "Multipolar Contributions to the Second Harmonic Response from Mixed DiA−SDS Molecular Aggregates": *J. Phys. Chem. C* **112**, 2716 (2008).
[5] S. Roke and G. Gonella, "Nonlinear Light Scattering and Spectroscopy of Particles and Droplets in Liquids": *Annu. Rev. Phys. Chem.* **63**, 353 (2012).
[6] D.M. Bishop, "Explicit Nondivergent Formulas for Atomic and Molecular Dynamic Hyperpolarizabilities": *J. Chem. Phys.* **100**, 6535 (1994).
[7] S. Brasselet and J. Zyss, "A Dual Molecular and Photonic Engineering Perspective in Molecular Nonlinear Optics: Ellipsometric Control of Optical Poling": *Pure Appl. Opt. J. Eur. Opt. Soc. Part A* **7**, 129 (1998).

[8] M. Barzoukas, C. Runser, A. Fort, and M. Blanchard-Desce, "A Two-State Description of (hyper) Polarizabilities of Push-Pull Molecules Based on a Two-Form Model": *Chem. Phys. Lett.* **257**, 531 (1996).

[9] S.K. Yang, H.C. Ahn, S.-J. Jeon, I. Asselberghs, K. Clays, A. Persoons, and B.R. Cho, "First Hyperpolarizabilities of Dipolar, Bis-Dipolar, and Octupolar Molecules": *Chem. Phys. Lett.* **403**, 68 (2005).

[10] P.C. Ray, "Size and Shape Dependent Second Order Nonlinear Optical Properties of Nanomaterials and Their Application in Biological and Chemical Sensing": *Chem. Rev.* **110**, 5332 (2010).

[11] E. Hendrickx, K. Clays, and A. Persoons, "Hyper-Rayleigh Scattering in Isotropic Solution": *Acc. Chem. Res.* **31**, 675 (1998).

[12] K. Clays and B.J. Coe, "Design Strategies versus Limiting Theory for Engineering Large Second-Order Nonlinear Optical Polarizabilities in Charged Organic Molecules": *Chem. Mater.* **15**, 642 (2003).

[13] S. Van Cleuvenbergen, I. Asselberghs, W. Vanormelingen, T. Verbiest, E. Franz, K. Clays, M.G. Kuzyk, and G. Koeckelberghs, "Record-High Hyperpolarizabilities in Conjugated Polymers": *J. Mater. Chem. C* **2**, 4533 (2014).

[14] D.L. Andrews, D.S. Bradshaw, and M.M. Coles, "Limitations and Improvements upon the Two-Level Approximation for Molecular Nonlinear Optics": *Proc. SPIE*, **7917** (2011), p. 1K.

[15] D.S. Bradshaw and D.L. Andrews, "Mechanisms of Light Energy Harvesting in Dendrimers and Hyperbranched Polymers": *Polymers* **3**, 2053 (2011).

[16] M.G. Kuzyk, "Quantum Limits of the Hyper-Rayleigh Scattering Susceptibility": *IEEE J. Sel. Top. Quantum Electron.* **7**, 774 (2001).

[17] M.G. Kuzyk, J. Pérez-Moreno, and S. Shafei, "Sum Rules and Scaling in Nonlinear Optics": *Sum Rules Scaling Nonlinear Opt.* **529**, 297 (2013).

[18] J. Perez-Moreno, K. Clays, and M.G. Kuzyk, "Why Do We Need Three Levels to Understand the Molecular Optical Response?": *Proc. SPIE*, **8113** (2011), p. 0L.

[19] Peter Atkins and Julio de Paula, *Atkins' Physical Chemistry*, 8th ed. (Oxford University Press, 2006).

[20] Y. Zhang, X. Wang, D. Fu, J. Cheng, Y. Shen, J. Liu, and Z. Lu, "Second-Order Optical Nonlinearity Study of CdS Nanoparticles via Hyper-Rayleigh Scattering": *J. Phys. Chem. Solids* **62**, 903 (2001).

[21] D.L. Andrews, "Harmonic Generation in Free Molecules": *J. Phys. B At. Mol. Phys.* **13**, 4091 (1980).

[22] D.L. Andrews, "The Role of Longitudinal Polarization in Surface Second Harmonic Generation": *J. Mod. Opt.* **40**, 939 (1993).

[23] D. Epperlein, B. Dick, G. Marowsky, and G.A. Reider, "Second-Harmonic Generation in Centro-Symmetric Media": *Appl. Phys. B* **44**, 5 (1987).

[24] E.A. Power and T. Thirunamachandran, "On the Nature of the Hamiltonian for the Interaction of Radiation with Atoms and Molecules: (e/mc)p.A, −μ.E, and All That": *Am. J. Phys.* **46**, 370 (1978).

[25] R.G. Woolley, "Gauge Invariance in Non–relativistic Electrodynamics": *Proc. R. Soc. Lond. Math. Phys. Eng. Sci.* **456**, 1803 (2000).

[26] D.L. Andrews and T. Thirunamachandran, "Hyper−Raman Scattering by Chiral Molecules": *J. Chem. Phys.* **70**, 1027 (1979).

[27] S. Kielich and Z. Ożgo, "Reversal Ratio of Double-Photon Scattering by Noncentro-Symmetric Molecules": *Opt. Commun.* **8**, 417 (1973).

[28] D.L. Andrews and T. Thirunamachandran, "Polarization Effects in Non-Linear Scattering": *Opt. Commun.* **22**, 312 (1977).

[29] D.L. Andrews and W.A. Ghoul, "Polarization Studies in Multiphoton Absorption Spectroscopy": *J. Chem. Phys.* **75**, 530 (1981).

[30] D.H. Friese, M.T.P. Beerepoot, and K. Ruud, "Rotational Averaging of Multiphoton Absorption Cross Sections": *J. Chem. Phys.* **141**, (2014).

[31] M. D. Williams, J. S. Ford, and D. L. Andrews, "Hyper-Rayleigh Scattering in Centrosymmetric Systems": *J. Chem. Phys.* **143**, 124301 (2015).

[32] D.A. Long and L. Stanton, "Studies of Nonlinear Phenomena. I. Theory of the Hyper Raman Effect": *Proc. R. Soc. Lond. Math. Phys. Eng. Sci.* **318**, 441 (1970).

[33] D.P. Shelton, "Accurate Hyper-Rayleigh Scattering Polarization Measurements": *Rev. Sci. Instrum.* **82**, (2011).

–

r =	Radiation scalar	Parallel	Perpendicular	Preserved	Flipped
1,2,14,15,16,17,29,30	(e' · e*)(e'* · e)(e · k')(e* · k')	0	0	0	0
3,13,18,28	(e* · e*)(e'* · e)(e · k')(e' · k')	0	0	0	0
4,5,19,20	(e · e')(e'* · e)(e* · k')^2	0	0	0	0
6,21	(e* · e*)(e · e')(e'* · e)(k' · k')	1	0	0	0
7,8,10,11,22,23,25,26	(e · e*)(e'* · e)(e* · k')(e' · k')	0	0	0	0
9,12,24,27	(e · e*)(e' · e*)(e'* · e)(k' · k')	1	0	1	0
31,32,92,93	(e · e)(e' · e*)(e* · k')(e'* · k')	0	0	0	0
33,91	(e · e)(e* · e*)(e' · k')(e'* · k')	0	0	0	0
34,35,37,40,98,99,101,104	(e · e*)(e · e')(e* · k')(e'* · k')	0	0	0	0
36,43,94,97	(e* · e*)(e · e')(e · k')(e'* · k')	0	0	0	0
38,41,102,105	(e · e*)^2(e' · k')(e'* · k')	0	0	0	0
39,42,44,45,95,96,100,103	(e · e*)(e' · e*)(e · k')(e'* · k')	0	0	0	0
46,47	(e · e)(e'* · e')(e* · k')^2	0	0	0	0
48	(e · e)(e* · e*)(e'* · e')(k' · k')	1	1	0	0
49,50,52,54,55,57,59,60	(e · e*)(e'* · e')(e · k')(e* · k')	0	0	0	0
51,58	(e* · e*)(e'* · e')(e · k')^2	0	0	0	0
53,56	(e · e*)^2(e'* · e')(k' · k')	1	1	1	1
61,62,76,77	(e · e)(e'* · e*)(e* · k')(e' · k')	0	0	0	0
63,78	(e · e)(e'* · e*)(e' · e*)(k' · k')	1	0	0	0
64,67,69,74,79,82,84,89	(e · e')(e'* · e*)(e · k')(e* · k')	0	0	0	0
65,70,72,75,80,85,87,90	(e · e*)(e'* · e*)(e · k')(e' · k')	0	0	0	0
66,73,81,88	(e'* · e*)(e' · e*)(e · k')^2	0	0	0	0
68,71,83,86	(e · e*)(e · e')(e'* · e*)(k' · k')	1	0	0	1

Table 6.3: Evaluation of the 105 radiation scalars $\left\{ f\, e_i\, e_j \bar{e}'_k\, \hat{k}'_l \bar{e}_m \bar{e}_n\, e'_o\, \hat{k}'_p \right\}_r$.

Symbols e and k stand for the **e** and $\hat{\mathbf{k}}$ vectors in equation (21), and an asterisk (*) denotes complex conjugation: $\mathrm{e}^* \equiv \bar{\mathbf{e}}$.

s =	Molecular scalar (natural invariant)
1,2,16,17	$K'_{a(ab)b} K'^{*}_{c(cd)d}$
3,18	$K'_{a(ab)b} K'^{*}_{c(dd)c}$
4,5,19,20	$K'_{a(ab)c} K'^{*}_{b(cd)d}$
6,21	$K'_{a(ab)c} K'^{*}_{b(dd)c}$
7,10,22,25	$K'_{a(ab)c} K'^{*}_{c(bd)d}$
8,11,23,26	$K'_{a(ab)c} K'^{*}_{d(bc)d}$
9,12,24,27	$K'_{a(ab)c} K'^{*}_{d(bd)c}$
13,28	$K'_{a(ab)c} K'^{*}_{c(dd)b}$
14,15,29,30	$K'_{a(ab)c} K'^{*}_{d(cd)b}$
31,32	$K'_{a(bb)a} K'^{*}_{c(cd)d}$
33	$K'_{a(bb)a} K'^{*}_{c(dd)c}$
34,35,37,40	$K'_{a(bc)a} K'^{*}_{b(cd)d}$
36,43	$K'_{a(bc)a} K'^{*}_{b(dd)c}$
38,41	$K'_{a(bc)a} K'^{*}_{d(bc)d}$
39,42,44,45	$K'_{a(bc)a} K'^{*}_{d(bd)c}$
46,47	$K'_{a(bb)c} K'^{*}_{a(cd)d}$
48	$K'_{a(bb)c} K'^{*}_{a(dd)c}$
49,50,52,55	$K'_{a(bc)b} K'^{*}_{a(cd)d}$
51,58	$K'_{a(bc)b} K'^{*}_{a(dd)c}$
53,56	$K'_{a(bc)d} K'^{*}_{a(bc)d}$
54,57,59,60	$K'_{a(bc)d} K'^{*}_{a(bd)c}$
61,76	$K'_{a(bb)c} K'^{*}_{c(ad)d}$
62,77	$K'_{a(bb)c} K'^{*}_{d(ac)d}$
63,78	$K'_{a(bb)c} K'^{*}_{d(ad)c}$
64,67,79,82	$K'_{a(bc)b} K'^{*}_{c(ad)d}$
65,70,80,85	$K'_{a(bc)b} K'^{*}_{d(ac)d}$
66,73,81,88	$K'_{a(bc)b} K'^{*}_{d(ad)c}$
68,71,83,86	$K'_{a(bc)d} K'^{*}_{b(ac)d}$
69,74,84,89	$K'_{a(bc)d} K'^{*}_{b(ad)c}$
72,75,87,90	$K'_{a(bc)d} K'^{*}_{d(ab)c}$
91	$K'_{a(bb)c} K'^{*}_{c(dd)a}$
92,93	$K'_{a(bb)c} K'^{*}_{d(cd)a}$
94,97	$K'_{a(bc)b} K'^{*}_{c(dd)a}$
95,96,100,103	$K'_{a(bc)b} K'^{*}_{d(cd)a}$
98,99,101,104	$K'_{a(bc)d} K'^{*}_{b(cd)a}$
102,105	$K'_{a(bc)d} K'^{*}_{d(bc)a}$

Table 6.4: Evaluation of the 105 molecular scalars $\left\{ g\, K'_{(ij)kl} \bar{K}'_{(mn)op} \right\}_s$.

Natural invariant	Parallel coefficient	Perpendicular coefficient	Preserved coefficient	Flipped coefficient
$K'_{a(ab)b}K'^{*}_{c(cd)d}$	– 2/945	1/1890	– 5/378	1/945
$K'_{a(ab)b}K'^{*}_{c(dd)c}$	– 1/945	1/378	1/189	1/1890
$K'_{a(ab)c}K'^{*}_{b(cd)d}$	– 2/945	1/1890	2/189	2/189
$K'_{a(ab)c}K'^{*}_{b(dd)c}$	8/945	– 13/1890	– 13/945	– 13/945
$K'_{a(ab)c}K'^{*}_{c(bd)d}$	– 2/945	1/189	– 5/378	2/189
$K'_{a(ab)c}K'^{*}_{d(bc)d}$	– 2/945	1/189	– 5/378	2/189
$K'_{a(ab)c}K'^{*}_{d(bd)c}$	16/945	– 13/945	11/189	– 26/945
$K'_{a(ab)c}K'^{*}_{c(dd)b}$	– 1/945	1/378	1/189	1/1890
$K'_{a(ab)c}K'^{*}_{d(cd)b}$	– 2/945	1/1890	– 5/378	1/945
$K'_{a(bb)a}K'^{*}_{c(cd)d}$	– 1/945	1/378	1/189	1/1890
$K'_{a(bb)a}K'^{*}_{c(dd)c}$	– 1/1890	– 11/1890	1/3780	1/3780
$K'_{a(bc)a}K'^{*}_{b(cd)d}$	– 2/945	1/189	2/189	– 5/378
$K'_{a(bc)a}K'^{*}_{b(dd)c}$	– 1/945	1/378	1/1890	1/189
$K'_{a(bc)a}K'^{*}_{d(bc)d}$	– 1/945	– 11/945	– 5/756	– 5/756
$K'_{a(bc)a}K'^{*}_{d(bd)c}$	– 2/945	1/189	– 5/378	2/189
$K'_{a(bb)c}K'^{*}_{a(cd)d}$	– 1/945	– 13/1890	1/189	1/189
$K'_{a(bb)c}K'^{*}_{a(dd)c}$	4/945	17/945	– 13/1890	– 13/1890
$K'_{a(bc)b}K'^{*}_{a(cd)d}$	– 2/945	– 13/945	– 5/378	– 5/378
$K'_{a(bc)b}K'^{*}_{a(dd)c}$	– 1/945	– 13/1890	1/189	1/189
$K'_{a(bc)d}K'^{*}_{a(bc)d}$	8/945	34/945	11/378	11/378
$K'_{a(bc)d}K'^{*}_{a(bd)c}$	– 2/945	– 13/945	– 5/378	– 5/378
$K'_{a(bb)c}K'^{*}_{c(ad)d}$	– 1/945	1/378	1/1890	1/189
$K'_{a(bb)c}K'^{*}_{d(ac)d}$	– 1/945	1/378	1/1890	1/189
$K'_{a(bb)c}K'^{*}_{d(ad)c}$	8/945	– 13/1890	– 13/945	– 13/945
$K'_{a(bc)b}K'^{*}_{c(ad)d}$	– 2/945	1/1890	1/945	– 5/378
$K'_{a(bc)b}K'^{*}_{d(ac)d}$	– 2/945	1/189	2/189	– 5/378
$K'_{a(bc)b}K'^{*}_{d(ad)c}$	– 2/945	1/1890	2/189	2/189
$K'_{a(bc)d}K'^{*}_{b(ac)d}$	16/945	– 13/945	– 26/945	11/189
$K'_{a(bc)d}K'^{*}_{b(ad)c}$	– 2/945	1/1890	1/945	– 5/378
$K'_{a(bc)d}K'^{*}_{d(ab)c}$	– 2/945	1/189	2/189	– 5/378
$K'_{a(bb)c}K'^{*}_{c(dd)a}$	– 1/1890	– 11/1890	1/3780	1/3780
$K'_{a(bb)c}K'^{*}_{d(cd)a}$	– 1/945	1/378	1/189	1/1890
$K'_{a(bc)b}K'^{*}_{c(dd)a}$	– 1/945	1/378	1/1890	1/189
$K'_{a(bc)b}K'^{*}_{d(cd)a}$	– 2/945	1/189	– 5/378	2/189
$K'_{a(bc)d}K'^{*}_{b(cd)a}$	– 2/945	1/189	2/189	– 5/378
$K'_{a(bc)d}K'^{*}_{d(bc)a}$	– 1/945	– 11/945	– 5/756	– 5/756

Table 6.5: Results for equation (24). The averaged-contraction is equal to a sum of all 36 natural invariants $K'K'^{*}$, each multiplied by a setup-specific coefficient.

Chapter 7: **Concluding comments**

All of the photonic processes analysed in this thesis have been shown to strongly depend on the precise system geometry – particularly the relative positions and orientations of each involved chromophore. The best example is section 6 of chapter 3b, which reports extremely complicated functions of lengths and angles, illustrative of the fine control that molecular geometries may exert on the efficiency of photonic processes: As seen in figure 3b.4, the energy-transfer process in question may be entirely forbidden in one case, but then become allowed after a very fine change of one chromophore's alignment.

The processes described in chapters 3a, 3b and 4a are distinguished by not entailing any net absorption or emission of external photons. Energy is transferred between chromophores without any involvement of distant sources/detectors of radiation: RET is a process internal to a two- or three-chromophore system; chapter 4a concerns a process of photon emission and immediate detection, with the detector included as part of a three-chromophore energy transfer system. In contrast, chapter 5 describes a process in which a radiation mode interacts with a molecule without the Fock number necessarily changing – in principle, this can become a form of weak measurement on the radiation state.[1–3]

The two parts of Chapter 4 therefore represent alternative treatments of similar processes, distinguished by very different ways of framing the system – either all photon paths are bound within the system, or emitted light escapes out and is considered a real photon. Very different quantum measurement issues arise in these two analyses, yielding experimentally-distinguishable outcomes. Treating emission-and-detection as a single four-event process may be conceptually superior, as back-coupling and degeneracy splitting are quantum effects that are excluded when emission is restricted to a photon with specified real properties. By including the detector as a coupled chromophore within the system and allowing for unspecified emitter states, chapter 4a reveals the particular emission behaviours characteristic of excitons, distinct from single-chromophore emission.[4] The results provide testable models for the idiosyncratic excitation behaviour of coupled nanoantennas, a family of systems of current technological interest.[5]

Chapter 3 gives a full MQED description of RET as a two- or four-interaction event process, with the coupling between chromophores mediated by virtual photons. In chapter 4a this result is directly applied to an entirely distinct energy-transfer process (more properly described as an *emission* process), thus illustrating the versatility of the MQED framework. The geometric analysis in chapter 4b may also inform the optimisation of multi-chromophore systems for energy exchange. This thesis contributes to understanding the very precise requirements of molecular geometry that must inform the design of energy-harvesting technology, and other systems where fine control of energy transfer is required.

For example, recent research seeks to develop laser technology using organic dye molecules in the solid state, optimising laser yield via a sequence of selective RET steps that populate the lasing chromophore's excited state.[6] Also, in light-harvesting systems, energy from the original absorption event is directed through a "cascade" of efficient one-way transfer steps toward the desired reaction centre.[7,8] The analysis of chapters 3 and 4 may be applied to give a more complete description of the energy transfer processes in such systems, and thence predict the optimum positions and orientations of chromophores within the solid matrix, and account for effects of quantum interference by nearby dye or host molecules.

If this work is to be developed into a full MQED description of real light-harvesting systems, then the absorption of light and all subsequent inter-chromophore energy transfer steps should be included together and treated as one process. The analysis of media-modified absorption provided by chapter 5 of this thesis must be combined with the analysis of media-modified transfer provided by chapter 3a, including all possible coupling configurations, then the system geometry can be holistically optimised for harvesting efficiency.

The anisotropy predictions of chapter 4b are an example of the MQED method reproducing results from complementary theoretical approaches.[9] The analysis in this chapter also explains advanced spectroscopic behaviours that would otherwise be considered anomalous, in particular the observation of extremely high anisotropy of fluorescence at short timescales.[10] The relative orientations of dipoles within a multi-chromophore molecule have been linked to obscure but measurable features of the total fluorescence behaviour. This has potential

applications in the study of protein folding and other molecular structure problems.

Chapters 3a, 4b, 5 and 6 first give rate equations for the given photonic process as a function of molecular orientation, then calculate the average value of that rate over all orientations of the active molecule. The static results are valuable in themselves, but they are directly applicable as rate predictions only if each active molecule's relative position and orientation is known to a reasonable precision. Such well-ordered molecules may be found in structured energy-harvesting materials or natural photosynthetic complexes,[8] but in the condensed phase the rotationally-averaged rate equations must be used. Further work should extend the geometric analyses in this thesis by challenging this static/stochastic dichotomy, exploring intermediate cases where chromophore orientation is subject to partial thermal disorder. For example, the θ parameter in chapter 4b should be unambiguously broken into its intrinsic and rotational components, in order for fluorescence anisotropy measurements to elicit more internal geometric information.

Chapters 5 and 6 describe high-order (nonlinear) light-interaction processes by single molecules of unspecified orientation. With no relative position vectors, the most important geometric variables are the propagation-direction and polarisation state of the input beams. Such beam parameters can be finely controlled, so the results of these chapters are well-suited to application in fluorescence spectroscopy experiments. The only other consideration is the set of averaged molecular response tensor components. Process selection rules are reducible to these symmetry properties,[11,12] and in chapter 6 the typical rules have been undermined by considering new forms of molecular response – a conventionally-forbidden process has been given a predicted efficiency.[13] The theoretical prospect of new forms of hyper-Rayleigh scattering opens the way to developments in the spectroscopy of high-symmetry molecules, with potential applications in new methods of characterising substances.

When there are many interactions of radiation with a molecule of unspecified orientation, the rotational averages of process rate must be very high order. Chapter 2b explains the general method, and chapter 6 provides a worked example of an eighth-rank average involving 105×105 matrix evaluation. It is

hoped that publication of this thesis provides a resource for any researchers considering similarly ambitious rotational-average calculations.

The intrinsic polarisability ($E1^2$ moment) of a molecule is used to quantify the molecule's propensity to undergo a two-interaction transition, just like transition dipole (E1) moment is commonly used in physical chemistry as a measure of a molecule's propensity to a single interaction. The polarisability becomes central to all photonic processes with cooperation between chromophores (discussed in chapters 3a, 3b and 4a) or the multi-photon interactions of single chromophores (chapters 4b, 5 and 6). Section 6 of chapter 2a provides a necessary discussion of polarisability's interpretation considering the problem of damping and resonance. Polarisability theory is then given a detailed application in section 5 of chapter 3a: With two virtual photons interacting with one chromophore, it is appropriate to derive the tensor in full, as a factor in the process quantum amplitude. Further, the polarisability of a medium molecule is related to the medium's bulk optical properties, as a means of accounting for advanced media effects.

At certain points in each of the chapters 3-6, limiting assumptions about the system geometry have been imposed which simplify the rate equations into a concise form. This approach has been necessary to render the predictions of each system's (possibly extremely complicated) dynamics into a set of reportable results – but it means that the results are limited to particular cases, which may not always be those of practical interest. Nonetheless, the calculations in this thesis may still serve as a template for the derivation of results for more useful cases: The reader may follow the methods explained in each chapter, and apply the general rate equations, then explore an alternative system geometry that is more relevant to their particular application.

[1] P. Grangier, J.A. Levenson, and J.-P. Poizat, "Quantum Non-Demolition Measurements in Optics": *Nature* **396**, 537 (1998).

[2] W.J. Munro, K. Nemoto, R.G. Beausoleil, and T.P. Spiller, "High-Efficiency Quantum-Nondemolition Single-Photon-Number-Resolving Detector": *Phys Rev A* **71**, 33819 (2005).

[3] D.S. Bradshaw and D.L. Andrews, "Laser-Modified One- and Two-Photon Absorption: Expanding the Scope of Optical Nonlinearity": *Phys Rev A* **88,** 33807 (2013).

[4] G. D. Scholes and G. Rumbles, "Excitons in Nanoscale Systems": *Nat. Mater.* **5,** 683 (2006).

[5] S.I. Schmid and J. Evers, "Interplay of Vacuum-Mediated Inter- and Intra-Atomic Couplings in a Pair of Atoms": *Phys Rev A* **81**, 63805 (2010).

[6] J. Ling, Z. Zheng, A. Köhler, and A.H.E. Müller, "Rod-Like Nano-Light Harvester": *Macromol. Rapid Commun.* **35,** 52 (2014).

[7] H. Nakanotani, T. Furukawa, and C. Adachi, "Light Amplification in an Organic Solid-State Film with the Aid of Triplet-to-Singlet Upconversion": *Adv. Opt. Mater.* **3,** 1381 (2015).

[8] D.L. Andrews and D.S. Bradshaw, "Optically Nonlinear Energy Transfer in Light-Harvesting Dendrimers": *J. Chem. Phys.* **121**, 2445 (2004).

[9] J. Lakowicz, "Fluorescence Anisotropy": *Princ. Fluoresc. Spectrosc.*, 2nd ed. (Kluwer Academic Plenum, New York, 1999), p. 291.

[10] G.G. Gurzadyan, T.-H. Tran-Thi, and T. Gustavsson, "Time-Resolved Fluorescence Spectroscopy of High-Lying Electronic States of Zn-Tetraphenylporphyrin": *J. Chem. Phys.* **108**, 385 (1998).

[11] D.L. Andrews and T. Thirunamachandran, "Hyper−Raman Scattering by Chiral Molecules": *J. Chem. Phys.* **70,** 1027 (1979).

[12] R. Piron, S. Brasselet, D. Josse, J. Zyss, G. Viscardi, and C. Barolo, "Matching Molecular and Optical Multipoles in Photoisomerizable Nonlinear Systems": *J Opt Soc Am B* **22**, 1276 (2005).

[13] M. D. Williams, J. S. Ford, and D. L. Andrews, "Hyper-Rayleigh Scattering in Centrosymmetric Systems": *J. Chem. Phys.* **143,** 124301 (2015).

–

Appendix 8a: **Time-ordering of interaction events: State-sequence diagrams**

This appendix outlines state-sequence diagrams as an alternative diagrammatic system to the Feynman diagrams employed in the main part of the thesis.

The elementary case of a quantum interaction process is a unitary system that undergoes one transformative event. As a state-sequence diagram, such a process is illustrated by figure 8a.1:

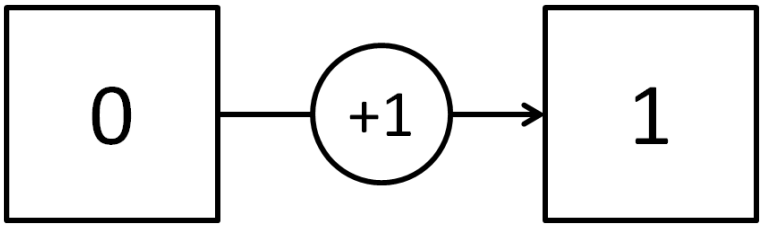

Figure 8a.1: Elementary single-event state-sequence diagram.

Time proceeds from left to right. The system, illustrated as a box, is shown in its initial state (left) labelled "0". The process of the system evolving into its final state can be seen by reading the diagram rightward, following the transformative event arrow "+1" that transitions the system from that initial state into its final state labelled "1".

If there is more than one event, then the different time-orderings turn the diagram into a network of the possible state sequences, as shown by figure 8a.2.

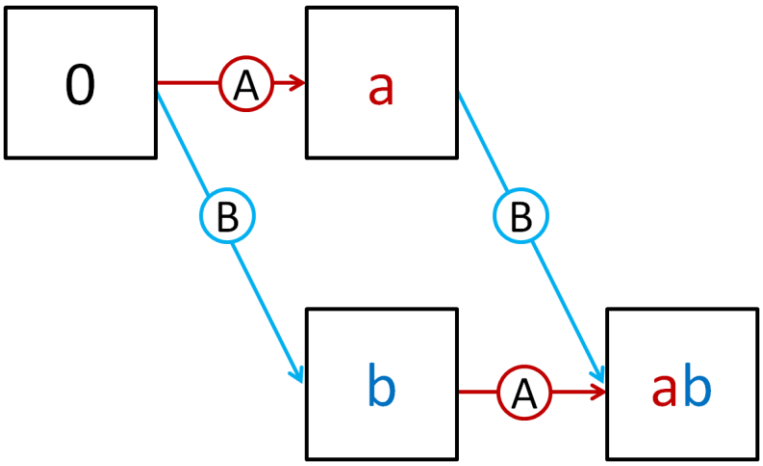

Figure 8a.2: Elementary two-event state-sequence diagram.

This two-event process consists of events (A) and (B). Event (A) adds the property "a" to the system's state; event (B) adds the property "b". In general, the property "x" should be understood as "event (X) is in the system's history". Therefore, the event arrows must all be drawn parallel to like events and orthogonal to all unlike events. The combination of both events transforms the system from initial state "0" to final state "ab". There are two allowed routes through the network – these are the two time-orderings, (A)(B) and (B)(A). It is this that creates two distinct possible states, "a" and "b", during the intermediate era.

For a practical example of this scheme used to describe a MQED problem, consider the RET process that is illustrated with two Feynman diagrams in figure 2a.2. This is represented by state-sequence diagram figure 8a.3.

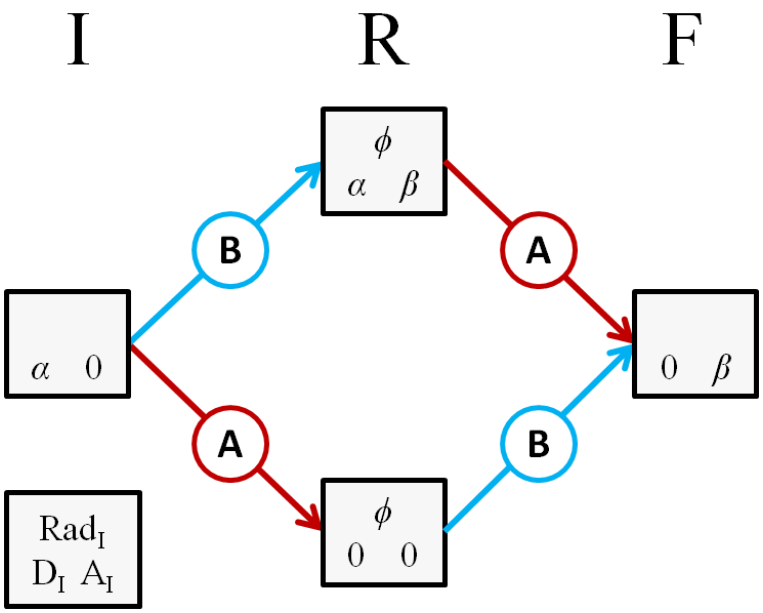

Figure 8a.3: State-sequence diagram for resonance energy transfer.

Each box displays a system state, displaying the states of the three subsystems: Radiation, Donor molecule, and Acceptor molecule. The lower path is the (A)(B) time-ordering and corresponds to the left Feynman diagram; the upper path is (B)(A) and corresponds to the right Feynman diagram. The advantage of the state-sequence approach is that both Feynman diagrams and their relationship are completely described with this one figure.

Figure 8a.4 is the abstract diagram with three events. Again, the occurrence of (C) adds the property "c" to the system's state. This network can be seen to be comprised of the two-event diagram doubled-up – the (A)+(B) parallelogram turning "0" to "ab" is reproduced, turning c to abc. Note that in moving from two events top three: the number of state-sequence routes from the initial to final state increases from 2*!* to 3*!*, and the total number of possible states increases from 2^2 to 2^3.

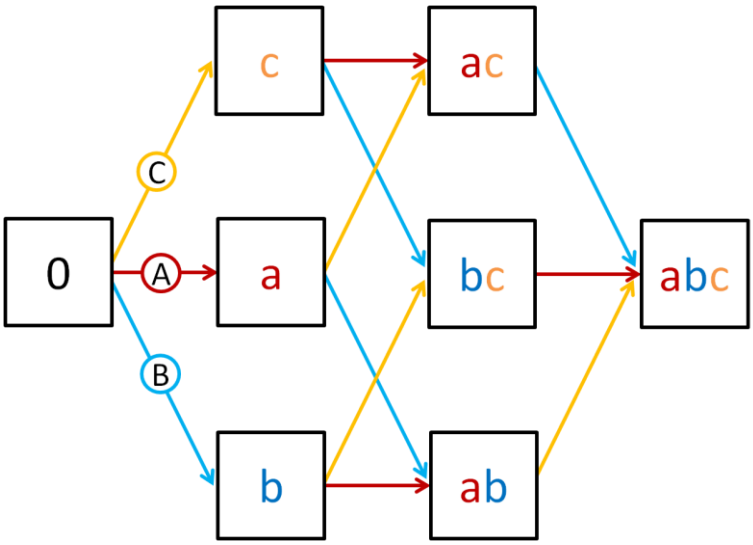

Figure 8a.4: Elementary three-event state-sequence diagram.

This diagram has the clear structure of a cube, with the three events defining the cardinal directions in a three-dimensional (A)(B)(C)-space. This mathematical feature arises from treating the events as fully independent and commutative – any time-ordering is allowed and each permutation of the same set of events has the same outcome. The combinatorial possibilities of three transitions occurring in any order map to a representation of a 3D state space, through which the system moves in unit-vector leaps from the initial state “0”, to the opposing vertex of the cube which is the final state “abc”.

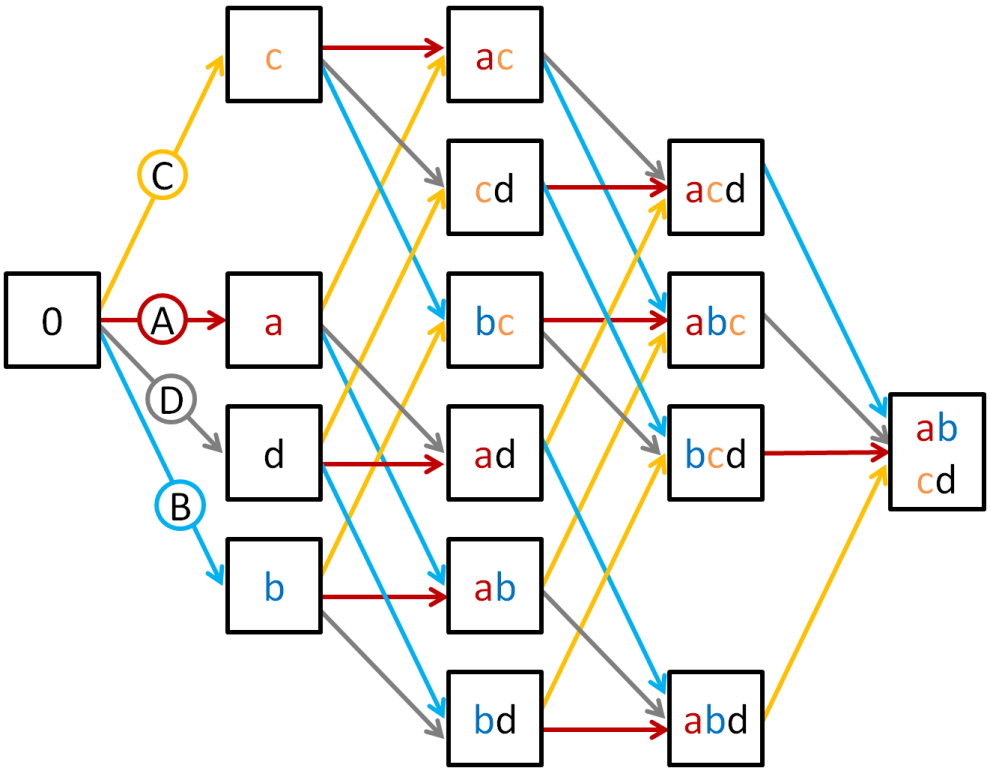

Figure 8a.5: Elementary four-event state-sequence diagram.

For a four-event process, the three-event diagram is doubled-up in the same way, constructing a tesseract (four-dimensional cube) in the 4D state-space defined by the four events. This state-sequence diagram covers 2^4 states and 4*!* time-ordering pathways. The network of the four-event diagram precisely emulates a tesseract projected into the 2D plane of this page: the 16 state-boxes align with vertices, and the 32 event-lines align with the cell-edges of a tesseract.

For an example of a real four-event process captured with a tesseract state-sequence diagram, consider the "MDA configuration" of third-body-modified RET, the focus of chapter 3a. This is represented by state-sequence diagram figure 8a.6.

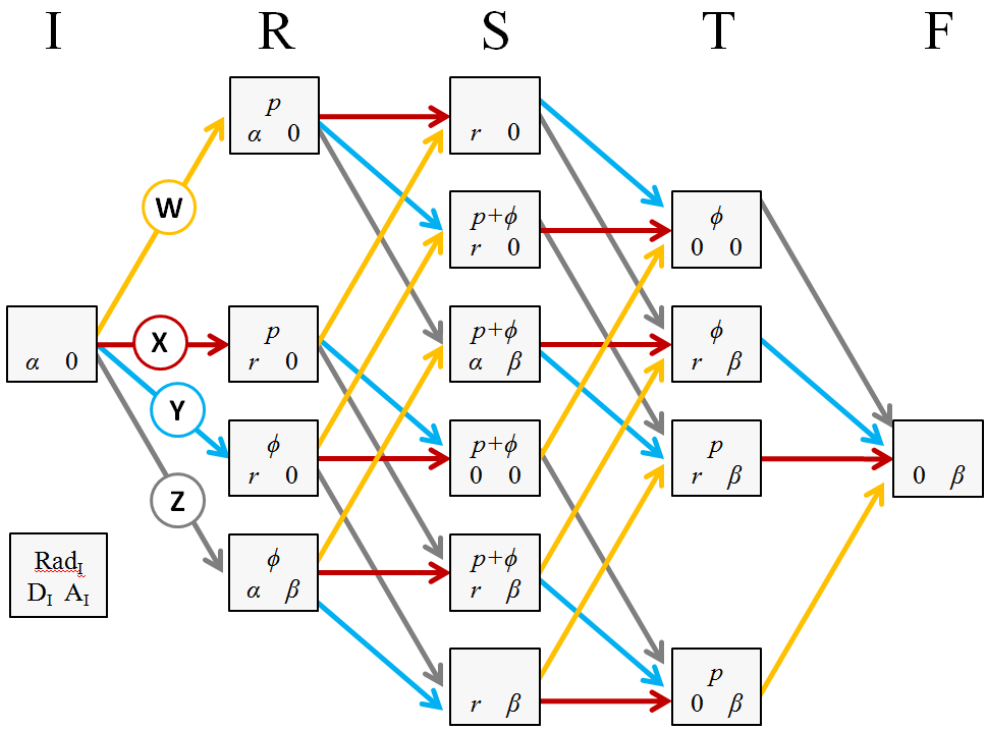

Figure 8a.6: State-sequence diagram for the "MDA configuration" of third-body-modified RET.

The electronic state of the chromophore M is not shown, as it remains M_0 throughout the process. The YZWX pathway through this network is illustrated by figure 3a.2. The other 23 time-orderings of the MDA-configuration process, which are enumerated separately at great length in Appendix 8c, are summarised systematically by this one figure.

The following patterns arise in a state-sequence diagram for an interaction process with N transition events. These are illustrated by figure 8a.7.

- The evolution of the system consists of N+1 "eras", separated by the N events;
- The state-sequence diagram covers 2^N possible states including the initial and final;
- There are N*!* possible sequence routes between the many intermediate states, identical to the time-order permutations of the N events;

- The diagram has the form of an N-dimensional cube with states as vertices and events as cell-edges;
- The diagram sorts the 2^N states between the N+1 eras according to the $(N+1)^{th}$ row of Pascal's Triangle.

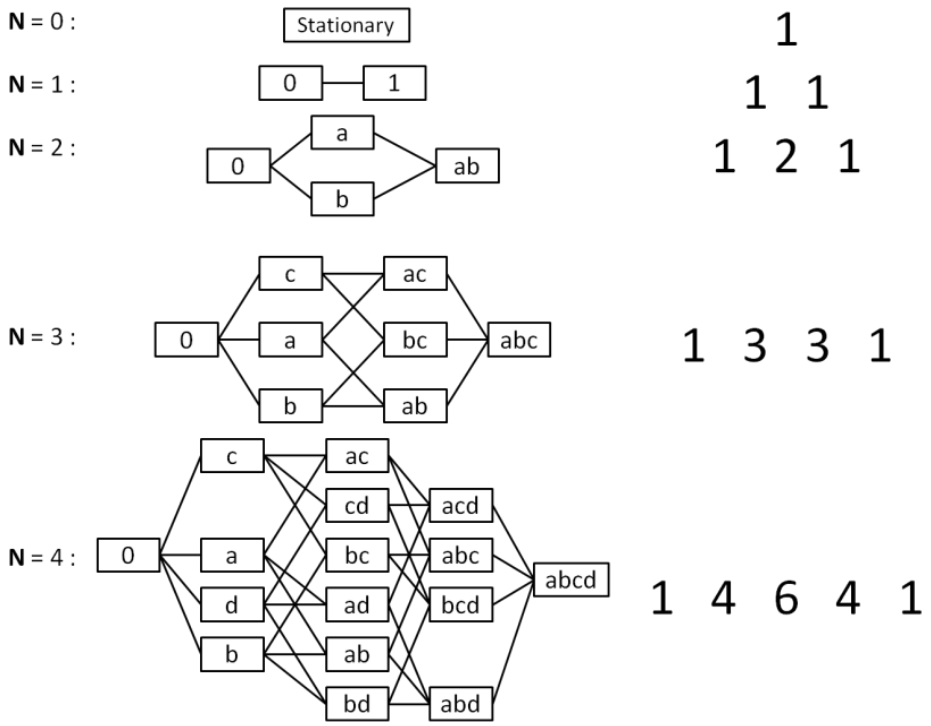

Figure 8a.7: The elementary state-sequence diagrams replicate Pascal's triangle. The trivial N=0 case is the diagram for a zero-event process, i.e. a stationary state.

–

Appendix 8b: **Rotational averaging of tensors: Complete matrices**

1. Sources

These are the results of the $I^{(N)}$ calculation method outlined in chapter 2b section 3, for even N values. The results for second, fourth and sixth ranks are as reported in Appendix 2 of the book [*Molecular Quantum Electrodynamics* by D. P. Craig and T. Thirunamachandran (Dover Publications, 1998)]. The results for the eighth rank rotational average are as reported in the article [D.L. Andrews and W.A. Ghoul, "Eighth Rank Isotropic Tensors and Rotational Averages": *J. Phys. Math. Gen.* **14**, 1281 (1981)].

2. Second rank average, N=2

The elementary tensor f is a single Kronecker delta in two i indices.

$$f^{(2)} = \delta_{i12}$$

As there is only one f, the matrix **S** has just one element, provided by a straightforward application of equation (2b.10).

$$S = f^{(2)} \cdot f^{(2)} = \delta_{ij}\delta_{ij} = 3$$

The single $m^{(2)}$ element is calculated as the inverse of S, which in the single-element limit is equal to the number's reciprocal.

$$m^{(2)} = S^{-1} = \frac{1}{3}$$

Finally, according to equation (2b.5), the result for $I^{(2)}$ is a double-tensor of one term.

$$I^{(2)} = f^{(2)} m^{(2)} g^{(2)} = \frac{1}{3}\delta_{i12}\,\delta_{\lambda 12}$$

This double-tensor is responsible for the "trace" function Tr( ) in chapter 3a section 5, and is used to evaluate equation (5.20).

3. Fourth rank average, *N*=4

The tensors $f_r^{(4)}$ are each a pair of Kronecker deltas in *i*. There are three possible permutations of four indices paired.

$$f_1^{(4)} = \delta_{i12}\delta_{i34}$$
$$f_2^{(4)} = \delta_{i13}\delta_{i24}$$
$$f_3^{(4)} = \delta_{i14}\delta_{i23}$$

Equation (2b.10) applies to each element of the dimension-three square matrix **S**.

$$\mathbf{S} = \begin{pmatrix} \delta_{ij}\delta_{kl}\delta_{ij}\delta_{kl} & \delta_{ij}\delta_{kl}\delta_{ik}\delta_{jl} & \delta_{ij}\delta_{kl}\delta_{il}\delta_{jk} \\ \delta_{ik}\delta_{jl}\delta_{ij}\delta_{kl} & \delta_{ik}\delta_{jl}\delta_{ik}\delta_{jl} & \delta_{ik}\delta_{jl}\delta_{il}\delta_{jk} \\ \delta_{il}\delta_{jk}\delta_{ij}\delta_{kl} & \delta_{il}\delta_{jk}\delta_{ik}\delta_{jl} & \delta_{il}\delta_{jk}\delta_{il}\delta_{jk} \end{pmatrix} = \begin{pmatrix} 9 & 3 & 3 \\ 3 & 9 & 3 \\ 3 & 3 & 9 \end{pmatrix}$$

The matrix $m^{(4)}$ is calculated via matrix-inversion.

$$m^{(4)} = \mathbf{S}^{-1} = \frac{1}{30}\begin{pmatrix} 4 & -1 & -1 \\ -1 & 4 & -1 \\ -1 & -1 & 4 \end{pmatrix}$$

Applying equation (2b.5), $I^{(4)}$ is a double-tensor of nine terms.

$$I^{(4)} = f_r^{(4)} m_{rs}^{(4)} g_s^{(4)} = \frac{1}{30}\begin{pmatrix} \delta_{i12}\delta_{i34} \\ \delta_{i13}\delta_{i24} \\ \delta_{i14}\delta_{i23} \end{pmatrix}^{\mathrm{T}} \begin{pmatrix} 4 & -1 & -1 \\ -1 & 4 & -1 \\ -1 & -1 & 4 \end{pmatrix} \begin{pmatrix} \delta_{\lambda 12}\delta_{\lambda 34} \\ \delta_{\lambda 13}\delta_{\lambda 24} \\ \delta_{\lambda 14}\delta_{\lambda 23} \end{pmatrix}$$

This result is central to chapter 4b section 4, and is employed in the evaluation of equations (5.21), (5.22), and (5.26).

4. Sixth rank average, *N*=6

The tensors $f_r^{(6)}$ are each a product of three Kronecker deltas in *i*. There are 15 of them, representing all possible permutations of six *i* indices in three pairings.

$$f_1^{(6)} = \delta_{i12}\delta_{i34}\delta_{i56} \qquad f_6^{(6)} = \delta_{i13}\delta_{i26}\delta_{i45} \qquad f_{11}^{(6)} = \delta_{i15}\delta_{i24}\delta_{i36}$$
$$f_2^{(6)} = \delta_{i12}\delta_{i35}\delta_{i46} \qquad f_7^{(6)} = \delta_{i14}\delta_{i23}\delta_{i56} \qquad f_{12}^{(6)} = \delta_{i15}\delta_{i26}\delta_{i34}$$
$$f_3^{(6)} = \delta_{i12}\delta_{i36}\delta_{i45} \qquad f_8^{(6)} = \delta_{i14}\delta_{i25}\delta_{i36} \qquad f_{13}^{(6)} = \delta_{i16}\delta_{i23}\delta_{i45}$$
$$f_4^{(6)} = \delta_{i13}\delta_{i24}\delta_{i56} \qquad f_9^{(6)} = \delta_{i14}\delta_{i26}\delta_{i35} \qquad f_{14}^{(6)} = \delta_{i16}\delta_{i24}\delta_{i35}$$
$$f_5^{(6)} = \delta_{i13}\delta_{i25}\delta_{i46} \qquad f_{10}^{(6)} = \delta_{i15}\delta_{i23}\delta_{i46} \qquad f_{15}^{(6)} = \delta_{i16}\delta_{i25}\delta_{i34}$$

The result for $m^{(6)}$ is reported by Craig & Thirunamachandran (1998) as part of their equation (A2.26). The method employed in this calculation is identical to the N=4 case that I have explained in full above, but involving a matrix-inversion computation of dimension 15.

$$m^{(6)} = \frac{1}{210}\begin{pmatrix}
16 & -5 & -5 & -5 & 2 & 2 & -5 & 2 & 2 & 2 & 2 & -5 & 2 & 2 & -5 \\
-5 & 16 & -5 & 2 & -5 & 2 & 2 & 2 & -5 & -5 & 2 & 2 & 2 & -5 & 2 \\
-5 & -5 & 16 & 2 & 2 & -5 & 2 & -5 & 2 & 2 & -5 & 2 & -5 & 2 & 2 \\
-5 & 2 & 2 & 16 & -5 & -5 & -5 & 2 & 2 & 2 & -5 & 2 & 2 & -5 & 2 \\
2 & -5 & 2 & -5 & 16 & -5 & 2 & -5 & 2 & -5 & 2 & 2 & 2 & 2 & -5 \\
2 & 2 & -5 & -5 & -5 & 16 & 2 & 2 & -5 & 2 & 2 & -5 & -5 & 2 & 2 \\
-5 & 2 & 2 & -5 & 2 & 2 & 16 & -5 & -5 & -5 & 2 & 2 & -5 & 2 & 2 \\
2 & 2 & -5 & 2 & -5 & 2 & -5 & 16 & -5 & 2 & -5 & 2 & 2 & 2 & -5 \\
2 & -5 & 2 & 2 & 2 & -5 & -5 & -5 & 16 & 2 & 2 & -5 & 2 & -5 & 2 \\
2 & -5 & 2 & 2 & -5 & 2 & -5 & 2 & 2 & 16 & -5 & -5 & -5 & 2 & 2 \\
2 & 2 & -5 & -5 & 2 & 2 & 2 & -5 & 2 & -5 & 16 & -5 & 2 & -5 & 2 \\
-5 & 2 & 2 & 2 & 2 & -5 & 2 & 2 & -5 & -5 & -5 & 16 & 2 & 2 & -5 \\
2 & 2 & -5 & 2 & 2 & -5 & -5 & 2 & 2 & -5 & 2 & 2 & 16 & -5 & -5 \\
2 & -5 & 2 & -5 & 2 & 2 & 2 & 2 & -5 & 2 & -5 & 2 & -5 & 16 & -5 \\
-5 & 2 & 2 & 2 & -5 & 2 & 2 & -5 & 2 & 2 & 2 & -5 & -5 & -5 & 16
\end{pmatrix}$$

Applying equation (2b.5) of this thesis, $I^{(6)}$ is a double-tensor of 225 terms given by the row-square-column matrix multiplication:

$$I^{(6)} = \begin{pmatrix}
\delta_{i12}\delta_{i34}\delta_{i56} \\
\delta_{i12}\delta_{i35}\delta_{i46} \\
\delta_{i12}\delta_{i36}\delta_{i45} \\
\delta_{i13}\delta_{i24}\delta_{i56} \\
\delta_{i13}\delta_{i25}\delta_{i46} \\
\delta_{i13}\delta_{i26}\delta_{i45} \\
\delta_{i14}\delta_{i23}\delta_{i56} \\
\delta_{i14}\delta_{i25}\delta_{i36} \\
\delta_{i14}\delta_{i26}\delta_{i35} \\
\delta_{i15}\delta_{i23}\delta_{i46} \\
\delta_{i15}\delta_{i24}\delta_{i36} \\
\delta_{i15}\delta_{i26}\delta_{i34} \\
\delta_{i16}\delta_{i23}\delta_{i45} \\
\delta_{i16}\delta_{i24}\delta_{i35} \\
\delta_{i16}\delta_{i25}\delta_{i34}
\end{pmatrix}^{\mathrm{T}} m^{(6)} \begin{pmatrix}
\delta_{\lambda 12}\delta_{\lambda 34}\delta_{\lambda 56} \\
\delta_{\lambda 12}\delta_{\lambda 35}\delta_{\lambda 46} \\
\delta_{\lambda 12}\delta_{\lambda 36}\delta_{\lambda 45} \\
\delta_{\lambda 13}\delta_{\lambda 24}\delta_{\lambda 56} \\
\delta_{\lambda 13}\delta_{\lambda 25}\delta_{\lambda 46} \\
\delta_{\lambda 13}\delta_{\lambda 26}\delta_{\lambda 45} \\
\delta_{\lambda 14}\delta_{\lambda 23}\delta_{\lambda 56} \\
\delta_{\lambda 14}\delta_{\lambda 25}\delta_{\lambda 36} \\
\delta_{\lambda 14}\delta_{\lambda 26}\delta_{\lambda 35} \\
\delta_{\lambda 15}\delta_{\lambda 23}\delta_{\lambda 46} \\
\delta_{\lambda 15}\delta_{\lambda 24}\delta_{\lambda 36} \\
\delta_{\lambda 15}\delta_{\lambda 26}\delta_{\lambda 34} \\
\delta_{\lambda 16}\delta_{\lambda 23}\delta_{\lambda 45} \\
\delta_{\lambda 16}\delta_{\lambda 24}\delta_{\lambda 35} \\
\delta_{\lambda 16}\delta_{\lambda 25}\delta_{\lambda 34}
\end{pmatrix}$$

This result is employed in the evaluation of equations (5.23), (5.24), (5.27) and (5.28).

5. Eighth rank average, *N*=8

Application of equation (2b.7) predicts 105 unique values for *r* and for *s*, and the set of 105 tensors $f_r^{(8)}$ may be constructed by following the same index-permutation pattern as in the above results. Table 8b.2 following this appendix describes these 105 tensors $f_r^{(8)}$, each of which is a product of four Kronecker deltas in i. It must be noted that this set is *overcomplete* – only 91 of these tensors $f_r^{(8)}$ are linearly independent, as the other 14 may be constructed as linear functions of the independent 91. Nonetheless, the overcomplete set is not incorrect because this redundancy does not introduce *degeneracy* as defined in chapter 2b section 4.

This overcompleteness means that there is not a unique solution for each of the 11025 elements $m_{rs}^{(8)}$. In the calculation performed by Andrews & Ghoul (1981), each element $m_{rs}^{(8)}$ is instead assigned a variable label. The assignment is based on the tensor structure of the corresponding element of the **S** matrix, $S_{rs} = f_r^{(8)} \cdot f_s^{(8)}$. For example, the top-right element is:

$$S_{1;105} = f_1^{(8)} \cdot f_{105}^{(8)} = \delta_{ij}\delta_{kl}\delta_{mn}\delta_{op}\delta_{ip}\delta_{jo}\delta_{kn}\delta_{lm} = \left(\delta_{ij}\delta_{jo}\delta_{op}\delta_{ip}\right)\left(\delta_{kl}\delta_{lm}\delta_{mn}\delta_{kn}\right)$$

What is of interest is that the inner product of eight deltas factorises into two self-contained cycles of four. This factorisation is diagnostic of a certain set of possible values for $m_{1;105}^{(8)}$. There are five distinct ways that each inner product of eight deltas may factorise into cycles, and these are each assigned a variable label in the set $\{A,B,C,D,E\}$. The ruleset of this algorithm is given by Table 8b.1.

S_{rs} factorisation	$m_{rs}^{(8)}$
$(\delta\,\delta)(\delta\,\delta)(\delta\,\delta)(\delta\,\delta)$	A
$(\delta\,\delta\,\delta\,\delta)(\delta\,\delta)(\delta\,\delta)$	B
$(\delta\,\delta\,\delta\,\delta)(\delta\,\delta\,\delta\,\delta)$	C
$(\delta\,\delta\,\delta\,\delta\,\delta\,\delta)(\delta\,\delta)$	D
$(\delta\,\delta\,\delta\,\delta\,\delta\,\delta\,\delta\,\delta)$	E

Table 8b.1: Rules for assigning the labels *A*,*B*,*C*,*D*,*E* to the elements $m_{rs}^{(8)}$, according to the tensor structure of the corresponding element S_{rs}. Adapted from Table 3 in Andrews & Ghoul (1981).

Tables 8b.3-8 following this appendix combine to show the resulting matrix $m^{(8)}$ in terms of the five variable labels *A*,*B*,*C*,*D*,*E*. These variables have possible values constrained by the equations (26-29) given by Andrews & Ghoul (1981). I have chosen to use the E=0 result, as this is the simplest form of $m^{(8)}$, most useful for direct application in the rotational-averaging calculations in this thesis.

$$\mathrm{A} = 19/630 \qquad \mathrm{B} = -23/3780 \qquad \mathrm{C} = 1/7560 \qquad \mathrm{D} = 1/756 \qquad \mathrm{E} = 0$$

Once again, $m^{(8)}$ enters equation (2b.5), to give $I^{(8)}$ as a double-tensor with 11025 terms. This result is employed in the evaluation of equations (5.25) and (5.29). Also, see chapter 6 section 5 of this thesis for a worked example of how $I^{(8)}$ is used to calculate a rotationally-averaged process rate.

–

r	δ_i		δ_i		δ_i		δ_i	
1	1	2	3	4	5	6	7	8
2	1	2	3	4	5	7	6	8
3	1	2	3	4	5	8	6	7
4	1	2	3	5	4	6	7	8
5	1	2	3	5	4	7	6	8
6	1	2	3	5	4	8	6	7
7	1	2	3	6	4	5	7	8
8	1	2	3	6	4	7	5	8
9	1	2	3	6	4	8	5	7
10	1	2	3	7	4	5	6	8
11	1	2	3	7	4	6	5	8
12	1	2	3	7	4	8	5	6
13	1	2	3	8	4	5	6	7
14	1	2	3	8	4	6	5	7
15	1	2	3	8	4	7	5	6
16	1	3	2	4	5	6	7	8
17	1	3	2	4	5	7	6	8
18	1	3	2	4	5	8	6	7
19	1	3	2	5	4	6	7	8
20	1	3	2	5	4	7	6	8
21	1	3	2	5	4	8	6	7
22	1	3	2	6	4	5	7	8
23	1	3	2	6	4	7	5	8
24	1	3	2	6	4	8	5	7
25	1	3	2	7	4	5	6	8
26	1	3	2	7	4	6	5	8
27	1	3	2	7	4	8	5	6
28	1	3	2	8	4	5	6	7
29	1	3	2	8	4	6	5	7
30	1	3	2	8	4	7	5	6
31	1	4	2	3	5	6	7	8
32	1	4	2	3	5	7	6	8
33	1	4	2	3	5	8	6	7
34	1	4	2	5	3	6	7	8
35	1	4	2	5	3	7	6	8
36	1	4	2	5	3	8	6	7
37	1	4	2	6	3	5	7	8
38	1	4	2	6	3	7	5	8
39	1	4	2	6	3	8	5	7
40	1	4	2	7	3	5	6	8
41	1	4	2	7	3	6	5	8
42	1	4	2	7	3	8	5	6
43	1	4	2	8	3	5	6	7
44	1	4	2	8	3	6	5	7
45	1	4	2	8	3	7	5	6
46	1	5	2	3	4	6	7	8
47	1	5	2	3	4	7	6	8
48	1	5	2	3	4	8	6	7
49	1	5	2	4	3	6	7	8
50	1	5	2	4	3	7	6	8
51	1	5	2	4	3	8	6	7
52	1	5	2	6	3	4	7	8
53	1	5	2	6	3	7	4	8
54	1	5	2	6	3	8	4	7
55	1	5	2	7	3	4	6	8
56	1	5	2	7	3	6	4	8
57	1	5	2	7	3	8	4	6
58	1	5	2	8	3	4	6	7
59	1	5	2	8	3	6	4	7
60	1	5	2	8	3	7	4	6
61	1	6	2	3	4	5	7	8
62	1	6	2	3	4	7	5	8
63	1	6	2	3	4	8	5	7
64	1	6	2	4	3	5	7	8
65	1	6	2	4	3	7	5	8
66	1	6	2	4	3	8	5	7
67	1	6	2	5	3	4	7	8
68	1	6	2	5	3	7	4	8
69	1	6	2	5	3	8	4	7
70	1	6	2	7	3	4	5	8
71	1	6	2	7	3	5	4	8
72	1	6	2	7	3	8	4	5
73	1	6	2	8	3	4	5	7
74	1	6	2	8	3	5	4	7
75	1	6	2	8	3	7	4	5
76	1	7	2	3	4	5	6	8
77	1	7	2	3	4	6	5	8
78	1	7	2	3	4	8	5	6
79	1	7	2	4	3	5	6	8
80	1	7	2	4	3	6	5	8
81	1	7	2	4	3	8	5	6
82	1	7	2	5	3	4	6	8
83	1	7	2	5	3	6	4	8
84	1	7	2	5	3	8	4	6
85	1	7	2	6	3	4	5	8
86	1	7	2	6	3	5	4	8
87	1	7	2	6	3	8	4	5
88	1	7	2	8	3	4	5	6
89	1	7	2	8	3	5	4	6
90	1	7	2	8	3	6	4	5
91	1	8	2	3	4	5	6	7
92	1	8	2	3	4	6	5	7
93	1	8	2	3	4	7	5	6
94	1	8	2	4	3	5	6	7
95	1	8	2	4	3	6	5	7
96	1	8	2	4	3	7	5	6
97	1	8	2	5	3	4	6	7
98	1	8	2	5	3	6	4	7
99	1	8	2	5	3	7	4	6
100	1	8	2	6	3	4	5	7
101	1	8	2	6	3	5	4	7
102	1	8	2	6	3	7	4	5
103	1	8	2	7	3	4	5	6
104	1	8	2	7	3	5	4	6
105	1	8	2	7	3	6	4	5

Table 8b.2: Each tensor $f_r^{(8)}$ is a product of four Kronecker deltas. The value of r specifies the permutation of the four i indices.

A	B	B	B	D	D	B	D	D	D	D	B	D	D	B	B	C	C	D	E	E	D	E	E	E	E	D	E	E	D	B	C	C	D	E
B	A	B	D	B	D	D	D	B	B	D	D	D	B	D	C	B	C	E	D	E	E	E	D	D	E	E	E	D	E	C	B	C	E	D
B	B	A	D	D	B	D	B	D	D	B	D	B	D	D	C	C	B	E	E	D	E	D	E	E	D	E	D	E	E	C	C	B	E	E
B	D	D	A	B	B	B	D	D	D	B	D	D	B	D	D	E	E	B	C	C	D	E	E	E	D	E	E	D	E	D	E	E	D	E
D	B	D	B	A	B	D	B	D	B	D	D	D	D	B	E	D	E	C	B	C	E	D	E	D	E	E	E	E	D	E	D	E	E	D
D	D	B	B	B	A	D	D	B	D	D	B	B	D	D	E	E	D	C	C	B	E	E	D	E	E	D	D	E	E	E	E	D	E	E
B	D	D	B	D	D	A	B	B	B	D	D	B	D	D	D	E	E	D	E	E	B	C	C	D	E	E	D	E	E	D	E	E	B	C
D	D	B	D	B	D	B	A	B	D	B	D	D	D	B	E	E	D	E	D	E	C	B	C	E	D	E	E	E	D	E	E	D	D	E
D	B	D	D	D	B	B	B	A	D	D	B	D	B	D	E	D	E	E	E	D	C	C	B	E	E	D	E	D	E	E	D	E	D	E
D	B	D	D	B	D	B	D	D	A	B	B	B	D	D	E	D	E	E	D	E	D	E	E	B	C	C	D	E	E	E	D	E	C	B
D	D	B	B	D	D	D	B	D	B	A	B	D	B	D	E	E	D	D	E	E	E	D	E	C	B	C	E	D	E	E	E	D	E	D
B	D	D	D	D	B	D	D	B	B	B	A	D	D	B	D	E	E	E	E	D	E	E	D	C	C	B	E	E	D	D	E	E	E	D
D	D	B	D	D	B	B	D	D	B	D	D	A	B	B	E	E	D	E	E	D	D	E	E	D	E	E	B	C	C	E	E	D	C	C
D	B	D	B	D	D	D	D	B	D	B	D	B	A	B	E	D	E	D	E	E	E	E	D	E	D	E	C	B	C	E	D	E	E	E
B	D	D	D	B	D	D	B	D	D	D	B	B	B	A	D	E	E	E	D	E	E	D	E	E	E	D	C	C	B	D	E	E	E	E
B	C	C	D	E	E	D	E	E	E	E	D	E	E	D	A	B	B	B	D	D	B	D	D	D	D	B	D	D	B	B	C	C	D	E
C	B	C	E	D	E	E	E	D	D	E	E	E	D	E	B	A	B	D	B	D	D	D	B	B	D	D	D	B	D	C	B	C	E	D
C	C	B	E	E	D	E	D	E	E	D	E	D	E	E	B	B	A	D	D	B	D	B	D	D	B	D	B	D	D	C	C	B	E	E
D	E	E	B	C	C	D	E	E	E	D	E	E	D	E	B	D	D	A	B	B	B	D	D	D	B	D	D	B	D	D	E	E	B	D
E	D	E	C	B	C	E	D	E	D	E	E	E	E	D	D	B	D	B	A	B	D	B	D	B	D	D	D	D	B	E	D	E	D	B
E	E	D	C	C	B	E	E	D	E	E	D	D	E	E	D	D	B	B	B	A	D	D	B	D	D	B	B	D	D	E	E	D	D	D
D	E	E	D	E	E	B	C	C	D	E	E	D	E	E	B	D	D	B	D	D	A	B	B	B	D	D	B	D	D	D	E	E	D	E
E	E	D	E	D	E	C	B	C	E	D	E	E	E	D	D	D	B	D	B	D	B	A	B	D	B	D	D	D	B	E	E	D	E	C
E	D	E	E	E	D	C	C	B	E	E	D	E	D	E	D	B	D	D	D	B	B	B	A	D	D	B	D	B	D	E	D	E	E	E
E	D	E	E	D	E	D	E	E	B	C	C	D	E	E	D	B	D	D	B	D	B	D	D	A	B	B	B	D	D	E	D	E	E	D
E	E	D	D	E	E	E	D	E	C	B	C	E	D	E	D	D	B	B	D	D	D	B	D	B	A	B	D	B	D	E	E	D	C	E
D	E	E	E	E	D	E	E	D	C	C	B	E	E	D	B	D	D	D	D	B	D	D	B	B	B	A	D	D	B	D	E	E	E	E
E	E	D	E	E	D	D	E	E	D	E	E	B	C	C	D	D	B	D	D	B	B	D	D	B	D	D	A	B	B	E	E	D	E	E
E	D	E	D	E	E	E	E	D	E	D	E	C	B	C	D	B	D	B	D	D	D	D	B	D	B	D	B	A	B	E	D	E	C	E
D	E	E	E	D	E	E	D	E	E	E	D	C	C	B	B	D	D	D	B	D	D	B	D	D	D	B	B	B	A	D	E	E	E	C
B	C	C	D	E	E	D	E	E	E	E	D	E	E	D	B	C	C	D	E	E	D	E	E	E	E	D	E	E	D	A	B	B	B	D
C	B	C	E	D	E	E	E	D	D	E	E	E	D	E	C	B	C	E	D	E	E	E	D	D	E	E	E	D	E	B	A	B	D	B
C	C	B	E	E	D	E	D	E	E	D	E	D	E	E	C	C	B	E	E	D	E	D	E	E	D	E	D	E	E	B	B	A	D	D
D	E	E	D	E	E	B	D	D	C	E	E	C	E	E	D	E	E	B	D	D	D	E	E	E	C	E	E	C	E	B	D	D	A	B
E	D	E	E	D	E	C	E	E	B	D	D	C	E	E	E	D	E	D	B	D	E	C	E	D	E	E	E	E	C	D	B	D	B	A
E	E	D	E	E	D	C	E	E	C	E	E	B	D	D	E	E	D	D	D	B	E	E	C	E	E	C	D	E	E	D	D	B	B	B
D	E	E	B	D	D	D	E	E	E	C	E	E	C	E	D	E	E	D	E	E	B	D	D	C	E	E	C	E	E	B	D	D	B	D
E	E	D	C	E	E	E	D	E	D	B	D	E	C	E	E	E	D	E	C	E	D	B	D	E	D	E	E	E	C	D	D	B	D	B
E	D	E	C	E	E	E	E	D	E	C	E	D	B	D	E	D	E	E	E	C	D	D	B	E	E	C	E	D	E	D	B	D	D	D
E	D	E	D	B	D	E	C	E	D	E	E	E	E	C	E	D	E	E	D	E	C	E	E	B	D	D	C	E	E	D	B	D	D	B
E	E	D	E	C	E	D	B	D	E	D	E	E	E	C	E	E	D	C	E	E	E	D	E	D	B	D	E	C	E	D	D	B	B	D
D	E	E	E	C	E	E	C	E	E	E	D	D	D	B	D	E	E	E	E	C	E	E	C	D	D	B	E	E	D	B	D	D	D	D
E	E	D	D	D	B	E	E	C	E	E	C	D	E	E	E	E	D	E	E	D	C	E	E	C	E	E	B	D	D	D	D	B	D	D
E	D	E	E	E	C	D	D	B	E	E	C	E	D	E	E	D	E	C	E	E	E	E	D	E	C	E	D	B	D	D	B	D	B	D
D	E	E	E	E	C	E	E	C	D	D	B	E	E	D	D	E	E	E	C	E	E	C	E	E	E	D	D	D	B	B	D	D	D	B
D	E	E	B	C	C	D	E	E	E	D	E	E	D	E	D	E	E	B	C	C	D	E	E	E	D	E	E	D	E	B	D	D	D	E
E	D	E	C	B	C	E	D	E	D	E	E	E	E	D	E	D	E	C	B	C	E	D	E	D	E	E	E	E	D	D	B	D	E	D
E	E	D	C	C	B	E	E	D	E	E	D	D	E	E	E	E	D	C	C	B	E	E	D	E	E	D	D	E	E	D	D	B	E	E
D	E	E	D	E	E	B	D	D	C	E	E	C	E	E	B	D	D	D	E	E	D	E	E	E	E	C	E	E	C	D	E	E	B	C
E	D	E	E	D	E	C	E	E	B	D	D	C	E	E	D	B	D	E	D	E	E	E	C	D	E	E	E	C	E	E	D	E	C	B
E	E	D	E	E	D	C	E	E	C	E	E	B	D	D	D	D	B	E	E	D	E	C	E	E	C	E	D	E	E	E	E	D	C	C
B	D	D	D	E	E	D	E	E	E	E	C	E	E	C	D	E	E	D	E	E	B	D	D	C	E	E	C	E	E	D	E	E	D	E
C	E	E	E	E	D	E	E	D	D	D	B	E	E	C	E	C	E	E	E	D	D	D	B	E	E	D	E	C	E	E	E	C	E	D

Table 8b.3: Elements $m_{rs}^{(8)}$, in the range $s \in \{1 \to 35\}$ and $r \in \{1 \to 53\}$. The edge of the $m^{(8)}$ matrix is bordered.

E	D	E	E	E	E	D	E	E	D	D	E	E	D	E	E	B	C	C	D	E	E	D	E	E	D	E	E	D	E	E	B	C	C	D
E	E	E	D	D	E	E	E	D	E	E	D	E	E	D	E	D	E	E	B	C	C	D	E	E	E	E	D	E	E	D	D	E	E	D
D	E	D	E	E	D	E	D	E	E	E	E	D	E	E	D	D	E	E	D	E	E	B	C	C	E	D	E	E	D	E	D	E	E	B
E	B	C	C	D	E	E	D	E	E	B	C	C	D	E	E	D	E	E	E	E	D	E	E	D	D	E	E	B	C	C	D	E	E	E
E	D	E	E	B	C	C	D	E	E	C	B	C	E	D	E	E	E	D	D	E	E	E	D	E	E	D	E	D	E	E	E	E	D	E
D	D	E	E	D	E	E	B	C	C	C	C	B	E	E	D	E	D	E	E	D	E	D	E	E	E	E	D	D	E	E	E	D	E	C
C	D	E	E	E	D	E	E	D	E	D	E	E	B	C	C	D	E	E	E	D	E	E	D	E	B	C	C	D	E	E	D	E	E	E
E	E	D	E	C	B	C	E	D	E	E	D	E	D	E	E	E	E	D	E	D	E	C	B	C	C	B	C	E	D	E	E	E	D	D
E	E	E	D	E	D	E	C	B	C	E	E	D	D	E	E	E	D	E	C	B	C	E	D	E	C	C	B	E	E	D	E	D	E	E
C	E	D	E	D	E	E	E	E	D	E	D	E	C	B	C	E	D	E	D	E	E	E	E	D	D	E	E	E	D	E	E	D	E	E
E	C	B	C	E	D	E	E	E	D	D	E	E	E	D	E	E	D	E	E	E	D	C	C	B	E	D	E	C	B	C	E	D	E	D
E	E	D	E	E	E	D	C	C	B	E	E	D	E	D	E	C	B	C	E	D	E	E	E	D	E	E	D	E	D	E	C	B	C	E
B	E	E	D	E	E	D	D	E	E	E	E	D	C	C	B	E	E	D	E	E	D	D	E	E	D	E	E	E	E	D	E	E	D	C
D	C	C	B	E	E	D	E	D	E	D	E	E	E	E	D	E	E	D	C	C	B	E	E	D	E	E	D	C	C	B	E	E	D	E
D	E	E	D	C	C	B	E	E	D	E	D	E	E	E	D	C	C	B	E	E	D	E	D	E	E	D	E	E	E	D	C	C	B	E
E	D	E	E	E	E	D	E	E	D	D	E	E	B	D	D	D	E	E	E	C	E	E	C	E	D	E	E	B	D	D	D	E	E	E
E	E	E	D	D	E	E	E	D	E	E	D	E	D	B	D	E	C	E	D	E	E	E	E	C	E	E	D	D	D	B	E	E	C	E
D	E	D	E	E	D	E	D	E	E	E	E	D	D	D	B	E	E	C	E	E	C	D	E	E	E	D	E	D	B	D	E	C	E	D
D	D	E	E	E	C	E	E	C	E	B	C	C	D	E	E	D	E	E	E	E	D	E	E	D	D	E	E	D	E	E	B	D	D	C
D	E	C	E	D	E	E	E	E	E	C	C	B	C	E	D	E	E	E	D	D	E	E	E	D	E	E	D	E	E	E	C	D	D	B	E
B	E	E	C	E	E	C	D	E	E	C	C	B	E	E	D	E	D	E	E	D	E	D	E	E	E	E	D	E	C	E	D	B	D	E
E	B	D	D	C	E	E	C	E	E	D	E	E	D	E	E	B	D	D	C	E	E	C	E	E	B	C	C	D	E	E	D	E	E	E
E	D	B	D	E	D	E	E	E	C	E	D	E	E	E	C	D	D	B	E	E	C	E	D	E	C	B	C	E	D	E	E	E	D	D
C	D	D	B	E	E	C	E	D	E	E	E	D	E	C	E	D	B	D	E	D	E	E	E	C	C	C	B	E	E	D	E	D	E	E
E	C	E	E	B	D	D	C	E	E	E	D	E	E	D	E	C	E	E	B	D	D	C	E	E	D	E	E	E	E	C	E	E	C	D
E	E	D	E	D	B	D	E	C	E	D	E	E	E	E	C	E	E	C	D	D	B	E	E	D	E	D	E	E	D	E	C	E	E	B
C	E	E	C	D	D	B	E	E	D	E	E	D	C	E	E	E	D	E	D	B	D	E	C	E	E	E	D	C	E	E	E	D	E	D
D	C	E	E	C	E	E	B	D	D	E	E	D	E	E	D	C	E	E	C	E	E	B	D	D	D	E	E	E	C	E	E	C	E	E
E	E	E	D	E	C	E	D	B	D	D	E	E	E	C	E	E	C	E	E	E	D	D	D	B	E	E	D	E	E	D	C	E	E	C
E	E	C	E	E	E	D	D	D	B	E	D	E	C	E	E	E	E	D	E	C	E	D	B	D	E	D	E	C	E	E	E	E	D	E
D	B	D	D	D	D	B	D	D	B	B	D	D	D	E	E	D	E	E	E	E	C	E	E	C	B	D	D	D	E	E	D	E	E	E
D	D	D	B	B	D	D	D	B	D	D	B	D	E	D	E	E	E	C	D	E	E	E	C	E	D	D	B	E	E	D	E	C	E	E
B	D	B	D	D	B	D	B	D	D	D	D	B	E	E	D	E	C	E	E	C	E	D	E	E	D	B	D	E	D	E	E	E	C	D
B	B	D	D	D	B	D	D	B	D	D	E	E	B	C	C	D	E	E	E	D	E	E	D	E	D	E	E	D	E	E	B	D	D	C
B	D	B	D	B	D	D	D	D	B	E	D	E	C	B	C	E	D	E	D	E	E	E	E	D	E	E	C	E	D	E	D	B	D	E
A	D	D	B	D	D	B	B	D	D	E	E	D	C	C	B	E	E	D	E	E	D	D	E	E	E	C	E	E	E	D	D	D	B	E
D	A	B	B	B	D	D	B	D	D	D	E	E	D	E	E	B	D	D	C	E	E	C	E	E	D	E	E	B	C	C	D	E	E	E
D	B	A	B	D	B	D	D	D	B	E	E	C	E	D	E	D	B	D	E	C	E	E	E	D	E	D	E	C	B	C	E	D	E	D
B	B	B	A	D	D	B	D	B	D	E	C	E	E	E	D	D	D	B	E	E	D	E	C	E	E	E	D	C	C	B	E	E	D	E
D	B	D	D	A	B	B	B	D	D	E	D	E	E	D	E	C	E	E	B	D	D	C	E	E	E	E	C	D	E	E	E	C	E	D
D	D	B	D	B	A	B	D	B	D	E	E	C	D	E	E	E	C	E	D	B	D	E	D	E	E	D	E	E	D	E	C	E	E	B
B	D	D	B	B	B	A	D	D	B	C	E	E	E	E	D	E	E	D	D	D	B	E	E	C	C	E	E	E	E	D	E	E	D	D
B	B	D	D	B	D	D	A	B	B	E	E	D	E	E	D	C	E	E	C	E	E	B	D	D	E	C	E	D	E	E	E	E	C	E
D	D	D	B	D	B	D	B	A	B	E	C	E	D	E	E	E	E	C	E	D	E	D	B	D	E	E	D	E	E	D	C	E	E	C
D	D	B	D	D	D	B	B	B	A	C	E	E	E	D	E	E	D	E	E	E	C	D	D	B	C	E	E	E	D	E	E	D	E	E
E	D	E	E	E	E	C	E	E	C	A	B	B	B	D	D	B	D	D	D	D	B	D	D	B	B	D	D	D	E	E	D	E	E	E
E	E	E	C	D	E	E	E	C	E	B	A	B	D	B	D	D	D	B	B	D	D	D	B	D	D	B	D	E	C	E	E	E	D	C
D	E	C	E	E	C	E	D	E	E	B	B	A	D	D	B	D	B	D	D	B	D	B	D	D	D	D	B	E	E	C	E	D	E	E
C	D	E	E	E	D	E	E	D	E	B	D	D	A	B	B	B	D	D	D	B	D	D	B	D	D	E	E	B	D	D	D	E	E	E
C	E	D	E	D	E	E	E	E	D	D	B	D	B	A	B	D	B	D	B	D	D	D	D	B	E	C	E	D	B	D	E	D	E	C
B	E	E	D	E	E	D	D	E	E	D	D	B	B	B	A	D	D	B	D	D	B	B	D	D	E	E	C	D	D	B	E	E	D	E
E	B	D	D	C	E	E	C	E	E	B	D	D	B	D	D	A	B	B	B	D	D	B	D	D	D	E	E	D	E	E	B	C	C	D
E	D	B	D	E	C	E	E	E	D	D	D	B	D	B	D	B	A	B	D	B	D	D	D	B	E	E	D	E	D	E	C	B	C	E

Table 8b.4: Elements $m_{rs}^{(8)}$, in the range $s \in \{36 \to 70\}$ and $r \in \{1 \to 53\}$. The edge of the $m^{(8)}$ matrix is bordered.

E	E	D	E	E	E	E	D	E	E	D	D	E	E	D	E	E	B	C	C	E	E	D	E	E	D	D	E	E	D	E	E	B	C	C
E	E	B	C	C	D	E	E	D	E	E	B	C	C	D	E	E	D	E	E	E	D	E	E	D	E	D	E	E	B	C	C	D	E	E
C	C	D	E	E	E	D	E	E	D	E	D	E	E	B	C	C	D	E	E	D	E	E	D	E	E	B	C	C	D	E	E	D	E	E
D	E	E	D	E	E	D	E	D	E	E	E	E	D	E	D	E	C	B	C	E	D	E	D	E	E	E	E	D	E	D	E	C	B	C
D	E	C	B	C	D	E	E	B	C	C	D	E	E	E	D	E	E	D	E	E	E	D	D	E	E	E	D	E	C	B	C	E	D	E
B	C	E	D	E	E	E	D	D	E	E	E	D	E	C	B	C	E	D	E	D	E	E	B	C	C	D	E	E	E	D	E	E	D	E
E	D	E	E	D	D	E	E	E	D	E	E	D	E	E	E	D	C	C	B	D	E	E	E	D	E	E	D	E	E	E	D	C	C	B
E	E	E	D	E	E	D	E	C	B	C	E	D	E	D	E	E	E	E	D	E	E	D	E	D	E	C	B	C	E	D	E	E	E	D
D	E	D	E	E	E	E	D	E	D	E	C	B	C	E	D	E	E	E	D	E	D	E	C	B	C	E	D	E	D	E	E	E	E	D
E	D	C	C	B	B	C	C	D	E	E	D	E	E	E	E	D	E	E	D	D	E	E	E	E	D	E	E	D	C	C	B	E	E	D
E	E	E	E	D	C	B	C	E	D	E	E	E	D	D	E	E	E	D	E	E	D	E	E	E	D	C	C	B	E	E	D	E	D	E
D	E	E	E	D	C	C	B	E	E	D	E	D	E	E	D	E	D	E	E	E	E	D	C	C	B	E	E	D	E	E	D	D	E	E
C	B	E	E	D	D	E	E	E	E	D	E	E	D	C	C	B	E	E	D	B	C	C	D	E	E	D	E	E	E	E	D	E	E	D
E	D	D	E	E	E	D	E	E	E	D	C	C	B	E	E	D	E	D	E	C	B	C	E	D	E	E	E	D	D	E	E	E	D	E
E	D	E	D	E	E	E	D	C	C	B	E	E	D	E	E	D	D	E	E	C	C	B	E	E	D	E	D	E	E	D	E	D	E	E
C	E	E	C	E	E	E	D	D	D	B	E	E	C	E	E	C	D	E	E	E	E	D	D	D	B	E	E	C	E	E	C	D	E	E
E	C	D	E	E	D	E	E	B	D	D	D	E	E	E	C	E	E	C	E	E	D	E	D	B	D	E	C	E	D	E	E	E	E	C
E	E	E	E	C	E	D	E	D	B	D	E	C	E	D	E	E	E	E	C	D	E	E	B	D	D	D	E	E	E	C	E	E	C	E
E	E	C	E	E	E	D	E	E	E	C	D	D	B	E	E	C	E	D	E	E	D	E	E	E	C	D	D	B	E	E	C	E	D	E
E	C	E	D	E	D	E	E	D	E	E	B	D	D	C	E	E	C	E	E	E	E	D	E	C	E	D	B	D	E	D	E	E	E	C
D	E	E	E	C	E	E	D	E	C	E	D	B	D	E	D	E	E	E	C	D	E	E	D	E	E	B	D	D	C	E	E	C	E	E
E	D	E	E	D	D	E	E	E	E	C	E	E	C	D	D	B	E	E	D	D	E	E	E	E	C	E	E	C	D	D	B	E	E	D
E	E	E	D	E	E	D	E	E	D	E	C	E	E	B	D	D	C	E	E	E	E	D	C	E	E	E	D	E	D	B	D	E	C	E
D	E	D	E	E	E	E	D	C	E	E	E	D	E	D	B	D	E	C	E	E	D	E	E	D	E	C	E	E	B	D	D	C	E	E
D	B	E	E	D	B	C	C	D	E	E	D	E	E	E	E	D	E	E	D	D	E	E	E	C	E	E	C	E	E	E	D	D	D	B
D	D	C	E	E	C	B	C	E	D	E	E	E	D	D	E	E	E	D	E	E	D	E	C	E	E	E	E	D	E	C	E	D	B	D
B	D	E	C	E	C	C	B	E	E	D	E	D	E	E	D	E	D	E	E	E	E	D	E	E	D	C	E	E	C	E	E	B	D	D
E	D	D	D	B	D	E	E	E	C	E	E	C	E	E	E	D	D	D	B	B	C	C	D	E	E	D	E	E	E	E	D	E	E	D
E	E	B	D	D	E	D	E	C	E	E	E	E	D	E	C	E	D	B	D	C	B	C	E	D	E	E	E	D	D	E	E	E	D	E
C	E	D	B	D	E	E	D	E	E	D	C	E	E	C	E	E	B	D	D	C	C	B	E	E	D	E	D	E	E	D	E	D	E	E
E	C	E	E	C	D	D	B	E	E	D	E	C	E	E	C	E	D	E	E	D	D	B	E	E	D	E	C	E	E	C	E	D	E	E
C	E	D	E	E	B	D	D	D	E	E	D	E	E	E	E	C	E	E	C	D	B	D	E	D	E	E	E	C	D	E	E	E	C	E
E	E	E	C	E	D	B	D	E	D	E	E	E	C	D	E	E	E	C	E	B	D	D	D	E	E	D	E	E	E	E	C	E	E	C
E	E	C	E	E	E	E	C	E	D	E	D	B	D	E	C	E	E	E	D	E	E	C	E	D	E	D	B	D	E	C	E	E	E	D
C	E	E	E	D	D	E	E	D	E	E	B	D	D	C	E	E	C	E	E	E	C	E	E	E	D	D	D	B	E	E	D	E	C	E
E	D	E	C	E	E	C	E	E	E	D	D	D	B	E	E	D	E	C	E	D	E	E	D	E	E	B	D	D	C	E	E	C	E	E
D	E	E	D	E	E	E	E	D	C	E	E	E	D	E	D	B	D	E	D	E	E	E	C	D	E	E	E	C	E	D	B	D	E	E
E	E	E	E	D	E	D	E	E	D	E	C	E	E	B	D	D	C	E	E	C	E	E	E	E	D	E	E	D	D	D	B	E	E	C
E	D	D	E	E	C	E	E	E	E	D	E	E	C	E	E	E	D	D	D	E	E	E	C	E	E	C	E	D	E	E	E	B	D	D
D	D	C	E	E	E	D	E	C	B	C	E	D	E	D	E	E	E	E	D	C	E	E	E	D	E	E	D	E	E	E	C	D	D	B
D	B	E	E	C	E	E	D	C	C	B	E	E	D	E	E	D	D	E	E	E	E	D	E	E	D	C	E	E	C	E	E	B	D	D
D	E	D	B	D	E	C	E	D	E	E	E	E	C	E	D	E	D	B	D	D	E	E	B	C	C	D	E	E	E	D	E	E	D	E
E	E	B	D	D	C	E	E	E	D	E	E	D	E	E	E	C	D	D	B	E	D	E	C	B	C	E	D	E	D	E	E	E	E	D
E	C	D	D	B	E	E	D	E	E	D	C	E	E	C	E	E	B	D	D	E	E	D	C	C	B	E	E	D	E	E	D	D	E	E
E	C	E	E	C	D	B	D	E	C	E	E	E	D	C	E	E	E	D	E	D	B	D	E	C	E	E	E	D	C	E	E	E	D	E
E	E	E	D	E	B	D	D	D	E	E	D	E	E	E	E	C	E	E	C	D	D	B	E	E	C	E	D	E	E	D	E	C	E	E
D	E	C	E	E	D	D	B	E	E	C	E	D	E	E	D	E	C	E	E	B	D	D	D	E	E	D	E	E	E	E	C	E	E	C
C	E	E	C	E	E	E	C	E	D	B	D	E	D	E	C	E	E	E	E	D	E	C	E	D	B	D	E	D	E	C	E	E	E	E	D
E	E	E	E	D	D	E	E	B	D	D	D	E	E	E	C	E	E	E	C	E	E	E	C	D	D	B	E	E	D	E	E	D	C	E	E
E	D	C	E	E	E	E	C	D	D	B	E	E	D	E	E	D	C	E	E	D	E	E	B	D	D	D	E	E	E	C	E	E	C	E
E	E	D	E	E	E	C	E	E	C	E	D	E	E	B	D	D	D	E	E	E	C	E	E	C	E	D	E	E	B	D	D	D	E	E
D	E	E	E	D	E	E	D	C	E	E	E	D	E	D	B	D	E	C	E	C	E	E	E	E	D	E	E	D	D	D	B	E	E	C

Table 8b.5: Elements $m_{rs}^{(8)}$, in the range $s \in \{71 \to 105\}$ and $r \in \{1 \to 53\}$. The edge of the $m^{(8)}$ matrix is bordered.

C E E E D E E D E E E C D D B E E C E D E D B D E C E E E D E C E E E
D B D E D E E E C D E E E C E E D E E D E C E E B D D C E E E D E E D
E C E E E D D D B E E D E C E C E E E E D E E D D D B E E C E E C D E
E C E D E E E E C E D E D B D E E C D E E E C E D B D E D E C E E E E
D D B E E D E C E E C E D E E E E D E E D C E E C E E B D D E E D E E
E E C E D E D B D E C E E E D C E E E D E E D E E E C D D B E C E D E
E E C D E E E C E D B D E D E E C E D E E E E C E D E D B D C E E E D
D E E D E E B C C D E E D E E D E E D E E B C C D E E D E E E B D D D E
E E D E D E C B C E D E E E D E E D E D E C B C E D E E E D D D B E E
E D E E E D C C B E E D E D E E D E E E D C C B E E D E D E D B D E C
D E E B D D D E E E C E E C E B D D D E E D E E E E C E E C D E E D E
E E D C E E E D E D B D E C E D D B E E C E D E E D E C E E E E D E D
E D E C E E E E D E C E D B D D B D E C E E E D C E E E D E E D E E E
B D D D E E D E E E E C E E C D E E B D D D E E E C E E C E D E E B D
C E E E E D E E D D D B E E C E E C D D B E E D E E D C E E E E C E D B
C E E E D E E E D E E E C D D B E C E D B D E D E C E E E E D E E C D D
D D B E E C E D E E D E C E E E E D C E E E D E D B D E C E E E D C E
E E C D D B E E D E E D C E E C E E E E D E E D D D B E E C E C E E C
E E C E E C D E E D E E B D D E C E E C E D E E B D D D E E C E E E E
D B D E C E E E D C E E E D E E D E C E E E E D E C E D B D E D E C E
E C E D B D E D E C E E E E D C E E E D E E D E E E C D D B E E C E E
E C E E C E D E E B D D D E E E C E E C D E E D E E B D D C E E E D
E D E E D E D E E B C C D E E E D E E D E D E E B C C D E E D B D E D
E E D D E E E D E C B C E D E E E D D E E E D E C B C E D E D D B E E
D E E E E D E E D C C B E E D D E E E E D E E D C C B E E D B D D C E
E D E D B D E C E D E E E E C D B D E D E E E C D E E E C E E D E E D
E E D E C E D B D E D E E E C D D B E E C E D E E D E C E E E E D D E
D E E E C E E C E E E D D D B B D D C E E C E E E E D E E D D E E E E
D B D E D E E E C D E E E C E E D E D B D E C E D E E E E C E D E D B
E C E E E D D D B E E D E C E E E C D D B E E D E E D C E E C E E B D
E C E D E E E E C E D E D B D C E E B D D C E E E D E E D E E E C D D
D D B E E C E D E E D E C E E E E D E C E D B D E D E E E C E E D E C
E E C D D B E E D E E D C E E E C E E E E D D D B E E D E C E C E E C E
E E C E E C D E E D E E B D D C E E C E E B D D D E E D E E E C E E E
B D D C E E C E E E E E D E E D D E E E C E E C E E E D D D B D E E E C
C E E B D D C E E E D E E D E E C E D E E E E C E D E D B D E E C E E
C E E C E E B D D D E E D E E E E C E E E C D E E D E E B D D E C E D E
E E D E E D D E E D E E B C C E E D E E D E E D D E E D E E B C C D D B E E
E D E D E E E E D E D E C B C E D E D E E E E D E D E C B C D B D E C
D E E E D E E D E E E D C C B D E E E D E E D E E E D C C B B D D C E
E E D D D B E E C E E C D E E D D B E E D E C E E E C E D E E E E D E E
E D E E E C D D B E E C E D E D B D E C E E E E D C E E E D E E D E D E
D E E E E C E E C D D B E E D B D D C E E C E E E E D E E D D E E E D
D D B E E D E C E E C E D E E E E D D D B E E C E E C D E E E E D D D
E E C E D E D B D E C E E E D E C E D B D E D E C E E E E D C E E B D
E E C D E E E C E D B D E D E C E E B D D C E E E D E E D E E C E D B
D B D E C E E E D C E E E D E E D E E E C D D B E E C E D E E D E E E
E C E D B D E D E C E E E E D E E C E D E D B D E C E E E D C E E E C E
E C E E C E D E E B D D D E E C E E C E E B D D D E E D E E E E C E D
B D D C E E C E E E E D E E D D E E E E C E E C D D B E E D D E E E E
C E E B D D C E E E D E E D E E E C D E E E C E D B D E D E E C E E C
C E E C E E B D D D E E D E E E C E E C E D E E B D D D E E E E C D E

Table 8b.6: Elements $m_{rs}^{(8)}$, in the range $s \in \{1 \to 35\}$ and $r \in \{54 \to 105\}$. The edge of the $m^{(8)}$ matrix is bordered.

D D D B E E D E C E D B D D D B B B A D D B D B D E D E E E D C C B E
E C E E B D D C E E E D B D D B D B D D A B B B D D E C E E C E D E E B
E E C E D B D E D E D D B B D D D B D B A B D B D E E D C E E E D E D
D E E D D D B E E C B D D D D D B D D B B B A D D B C E E E E D E E D D
D C E E C E E B D D D D B D D B B D D B D D A B B E E C E E C D E E D
E E E C E D E D B D D B D B D D D D B D B D B A B E D E C E E E E D E
E E D E E E C D D B B D D D B D D B D D D B B B A C E E E D E E D E E
E D E E E E C E E C B D D D E E D E E E E C E E E C A B B B D D B D D D
C E D E E D E C E E D B D E C E E E D C E E E D E B A B D B D D D B B
E E E D C E E E D E D D B E E C E D E E D E C E E B B A D D B D B D D
E B C C D E E D E E D E E B D D D E E E C E E C E B D D A B B B D D D
E C B C E D E E E D E C E D B D E D E C E E E E D D B D B A B D B D B
D C C B E E D E D E E E C D D B E E D E E D C E E D D B B B A D D B D
D D E E E C E E C E D E E D E E B C C D E E D E E E B D D B D D A B B B
D E D E C E E E E D E E D E D E C B C E D E E E D D D B D B D B A B D
B E E D E E D C E E E D E E E D C C B E E D E D E D B D D D B B B A D
E E D E D B D E C E E C E E E C E D E E B D D D E E D B D D B D B D D A
E D E E B D D D E E E E D C E E E D E D B D E C E D D B B D D D B D B
D E E D D D B E E C C E E E E D E E D D D B E E C B D D D D B D D B B
E E E D E C E D B D E E C E E C D E E D E E B D D D D B D D B B D D B
C D E E D E E B D D E D E C E E E E D E C E D B D D B D B D D D D B D
E E D E E E C D D B C E E E D E E D E E E C D D B B D D D B D D B D D
E E E C D E E E C E D B D E D E E E C D E E E C E B D D C E E C E E E
C E D E E D E C E E B D D C E E C E E E E D E E D D B D E D E E E C D
E C E E E E D E E D D D B E E C E D E E D E C E E D D B E E C E D E E
E D E E B C C D E E E D E D B D E C E D E E E E C C E E B D D C E E E
E E D E C B C E D E C E E B D D C E E E D E E D E E D E D B D E C E D
D E E D C C B E E D E E C D D B E E D E E D C E E E E E C D D B E E D E
D E C E D E E E E C E D E E D E D E E B C C D E E C E E C E E B D D D
D C E E E D E E D E E E D D E E E D E C B C E D E E E D E C E D B D E
B E E D E E D C E E D E E E E D E E D C C B E E D E C E E E D D D B E
E D B D E D E E E C C E E C E E B D D D E E D E E E D E E D E E B
E B D D D E E D E E E E D E C E D B D E D E E E C E E D D E E E D E C
D D D B E E D E C E E E C E E E D D D B E E D E C E D E E E E D E E D C
E E C E E E D D D B E E C E E C D E E D E E B D D E E C E E C D E E D
C D E E D E E B D D D E E E C E E C E E E D D D B E C E D E E E E C E
E E E C E D E D B D E C E D E E E E C E D E D B D D E E E C E E C E E
D E C E E C E D E E D D B E E D E C E E C E D E E B D D C E E C E E E
E E E D C E E E D E B D D C E E C E E E E D E E D D D B E E D E C E E
E C E E E E D E E D D B D E C E E E D C E E E D E D B D E C E E E D C
D D E E D E E B C C E E D D D B E E C E E C D E E C E E B D D C E E E
E E E D E D E C B C C E E B D D C E E E D E E D E E E D D D B E E C E
E E D E E E D C C B E C E D B D E D E C E E E E D E C E D B D E D E C
B E E C E E C D E E E E D E E D D E E D E E B C C C E E C E E B D D D
D C E E E D E E D E E D E D E E E E D E D E C B C E D E E E C D D B E
D E D E C E E E E E D D E E E D E E D E E E E D C C B E E C E D E D B D E
C D D B E E C E D E C E E C E E B D D D E E D E E E E D E E D D E E D
E B D D D E E D E E E D E E E C D D B E E C E D E E D E D E E E E D E
E D B D E C E E E D E E C E D E D B D E C E E E D D E E E D E E D E E
C E E C D D B E E D E C E E C E D E E B D D D E E E C E E C E D E E B
E D E E B D D D E E D E E E E C E E C D D B E E D E E E C D E E E C E D
E E C E D B D E D E E E C D E E E C E D B D E D E D E E E E C E E C D

Table 8b.7: Elements $m_{rs}^{(8)}$, in the range $s \in \{36 \to 70\}$ and $r \in \{54 \to 105\}$. The edge of the $m^{(8)}$ matrix is bordered.

E	D	E	D	E	C	E	E	E	E	D	E	E	D	D	D	B	E	E	C	E	E	D	C	E	E	E	D	E	D	B	D	E	C	E
D	D	D	E	E	D	E	E	D	E	E	B	C	C	D	E	E	D	E	E	E	E	C	E	E	C	D	E	E	D	E	E	B	D	D
B	D	E	C	E	E	E	D	E	D	E	C	B	C	E	D	E	E	E	D	C	E	E	E	D	E	E	D	E	E	E	C	D	D	B
D	B	E	E	C	E	D	E	E	E	D	C	C	B	E	E	D	E	D	E	E	D	E	C	E	E	E	E	D	E	C	E	D	B	D
E	E	B	D	D	E	E	C	E	E	C	D	E	E	D	E	E	B	D	D	D	E	E	D	E	E	B	C	C	D	E	E	D	E	E
C	E	D	B	D	C	E	E	E	D	E	E	D	E	E	E	C	D	D	B	E	E	D	E	D	E	C	B	C	E	D	E	E	E	D
E	C	D	D	B	E	D	E	C	E	E	E	E	D	E	C	E	D	B	D	E	D	E	E	E	D	C	C	B	E	E	D	E	D	E
D	B	D	D	B	B	D	D	C	E	E	C	E	E	E	E	D	E	E	D	B	D	D	C	E	E	C	E	E	E	E	D	E	E	D
D	D	D	B	D	D	B	D	E	D	E	E	E	C	D	E	E	E	C	E	D	D	B	E	E	C	E	D	E	E	D	E	C	E	E
B	D	B	D	D	D	D	B	E	E	C	E	D	E	E	D	E	C	E	E	D	B	D	E	D	E	E	E	C	D	E	E	E	C	E
B	D	D	B	D	C	E	E	B	D	D	C	E	E	E	D	E	E	D	E	C	E	E	B	D	D	C	E	E	E	D	E	E	D	E
D	D	D	D	B	E	D	E	D	B	D	E	C	E	D	E	E	E	E	C	E	E	C	D	D	B	E	E	D	E	E	D	C	E	E
D	B	B	D	D	E	E	C	D	D	B	E	E	D	E	E	D	C	E	E	E	D	E	D	B	D	E	C	E	D	E	E	E	E	C
D	D	B	D	D	C	E	E	C	E	E	B	D	D	D	E	E	D	E	E	C	E	E	C	E	E	B	D	D	D	E	E	D	E	E
B	D	D	D	B	E	E	D	E	C	E	D	B	D	E	D	E	E	E	C	E	C	E	E	E	D	D	D	B	E	E	D	E	C	E
D	B	D	B	D	E	C	E	E	E	D	D	D	B	E	E	D	E	C	E	E	E	D	E	C	E	D	B	D	E	D	E	E	E	C
B	B	B	D	D	E	D	E	E	D	E	D	E	E	B	C	C	D	E	E	E	E	C	E	E	C	D	E	E	D	E	E	B	D	D
A	B	D	B	D	E	E	D	D	E	E	E	D	E	C	B	C	E	D	E	E	C	E	D	E	E	E	E	C	E	D	E	D	B	D
B	A	D	D	B	D	E	E	E	E	D	E	E	D	C	C	B	E	E	D	D	E	E	E	C	E	E	C	E	E	E	D	D	D	B
D	D	A	B	B	E	E	C	E	E	C	D	E	E	D	E	E	B	D	D	E	D	E	E	D	E	D	E	E	B	C	C	D	E	E
B	D	B	A	B	E	C	E	D	E	E	E	E	C	E	D	E	D	B	D	E	E	D	D	E	E	E	D	E	C	B	C	E	D	E
D	B	B	B	A	D	E	E	E	C	E	E	C	E	E	E	D	D	D	B	D	E	E	E	E	D	E	E	D	C	C	B	E	E	D
E	D	E	E	D	A	B	B	B	D	D	B	D	D	D	D	B	D	D	B	B	D	D	C	E	E	C	E	E	E	E	D	E	E	D
E	E	E	C	E	B	A	B	D	B	D	D	D	B	B	D	D	D	B	D	D	B	D	E	C	E	E	E	D	C	E	E	E	D	E
D	E	C	E	E	B	B	A	D	D	B	D	B	D	D	B	D	B	D	D	D	D	B	E	E	D	E	C	E	E	C	E	D	E	E
D	E	E	D	E	B	D	D	A	B	B	B	D	D	D	B	D	D	B	D	C	E	E	B	D	D	C	E	E	E	D	E	E	D	E
E	E	E	E	C	D	B	D	B	A	B	D	B	D	B	D	D	D	D	B	E	C	E	D	B	D	E	D	E	C	E	E	E	E	D
E	D	C	E	E	D	D	B	B	B	A	D	D	B	D	D	B	B	D	D	E	E	D	D	D	B	E	E	C	E	E	C	D	E	E
E	E	D	E	E	B	D	D	B	D	D	A	B	B	B	D	D	B	D	D	C	E	E	C	E	E	B	D	D	D	E	E	D	E	E
D	E	E	E	C	D	D	B	D	B	D	B	A	B	D	B	D	D	D	B	E	E	C	E	D	E	D	B	D	E	C	E	E	E	D
E	D	E	C	E	D	B	D	D	D	B	B	B	A	D	D	B	D	B	D	E	E	E	E	C	D	D	B	E	E	C	E	D	E	
C	C	D	E	E	D	B	D	D	B	D	B	D	D	A	B	B	B	D	D	E	C	E	E	C	E	D	E	E	B	D	D	D	E	E
B	C	E	D	E	D	D	B	B	D	D	D	B	D	B	A	B	D	B	D	E	E	C	D	E	E	E	C	E	D	B	D	E	D	E
C	B	E	E	D	B	D	D	D	D	B	D	D	B	B	B	A	D	D	B	D	E	E	E	E	C	E	E	C	D	D	B	E	E	D
E	E	B	D	D	D	D	B	D	D	B	B	D	D	B	D	D	A	B	B	E	E	D	E	E	D	D	E	E	D	E	E	B	C	C
D	E	D	B	D	D	B	D	B	D	D	D	D	B	D	B	D	B	A	B	E	D	E	D	E	E	E	E	D	E	D	E	C	B	C
E	D	D	D	B	B	D	D	D	B	D	D	B	D	D	D	B	B	B	A	D	E	E	E	D	E	E	D	E	E	E	D	C	C	B
E	D	E	E	D	B	D	D	C	E	E	C	E	E	E	E	D	E	E	D	A	B	B	B	D	D	B	D	D	D	D	B	D	D	B
C	E	D	E	E	D	B	D	E	C	E	E	E	D	C	E	E	E	D	E	B	A	B	D	B	D	D	D	B	B	D	D	D	B	D
E	E	E	D	E	D	D	B	E	E	D	E	C	E	E	C	E	D	E	E	B	B	A	D	D	B	D	B	D	D	B	D	B	D	D
D	E	E	D	E	C	E	E	B	D	D	C	E	E	E	D	E	E	D	E	B	D	D	A	B	B	B	D	D	D	B	D	D	B	D
E	C	D	E	E	E	C	E	D	B	D	E	D	E	C	E	E	E	E	D	D	B	D	B	A	B	D	B	D	B	D	D	D	D	B
E	E	E	E	D	E	E	D	D	D	B	E	E	C	E	E	C	D	E	E	D	D	B	B	B	A	D	D	B	D	D	B	B	D	D
E	E	D	E	E	C	E	E	C	E	E	B	D	D	D	E	E	D	E	E	B	D	D	B	D	D	A	B	B	B	D	D	B	D	D
E	C	E	D	E	E	E	C	E	D	E	D	B	D	E	C	E	E	E	D	D	D	B	D	B	D	B	A	B	D	B	D	D	D	B
C	E	E	E	D	E	D	D	E	E	E	C	D	D	B	E	E	C	E	D	E	D	B	D	D	D	B	B	B	A	D	D	B	D	B	D
E	E	B	C	C	E	C	E	E	E	C	E	D	E	E	B	D	D	D	E	E	D	B	D	D	B	D	B	D	D	A	B	B	B	D	D
D	E	C	B	C	E	E	C	D	E	E	E	C	E	D	B	D	E	D	E	D	D	B	B	D	D	D	B	D	B	A	B	D	B	D
E	D	C	C	B	D	E	E	E	E	C	E	E	C	D	D	B	E	E	D	B	D	D	D	D	B	D	D	B	B	B	A	D	D	B
D	D	D	E	E	E	E	D	E	E	D	D	E	E	D	E	E	B	C	C	D	D	B	D	D	B	B	D	D	B	D	D	A	B	B
B	D	E	D	E	E	D	E	D	E	E	E	E	D	E	D	E	C	B	C	D	B	D	B	D	D	D	D	B	D	B	D	B	A	B
D	B	E	E	D	D	E	E	E	D	E	E	D	E	E	E	D	C	C	B	B	D	D	D	B	D	D	B	D	D	D	B	B	B	A

Table 8b.8: Elements $m_{rs}^{(8)}$, in the range $s \in \{71 \to 105\}$ and $r \in \{54 \to 105\}$. The edge of the $m^{(8)}$ matrix is bordered.

Appendix 8c: **Resonance energy transfer: Explicit coupling V_{ij} derivation**

As shown in chapter 3a, third-body-modified RET comprises four interaction events, which may occur in any of 24 possible time-orderings. For *any one* time-ordering, the MDA-configuration of the process has quantum amplitude given by equation (3a.4):

$$M_{FI} = \left(\frac{\hbar c}{2\varepsilon_0 V}\right)^2 \sum_{p,e_{(p)},\phi,e_{(\phi)}} \frac{p\phi\ \ \bar{e}_{(p)a} e_{(p)b} \bar{e}_{(\phi)c} e_{(\phi)d}\ \ \mu_i^{M_o M_o} \mu_j^{D_o D_r} \mu_k^{D_r D_\alpha} \mu_l^{A_\beta A_o}}{\left[E^{\mathrm{D}}_{\alpha T} + E^{\mathrm{A}}_{0T} - E^{rad}_{T}\right]\left[E^{\mathrm{D}}_{\alpha S} + E^{\mathrm{A}}_{0S} - E^{rad}_{S}\right]\left[E^{\mathrm{D}}_{\alpha R} + E^{\mathrm{A}}_{0R} - E^{rad}_{R}\right]} \times \exp\left(i\mathbf{p}.(\mathbf{r}_{pAnn.} - \mathbf{r}_{pCre.}) + i\boldsymbol{\varphi}.(\mathbf{r}_{\phi Ann.} - \mathbf{r}_{\phi Cre.})\right)$$

This appendix contains the generalisation this result to find the quantum amplitude of the overall process. This will be simply the sum of 24 terms with this form, at the limit of infinite volume *V*.

The indices *a*, *b*, *c*, *d* are hereafter chosen to be fixed and *i*, *j*, *k*, *l* to vary according to the rules set out in chapter 3a – therefore, the $\bar{e}_a e_b \bar{e}_c e_d$ factor is common to all 24 terms and factors out. The photon annihilation and creation positions $\mathbf{r}_{pAnn}$ and $\mathbf{r}_{pCre}$ will in every case be the positions of chromophores D and M, or vice versa. The positions $\mathbf{r}_{\phi Ann}$ and $\mathbf{r}_{\phi Cre}$ will in every case be the positions of chromophores A and D, or vice versa.

What follows are the *numerators* of the 24 versions of Equation (3a.4) for each time-ordering of the four events (W), (X), (Y), (Z).

$$WXYZ = \left(\frac{\hbar c}{2\varepsilon_0 V}\right)^2 \boldsymbol{\mu}_a^{M_o M_o} \boldsymbol{\mu}_c^{D_o D_r} \boldsymbol{\mu}_b^{D_r D_\alpha} \boldsymbol{\mu}_d^{A_\beta A_o} \sum_{p,\phi} p\phi \bar{e}_{(p)a} e_{(p)b} \bar{e}_{(\phi)c} e_{(\phi)d} \exp\left(ip\cdot(r_D - r_M) + i\phi\cdot(r_A - r_D)\right)$$

$$WXZY = \left(\frac{\hbar c}{2\varepsilon_0 V}\right)^2 \boldsymbol{\mu}_a^{M_o M_o} \boldsymbol{\mu}_d^{D_o D_r} \boldsymbol{\mu}_b^{D_r D_\alpha} \boldsymbol{\mu}_c^{A_\beta A_o} \sum_{p,\phi} p\phi \bar{e}_{(p)a} e_{(p)b} \bar{e}_{(\phi)c} e_{(\phi)d} \exp\left(ip\cdot(r_D - r_M) + i\phi\cdot(r_D - r_A)\right)$$

$$WYXZ = \left(\frac{\hbar c}{2\varepsilon_0 V}\right)^2 \boldsymbol{\mu}_a^{M_o M_o} \boldsymbol{\mu}_b^{D_o D_r} \boldsymbol{\mu}_c^{D_r D_\alpha} \boldsymbol{\mu}_d^{A_\beta A_o} \sum_{p,\phi} p\phi \bar{e}_{(p)a} e_{(p)b} \bar{e}_{(\phi)c} e_{(\phi)d} \exp\left(ip\cdot(r_D - r_M) + i\phi\cdot(r_A - r_D)\right)$$

$$WYZX = \left(\frac{\hbar c}{2\varepsilon_0 V}\right)^2 \boldsymbol{\mu}_a^{M_o M_o} \boldsymbol{\mu}_b^{D_o D_r} \boldsymbol{\mu}_c^{D_r D_\alpha} \boldsymbol{\mu}_d^{A_\beta A_o} \sum_{p,\phi} p\phi \bar{e}_{(p)a} e_{(p)b} \bar{e}_{(\phi)c} e_{(\phi)d} \exp\left(ip\cdot(r_D - r_M) + i\phi\cdot(r_A - r_D)\right)$$

$$WZXY = \left(\frac{\hbar c}{2\varepsilon_0 V}\right)^2 \boldsymbol{\mu}_a^{M_o M_o} \boldsymbol{\mu}_d^{D_o D_r} \boldsymbol{\mu}_b^{D_r D_\alpha} \boldsymbol{\mu}_c^{A_\beta A_o} \sum_{p,\phi} p\phi \bar{e}_{(p)a} e_{(p)b} \bar{e}_{(\phi)c} e_{(\phi)d} \exp\left(ip\cdot(r_D - r_M) + i\phi\cdot(r_D - r_A)\right)$$

$$WZYX = \left(\frac{\hbar c}{2\varepsilon_0 V}\right)^2 \boldsymbol{\mu}_a^{M_o M_o} \boldsymbol{\mu}_b^{D_o D_r} \boldsymbol{\mu}_d^{D_r D_\alpha} \boldsymbol{\mu}_c^{A_\beta A_o} \sum_{p,\phi} p\phi \bar{e}_{(p)a} e_{(p)b} \bar{e}_{(\phi)c} e_{(\phi)d} \exp\left(ip\cdot(r_D - r_M) + i\phi\cdot(r_D - r_A)\right)$$

$$XWYZ = \left(\frac{\hbar c}{2\varepsilon_0 V}\right)^2 \boldsymbol{\mu}_b^{M_o M_o} \boldsymbol{\mu}_c^{D_o D_r} \boldsymbol{\mu}_a^{D_r D_\alpha} \boldsymbol{\mu}_d^{A_\beta A_o} \sum_{p,\phi} p\phi \bar{e}_{(p)a} e_{(p)b} \bar{e}_{(\phi)c} e_{(\phi)d} \exp\left(ip\cdot(r_M - r_D) + i\phi\cdot(r_A - r_D)\right)$$

$$XWZY = \left(\frac{\hbar c}{2\varepsilon_0 V}\right)^2 \boldsymbol{\mu}_b^{M_o M_o} \boldsymbol{\mu}_d^{D_o D_r} \boldsymbol{\mu}_a^{D_r D_\alpha} \boldsymbol{\mu}_c^{A_\beta A_o} \sum_{p,\phi} p\phi \bar{e}_{(p)a} e_{(p)b} \bar{e}_{(\phi)c} e_{(\phi)d} \exp\left(ip\cdot(r_M - r_D) + i\phi\cdot(r_D - r_A)\right)$$

$$XYWZ = \left(\frac{\hbar c}{2\varepsilon_0 V}\right)^2 \boldsymbol{\mu}_b^{M_o M_o} \boldsymbol{\mu}_c^{D_o D_r} \boldsymbol{\mu}_a^{D_r D_\alpha} \boldsymbol{\mu}_d^{A_\beta A_o} \sum_{p,\phi} p\phi \bar{e}_{(p)a} e_{(p)b} \bar{e}_{(\phi)c} e_{(\phi)d} \exp\left(ip\cdot(r_M - r_D) + i\phi\cdot(r_A - r_D)\right)$$

$$XYZW = \left(\frac{\hbar c}{2\varepsilon_0 V}\right)^2 \boldsymbol{\mu}_b^{M_o M_o} \boldsymbol{\mu}_c^{D_o D_r} \boldsymbol{\mu}_a^{D_r D_\alpha} \boldsymbol{\mu}_d^{A_\beta A_o} \sum_{p,\phi} p\phi \bar{e}_{(p)a} e_{(p)b} \bar{e}_{(\phi)c} e_{(\phi)d} \exp\left(ip\cdot(r_M - r_D) + i\phi\cdot(r_A - r_D)\right)$$

$$XZWY = \left(\frac{\hbar c}{2\varepsilon_0 V}\right)^2 \boldsymbol{\mu}_b^{M_o M_o} \boldsymbol{\mu}_d^{D_o D_r} \boldsymbol{\mu}_a^{D_r D_\alpha} \boldsymbol{\mu}_c^{A_\beta A_o} \sum_{p,\phi} p\phi \bar{e}_{(p)a} e_{(p)b} \bar{e}_{(\phi)c} e_{(\phi)d} \exp\left(ip\cdot(r_M - r_D) + i\phi\cdot(r_D - r_A)\right)$$

$$XZYW = \left(\frac{\hbar c}{2\varepsilon_0 V}\right)^2 \boldsymbol{\mu}_b^{M_o M_o} \boldsymbol{\mu}_d^{D_o D_r} \boldsymbol{\mu}_a^{D_r D_\alpha} \boldsymbol{\mu}_c^{A_\beta A_o} \sum_{p,\phi} p\phi \bar{e}_{(p)a} e_{(p)b} \bar{e}_{(\phi)c} e_{(\phi)d} \exp\left(ip\cdot(r_M - r_D) + i\phi\cdot(r_D - r_A)\right)$$

$$YWXZ = \left(\frac{\hbar c}{2\varepsilon_0 V}\right)^2 \boldsymbol{\mu}_a^{M_o M_o} \boldsymbol{\mu}_b^{D_o D_r} \boldsymbol{\mu}_c^{D_r D_\alpha} \boldsymbol{\mu}_d^{A_\beta A_o} \sum_{p,\phi} p\phi \bar{e}_{(p)a} e_{(p)b} \bar{e}_{(\phi)c} e_{(\phi)d} \exp\left(ip\cdot(r_D - r_M) + i\phi\cdot(r_A - r_D)\right)$$

$$YWZX = \left(\frac{\hbar c}{2\varepsilon_0 V}\right)^2 \boldsymbol{\mu}_a^{M_o M_o} \boldsymbol{\mu}_b^{D_o D_r} \boldsymbol{\mu}_c^{D_r D_\alpha} \boldsymbol{\mu}_d^{A_\beta A_o} \sum_{p,\phi} p\phi \bar{e}_{(p)a} e_{(p)b} \bar{e}_{(\phi)c} e_{(\phi)d} \exp\left(ip\cdot(r_D - r_M) + i\phi\cdot(r_A - r_D)\right)$$

$$YXWZ = \left(\frac{\hbar c}{2\varepsilon_0 V}\right)^2 \boldsymbol{\mu}_b^{M_o M_o} \boldsymbol{\mu}_a^{D_o D_r} \boldsymbol{\mu}_c^{D_r D_\alpha} \boldsymbol{\mu}_d^{A_\beta A_o} \sum_{p,\phi} p\phi \bar{e}_{(p)a} e_{(p)b} \bar{e}_{(\phi)c} e_{(\phi)d} \exp\left(ip\cdot(r_M - r_D) + i\phi\cdot(r_A - r_D)\right)$$

$$YXZW = \left(\frac{\hbar c}{2\varepsilon_0 V}\right)^2 \boldsymbol{\mu}_b^{M_o M_o} \boldsymbol{\mu}_a^{D_o D_r} \boldsymbol{\mu}_c^{D_r D_\alpha} \boldsymbol{\mu}_d^{A_\beta A_o} \sum_{p,\phi} p\phi \bar{e}_{(p)a} e_{(p)b} \bar{e}_{(\phi)c} e_{(\phi)d} \exp\left(ip\cdot(r_M - r_D) + i\phi\cdot(r_A - r_D)\right)$$

$$YZWX = \left(\frac{\hbar c}{2\varepsilon_0 V}\right)^2 \boldsymbol{\mu}_a^{M_o M_o} \boldsymbol{\mu}_b^{D_o D_r} \boldsymbol{\mu}_c^{D_r D_\alpha} \boldsymbol{\mu}_d^{A_\beta A_o} \sum_{p,\phi} p\phi \bar{e}_{(p)a} e_{(p)b} \bar{e}_{(\phi)c} e_{(\phi)d} \exp\left(ip\cdot(r_D - r_M) + i\phi\cdot(r_A - r_D)\right)$$

$$YZXW = \left(\frac{\hbar c}{2\varepsilon_0 V}\right)^2 \boldsymbol{\mu}_b^{M_o M_o} \boldsymbol{\mu}_a^{D_o D_r} \boldsymbol{\mu}_c^{D_r D_\alpha} \boldsymbol{\mu}_d^{A_\beta A_o} \sum_{p,\phi} p\phi \bar{e}_{(p)a} e_{(p)b} \bar{e}_{(\phi)c} e_{(\phi)d} \exp\left(ip\cdot(r_M - r_D) + i\phi\cdot(r_A - r_D)\right)$$

$$ZWXY = \left(\frac{\hbar c}{2\varepsilon_0 V}\right)^2 \boldsymbol{\mu}_a^{M_o M_o} \boldsymbol{\mu}_d^{D_o D_r} \boldsymbol{\mu}_b^{D_r D_\alpha} \boldsymbol{\mu}_c^{A_\beta A_o} \sum_{p,\phi} p\phi \bar{e}_{(p)a} e_{(p)b} \bar{e}_{(\phi)c} e_{(\phi)d} \exp\left(ip\cdot(r_D - r_M) + i\phi\cdot(r_D - r_A)\right)$$

$$ZWYX = \left(\frac{\hbar c}{2\varepsilon_0 V}\right)^2 \boldsymbol{\mu}_a^{M_o M_o} \boldsymbol{\mu}_b^{D_o D_r} \boldsymbol{\mu}_d^{D_r D_\alpha} \boldsymbol{\mu}_c^{A_\beta A_o} \sum_{p,\phi} p\phi \bar{e}_{(p)a} e_{(p)b} \bar{e}_{(\phi)c} e_{(\phi)d} \exp\left(ip\cdot(r_D - r_M) + i\phi\cdot(r_D - r_A)\right)$$

$$ZXWY = \left(\frac{\hbar c}{2\varepsilon_0 V}\right)^2 \boldsymbol{\mu}_b^{M_o M_o} \boldsymbol{\mu}_d^{D_o D_r} \boldsymbol{\mu}_a^{D_r D_\alpha} \boldsymbol{\mu}_c^{A_\beta A_o} \sum_{p,\phi} p\phi \bar{e}_{(p)a} e_{(p)b} \bar{e}_{(\phi)c} e_{(\phi)d} \exp\left(ip\cdot(r_M - r_D) + i\phi\cdot(r_D - r_A)\right)$$

$$ZXWY = \left(\frac{\hbar c}{2\varepsilon_0 V}\right)^2 \boldsymbol{\mu}_b^{M_o M_o} \boldsymbol{\mu}_d^{D_o D_r} \boldsymbol{\mu}_a^{D_r D_\alpha} \boldsymbol{\mu}_c^{A_\beta A_o} \sum_{p,\phi} p\phi \bar{e}_{(p)a} e_{(p)b} \bar{e}_{(\phi)c} e_{(\phi)d} \exp\left(ip\cdot(r_M - r_D) + i\phi\cdot(r_D - r_A)\right)$$

$$ZYWX = \left(\frac{\hbar c}{2\varepsilon_0 V}\right)^2 \boldsymbol{\mu}_a^{M_o M_o} \boldsymbol{\mu}_b^{D_o D_r} \boldsymbol{\mu}_d^{D_r D_\alpha} \boldsymbol{\mu}_c^{A_\beta A_o} \sum_{p,\phi} p\phi \bar{e}_{(p)a} e_{(p)b} \bar{e}_{(\phi)c} e_{(\phi)d} \exp\left(ip\cdot(r_D - r_M) + i\phi\cdot(r_D - r_A)\right)$$

$$ZYXW = \left(\frac{\hbar c}{2\varepsilon_0 V}\right)^2 \boldsymbol{\mu}_b^{M_o M_o} \boldsymbol{\mu}_a^{D_o D_r} \boldsymbol{\mu}_d^{D_r D_\alpha} \boldsymbol{\mu}_c^{A_\beta A_o} \sum_{p,\phi} p\phi \bar{e}_{(p)a} e_{(p)b} \bar{e}_{(\phi)c} e_{(\phi)d} \exp\left(ip\cdot(r_M - r_D) + i\phi\cdot(r_D - r_A)\right)$$

These 24 terms factorise into four terms with unique exponential factors, each a sum of six unique fractions. Within each term, the six fractions group into two unique numerators – the first and fourth terms have five fractions with the same numerator and one exception, the second and third terms have three fractions with each numerator.

$$\begin{aligned}
M_{fi} = \left(\frac{\hbar c}{2\varepsilon_0 V}\right)^2 & \sum_{p,\phi} p\phi \bar{e}_{(p)a} e_{(p)b} \bar{e}_{(\phi)c} e_{(\phi)d} \\
\times \Bigg\{ \Bigg(& \frac{\boldsymbol{\mu}_a^{M_o M_o} \boldsymbol{\mu}_c^{D_o D_r} \boldsymbol{\mu}_b^{D_r D_\alpha} \boldsymbol{\mu}_d^{A_\beta A_o}}{\left[-\hbar c p\right]\left[E_{\alpha r}^D\right]\left[E_{\alpha 0}^D - \hbar c\phi\right]} \\
& + \frac{\boldsymbol{\mu}_a^{M_o M_o} \boldsymbol{\mu}_b^{D_o D_r} \boldsymbol{\mu}_c^{D_r D_\alpha} \boldsymbol{\mu}_d^{A_\beta A_o}}{\left[-\hbar c p\right]\left[E_{\alpha r}^D - \hbar c(p+\phi)\right]\left[E_{\alpha 0}^D - \hbar c\phi\right]} \\
& + \frac{\boldsymbol{\mu}_a^{M_o M_o} \boldsymbol{\mu}_b^{D_o D_r} \boldsymbol{\mu}_c^{D_r D_\alpha} \boldsymbol{\mu}_d^{A_\beta A_o}}{\left[-\hbar c p\right]\left[E_{\alpha r}^D - \hbar c(p+\phi)\right]\left[E_{\alpha r}^D + E_{0\beta}^A - \hbar c p\right]} \\
& + \frac{\boldsymbol{\mu}_a^{M_o M_o} \boldsymbol{\mu}_b^{D_o D_r} \boldsymbol{\mu}_c^{D_r D_\alpha} \boldsymbol{\mu}_d^{A_\beta A_o}}{\left[E_{\alpha r}^D - \hbar c\phi\right]\left[E_{\alpha r}^D - \hbar c(p+\phi)\right]\left[E_{\alpha 0}^D - \hbar c\phi\right]} \\
& + \frac{\boldsymbol{\mu}_a^{M_o M_o} \boldsymbol{\mu}_b^{D_o D_r} \boldsymbol{\mu}_c^{D_r D_\alpha} \boldsymbol{\mu}_d^{A_\beta A_o}}{\left[E_{\alpha r}^D - \hbar c\phi\right]\left[E_{\alpha r}^D - \hbar c(p+\phi)\right]\left[E_{\alpha r}^D + E_{0\beta}^A - \hbar c p\right]} \\
& + \frac{\boldsymbol{\mu}_a^{M_o M_o} \boldsymbol{\mu}_b^{D_o D_r} \boldsymbol{\mu}_c^{D_r D_\alpha} \boldsymbol{\mu}_d^{A_\beta A_o}}{\left[E_{\alpha r}^D - \hbar c\phi\right]\left[E_{\alpha r}^D + E_{0\beta}^A\right]\left[E_{\alpha r}^D + E_{0\beta}^A - \hbar c p\right]} \Bigg) \\
& \times \exp\left(ip\cdot\left[r_D - r_M\right] + i\phi\cdot\left[r_A - r_D\right]\right)
\end{aligned}$$

$$
+\left(\begin{array}{l}
\dfrac{\boldsymbol{\mu}_a^{M_o M_o}\boldsymbol{\mu}_d^{D_o D_r}\boldsymbol{\mu}_b^{D_r D_\alpha}\boldsymbol{\mu}_c^{A_\beta A_o}}{\left[E_{\alpha r}^D+E_{0\beta}^A-\hbar c\phi\right]\left[E_{\alpha r}^D\right]\left[-\hbar cp)\right]} \\
+\dfrac{\boldsymbol{\mu}_a^{M_o M_o}\boldsymbol{\mu}_d^{D_o D_r}\boldsymbol{\mu}_b^{D_r D_\alpha}\boldsymbol{\mu}_c^{A_\beta A_o}}{\left[E_{\alpha r}^D+E_{0\beta}^A-\hbar c\phi\right]\left[E_{0\beta}^A-\hbar c(p+\phi)\right]\left[-\hbar cp\right]} \\
+\dfrac{\boldsymbol{\mu}_a^{M_o M_o}\boldsymbol{\mu}_b^{D_o D_r}\boldsymbol{\mu}_d^{D_r D_\alpha}\boldsymbol{\mu}_c^{A_\beta A_o}}{\left[E_{\alpha r}^D+E_{0\beta}^A-\hbar cp\right]\left[E_{0\beta}^A-\hbar c(p+\phi)\right]\left[-\hbar cp\right]} \\
+\dfrac{\boldsymbol{\mu}_a^{M_o M_o}\boldsymbol{\mu}_d^{D_o D_r}\boldsymbol{\mu}_b^{D_r D_\alpha}\boldsymbol{\mu}_c^{A_\beta A_o}}{\left[E_{\alpha r}^D+E_{0\beta}^A-\hbar c\phi\right]\left[E_{0\beta}^A-\hbar c(p+\phi)\right]\left[E_{0\beta}^A-\hbar c\phi\right]} \\
+\dfrac{\boldsymbol{\mu}_a^{M_o M_o}\boldsymbol{\mu}_b^{D_o D_r}\boldsymbol{\mu}_d^{D_r D_\alpha}\boldsymbol{\mu}_c^{A_\beta A_o}}{\left[E_{\alpha r}^D+E_{0\beta}^A-\hbar cp\right]\left[E_{0\beta}^A-\hbar c(p+\phi)\right]\left[E_{0\beta}^A-\hbar c\phi\right]} \\
+\dfrac{\boldsymbol{\mu}_a^{M_o M_o}\boldsymbol{\mu}_b^{D_o D_r}\boldsymbol{\mu}_d^{D_r D_\alpha}\boldsymbol{\mu}_c^{A_\beta A_o}}{\left[E_{\alpha r}^D+E_{0\beta}^A-\hbar cp\right]\left[E_{\alpha r}^D+E_{0\beta}^A\right]\left[E_{0\beta}^A-\hbar c\phi\right]}
\end{array}\right) \\
\times\exp\left(ip\cdot\left[r_D-r_M\right]+i\phi\cdot\left[r_D-r_A\right]\right)
$$

$$
+\left(\begin{array}{l}
\dfrac{\boldsymbol{\mu}_b^{M_o M_o}\boldsymbol{\mu}_c^{D_o D_r}\boldsymbol{\mu}_a^{D_r D_\alpha}\boldsymbol{\mu}_d^{A_\beta A_o}}{\left[E_{\alpha 0}^D-\hbar c\phi\right]\left[E_{\alpha r}^D\right]\left[E_{\alpha r}^D-\hbar cp\right]} \\
+\dfrac{\boldsymbol{\mu}_b^{M_o M_o}\boldsymbol{\mu}_c^{D_o D_r}\boldsymbol{\mu}_a^{D_r D_\alpha}\boldsymbol{\mu}_d^{A_\beta A_o}}{\left[E_{\alpha 0}^D-\hbar c\phi\right]\left[E_{\alpha 0}^D-\hbar c(p+\phi)\right]\left[E_{\alpha r}^D-\hbar cp\right]} \\
+\dfrac{\boldsymbol{\mu}_b^{M_o M_o}\boldsymbol{\mu}_c^{D_o D_r}\boldsymbol{\mu}_a^{D_r D_\alpha}\boldsymbol{\mu}_d^{A_\beta A_o}}{\left[E_{\alpha 0}^D+E_{0\beta}^A-\hbar cp\right]\left[E_{\alpha 0}^D-\hbar c(p+\phi)\right]\left[E_{\alpha r}^D-\hbar cp\right]} \\
+\dfrac{\boldsymbol{\mu}_b^{M_o M_o}\boldsymbol{\mu}_a^{D_o D_r}\boldsymbol{\mu}_c^{D_r D_\alpha}\boldsymbol{\mu}_d^{A_\beta A_o}}{\left[E_{\alpha 0}^D-\hbar c\phi\right]\left[E_{\alpha 0}^D-\hbar c(p+\phi)\right]\left[E_{\alpha r}^D-\hbar c\phi\right]} \\
+\dfrac{\boldsymbol{\mu}_b^{M_o M_o}\boldsymbol{\mu}_a^{D_o D_r}\boldsymbol{\mu}_c^{D_r D_\alpha}\boldsymbol{\mu}_d^{A_\beta A_o}}{\left[E_{\alpha 0}^D+E_{0\beta}^A-\hbar cp\right]\left[E_{\alpha 0}^D-\hbar c(p+\phi)\right]\left[E_{\alpha r}^D-\hbar c\phi\right]} \\
+\dfrac{\boldsymbol{\mu}_b^{M_o M_o}\boldsymbol{\mu}_a^{D_o D_r}\boldsymbol{\mu}_c^{D_r D_\alpha}\boldsymbol{\mu}_d^{A_\beta A_o}}{\left[E_{\alpha 0}^D+E_{0\beta}^A-\hbar cp\right]\left[E_{\alpha r}^D+E_{0\beta}^A\right]\left[E_{\alpha r}^D-\hbar c\phi\right]}
\end{array}\right) \\
\times\exp\left(ip\cdot\left[r_M-r_D\right]+i\phi\cdot\left[r_A-r_D\right]\right)
$$

$$
+\Bigg(\frac{\boldsymbol{\mu}_b^{M_o M_o}\boldsymbol{\mu}_d^{D_o D_r}\boldsymbol{\mu}_a^{D_r D_\alpha}\boldsymbol{\mu}_c^{A_\beta A_o}}{\left[E_{\alpha r}^D + E_{0\beta}^A - \hbar c\phi\right]\left[E_{\alpha r}^D\right]\left[E_{\alpha r}^D - \hbar cp\right]}
$$

$$
+\frac{\boldsymbol{\mu}_b^{M_o M_o}\boldsymbol{\mu}_d^{D_o D_r}\boldsymbol{\mu}_a^{D_r D_\alpha}\boldsymbol{\mu}_c^{A_\beta A_o}}{\left[E_{\alpha r}^D + E_{0\beta}^A - \hbar c\phi\right]\left[E_{\alpha r}^D + E_{0\beta}^A - \hbar c(p+\phi)\right]\left[E_{\alpha r}^D - \hbar cp\right]}
$$

$$
+\frac{\boldsymbol{\mu}_b^{M_o M_o}\boldsymbol{\mu}_d^{D_o D_r}\boldsymbol{\mu}_a^{D_r D_\alpha}\boldsymbol{\mu}_c^{A_\beta A_o}}{\left[E_{\alpha 0}^D + E_{0\beta}^A - \hbar cp\right]\left[E_{\alpha r}^D + E_{0\beta}^A - \hbar c(p+\phi)\right]\left[E_{\alpha r}^D - \hbar cp\right]}
$$

$$
+\frac{\boldsymbol{\mu}_b^{M_o M_o}\boldsymbol{\mu}_d^{D_o D_r}\boldsymbol{\mu}_a^{D_r D_\alpha}\boldsymbol{\mu}_c^{A_\beta A_o}}{\left[E_{\alpha r}^D + E_{0\beta}^A - \hbar c\phi\right]\left[E_{\alpha r}^D + E_{0\beta}^A - \hbar c(p+\phi)\right]\left[E_{0\beta}^A - \hbar c\phi\right]}
$$

$$
+\frac{\boldsymbol{\mu}_b^{M_o M_o}\boldsymbol{\mu}_d^{D_o D_r}\boldsymbol{\mu}_a^{D_r D_\alpha}\boldsymbol{\mu}_c^{A_\beta A_o}}{\left[E_{\alpha 0}^D + E_{0\beta}^A - \hbar cp\right]\left[E_{\alpha r}^D + E_{0\beta}^A - \hbar c(p+\phi)\right]\left[E_{0\beta}^A - \hbar c\phi\right]}
$$

$$
+\frac{\boldsymbol{\mu}_b^{M_o M_o}\boldsymbol{\mu}_a^{D_o D_r}\boldsymbol{\mu}_d^{D_r D_\alpha}\boldsymbol{\mu}_c^{A_\beta A_o}}{\left[E_{\alpha 0}^D + E_{0\beta}^A - \hbar cp\right]\left[E_{\alpha r}^D + E_{0\beta}^A\right]\left[E_{0\beta}^A - \hbar c\phi\right]}\Bigg)
$$

$$
\times \exp\left(ip\cdot\left[r_M - r_D\right] + i\phi\cdot\left[r_D - r_A\right]\right) \quad \Big\}.
$$

The quantity $E_{\alpha 0}^D$ is the electronic energy lost by chromophore D. Similarly, the quantity $E_{0\beta}^A$ is the electronic energy "lost" by chromophore A. Since RET is the conservative process of energy transferred from D to A, chromophore A must *gain* exactly the amount of energy that D loses, which is to say $E_{\alpha 0}^D = -E_{0\beta}^A$. Replacing all instances of the variable $E_{\alpha 0}^D$ with $-E_{0\beta}^A$ simplifies the unique denominators, yielding just 8 terms:

$$
\begin{aligned}
M_{fi} = & \left(\frac{\hbar c}{2\varepsilon_0 V}\right)^2 \sum_{p,\phi} p\phi \bar{e}_{(p)a} e_{(p)b} \bar{e}_{(\phi)c} e_{(\phi)d} \\
& \times \Bigg\{ \Bigg(\frac{\boldsymbol{\mu}_a^{M_o M_o} \boldsymbol{\mu}_c^{D_o D_r} \boldsymbol{\mu}_b^{D_r D_\alpha} \boldsymbol{\mu}_d^{A_\beta A_o}}{\left[-\hbar cp\right]\left[E_{\alpha r}^{D}\right]\left[-E_{0\beta}^{A} - \hbar c\phi\right]} \\
& \quad + \frac{\boldsymbol{\mu}_a^{M_o M_o} \boldsymbol{\mu}_b^{D_o D_r} \boldsymbol{\mu}_c^{D_r D_\alpha} \boldsymbol{\mu}_d^{A_\beta A_o}}{\left[-\hbar cp\right]\left[E_{\alpha r}^{D} + E_{0\beta}^{A}\right]\left[-E_{0\beta}^{A} - \hbar c\phi\right]} \Bigg) \exp\left(ip \cdot \left[r_D - r_M\right] + i\phi \cdot \left[r_A - r_D\right]\right) \\
& + \Bigg(\frac{\boldsymbol{\mu}_a^{M_o M_o} \boldsymbol{\mu}_d^{D_o D_r} \boldsymbol{\mu}_b^{D_r D_\alpha} \boldsymbol{\mu}_c^{A_\beta A_o}}{\left[-\hbar cp\right]\left[E_{\alpha r}^{D}\right]\left[E_{0\beta}^{A} - \hbar c\phi\right]} \\
& \quad + \frac{\boldsymbol{\mu}_a^{M_o M_o} \boldsymbol{\mu}_b^{D_o D_r} \boldsymbol{\mu}_d^{D_r D_\alpha} \boldsymbol{\mu}_c^{A_\beta A_o}}{\left[-\hbar cp\right]\left[E_{\alpha r}^{D} + E_{0\beta}^{A}\right]\left[E_{0\beta}^{A} - \hbar c\phi\right]} \Bigg) \exp\left(ip \cdot \left[r_D - r_M\right] + i\phi \cdot \left[r_D - r_A\right]\right) \\
& + \Bigg(\frac{\boldsymbol{\mu}_b^{M_o M_o} \boldsymbol{\mu}_c^{D_o D_r} \boldsymbol{\mu}_a^{D_r D_\alpha} \boldsymbol{\mu}_d^{A_\beta A_o}}{\left[-\hbar cp\right]\left[E_{\alpha r}^{D}\right]\left[-E_{0\beta}^{A} - \hbar c\phi\right]} \\
& \quad + \frac{\boldsymbol{\mu}_b^{M_o M_o} \boldsymbol{\mu}_a^{D_o D_r} \boldsymbol{\mu}_c^{D_r D_\alpha} \boldsymbol{\mu}_d^{A_\beta A_o}}{\left[-\hbar cp\right]\left[E_{\alpha r}^{D} + E_{0\beta}^{A}\right]\left[-E_{0\beta}^{A} - \hbar c\phi\right]} \Bigg) \exp\left(ip \cdot \left[r_M - r_D\right] + i\phi \cdot \left[r_A - r_D\right]\right) \\
& + \Bigg(\frac{\boldsymbol{\mu}_b^{M_o M_o} \boldsymbol{\mu}_d^{D_o D_r} \boldsymbol{\mu}_a^{D_r D_\alpha} \boldsymbol{\mu}_c^{A_\beta A_o}}{\left[-\hbar cp\right]\left[E_{\alpha r}^{D}\right]\left[E_{0\beta}^{A} - \hbar c\phi\right]} \\
& \quad + \frac{\boldsymbol{\mu}_b^{M_o M_o} \boldsymbol{\mu}_a^{D_o D_r} \boldsymbol{\mu}_d^{D_r D_\alpha} \boldsymbol{\mu}_c^{A_\beta A_o}}{\left[-\hbar cp\right]\left[E_{\alpha r}^{D} + E_{0\beta}^{A}\right]\left[E_{0\beta}^{A} - \hbar c\phi\right]} \Bigg) \exp\left(ip \cdot \left[r_M - r_D\right] + i\phi \cdot \left[r_D - r_A\right]\right) \Bigg\}
\end{aligned}
$$

The common factor $[-\hbar cp]^{-1}$ immediately cancels with the top line. Factorising out common numerators, combining denominator sums and collecting like terms yields the relatively concise quantum amplitude expression:

$$
\begin{aligned}
M_{FI} = & -\hbar c \left(2\varepsilon_0 V\right)^{-2} \sum_{p, e_{(p)}, \phi, e_{(\phi)}} \phi\, \bar{e}_{(p)a} e_{(p)b} \bar{e}_{(\phi)c} e_{(\phi)d} \\
& \times \Bigg\{ \Bigg(\frac{\mu_c^{D_o D_r} \mu_d^{A_\beta A_o} \exp\left(+i\boldsymbol{\varphi} \cdot \mathbf{R}_{DA}\right)}{\left[E_{\alpha r}^{D}\right]\left[-E_{0\beta}^{A} - \hbar c\phi\right]} + \frac{\mu_d^{D_o D_r} \mu_c^{A_\beta A_o} \exp\left(-i\boldsymbol{\varphi} \cdot \mathbf{R}_{DA}\right)}{\left[E_{\alpha r}^{D}\right]\left[E_{0\beta}^{A} - \hbar c\phi\right]} \Bigg) \\
& \quad \times \left[\mu_a^{M_o M_o} \mu_b^{D_r D_\alpha} \exp\left(+i\mathbf{p} \cdot \mathbf{R}_{MD}\right) + \mu_b^{M_o M_o} \mu_a^{D_r D_\alpha} \exp\left(-i\mathbf{p} \cdot \mathbf{R}_{MD}\right)\right] \\
& + \Bigg(\frac{\mu_c^{D_r D_\alpha} \mu_d^{A_\beta A_o} \exp\left(+i\boldsymbol{\varphi} \cdot \mathbf{R}_{DA}\right)}{\left[E_{\alpha r}^{D} + E_{0\beta}^{A}\right]\left[-E_{0\beta}^{A} - \hbar c\phi\right]} + \frac{\mu_d^{D_r D_\alpha} \mu_c^{A_\beta A_o} \exp\left(-i\boldsymbol{\varphi} \cdot \mathbf{R}_{DA}\right)}{\left[E_{\alpha r}^{D} + E_{0\beta}^{A}\right]\left[E_{0\beta}^{A} - \hbar c\phi\right]} \Bigg) \\
& \quad \times \left[\mu_a^{M_o M_o} \mu_b^{D_o D_r} \exp\left(+i\mathbf{p} \cdot \mathbf{R}_{MD}\right) + \mu_b^{M_o M_o} \mu_a^{D_o D_r} \exp\left(-i\mathbf{p} \cdot \mathbf{R}_{MD}\right)\right] \Bigg\}
\end{aligned}
$$

It is now appropriate to expand the quantisation volume to infinity. Moving from an enclosed finite system to a regime of infinite space modifies the nature of the sum over **p** and $\mathbf{e}_{(p)}$ described by the big sigma operator. This is now a continuous sum over all possible vectors **p**, a definite integral over all of **p**-space (triple-integration).

$$\lim_{V\to\infty}\frac{1}{V}\sum_{p} \equiv \int_0^\infty \frac{d^3p}{(2\pi)^3}$$

The polarisation vectors $\bar{e}_{(p)}$ and $e_{(p)}$ form an orthogonal triad with the wavevector **p**, while $\bar{e}_{(\phi)}$, $e_{(\phi)}$ and **ϕ** form a triad likewise. In Cartesian unit-vector notation, this implies:

$$\sum_{p,e_{(p)}} \bar{e}_{(p)a} e_{(p)b} = \delta_{ab} - \hat{p}_a \hat{p}_b$$

The common factor of $\bar{e}_a e_b \bar{e}_c e_d$ involves the indices *a, b, c, d* being used to describe the two elementary polarisation vectors for each photon. In the integration over both **p** and over **ϕ**, this becomes:

$$\lim_{V\to\infty} V^{-2} \sum_{p,e_{(p)},\phi,e_{(\phi)}} \bar{e}_{(p)a} e_{(p)b} \bar{e}_{(\phi)c} e_{(\phi)d} = (2\pi)^{-6} \int_0^\infty\int_0^\infty \left(\delta_{ab} - \hat{p}_a\hat{p}_b\right)\left(\delta_{cd} - \hat{\phi}_c\hat{\phi}_d\right) d^3\mathbf{p} d^3\boldsymbol{\varphi}$$

Due to Kronecker deltas, the indices *a* and *b* are now symmetric with respect to each other, likewise *c* and *d*. Henceforth, μ_b and μ_d have been suppressed into μ_a and μ_c respectively, implying that $\mu_a\mu_a=\mu_a\mu_b$ or $\mu_b\mu_a$.

$$\begin{aligned} M_{fi} = {} & -(2\pi)^{-6}\hbar c\left(2\varepsilon_0\right)^{-2} \mu_a^{M_o M_o}\mu_c^{A_\beta A_o} \int_0^\infty\int_0^\infty \left(\delta_{ab} - \hat{p}_a\hat{p}_b\right)\left(\delta_{cd} - \hat{\phi}_c\hat{\phi}_d\right)\phi \\ & \times\Bigg\{ \mu_c^{D_o D_r}\mu_a^{D_r D_\alpha}\left(\frac{\exp\left(+i\boldsymbol{\varphi}\cdot\mathbf{R}_{DA}\right)}{\left[E^D_{\alpha r}\right]\left[-E^A_{0\beta}-\hbar c\phi\right]} + \frac{\exp\left(-i\boldsymbol{\varphi}\cdot\mathbf{R}_{DA}\right)}{\left[E^D_{\alpha r}\right]\left[E^A_{0\beta}-\hbar c\phi\right]}\right) \\ & \quad + \mu_a^{D_o D_r}\mu_c^{D_r D_\alpha}\left(\frac{\exp\left(+i\boldsymbol{\varphi}\cdot\mathbf{R}_{DA}\right)}{\left[E^D_{\alpha r}+E^A_{0\beta}\right]\left[-E^A_{0\beta}-\hbar c\phi\right]} + \frac{\exp\left(-i\boldsymbol{\varphi}\cdot\mathbf{R}_{DA}\right)}{\left[E^D_{\alpha r}+E^A_{0\beta}\right]\left[E^A_{0\beta}-\hbar c\phi\right]}\right)\Bigg\} \\ & \times\left[\exp\left(+i\mathbf{p}\cdot\mathbf{R}_{MD}\right)+\exp\left(-i\mathbf{p}\cdot\mathbf{R}_{MD}\right)\right] d^3\mathbf{p}\; d^3\boldsymbol{\varphi} \end{aligned}$$

The terms pertaining to the two photons *p* and ϕ may be separated out into two definite integrals over three-dimensional wavevector spaces:

$$
\begin{aligned}
M_{FI} = {} & -(2\pi)^{-6}\hbar c\left(2\varepsilon_0\right)^{-2}\mu_a^{M_o M_o}\mu_c^{A_\beta A_o} \\
& \times\int_0^\infty\left(\delta_{ab}-\hat{p}_a\hat{p}_b\right)\left[\exp\left(+i\mathbf{p}\cdot\mathbf{R}_{MD}\right)+\exp\left(-i\mathbf{p}\cdot\mathbf{R}_{MD}\right)\right]d^3\mathbf{p} \\
& \times\int_0^\infty\phi\left(\delta_{cd}-\hat{\phi}_c\hat{\phi}_d\right) \\
& \quad\times\Bigg\{\quad\mu_c^{D_o D_r}\mu_a^{D_r D_\alpha}\left(\frac{\exp\left(+i\boldsymbol{\varphi}\cdot\mathbf{R}_{DA}\right)}{\left[E_{\alpha r}^D\right]\left[-E_{0\beta}^A-\hbar c\phi\right]}+\frac{\exp\left(-i\boldsymbol{\varphi}\cdot\mathbf{R}_{DA}\right)}{\left[E_{\alpha r}^D\right]\left[E_{0\beta}^A-\hbar c\phi\right]}\right) \\
& \qquad+\mu_a^{D_o D_r}\mu_c^{D_r D_\alpha}\left(\frac{\exp\left(+i\boldsymbol{\varphi}\cdot\mathbf{R}_{DA}\right)}{\left[E_{\alpha r}^D+E_{0\beta}^A\right]\left[-E_{0\beta}^A-\hbar c\phi\right]}+\frac{\exp\left(-i\boldsymbol{\varphi}\cdot\mathbf{R}_{DA}\right)}{\left[E_{\alpha r}^D+E_{0\beta}^A\right]\left[E_{0\beta}^A-\hbar c\phi\right]}\right)\Bigg\}d^3\boldsymbol{\varphi}
\end{aligned}
$$

Since chromophore A only interacts with photon ϕ and likewise M with p, we may choose to assign either a or b to the interaction on M (event W), and either c or d to the interaction on A (event Z). The strict correspondence between the indices a, b, c, d and the four unique photon creation/annihilation events no longer exists, although a and b still correspond to p, likewise c and d to ϕ.

The p integral evaluates as follows. In converting to spherical coordinates, we use the vector identity $\mathbf{p}\cdot\mathbf{R} = pR\cos(\theta)$, which suppresses the vectors into scalar variables.

$$
\begin{aligned}
& \int_0^\infty\left(\delta_{ab}-\hat{p}_a\hat{p}_b\right)\left[\exp\left(+i\mathbf{p}\cdot\mathbf{R}_{MD}\right)+\exp\left(-i\mathbf{p}\cdot\mathbf{R}_{MD}\right)\right]d^3\mathbf{p} \\
& = 2\int_0^{2\pi}\int_{-1}^{+1}\int_0^\infty\left(\delta_{ab}-\hat{p}_a\hat{p}_b\right)p^2\exp\left(\pm ipR_{MD}\right)dp\;d\cos\theta\;d\psi \\
& = -2\left(\nabla^2\delta_{ab}-\nabla_a\nabla_b\right)\int_0^{2\pi}\int_{-1}^{+1}\int_0^\infty\exp\left(\pm ipR_{MD}\right)dp\;d\cos\theta\;d\psi \\
& = -4\pi\left(\nabla^2\delta_{ab}-\nabla_a\nabla_b\right)\int_{-1}^{+1}\int_0^\infty\exp\left(\pm ipR_{MD}\right)dp\;d\cos\theta \\
& = -4\pi\left(\nabla^2\delta_{ab}-\nabla_a\nabla_b\right)\int_0^\infty\frac{\exp\left(\pm ipR_{MD}\right)-\exp\left(\mp ipR_{MD}\right)}{\pm ipR_{MD}}dp \\
& = -8\pi\left(\nabla^2\delta_{ab}-\nabla_a\nabla_b\right)\int_0^\infty\frac{\sin\left(pR_{MD}\right)}{pR_{MD}}dp \\
& = -4\pi^2\left(\nabla^2\delta_{ab}-\nabla_a\nabla_b\right)R_{MD}^{-1} \\
& N.B.\quad\nabla_j\equiv\partial\big/\partial R_{MD\,j}
\end{aligned}
$$

The φ integral evaluates as follows. The overall energy difference is best expressed as a reciprocal length, $k = -E^A_{0\beta}/\hbar c$.

$$\int_0^\infty \phi\left(\delta_{cd} - \hat{\phi}_c\hat{\phi}_d\right)\left\{ \mu_c^{D_oD_r}\mu_a^{D_rD_\alpha}\left(\frac{\exp\left(+i\boldsymbol{\varphi}\cdot\mathbf{R}_{DA}\right)}{\left[E^D_{\alpha r}\right]\left[\hbar ck - \hbar c\phi\right]} + \frac{\exp\left(-i\boldsymbol{\varphi}\cdot\mathbf{R}_{DA}\right)}{\left[E^D_{\alpha r}\right]\left[-\hbar ck - \hbar c\phi\right]}\right)\right.$$
$$\left. + \mu_a^{D_oD_r}\mu_c^{D_rD_\alpha}\left(\frac{\exp\left(+i\boldsymbol{\varphi}\cdot\mathbf{R}_{DA}\right)}{\left[E^D_{\alpha r} - \hbar ck\right]\left[\hbar ck - \hbar c\phi\right]} + \frac{\exp\left(-i\boldsymbol{\varphi}\cdot\mathbf{R}_{DA}\right)}{\left[E^D_{\alpha r} - \hbar ck\right]\left[-\hbar ck - \hbar c\phi\right]}\right)\right\} d^3\boldsymbol{\varphi}$$
$$= \left\{\frac{\mu_c^{D_oD_r}\mu_a^{D_rD_\alpha}}{E^D_{\alpha r}} + \frac{\mu_a^{D_oD_r}\mu_c^{D_rD_\alpha}}{E^D_{\alpha r} - \hbar ck}\right\}\int_0^\infty \phi\left(\delta_{cd} - \hat{\phi}_c\hat{\phi}_d\right)\left(\frac{\exp\left(+i\boldsymbol{\phi}\cdot R_{DA}\right)}{\hbar ck - \hbar c\phi} + \frac{\exp\left(-i\boldsymbol{\phi}\cdot R_{DA}\right)}{-\hbar ck - \hbar c\phi}\right) d^3\boldsymbol{\varphi}$$
$$= 8\pi(\hbar c)^{-1}\left\{\frac{\mu_c^{D_oD_r}\mu_a^{D_rD_\alpha}}{E^D_{\alpha r}} + \frac{\mu_a^{D_oD_r}\mu_c^{D_rD_\alpha}}{E^D_{\alpha r} - \hbar ck}\right\}\left(\nabla'^2\delta_{cd} - \nabla'_c\nabla'_d\right)\int_0^\infty \frac{\sin(\phi R_{DA})}{2R_{DA}}\left(\frac{1}{k-\phi} + \frac{1}{-k-\phi}\right) d\phi$$
$$= 4\pi^2(\hbar c)^{-1}\left\{\frac{\mu_c^{D_oD_r}\mu_a^{D_rD_\alpha}}{E^D_{\alpha r}} + \frac{\mu_a^{D_oD_r}\mu_c^{D_rD_\alpha}}{E^D_{\alpha r} - \hbar ck}\right\}\left(\nabla'^2\delta_{cd} - \nabla'_c\nabla'_d\right)R_{DA}^{-1}\exp\left(ikR_{DA}\right)$$

N.B. $\nabla'_j \equiv \partial/\partial R_{DA\,j}$

Combining these results gives the true quantum amplitude of the MDA configuration, containing an explicit summation over all physically-realisable virtual states D_r.

$$M_{FI} = (2\pi)^{-2}\left(2\varepsilon_0\right)^{-2}\left(\nabla^2\delta_{ab} - \nabla_a\nabla_b\right)R_{MD}^{-1}\left(\nabla'^2\delta_{cd} - \nabla'_c\nabla'_d\right)R_{DA}^{-1}\exp\left(ikR_{DA}\right)$$
$$\times \mu_a^{M_oM_o}\mu_d^{A_\beta A_o}\sum_{D_r}\left\{\frac{\mu_b^{D_oD_r}\mu_c^{D_rD_\alpha}}{E^D_{\alpha r}} + \frac{\mu_c^{D_oD_r}\mu_b^{D_rD_\alpha}}{E^D_{\alpha r} - \hbar ck}\right\}$$

This is the final amplitude result, reported as Equation (3a.5).

–

Appendix 8d: **Delocalised excitation: Exciton splitting**

This appendix calculates the difference in energy between the two delocalised-excitation (exciton) states of chapter 4a, section 4.

The two-emitter subsystem is in an unspecified state of excitation, with the states of localised-excitation as the base states:

- Base state A is the state of excitation localised on emitter A, represented by the Dirac ket $\left|A_m, B_0\right\rangle$.
- Base state B is the state of excitation localised on emitter B, represented by the Dirac ket $\left|A_0, B_m\right\rangle$.

The relevant molecular Hamiltonian matrix for these two ket eigenvectors is:

$$H = \begin{bmatrix} E_{\mathrm{A}} & M_{\mathrm{AB}} \\ M_{\mathrm{BA}} & E_{\mathrm{B}} \end{bmatrix}$$

E is the total energy of the subsystem in one of the base states and M is the quantum amplitude of a transition from one to the other. Due to the symmetry of the subsystem, the two base states are so similar that $E_{\mathrm{A}} = E_{\mathrm{B}}$ and $M_{\mathrm{AB}} = M_{\mathrm{BA}}$. The transition between the base states is a process of RET between A and B, as reported by equation (4a.15):

$$\begin{aligned} M_{\mathrm{AB}} &= \mu_i^{A_m A_0} V_{ij}\left(k; \mathbf{R}_{AB}\right) \mu_j^{B_0 B_m} \\ &= \left(4\pi\varepsilon_0\right)^{-1} R_{AB}^{-3} \exp\left(ikR_{AB}\right) \left|\boldsymbol{\mu}^{A_m A_0}\right| \left|\boldsymbol{\mu}^{B_0 B_m}\right| \\ &\quad \times \left\{\left[2ikR_{AB} - 2\right]\sin^2\theta\cos^2\phi + \left[1 - ikR_{AB} - k^2 R_{AB}^2\right]\left(\sin^2\theta\sin^2\phi + \cos^2\theta\right)\right\} \end{aligned}$$

The delocalised exciton states (blue arrows on Figure 4a.4) are each some combination of the base states, defined by some specific values for the superposition coefficients c_{A} and c_{B}:

$$\left|\Psi\right\rangle = c_A \left|A_m, B_0\right\rangle + c_B \left|A_0, B_m\right\rangle$$

Substituting this generic combination wavefunction into the time-dependent Schrödinger equation, $H\left|\Psi\right\rangle = i\hbar\partial\Psi/\partial t$, yields the following differential equations:

$$i\hbar c_A = c_A E_{\mathrm{A}} + c_B M_{\mathrm{AB}}$$
$$i\hbar c_B = c_B E_{\mathrm{A}} + c_A M_{\mathrm{AB}}$$

Integration leads to linear expressions for the two base state coefficients:

$$c_A = \frac{G_+}{2}\exp\left(-i\hbar^{-1}\left(E_{\mathrm{A}} + M_{\mathrm{AB}}\right)t\right) + \frac{G_-}{2}\exp\left(-i\hbar^{-1}\left(E_{\mathrm{A}} - M_{\mathrm{AB}}\right)t\right)$$
$$c_B = \frac{G_+}{2}\exp\left(-i\hbar^{-1}\left(E_{\mathrm{A}} + M_{\mathrm{AB}}\right)t\right) - \frac{G_-}{2}\exp\left(-i\hbar^{-1}\left(E_{\mathrm{A}} - M_{\mathrm{AB}}\right)t\right)$$

Here, G_+ and G_- are constants of integration determined by initial conditions. These contain information about which particular combination of base states the subsystem occupies:

- The symmetric exciton $\left|I^+\right\rangle$ is defined by $G_+=1$, $G_-=0$.
- The antisymmetric exciton $\left|I^-\right\rangle$ is defined by $G_+=0$, $G_-=1$.

Any combination-state Ψ has total energy labelled E_Ψ. This can be calculated with the Schrödinger equation by factoring out the shared time-dependent phase factor K_Ψ from the coefficients c_{A} and c_{B}:

$$\left|\Psi\right\rangle = K_\Psi\left(\ K_\Psi^{-1}c_A\left|A_m, B_0\right\rangle + K_\Psi^{-1}c_B\left|A_0, B_m\right\rangle\ \right)$$
$$K_\Psi \equiv \exp\left(-i\hbar^{-1}E_\Psi\, t\right)$$

Applying this factorisation to the $G_+=1$, $G_-=0$ case yields the total $\left|I^+\right\rangle$ energy.

$$E_{\mathrm{I}+} = E_{\mathrm{A}} + M_{\mathrm{AB}}$$

Applying this factorisation to the $G_+=0$, $G_-=1$ case yields the total $\left|I^-\right\rangle$ energy.

$$E_{\mathrm{I}-} = E_{\mathrm{A}} - M_{\mathrm{AB}}$$

So the energy difference between the two excitons is:

$$E_{\mathrm{I}+} - E_{\mathrm{I}-} = 2M_{\mathrm{AB}}$$